Italian SKA White Book

Editors: L. Feretti & I. Prandoni
On behalf of the SKA-Italy WG

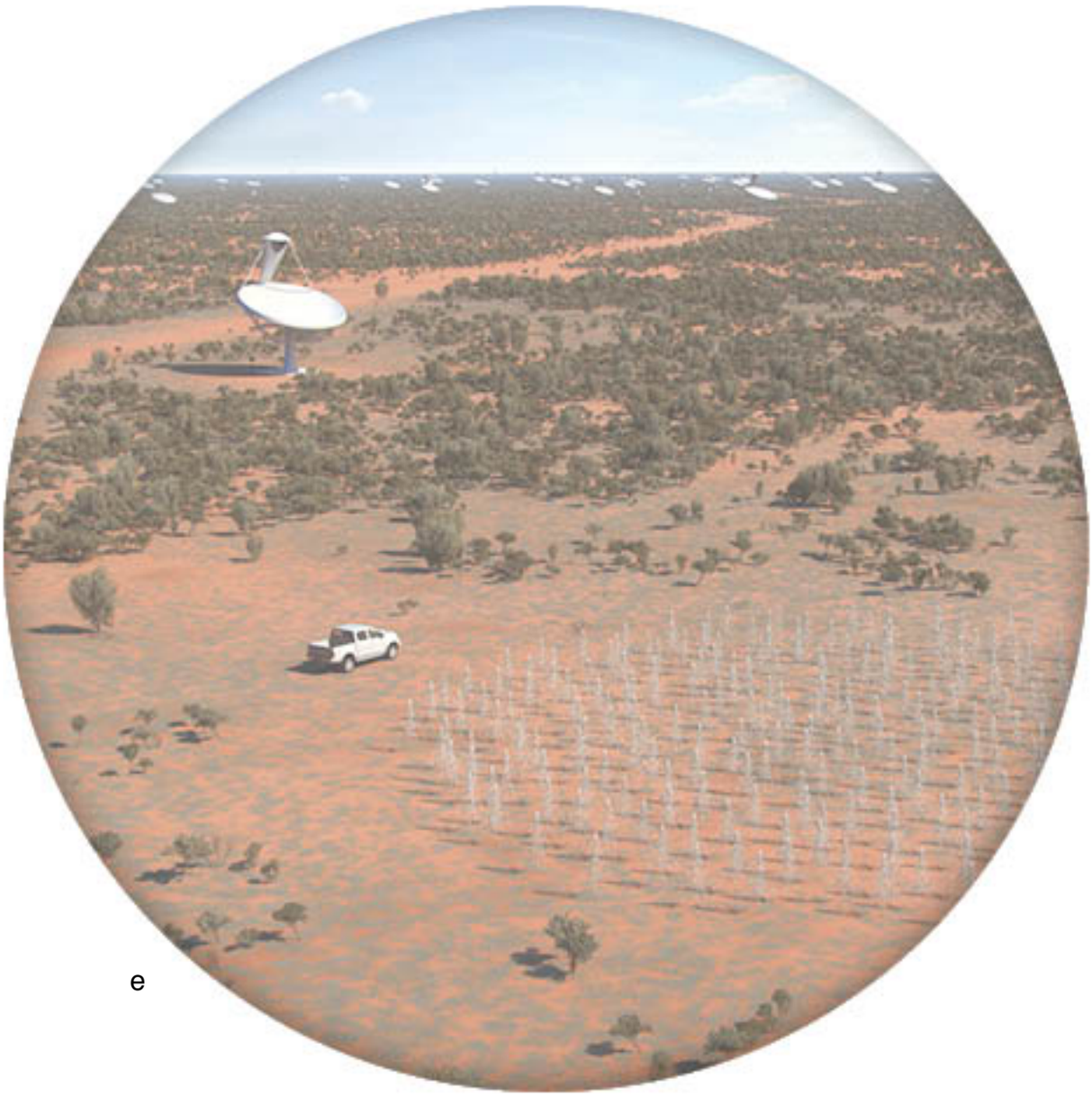

Endorsed by
Scientific Director & Scientific Council

PRESS

978-88-98985-00-

e

Italian SKA White Book

June 28, 2013

Editors[1] *& Contributors:*

L. Feretti[1], I. Prandoni[1], G. Brunetti[1], C. Burigana[2,35], A. Capetti[3], M. Della Valle[4], A. Ferrara[5], G. Ghirlanda[6], F. Govoni[7], S. Molinari[8], A. Possenti[7], R. Scaramella[9], L. Testi[10,11], P. Tozzi[11], G. Umana[12], A. Wolter[13]

Other Contributors:

L. Amati[2], C. Baccigalupi[14], M.T. Beltrán[11], G. Bonnoli[6], S. Borgani[15,16,17], E. Branchini[18], J.R. Brucato[11], C. Buemi[12], Z.-Y. Cai[15], S. Campana[6], S. Capozziello[19,20], V. Casasola[1], P. Caselli[21,11], R. Cassano[1], P. Castangia[7], , C. Ceccarelli[22,11], R. Cesaroni[11], C. Codella[11], L. Costamante[23], S. Covino[6], G. Cresci[24], P. D'Avanzo[6], M. De Laurentis[19,20], G. De Lucia[15], A. De Rosa[2], G. de Zotti[25], I. Donnarumma[8,31], S. Ettori[24], M. Feroci[8,36], F. Finelli[2], F. Fontani[11], F. Fraternali[26], F. Gastaldello[27], G. Ghisellini[6], G. Giovannini[26,1], M. Giroletti[1], M. Gitti[26,24], A. Gruppuso[2], D. Guidetti[1], L. Guzzo[6], L. Hunt[11], P. Leto[1], C. Maccone[28], M. Magliocchetti[8], F. Mannucci[11], A. Marconi[29], M. Massardi[1], S. Matarrese[30], P. Mazzotta[31], A. Melandri[6], A. Melchiorri[32], N. Menci[9], A. Mesinger[5], M. Murgia[7], M. Negrello[25], M.E. Palumbo[12], F. Panessa[8], D. Paoletti[2], P. Parma[1], F. Perrotta[16], C. M. Raiteri[3], E. M. Rossi[33], A. C. Ruggeri[19,20], R. Salvaterra[27], L. Stella[9], G. Tagliaferri[6], F. Tavecchio[6], A. Tarchi[7], A. Tramacere[34], C. Trigilio[12], G. Trinchieri[13], T. Trombetti[2], S. Turriziani[31], V. Vacca[1], T. Venturi[1], D. Vergani[2], M. Viel[16,17], L. Zampieri[25]

[1] *E-mail to:* l.feretti@ira.inaf.it,i.prandoni@ira.inaf.it

Affiliations:

[1]INAF – IRA,Via Piero Gobetti 101, I-40129, Bologna, Italy
[2]INAF – IASF, Via Piero Gobetti 101, I-40129, Bologna, Italy
[3]INAF – OA Torino, Strada Osservatorio 20, I-10025, Pino Torinese (To), Italy
[4]INAF – OA Capodimonte, Salita Moiariello 16, I-80131, Napoli, Italy
[5]Scuola Normale Superiore, Piazza dei Cavalieri 7, I-56126, Pisa, Italia
[6]INAF – OA Brera, via Bianchi 46, I-23807, Merate, Italy
[7]INAF – OA Cagliari, loc. Poggio dei Pini, Strada 54, I-09012 Capoterra
[8]INAF – IAPS Roma, Via Fosso del Cavalaiere 100, I-00133, Roma, Italy
[9]INAF – OA Roma, Via Frascati 33, I-00040, Monte Porzio Catone (RM), Italy
[10]ESO – Karl-Schwarzshild-Strasse 2, D-85748, Garching b. München, Germany
[11]INAF, OA Arcetri, Largo E. Fermi 5, I-50125, Firenze, Italy
[12]INAF, OA Catania, via S. Sofia 78, I-95123, Catania, Italy
[13]INAF – OA Brera, via Brera 28, I-20121, Milano, Italy
[14]SISSA, via S. Sofia 78, I-95123, Triestre, Italy
[15]Università di Trieste, Dipartimento di Fisica, via Valerio 2, I-34127, Trieste, Italy
[16]INAF – OA Trieste, via G.B. Tiepolo 11, I-34143, Trieste, Italy
[17]INFN - Sez. di Trieste, Università di Trieste, via Valerio 2, I-34127, Italy
[18]Università di Roma Tre, Dip. di Matematica e Fisica, via della Vasca Navale 84, I-00146, Roma, Italy
[19]Università di Napoli "Federico II", Dip. di Scienze Fisiche, Complesso Universitario di Monte S. Angelo Ed.G, Via Cinthia, I-80126, Napoli, Italy
[20]INFN, Sez. di Napoli, Complesso Universitario di Monte S. Angelo Ed.G, Via Cinthia, I-80126, Napoli, Italy
[21]School of Physics and Astronomy, University of Leeds, Leeds LS2 9JT, UK
[22]Institut de Planétologie et d'Astrophysique de Grenoble (IPAG) UMR 5274, UJF-Grenoble 1/CNRS-INSU, Grenoble F-38041, France
[23]University of Perugia, I-06123 Perugia, Italy
[24]INAF – OA Bologna, Via Ranzani 2, I–40126, Bologna, Italy
[25]INAF – OA Padova, Vicolo dell'Osservatorio 5, I-35122, Padova, Italy
[26]Universitá di Bologna, Dip. di Astronomia, Via Ranzani 2, I-40126, Bologna, Italy
[27]INAF – IASF, via Bassini 15, I-20133, Milano, Italy
[28]International Academy of Astronautics (IAA), P.O. Box 1268-16, F-75766, Paris Cedex 16, France
[29]Universitá di Firenze, Dipartimento di Fisica e Astronomia, Via Sansone 1, I-50019, Sesto Fiorentino (Firenze), Italy
[30]Universitá di Padova, Dipartimento di Fisica, Via Marzolo 8, I-35131, Padova, Italy
[31]Universitá di Roma "Tor Vergata", Dipartimento di Fisica, Via della Ricerca Scientifica, 1, I-00133, Roma, Italy
[32]Universitá di Roma "La Sapienza", Dipartimento di Fisica, P.le Aldo Moro 2, I-00185, Roma, Italy
[33]Leiden Observatory, Leiden University, P.O. Box 9513, 2300 RA, Leiden, The Netherlands
[34]ISDC, Geneve University, Chemin d'Ecogia 16, F-1290 Versoix, Switzerland
[35]Universitá di Ferrara, Dipartimento di Fisica e Scienze della Terra, Via Giuseppe Saragat 1, I-44100, Ferrara, Italy
[36]INFN, Sez. di Roma "Tor Vergata", Via della Ricerca Scientifica, 1, I-00133, Roma, Italy

This Book has been produced in the framework of SKA–related INAF initiatives
and has been endorsed by the INAF Scientific Council

Contents

Preface

Radio astronomy is in the midst of a transformation. State-of-the-art technology, together with developments in high-speed digital signal processing and broad-band optical fibre links between antennas, have enabled a ten-fold sensitivity boosts to existing radio facilities (e.g. e-MERLIN, JVLA, ATCA-CABB, eEVN, APERTIF), and are leading to next-generation radio telescopes (e.g. LOFAR, MWA, ASKAP, MeerKAT). All these efforts will ultimately lead to a new global facility, the Square Kilometre Array (SKA), a revolutionary, gigantic, radio telescope with a total collective area of 1 square km. These upgraded/next-generation facilities (referred to as *SKA pathfinders* and/or *precursors*) are or are becoming soon operational, and are essential technological and scientific test-beds for the first phase of the SKA, expected to start scientific observations in 2020. The expected advances in sensitivity, field-of-view, frequency range and spectral resolution will yield transformational science in many research fields, from cosmology to astrophysics.

Italy is one of the founding members of the *SKA Organization*, an independent body that will seek funding and will coordinate the design phase of the SKA project. Thanks to their internationally recognized expertise, several Italian researchers are already involved in major legacy projects planned for SKA pathfinders/precursors, in some cases with leading roles. Moreover, the scientific interest to the SKA is rapidly growing in the Italian community as a whole. This *Book* represents the first Italian SKA-driven coordinated effort to exploit existing synergies and scientific expertise/excellence in a variety of research fields, to build an Italian science roadmap to the SKA.

This *Book* briefly presents SKA–driven scientific activities currently on-going in Italy, and a collection of science cases and/or topics, in which the Italian community has strong expertise, where SKA, in its various phases of implementation (from SKA pathfinfders and precursors to SKA phase 1 and 2), is expected to play a major role.

Part I

Introduction

1 The SKA and its Scientific Perspectives

With a collecting area of about a square kilometre, the SKA will be far superior in sensitivity and/or observing speed to all current radio facilities. In the lead-up to the SKA, several next-generation radio telescopes are being constructed around the world (see e.g. [1] for a nice review), including the two official SKA precursors: ASKAP (Australian SKA Pathfinder) and MeerKAT.

ASKAP ([2–4]) is a new radio interferometer being built in Western Australia, and is expected to start operations in 2014 with a limited number of antennas. In its final design, ASKAP will consist of 36 12-m antennas distributed over a region of 6 km in diameter. Each antenna will be equipped with a PAF (Phased Array Feed), operating in a frequency band of $0.7 - 1.8$ GHz. PAF technology allows very wide field of views (~ 30 deg^2 at 1.4 GHz), at the expenses of sensitivity. This makes ASKAP best suited for wide-/all-sky surveys, rather than pointed deep integrations.

Meerkat ([5]) is the South African SKA precursor telescope. It will be constructed in two phases. Meerkat 1 (2016) will consist of 64 13-m antennas distributed over a region of 8 km in diameter. It will be equipped with single-pixel receivers, operating in a limited frequency range ($0.9 - 1.7$ GHz). The frequency range will be significantly extended in phase 2 (Meerkat 2, 2018), with operational bands $0.6 - 1.7$ GHz and $8 - 14.5$ GHz. For Meerkat 2 the telescope baselines will be possibly increased up to 16 km, allowing better spatial resolution and consequently deeper integrations.

The SKA is designed to be built in phases. The first (SKA 1) is expected to become fully operational by 2020, while the second (SKA 2) should become available around 2025 (or a few years later), and is expected to yield a factor 10 increase in sensitivity over SKA 1. According to current plans, both phases should consist of three elements: one operating at low frequency (SKA_low), one at intermediate/high frequency (SKA_mid), and one optimized for surveys (SKA_survey). In principle a third SKA phase (SKA 3) is envisaged, that should extend SKA operations to high radio frequencies (> 20 GHz). Such phase has yet to be confirmed.

The main technical specifications for SKA 1, SKA 2 and SKA precursors (Meerkat and ASKAP), to which we refer in this Book, are reported in Appendix A.

1.1 SKA Science Drivers

In the following we briefly summarize the main SKA science drivers, as from the SKA Science Book *Science with the Square Kilometre Array* ([6]). In addition, it is important to bear in mind that the SKA will permit improvements in many other research fields, besides those mentioned here, and will certainly discover new phenomena beyond what we can currently predict or even imagine.

1.1.1 Probing the Dark Ages

The aim is to investigate the formation of the first structures, as the Universe made the transition from largely neutral to its largely ionized state today. Our understanding of cosmology has expanded greatly in recent years. On the one hand, detailed observations of the cosmic microwave background

have shown a picture of the universe as it was only 300,000 years after the Big Bang, when the gas was smoothly distributed and electrically neutral, and lumps of matter such as galaxies, stars, and planets did not yet exist. On the other hand, technological advances in optical, X–ray, and radio telescopes allowed us to observe the detailed properties of galaxies and quasars at extreme distances, i.e. when the Universe was about one billion years old. At that time, protogalaxies were beginning to merge to form the galaxies (and clusters of galaxies) that we see today.

The last frontier of cosmology is to explore the time between these two epochs: the Dark Ages during which the first protogalaxies and quasars formed. Once the first objects grew, their light ionized the gas around them, therefore this event is labeled as *Epoch of Reionisation*. This era has proven difficult to study. The protogalaxies are distant and extremely faint; moreover, much of their light is absorbed as it travels toward us. Observations with the Wilkinson Microwave Anisotropy Probe (WMAP) found a surprisingly large electron scattering optical depth to the cosmic microwave background (CMB) radiation, implying that reionization began at $z \sim 20$; high redshift quasars selected from the Sloan Digital Sky Survey (SDSS) have shown evidence for a sharp rise in the neutral fraction of the intergalactic medium (IGM) at $z \sim 6$, implying that epoch of reionization ends at this time. Reconciling these observations requires reionisation to be a complex process, with the ionising sources having qualitatively different (and time-dependent) characteristics from all galaxies that we can currently observe and with feedback from protogalaxies playing a crucial role in regulating the formation of subsequent generations of objects. The emission from a patch of the IGM depends on its density, temperature, and neutral fraction. When the first sources of light turn on, the IGM is visible first in absorption and then in emission as these sources heat their surroundings. Fluctuations across the sky will show us how structures grow (through density variations) and how the heating occurs (whether through shocks or radiation from the first objects).

The Square Kilometre Array will study the detailed properties of the first luminous objects in the universe, taking snapshots of the 21 cm emission at many different epochs, before, during and after reionisation, yielding detailed information about the formation of the first structures in the universe. It will provide the best measurements available of the characteristics of the first light sources in the universe. Moreover, the SKA will have the sensitivity to make high-resolution spectra of high-redshift radio sources. These spectra will yield detailed information about the early evolution of the cosmic web, the growth of ionised regions around protogalaxies, and even provide the only known direct way to observe minihalos, small clumps of dark matter and gas in the IGM.

For more details see the chapter *Probing the Dark Ages with the Square Kilometre Array* (Carilli et al., [6]).

1.1.2 Galaxy Evolution, Cosmology and Dark Energy

This project is aimed at probing the structure of the Universe and its fundamental constituent, galaxies, by carrying out all-sky surveys of continuum emission and of HI to a redshift $z \sim 2$. HI surveys can probe both the properties of galaxy assembly and evolution (including dark matter) and cosmology (including dark energy). Hydrogen is the most abundant element in the Universe and it is the raw material from which stars form. The SKA will revolutionize the study of how galaxies form and transform their gas into stars, by detecting hydrogen gas in as many as a billion galaxies, at much larger distances than it is possible to detect today. It will also allow us to study the morphology of the hydrogen in galaxies, , to detect clouds in between galaxies, and to derive information on their origin. It is possible that powerful winds from hot, young stars can blow some of the gas belonging to a galaxy to large distances from the galaxy itself, or alternatively that gas clouds are made of *pristine* or *primordial* material from the very early Universe. The latter possibility would imply that not all of the hydrogen in the Universe has been captured within galaxies. The map of the cosmic

distribution of hydrogen will allow the investigation of the Universe expansion, and help identify the nature of the mysterious dark energy. There are two broad approaches that the SKA will pursue in studying cosmology and dark energy. The first involves a large survey of galaxies, searching for their (redshifted) 21 cm hydrogen emission. An extremely large survey of galaxies is required in order to sample a large enough volume of the Universe to detect relatively subtle effects. Another approach is to observe the gravitational lensing effects of galaxies and clusters of galaxies on the path of radio waves through the Universe by measuring the shapes of large numbers of galaxies. In addition to detecting vast numbers of HI emission line galaxies, the SKA can also perform the deepest ever radio continuum survey, probing the star formation history of the Universe as a function of redshift in a manner independent of the dust extinction, that confuses experiments in optical wavebands.

For more details see the chapter *Galaxy evolution, cosmology and dark energy with the Square Kilometre Array* (Rawlings et al., [6]).

1.1.3 Strong Field Tests of Gravity

High precision timing measurements can be conducted from the study of pulsars, the best clocks in the Universe, to investigate the nature of gravity and of space-time, and challenge the theory of general relativity in the presence of strong gravitational fields. Pulsars orbiting really massive objects like black holes are expected to be very rare, but with the unique sensitivity of the SKA these systems can be found in the disk of our Galaxy. Pulsars in orbit around the super-massive black hole in the centre of the Galaxy may also be detected. By studying the regularity of the received pulsar ticks, we can not only test general relativity under very strong-field gravity conditions, but we can also study the black hole properties at the same time. General relativity makes clear predictions about the nature of black holes. Observations with the SKA can measure these properties and hence provide the ultimate test for general relativity. Einstein′s theory also predicts the existence of waves propagating in space-time as a result of the motion or collapse of massive objects. Both the birth of the Universe in the Big Bang and the much later collision of super-massive black holes in the centre of galaxies would be expected to produce gravitational waves that still propagate through our neighborhood. The accurate pulsar clocks represented by millisecond pulsars, together termed a Pulsar Timing Array (PTA), in combination with the SKA telescope, will provide us with a unique opportunity to find these elusive gravitational waves at wavelengths that no other planned instruments will be able to detect.

The SKA will detect many more millisecond pulsars than is currently possible, and allow them to be timed to very high precision ($\leq$ 100 ns), making them very sensitive to the small space-time perturbations of gravitational waves. This *device*, with the SKA at its heart, will be sensitive to gravitational waves at frequencies of nHz thereby complementing the much higher frequencies accessible to Advanced LIGO ($\sim$ 100 Hz) and LISA ($\sim$ mHz).

For more details see the chapter *Strong-Field Tests of Gravity Using Pulsars and Black Holes* (Kramer et al., [6]).

1.1.4 The Origin and Evolution of Cosmic Magnetism

Magnetic fields are an essential part of many astrophysical phenomena, but fundamental questions remain about their evolution, structure and origin. The goal of this project is to trace magnetic field evolution and structure across cosmic time. Understanding the Universe is impossible without understanding magnetic fields. They fill intracluster and interstellar space, affect the evolution of galaxies and galaxy clusters, contribute significantly to the total pressure of interstellar gas, are essential for the onset of star formation, and control the density and distribution of cosmic rays in the interstellar medium (ISM). In spite of their importance, the origin of magnetic fields is still an open problem in

fundamental physics and astrophysics. Did significant primordial fields exist before the first stars and galaxies? If not, when and how were magnetic fields subsequently generated? What maintains the present-day magnetic fields of galaxies, stars and planets?

The SKA will detect millions of faint polarized sources that can be used to study the magnetic field throughout the Universe, using Faraday rotation. The resulting tri-dimensional maps of the Milky Way, nearby galaxies, and galaxy clusters will be used to study the processes that formed the fields observed today through the comparison with the predictions of models for magnetic field generation. Fundamental to all these issues is the search for magnetic fields in the intergalactic medium (IGM). All of empty space may be magnetised, either by outflows from galaxies, by relic lobes of radio galaxies, or as part of the cosmic web structure. Such a field has not yet been detected, but its role as the likely seed field for galaxies and clusters, plus the prospect that the IGM field might trace and regulate structure formation in the early Universe, places considerable importance on its discovery. Finally, detailed studies of the magnetic field configuration of individual objects at different redshifts, including the youngest galaxies and proto-galaxies, allow us to understand how magnetized structures evolve and amplify as galaxies mature, and distinguish between primordial and seed origins for present-day magnetic fields. The main platform on which SKA studies of cosmic magnetism is based is an All-Sky SKA Rotation Measure Survey, in which a year of observing time will yield Faraday rotation measures (RMs) for 10 million compact polarized extragalactic sources. This data-set will provide an all-sky grid of RMs at a spacing of just $20 - 30$ arcsec between sources; many of these sources will have redshifts from the Sloan Digital Sky Survey (SDSS) and its successors. Using the unique sensitivity of the SKA, it may even be feasible to measure Faraday rotation against the Cosmic Microwave Background produced by primordial magnetic fields. This all-pervading cosmic magnetic field can finally be identified through the all-sky RM survey proposed above. Just as the correlation function of galaxies yields the power spectrum of matter, the analogous correlation function of this RM distribution can then provide the magnetic power spectrum of the IGM as a function of cosmic epoch and over a wide range of spatial scales. Such measurements will allow us to develop a detailed model of the magnetic field geometry of the IGM and of the overall Universe.

For more details see the chapter *The Origin and Evolution of Cosmic Magnetism* (Gaensler et al., [6]).

1.1.5 The Cradle of Life

The goal of this project is to probe the full range of astrobiology, from the formation of prebiotic molecules in the interstellar medium to the emergence of technological civilisations on habitable planets. Searching for extraterrestrial life and planets is one of the most fundamental issues humanity has contemplated since the beginning of history.

Recent discoveries have shown that giant gaseous planets (similar to Jupiter) are common around other stars like the Sun, and the first handful of potentially habitable, rocky planets not much larger than the Earth (the so-called super-Earths) are being found mostly around smaller stars, but are deemed to be ubiquitous in the Galaxy.

The SKA will image the thermal emission from dust in the habitable zone with unprecedented detail. In particular, the SKA will show where dust evolves from micron sized interstellar particles to centimeter sized *pebbles*, the first step in assembling Earth-like planets. Fortunately there are hundreds of these young stars within about 500 light years of the Sun, and many thousands more at greater distances. If placed at 500 light years distance, our own Solar System would be about 1 arcsecond, so observations at high angular resolution are very important, enabling us to probe the *habitable zone* of Sun-like protostars, i.e. the region where environment is favorable for the development of life.

Giant planets may form by the slow growth of dust grains into large rocks that capture gas, or by rapid gravitational instabilities that disrupt the surrounding disk. The SKA will discern which mechanisms are active, and where in the disk they occur, which will reveal the impact of newborn giant planets on their Earth-like counterparts. In addition, the SKA offers the possibility of detecting radio transmissions that would provide evidence for intelligent life among the stars; in particular it will be able to detect extremely weak extraterrestrial signals and may even spot other planets capable of supporting life. Astrobiologists will use the SKA to search for amino acids, the building blocks of life, by identifying spectral lines at specific frequencies.

For more details see the chapter *The Cradle of Life* (Lazio et al., [6]).

2 Italian Involvement in Preparatory Work for the SKA

2.1 SKA-driven Scientific Activity

2.1.1 Introduction

In the following we briefly present the main SKA pathfinders and the two SKA precursors: MeerKAT and ASKAP, with special focus on the instruments which are of particular interest for the Italian community. Scientific key-projects, which the Italian community is involved in, are briefly presented as well (for a complete review of the planned radio–continuum radio surveys with SKA pathfinders and precursors and their scientific impact, see [1]).

2.1.2 e-MERLIN

MERLIN is an array of seven radio telescopes across the UK, connected to a central correlator at Jodrell Bank Observatory (JBO) and operated as a dedicated radio interferometer to produce high-resolution images. With a maximum baseline length of 220 km, MERLIN provides a unique capability for radio imaging at $0.01 - 0.15$ arcsec resolution at frequencies of 1.5, 5 and 22 GHz (L, C and K bands). The e-MERLIN project is a major upgrade to the instrument involving the installation of new receivers, analogue and digital electronics, optical-fibre links to each telescope and a new correlator at JBO. This increases the useable bandwidth by more than two orders of magnitude, and hence the continuum sensitivity by more than 10×. In addition, the increase in bandwidth dramatically improves aperture coverage for continuum observations resulting in enhanced image fidelity together with simultaneous spectral-index imaging. For more information see http://www.e-merlin.ac.uk.

The e-MERGE Legacy Project

With more than 900 hours allocated, the e-MERGE (e-MERLIN Galaxy Evolution) Survey is the largest single element of the approved e-MERLIN Legacy programme, accounting alone for about 30% of the total amount of time available to the whole Programme.

The e-MERGE Survey project intends to exploit the e-Merlin's unique combination of sensitivity and spatial resolution to study the formation and evolution of star-forming galaxies and AGN out to $z > 5$, through the deepest high resolution radio imaging of two well studied extragalactic fields. The first field (referred to as Tier 1), centered at the GOODS-N region, will be observed in both L- and C-Bands. This is aimed at studying star-formation and AGN activities in high redshift ($1 < z < 4$) galaxies, with special focus on possible co-existence and co-evolution of the two phenomena.

The second field (refereed to as Tier 0), observed in L-Band only, is centered at an Abell cluster, which will be used as a magnification lens to detect the background higher redshift (radio) galaxy population (up to $z > 5$).

With a resolution of $50 - 200$ milliarcsec (mas) in C- and L-Bands respectively, corresponding to $< 0.5 - 1.5$ kpc at $z > 1$, e-MERLIN gives us our first truly reliable view of the distribution of star formation within typical galaxies at the epoch where the bulk of the stars in the present-day Universe

were being formed. e-MERLIN will disentangle the contributions of AGN and star-formation, an essential step given the apparently simultaneous growth of the black holes and stellar populations in galaxies.

[The Italian contribution and leadership is related to AGN studies and data reduction and analysis of Tier 1 C-Band.]

2.1.3 e-European VLBI Network (eEVN)

The SKA will be a real-time instrument, with preferably 20% of its collecting area forming long baselines that extend to > 200 km. Data caching and transportation, distribution of the clock signal, and operations of this array will present a great technical challenge. The European VLBI Network (EVN) as a SKA pathfinder is addressing these issues within the framework of the NEXPReS EC project (http://www.nexpres.eu/). The primary goal of NEXPReS is to support and develop real-time electronic-VLBI (e-VLBI) operations in the EVN and on global scales.

Science observations with the e-EVN have routinely been carried out since 2006. The possibility of operating a real-time VLBI array with baselines exceeding 12,000 km was recently demonstrated by [7]. Relaxing the data storage limitations at the telescopes creates an obvious advantage for the EVN. This allows for more flexible operations to carry out transient science, it may provide seamless data transport at > 1 Gbps data rates for superior sensitivity, and makes it possible to conduct automated observations for efficient VLBI surveys, or to respond to external triggers.

The importance of long baselines (and even the possibility of baselines to space) for the SKA are currently under discussion. Sensitive e-VLBI observations could bring new evidence on the possible role of long (≥ 1000 km) baselines for the SKA.

[Italy is one of the members of EVN, contributing to it with three antennas (Medicina, Noto and SRT). As such it is well represented in the EVN governing bodies and commitees. The Italian community regularly submits and obtains observing time at the e-EVN.]

2.1.4 Karl G. Jansky Very Large Array (JVLA)

The Karl G. Jansky Very Large Array (JVLA) represents a major upgrade to the VLA, a facility open to researchers around the world. Its high sensitivity, continuous frequency coverage, flexible wideband correlator, and scaled array configurations make the JVLA a useful complement to the dedicated pathfinders, and to the all-sky continuum surveys that are being planned.

Thanks to its sensitivity and angular resolution, the JVLA can be used to provide important constraints to the SKA design. For instance the ultimate continuum sensitivity limits (source confusion or dynamic range) of the full SKA depend on the surface density on the sky of sub-μJy sources. If dynamic range permits, by imaging a single field at 20 cm to the confusion limit with 5 arcsec resolution, the JVLA in its B configuration will place a tight statistical constraint on the source density of objects fainter than 1 μJy.

[The Italian community regularly submits and obtains observing time at the JVLA.]

2.1.5 Aperture Tiles In Focus (APERTIF)

APERTIF, the new Phased Array Feed (PAF) receiver system for the Westerbork Synthesis Radio Telescope (WSRT) will dramatically enlarge the instantaneous field of view (FOV) of the WSRT ([8]) by replacing the current single front-end feeds by PAFs. Each of the PAFs consists of 121 Vivaldi elements and will detect the radiation field (in dual polarisation) in the focal plane of each dish over an area of about one square metre at an observing frequency of 1.4 GHz. Because of this, many beams can be formed simultaneously for each dish making it possible to image an area of about 8 square degrees on the sky, which is an increase of about a factor of 30 compared to the current

WSRT. Its large 300 MHz bandwidth will not only cater for sensitive continuum imaging, but is also crucial for efficient HI and OH emission surveys and for studies of polarised emission from large areas.

Apertif survey key-projects

Legacy projects for the APERTIF first years of operation are currently being selected. Among them is the WODAN (Westerbork Observations of the Deep APERTIF Northern-Sky) survey ([9]). The WODAN project is aimed at using APERTIF to undertake a radio-continuum survey of the northern 25% of the sky (i.e. North of declination $+30^o$) that is inaccessible to ASKAP (see below), to a target rms sensitivity of 10 μJy/beam at a spatial resolution of 15 arcsec, although confusion noise with a 15-arcsec beam may increase the observed rms noise level to about 20 μJy/beam.

Another proposed key-project is aimed at undertaking a blind, medium-deep survey of neutral hydrogen out to $z = 0.25$ over an area of 25×20 deg^2. Such survey intends to cover the nearby CVn-I, M101, CVn-II and UMa groups, while also including 100 distant Abell clusters. The proposed area is covered by both the SDSS and the UKIDSS-LAS surveys to ensure available optical and NIR photometry for all detected sources. The main scientific drivers are 1) to explore the HI mass function down to a minimum HI mass of 2×10^5 M_{Sun}; 2) to map and measure in detail the extended morphologies and kinematics of the neutral hydrogen in and around galaxies in different environments; and 3) to determine the cosmic evolution of the gas content of galaxies over the past 3 Gyr. A survey of this kind can only be surpassed by the Square Kilometre Array.

[Several Italian researchers are involved in both projects.]

2.1.6 Low Frequency Array (LOFAR)

LOFAR, the Low Frequency Radio Array, is a pan- European radio phased-array telescope that is currently being commissioned. The two types of antenna, one optimised for 30 – 80 MHz and the other for 110 – 240 MHz, are grouped together in stations a few hundreds meter wide. 40 stations are distributed over an area of diameter of 100 km in The Netherlands, and a further eight stations are located in Germany, UK, Sweden, and France. The signals from the antennas are digitised to form many beams on the sky, making LOFAR an extremely efficient survey instrument. LOFAR has already generated images that are the deepest ever at these low frequencies.

The LOFAR Survey key-project

A key motivation of LOFAR is to provide the entire international astronomical community with surveys of the radio sky that have a long-lasting legacy value for a broad range of astrophysical research. The LOFAR continuum survey ([10]) will cover the northern half of the sky. LOFAR will be especially complementary to WODAN and EMU (see below) in surveying the sky at high sensitivity and resolution but at a much lower frequency.

The three fundamental areas of astrophysics that have driven the design of the planned LOFAR surveys are: *(i)* the formation of massive galaxies at the epoch of reionisation, *(ii)* magnetic fields and shocked hot gas associated with the first bound clusters of galaxies, and *(iii)* star formation processes in distant galaxies.

To achieve the goals of the LOFAR surveys, a three-tiered approach has been adopted (Röttgering et al. 2010a). Tier 1 is a 2π steradian survey reaching an rms of 0.07 mJy at 15 – 65 and 120 – 180 MHz, and is designed to detect 100 cluster halos at $z > 0.6$ and 100 $z > 6$ radio galaxies. Tier 2 is a deep survey over 500 deg^2 at 30, 60, and 150 MHz, to be undertaken on 55 pre-selected sky regions/targets. Tier 3 is an "ultra-deep" survey at 150 MHz covering a single pointing of 100 deg^2 reaching the confusion level of 7 μJy/beam rms.

[Italy is involved in several of the science topics listed above, and leads the cluster science case.]

The LOFAR Magnetism key-project

This project aims at investigating fundamental astrophysical questions on the distribution of magnetic fields in the Universe, with the goal of understanding the origin of cosmic magnetism. The project makes use of the LOFAR capacity to detect linear polarisation and hence widens the horizon of the instrument.

Measuring polarised radio waves at low frequencies offers a new window to study cosmic magnetism, and LOFAR is the first radio telescope of sufficient sensitivity to open this window. Targets of this project are the Milky Way, pulsars, nearby galaxies, giant radio galaxies, galaxy groups and filaments.

Many synchrotron radio sources, like galaxies, have "steep" spectra, therefore they are better studied at low frequencies where their intensity is much larger. Another important tool to measure cosmic magnetic fields is the effect of Faraday rotation, which is proportional to the square of the wavelength. Therefore weak fields and/or low plasma densities, as expected e.g. in galaxy halos and filaments, can be measured with much higher precision at low frequencies / long wavelengths.

[Several Italian researchers are involved in this project.]

2.1.7 Australian SKA Pathfinder (ASKAP)

The Australian SKA Pathfinder (ASKAP; [2–4]) is a new radio telescope being built on the Australian SKA site in Western Australia, at the Murchison Radio-astronomy Observatory, with a planned completion date of 2013-14. It will consist of 36 12-metre antennas distributed over a region 6 km in diameter. Each antenna is equipped with a PAF of 96 dual-polarisation pixels operating in a frequency band of $700 - 1800$ MHz. As a result, ASKAP will have a field of view up to 30 deg^2. To ensure good calibration, the antennas are a novel 3-axis design, with the feed and reflector rotating to mimic the effect of an equatorial mount, ensuring a constant position angle of the PAF and sidelobes on the sky.

The EMU Key Project

EMU (Evolutionary Map of the Universe, [11]) is a radio sky survey project which will use the new ASKAP telescope to make a deep ($\sim$ 10 μJy rms) radio continuum survey covering the entire Southern Sky (perhaps as far North as 30^o). It can be characterised as a *Southern NVSS*, except that it will have about 40 times the sensitivity of the NVSS and about 5 times better angular resolution (10 arcsec). The EMU all-sky survey is particularly significant because of the growth in number of cutting-edge southern hemisphere telescopes and associated major surveys being planned spanning all wavelengths. EMU is one of the two equal-top-ranked key-projects selected for ASKAP.

The key science goals for EMU are:

- To trace the evolution of star-forming galaxies from $z \sim 2$ to the present day, using a wavelength unbiased by dust or molecular emission.
- To trace the evolution of massive black holes throughout the history of the Universe, up to the very edge of it, and understand their relationship to star-formation.
- To use the distribution of radio sources to explore the large-scale structure and cosmological parameters of the Universe.

- To explore an uncharted region of observational parameter space, almost certainly finding new classes of object.
- To create the most sensitive wide-field atlas of Galactic continuum emission yet made in the Southern Hemisphere, addressing areas such as star formation, supernovae, and Galactic structure.

[The Italian community is involved in all science topics listed above, and actively participate to the various working groups formed for the EMU design phase.]

The COAST Key Project

COAST (Compact Objects with ASKAP: Survey and Timing) is a multi-purposes experiment, which will use the capabilities of ASKAP of simultaneously observing many radio pulsars in order to face many key questions of current physics and astrophysics, among which:

- How did galaxies form? Did the galaxy formation process leave a background of gravitational waves?
- Was Einstein right?
- Are there exotic companions to pulsars?
- How many kinds of neutron stars are harboured in our Galaxy? Is there a link between them?
- What is the shape of the magnetic field pervading our Galaxy?
- Which are the physical processes which make a pulsar to shine in radio and other electromagnetic bands? Are pulsars also gravitational waves emitters?
- Which forces act in the ultra-high dense matter of a neutron star?

[All the subjects above are in the focus of the italian pulsar community, which is significantly represented in the working groups related to this project.]

The VAST Key Project

This is a survey for Variables And Slow Transients (VAST), the main aims of which are:

- to determine the origin and nature of the structures responsible for extreme scattering events;
- to provide a direct detection of baryons in the intergalactic medium;
- to detect and monitor 'orphan' gamma-ray burst afterglows to understand their nature;
- to conduct an unbiased survey of radio supernovae in the local Universe;
- to discover flaring magnetars, intermittent or deeply nulling radio pulsars, and rotating radio transients through changes in their pulse-averaged emission;
- to detect and monitor flare stars, cataclysmic variables and X-ray binaries in our Galaxy

[The italian community is interested in most of these subjects and is represented in the Science working group of this collaboration.]

2.1.8 MeerKAT

MeerKAT ([5]) is the South African SKA pathfinder telescope. Meerkat Phase 1 will consist of 64 dishes, each 13.5m in diameter, equipped with single-pixel receivers. MeerKAT's 64 dish array layout will be distributed over two components. A dense inner component will contain 70% of the dishes with a Gaussian uv-distribution with a dispersion of 300 m. The outer component will contain the remaining 30% of the dishes, having a Gaussian uv-distribution with a dispersion of 2500 m and a longest baseline of 8 km. A potential future extension (Meerkat Phase 2) could see 7 additional dishes being added to extend the longest baselines to about 16 km. MeerKAT will support a wide range of observing modes, including deep continuum, polarisation and spectral line imaging, pulsar timing, and transient searches. The plan is to provide standard data products, including an imaging pipeline.

70% of observing time on MeerKAT, for the first few years, is allocated for large survey projects of 1000 hours or more, while the remaining 30% is reserved for smaller PI driven proposals (of which 5% will be Director's Discretionary Time). Proposals for key projects were solicited in 2010, and 10 projects were selected. Two (a pulsar timing and a deep HI survey) were chosen as top priority, and a further eight as second priority.

[In the highly ranked pulsar timing project there is a significant involvement of the italian community, which will lead the "1000 Pulsar Array" program, expected to be run for about 1000 hours of observing time over 5 years.]

The MIGHTEE Survey

The MIGHTEE (MeerKAT International Giga-Hertz Tiered Extragalactic Exploration) Survey is one of the accepted key-projects. MIGHTEE is a very ambitiuous tiered continuum survey aimed at investigating the evolution of AGN, star-forming galaxies (SFG) and galaxy clusters from the epoch of reionization through to the present day ($0 < z < 6$).

The survey is designed to fully utilize MeerKAT's unique capabilities, namely a high-resolution coupled with a large survey speed and sensitivity (outperforming both ASKAP and JVLA), to make the most precise measurement of the radio luminosity function for radio-loud & radio-quiet AGN and star-forming galaxies over the full range in radio luminosity.

The MIGHTEE survey aims to probe to much fainter flux densities ($0.1 - 1$ μJy/beam rms) than the EMU/WODAN surveys, over smaller areas at higher angular resolution, at an observing frequency of 1.4 GHz. The higher sensitivity and resolution will enable exploration of AGN, star-forming galaxies and galaxy clusters from the epoch of eionisation through to the present day. The two-tiered approach (a $\sim$ 35 deg^2 pointing down to 1 μJy/beam rms plus a $\sim$ 1 deg^2 down to 0.1 μJy/beam rms) maximizes the scientific outcome of the survey, by allowing us to assess the evolutionary status of galaxies both as a function of their luminosity and of their environment.

[Italy is involved in several of the science topics listed above, and leads the AGN science case.]

2.2 Synergies with Other Future Facilities

In addition to the ongoing SKA- driven activity outlined in the previous Sections, there are important synergies to be exploited with several of the planned and/or proposed future facilities, which are expected to become available on a timescale similar to the SKA one ($>$ 2020). Such synergies are highlighted in the following chapters describing the Italian astrophysical science interests (see Part II of this Book), with particular focus on those facilities, which the Italian community is strongly involved in, or has expressed strong interest for (Euclid, LOFT, CTA, etc.).

Part II

Italian Astrophysical Science Interests

3 Cosmology

3.1 Studying the Dark Ages and Cosmic Dawn with the Square Kilometer Array

A. Mesinger & A. Ferrara

3.1.1 Summary

The best probe of the early Universe is the redshifted 21cm line from neutral hydrogen. The Square Kilometer Array (SKA) offers us an unprecedented opportunity to study the cosmic Dark Ages, the dawn of the first galaxies and the subsequent reionization of the Universe. However, efficient modeling tools are neccessary to robustly interpret the observations.

3.1.2 Introduction

Following recombination, the Universe entered the so-called Dark Ages. Perturbations in the baryonic fluid were allowed to grow, accreting onto the evolving dark matter (DM) structures. Eventually, the first astrophysical objects (stars and black holes) formed out of the baryons, perhaps as early as $z \sim 50$ (e.g. [26]). Their radiation spread out from their host DM halos, signaling the Cosmic Dawn, with a dramatic impact on their surroundings. Eventually the radiation from these first galaxies and their descendents permeated the Universe, culminating in the last global phase change of our Universe: the epoch of reionization (EoR). This process is fundamentally important, allowing us to study the first galaxies as well as the majority of the baryonic matter spread out between them in the intergalactic medium (IGM).

These early epochs correspond to the bulk of our light cone, enclosing orders of magnitude more linear modes than the much-studied cosmic microwave background (CMB; e.g. [17]). Unlocking this mystery is vital in furthering our understanding of the thermal and ionization history of baryons, its impact on structure formation, and the nature of the first galaxies. Indirect probes, such as the EoR, will be the only way of studying most of the first galaxies, since the majority of them will be too faint to be directly detected with next-generation infrared telescopes, such as the James Webb Space Telescope (JWST; e.g. [27]).

The most promising probe of the early Universe is the redshifted 21cm line. This line corresponds to the spin-flip transition in the ground state of neutral hydrogen. As a cosmological probe, the 21cm signal is usually represented in terms of the offset of the 21cm brightness temperature from the CMB temperature, T_γ, along a line of sight at observed frequency ν (c.f. [14]):

$$\delta T_b(\nu) = \frac{T_\mathrm{S} - T_\gamma}{1+z}(1 - e^{-\tau_{\nu_0}}) \approx$$
$$27 x_\mathrm{HI}\left(1 - \frac{T_\gamma}{T_\mathrm{S}}\right)(1+\delta_\mathrm{nl})\left(\frac{H}{dv_r/dr + H}\right)\sqrt{\frac{1+z}{10}\frac{0.15}{\Omega_\mathrm{M}h^2}}\left(\frac{\Omega_b h^2}{0.023}\right)\mathrm{mK},$$

where T_S is the gas spin temperature, τ_{ν_0} is the optical depth at the 21cm frequency ν_0, $\delta_\mathrm{nl}(\mathbf{x}, z) \equiv \rho/\bar{\rho} - 1$ is the evolved (Eulerian) density contrast, $H(z)$ is the Hubble parameter, dv_r/dr is the comoving gradient of the line of sight component of the comoving velocity, and all quantities are evaluated

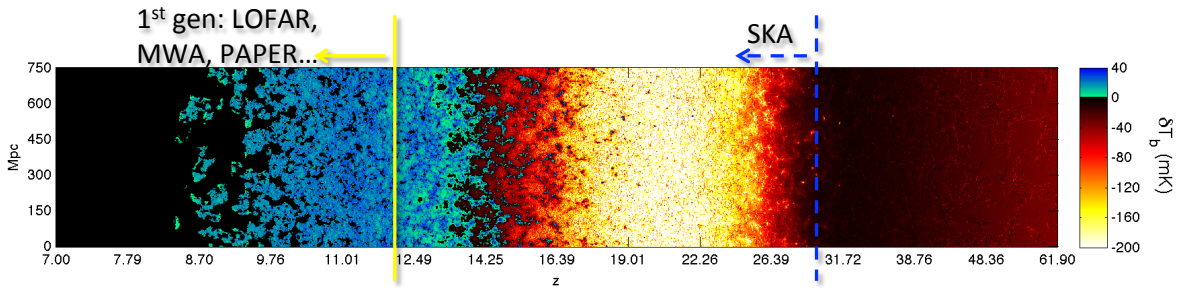

Figure 3.1. Slice through the 21cm brightness temperature field, computed with 21CMFAST. The horizontal axis shows evolution along the comoving line-of-sight coordinate, from $z \approx 62$ to $z \approx 7$. From right to left we see the expected major milestones in the signal: (i) collisional decoupling (*red→black*); (ii) WF coupling (*black→yellow*); (iii) IGM heating (*yellow→blue*); (iv) reionization (*blue→black*). The redshift limit accessible to SKA pathfinders roughly corresponds to the vertical yellow line; the SKA should probe out to roughly the vertical blue line ([20]). The slice is 750 Mpc in height and 1.5 Mpc (i.e. 1 cell) thick.

at redshift $z = \nu_0/\nu - 1$. The cosmological 21cm signal uses the CMB as a backlight: if $T_S < T_\gamma$, then the gas is seen in absorption, while if $T_S > T_\gamma$, the gas is seen in emission.

The 21cm signal is a line transition, which redshifts from the EoR into the FM band [for comparison, $\nu = 200$ (70) MHz corresponds to $z \approx 6$ (20)]. This means that each observed frequency corresponds to a redshift slice, making 21cm interferometry a powerful tomographical probe of the early Universe. From eq. (1) we can see that it is sensitive to both the thermal (T_S) and ionization (x_{HI}) evolution of the IGM, as well as fundamental cosmology (the last four terms of eq. 1). Bellow we elaborate on these epochs and the prospects for detection and interpretation of the corresponding 21cm signature. For more details, see the recent review in [20].

3.1.3 Epochs of the Cosmological 21cm Signal

The spin temperature, T_S, interpolates between the CMB temperature, T_γ, and the gas kinetic temperature, T_K. Since the observation uses the CMB as a backlight, a signal is only obtained if $T_S \to T_K$. This coupling is achieved through either: (i) collisions, which are effective in the IGM at high redshifts, $z \gtrsim 50$; or (ii) a Lyman alpha background [so-called Wouthuysen-Field (WF) coupling; [12; 32]], effective soon after the first sources turn on.

In Fig. 3.1, we show a slice through the δT_b field in a "fiducial" model (for more details, see [22]). It is immediately obvious that the 21cm signal is a physics-rich probe, encoding information on various processes during and before reionization. Although the exact timing of the cosmic epochs is uncertain, the relative order is robustly predicted (c.f. [13]; §2.1 in [19]):

1. **Collisional coupling**: The IGM is dense at high redshifts, so the spin temperature is uniformly collisionally coupled to the gas kinetic temperature, $T_K = T_S \lesssim T_\gamma$. Following thermal decoupling from the CMB ($z \lesssim 300$), the IGM cools adiabatically as $T_K \propto (1+z)^2$, faster than the CMB $T_\gamma \propto (1+z)$. Thus δT_b is negative. This epoch, serving as a *clean probe of the mater power spectrum* at $z \gtrsim 100$, is not shown in Fig. 3.1.
2. **Collisional decoupling**: The IGM becomes less dense as the Universe expands. The spin temperature starts to decouple from the kinetic temperature, and begins to approach the CMB temperature again, $T_K < T_S \lesssim T_\gamma$. Thus δT_b starts rising towards zero. Decoupling from T_K occurs as a function of the local gas density, with underdense regions decoupling first. Fluctuations are sourced by the density field, and again *offer a direct probe of cosmology*.

Eventually ($z \sim 25$), all of the IGM is decoupled and there is little or no signal. This epoch corresponds to the red→black transition on the right edge of Fig. 3.1.

3. **WF coupling (i.e. Lyα pumping)**: The first astrophysical sources turn on, and begin coupling T_S and T_K, this time through the Lyα background. δT_b becomes more negative, reaching values as low as $\delta T_b \sim$ 100–200 (depending on the offset of the WF coupling and X-ray heating epochs). This epoch, offering a window on the *very first stars in our Universe*, corresponds to the black→yellow transition in Fig. 3.1.
4. **IGM heating**: The IGM is heated, with the spin temperature now coupled to the gas temperature, $T_K = T_S$. As the gas temperature surpasses T_γ, the 21cm signal changes from absorption to emission, becoming insensitive to the actual value of T_S (see eq. 1). This epoch probes all processes which heat the IGM, *both astrophysical and cosmological*. The dominant source of heating is likely the X-rays from early accreting black holes (e.g. [13]); however in some models more exotic processes dominate, such as the evaporation of cosmic strings, or DM annihilation (e.g. [30]). This epoch (assuming X-ray dominated heating) corresponds to the yellow→blue transition in the panels of Fig. 3.1.
5. **Reionization**: as the abundance of *early galaxies* increases, the IGM gradually becomes ionized, a process which is inside-out on large scales. The tomography of this process is sensitive to the nature and clustering of the dominant UV sources (e.g. [18]). The cosmic 21cm signal decreases, approaching zero. This epoch corresponds to the blue→black transition in the panels of Fig. 3.1.

We see that the last three stages are sensitive to early astrophysical sources (and sinks) of cosmic radiation fields, while the first two (the Dark Ages) allow us to probe cosmology at redshifts much lower than recombination. Furthermore, if there is a substantial delay between two of the astrophysical epochs (such as would be the case if thermal feedback was efficient in turning off the first galaxies following IGM heating; [22]), then the matter power spectrum could be probed at lower, more accessible epochs than the Dark Ages.

SKA pathfinders, like the Low Frequency Array (LOFAR; [15])[1] and the Murchison Wide Field Array (MWA; [28])[2] are coming on-line, promising to measure the 21cm power spectrum during $7 \lesssim z \lesssim 12$. Given that the measurement of the Thompson scattering optical depth by the WMAP satelite ($\tau_e = 0.088 \pm 0.015$; [16]) places the mid-point of reionization at around $z \sim 10$, these first generation instruments have a strong chance of detecting the last half of reionization, at least statistically.

However, as can be seen in Fig. 3.1, this is just the tail end of the physical bounty encoded in the cosmic 21cm signal. *SKA is therefore invaluable!* With a frequency coverage of ~ 70–200 MHz, *SKA-low* would be able to cover not only the entire EoR, but likely also the epoch of IGM heating. If this coverage was extended down to $\nu \sim 50$ MHz as proposed by the European SKA science working group ([20]), we would be able to measure the radiation from the very first generations of galaxies (through WF coupling), as well as probe fundamental cosmology through: (i) the matter power spectrum between the astrophysical transitions outlined above (when $\bar{x}_{\rm HI} \approx 1$ and $T_S \approx T_K$); and (ii) the velocity offset between the baryons and DM which can imprint a delay and a large-scale baryon acoustic oscillation (BAO) feature in the Lyα and X-ray radiation fields (e.g. [19; 29]). Furthermore, the frequency resolution of SKA-low can be optimized for EoR tomography (~ 100 KHz), or increased to ~ 1 KHz to enable line studies and small-scale matter power spectrum measurements, as well as facilitating removal of radio frequency interference.

[1] http://www.lofar.org
[2] http://web.haystack.mit.edu/arrays/MWA/

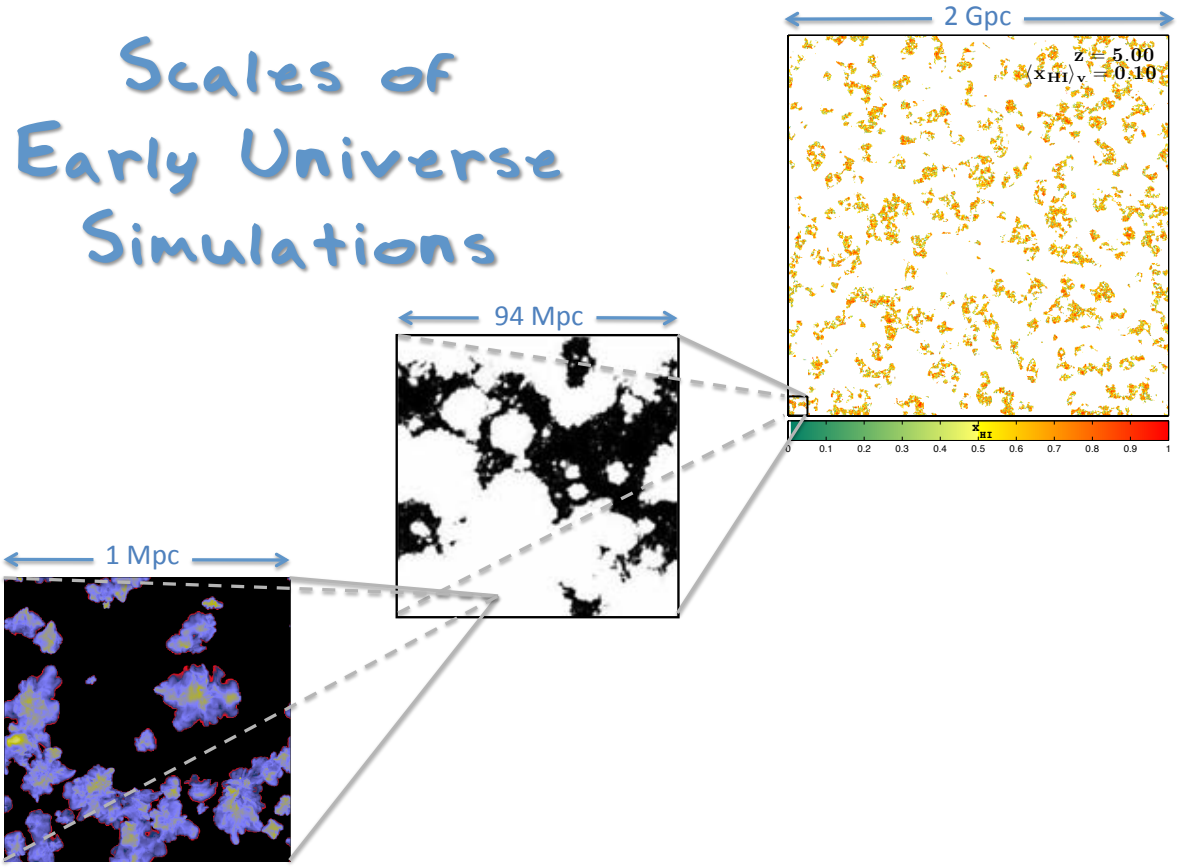

Figure 3.2. Scales of some early Universe simulations, with box sizes indicated in comoving units. Slices correspond to metallicity maps from [31], and ionization structure from [18] and [21], *left to right*. The left and middle panels roughly correspond to the current maximum box sizes of state-of-the-art numerical simulations of the first stars and the middle stages of reionization, respectively. This figure highlights the daunting dynamic range of cosmological processes such as reionization.

3.1.4 What can we learn from the observations?

As noted in the previous section, the cosmic 21cm signal is rich in physics and a powerful probe of the early Universe. However, extracting information from the observation is not straightforward. A fundamental question arises: *what can we learn from a given 21cm measurement?* Interpreting the observations is limited by our ability to model the impact of the early sources and sinks of radiation fields (X-ray, Lyα, and ionizing UV).

There has been exciting recent progress in simulating the first galaxies. However, putting these results in a cosmological context remains very difficult. There are two main challenges to overcome: (1) an extremely large parameter space, due to our poor understanding of the high-redshift Universe; (2) an enormous dynamic range (i.e. range of relevant scales; see Fig. 3.2). Theoretically, the early Universe could be modeled from first principles using numerical simulations. In practice, simulating reionization and other cosmological processes requires enormous simulation boxes. Gigaparsec scales are required to statistically model ionized regions, distributions of absorption systems, and highly-biased quasars. At the same time, the simulations require resolution high enough to resolve

the underlying stars and the complex small-scale feedback mechanisms which regulate them. Thus one is forced to make compromises: deciding which physical processes can be ignored, and how the others can be parameterized and efficiently folded-in to large-scale models.

In order to help surmount these difficulties, we developed a "semi-numerical" simulation, DexM ([23]; http://homepage.sns.it/mesinger/Sim). Our simulation uses approximate but efficient methods for generating 3D density, velocity, halo fields, ionization, UV radiation, spin temperature and cosmological 21cm fields. Recently, we also created 21cmFAST: an even faster, portable (with low memory requirements) version of DexM, which bypasses the halo finder, operating directly on the evolved density field; *a 3D realization of reionization is obtained in just a few minutes on a single CPU.* Thus we are able to account for the ionizing contribution of sources which are too small to be resolved by numerical simulations, at a mere fraction of the computing cost.

Each step of DexM and 21cmFAST has been tested against cosmological numeric simulations, and we find excellent agreement well into the quasi-linear regime [23; 24; 34]. *Both codes are publicly available, and will continue to be in future releases.* In just over two years since its launch, 21CMFAST is being used by research groups in eleven countries and is being implemented by most of the SKA pathfinders 21cm collaborations, including the LOFAR, the MWA, and the 21 Centimeter Array (21CMA).

Recently our semi-numeric algorithms gave birth to the exciting field of astrophysical parameter studies: using $\gtrsim 100$ realizations of the EoR, [33] and [25] recently interpreted the South Pole Telescope limits on the kinetic Sunyaev-Zel'dovich (kSZ) signal. Thanks to these parameter studies, in [25] we were able to conclude that either: (i) the early stages of reionization occurred in a much more homogeneous manner than suggested by fiducial, stellar-driven scenarios, such as would be the case if X-rays or exotic particles contributed significantly; and/or (ii) that there is a significant correlation between the cosmic infrared background and the thermal SZ. *Extensive parameter studies such as these will be required for any quantitative and robust interpretation of upcoming 21cm observations.*

3.1.5 Conclusions

The cosmological 21cm signal is very rich in information, containing both cosmological and astrophysical components. Pre-reionization epochs allow us to study processes which heat the IGM, as well measure as the matter power spectrum. Furthermore, astrophysical milestones such as reionization are the only practical way of observing the primordial zoo of astrophysical objects in the near future.

Although SKA pathfinders are an invaluable starting point (measuring the 21cm power spectrum during the latter stages of the EoR), *we need the SKA* in order to: (i) make certain we can detect even early reionization; (ii) facilitate tomography of the EoR; (iii) probe pre-reionization epochs of the first stars and black holes; (iv) probe cosmological signals. Given that the range of scales and unknown parameter space is enormous, we need efficient modeling tools (such as 21CMFAST) in order to robustly interpret observations.

3.2 Dark energy observational tests and the SKA perspective

S. Capozziello, M. De Laurentis, A. C. Ruggeri

3.2.1 Introduction

The increasing bulk of data that have been accumulated in the last fifteen years have pointed out the emergence of a new standard cosmological model usually referred to as the *concordance model*. The Hubble diagram of Type Ia Supernovae (SNeIa), measured by both the Supernova Cosmology

Project [35] and the High - z Team [36] up to redshift $z \sim 1$, was the first evidence that the universe is undergoing a phase of accelerated expansion. On the other hand, balloon born experiments, such as BOOMERanG [37] and MAXIMA [38], determined the location of the first and second peak in the anisotropy spectrum of cosmic microwave background radiation (CMBR) strongly pointing out that the geometry of the universe is spatially flat. If combined with constraints coming from galaxy clusters on the matter density parameter Ω_M, these data indicate that the universe is dominated by a non-clustered fluid with negative pressure, generically called *dark energy* (DE). Such a fluid should be able to drive the accelerated expansion. This picture has been further strengthened by the more precise measurements of the CMBR spectrum, due to the WMAP experiment [39], and by the extension of the SNeIa Hubble diagram to redshifts higher than 1 [40]. The simplest explanation is claiming for the well known cosmological constant Λ [41]. Although the best fit to most of the available astrophysical data, the ΛCDM model fails in explaining why the inferred value of Λ is so tiny (120 orders of magnitude lower) compared to the typical vacuum energy values predicted by particle physics and why its energy density is today comparable to the matter density (i.e. the *coincidence problem*). As a tentative solution, many authors have replaced the cosmological constant with a scalar field rolling down its potential and giving rise to the model referred to as *quintessence* [42]. Even if successful in fitting the data, the quintessence approach to DE is still plagued by the coincidence problem since the DE and matter densities evolve differently and reach comparable values for a very limited portion of the universe evolution coinciding at present era. In this case, the coincidence problem is replaced with a fine-tuning problem. Moreover, it is not clear where this scalar field originates from thus leaving a great uncertainty on the choice of the scalar field potential. The subtle and elusive nature of DE has led many authors to look for completely different scenarios able to give a quintessential behavior without the need of exotic components. So it could be possible to explain the accelerated expansion by introducing a single cosmic fluid with an equation of state causing it to act like dark matter (DM) at high densities and DE at low densities. An attractive feature of these models, usually referred to as *Unified Dark Energy* (UDE) or *Unified Dark Matter* (UDM) models, is that such an approach naturally solves, at least phenomenologically, the coincidence problem. The main ingredient of the approach is that a generalized equation of state can be always obtained and observational data can be fitted. Actually, there is still a different way to face the problem of cosmic acceleration. It is possible that the observed acceleration is not the manifestation of another ingredient in the cosmic pie, but rather the first signal of a breakdown of our understanding of the laws of gravitation. It is worth noting that these alternative schemes provide naturally a cosmological component with negative pressure whose origin is related to the geometry of the universe thus overcoming the problems linked to the physical meaning of the scalar field. This abundance of models is from one hand the signal of the fact that we have a limited number of cosmological tests to discriminate among rival theories, and, from the other hand, that a urgent degeneracy problem has to be faced. To this aim, it is useful to remember that both the SNeIa Hubble diagram and the angular size - redshift relation of compact radio sources [43; 44] are distance based methods to probe cosmological models so then systematic errors and biases could be iterated. From this point of view, it is interesting to look for tests based on time-dependent observables. For example, one can take into account the *lookback time* to distant objects since this quantity can discriminate among different cosmological models. The lookback time is observationally estimated as the difference between the present day age of the universe and the age of a given object at redshift z. Such an estimate is possible if the object is a galaxy observed in more than one photometric band since its color is determined by its age as a consequence of stellar evolution. It is thus possible to get an estimate of the galaxy age by measuring its magnitude in different bands and then using stellar evolutionary codes to choose the model that reproduces the observed colors at best. This paper is devoted to briefly review different classes of DE models discussing some methods

to constrain them. Far from being exhaustive and complete, our aim is to point out the degeneracy problem and the fact that we need further and self-consistent observational surveys at *all* redshifts to remove it. In particular, we face the possibility to use the SKA radio-telescope as a tool to investigate DE models.

3.2.2 Dark energy models

As a simple classification scheme, we may divide the different cosmological models in three wide classes. According to the models of the first class, the DE is a new ingredient of the cosmic Hubble flow, the simplest case being the ΛCDM scenario and its quintessential generalization which we will refer to as QCDM models. This is in sharp contrast with the assumption of UDE models (the second class) where there is a single fluid described by an equation of state comprehensive of all regimes of cosmic evolution [45; 46] which we will consider here referring to it as the *parametric density models* or generalized *EoS*[3] models. Finally, but it will not be discussed in detail, according to the third class models, accelerated expansion is the first evidence of a breakdown of the Einstein General Relativity (and thus of the Friedmann equations) which has to be considered as a particular case of more general theories of gravity. In the following, we will sketch DE approaches and derive some of the main quantities which we need for matching observations.

The ΛCDM model and its generalization toward quintessence (QCDM) models

Cosmological constant Λ has become a sort of textbook candidate to drive the accelerated expansion of spatially flat universe. Despite its *conceptual* problems, the ΛCDM model turns out to be the best fit to a combined analysis of completely different astrophysical data ranging from SNeIa to CMBR anisotropy spectrum and galaxy clustering. As a simple generalization, one may consider the QCDM scenario in which the barotropic factor $w \equiv p/\rho$ takes at a certain epoch a negative value with $w = -1$ corresponding to the standard cosmological constant. Testing whether such a barotropic factor deviates or not from -1 is one of the main issue of modern observational cosmology. How such a negative pressure fluid drives the cosmic acceleration may be easily understood by looking at the Friedmann equations:

$$H^2 \equiv \left(\frac{\dot{a}}{a}\right)^2 = \frac{8\pi G}{3}(\rho_M + \rho_Q)\,, \tag{3.2.1}$$

$$2\left(\frac{\ddot{a}}{a}\right) + H^2 = -8\pi G p_Q = -8\pi G w \rho_Q\,, \tag{3.2.2}$$

where the dot denotes differentiation with respect to cosmic time t, H is the Hubble parameter and the universe is assumed spatially flat as suggested by the position of the first peak in the CMBR anisotropy spectrum [37; 38].
Taking in account the continuity equation, $\dot{\rho} + 3H(\rho + p) = 0$, the SNeIa Hubble diagram, the large scale galaxy clustering and the CMBR anisotropy spectrum can all be fitted by the ΛCDM model and the universe turns out to be in an accelerated expansion phase. The simplicity of the model and its capability of fitting the most of the data are the reasons why the ΛCDM scenario is the leading candidate to explain the DE cosmology. Nonetheless, its generalization, QCDM models, i.e. mechanisms allowing the evolution of Λ from the past, are invoked to remove the Λ-problem and the *coincidence problem*.

[3] EoS for Equation of State.

Generalizing the EoS: the parametric density models

In the framework of UDE models, it has been proposed [46] a phenomenological class of models by introducing a single fluid[4] which can be written as a function of the redshift z:

$$\rho(z) = A_{norm}\left(1+\frac{1+z}{1+z_s}\right)^{\beta-\alpha}\left[1+\left(\frac{1+z}{1+z_b}\right)^{\alpha}\right] \tag{3.2.3}$$

having defined $z_s = 1/s - 1$ and $z_b = 1/b - 1$ (with $s < b$). It is easy to show that $\rho \propto a^{-\beta}$ for $a << s$, $\rho \propto a^{-\alpha}$ for $s << a << b$ and $\rho \propto const.$ for $a >> b$. By setting $(\alpha,\beta) = (3,4)$ the energy density smoothly interpolates from a radiation dominated phase to a matter dominated period finally approaching a de Sitter phase. The normalization constant A_{norm} may be estimated. The continuity equation may be recast in a form that allows to compute the pressure and the barotropic factor $w = p/\rho$, showing that it strongly depends on the scale factor (and hence on the redshift). Combining the Friedmann equations, the deceleration parameter $q = (1+3w)/2$ in the present day (namely at $a = 1$) we have:

$$q_0 = \frac{(y-1)\alpha + z_s[\alpha\, y - 2(1+y)] + (\beta-4)(1+y)}{2(2+z_s)(1+y)} \tag{3.2.4}$$

with $y = (1+z_b)^{-\alpha}$. It is convenient to solve Eq.(3.2.4) with respect to z_b in order to express this one as a function of q_0 and z_s. It is:

$$z_b = \left[\frac{\alpha(1+z_s)+\beta-(2+z_s)(2q_0+2)}{\alpha-\beta+(2+z_s)(2q_0+2)}\right]^{1/\alpha} - 1\,. \tag{3.2.5}$$

Such a parametric density model is fully characterized by five parameters which are chosen to be the two asymptotic slopes (α,β), the present day values of the deceleration parameter and of the Hubble constant (q_0, H_0) and the scaling redshift z_s. We will set $(\alpha,\beta) = (3,4)$ and $z_s = 3454$ so that (q_0, H_0) will be the two parameters to be constrained by the data. Any generalized EoS approach can be reduced to this scheme which is useful to fit the data. However, the phenomenological parameters, can often have a fundamental physics counterpart.

3.2.3 Methods to constrain models

Now, we will discuss how cosmological models can be constrained, in principle, using suitable distance and/or time indicators. As a general remark, solutions coming from cosmological models have to be matched with observations by using the redshift z as the natural time variable for the Hubble parameter, i.e.

$$H(z) = -\frac{\dot{z}}{z+1}\,. \tag{3.2.6}$$

Interesting ranges for z are: $100 < z < 1000$ for early universe (CMBR data), $10 < z < 100$ (LSS), $0 < z < 10$ (SNeIa, radio-galaxies, etc.). The method consists in building up a reasonable patchwork of data coming from different epochs and then matching them with the same cosmological solution ranging, in principle, from inflation to present accelerated era. In order to constrain the parameters characterizing the cosmological solution, a reasonable approach is to maximize the following likelihood function :

$$\mathcal{L} \propto \exp\left[-\frac{\chi^2(\mathbf{p})}{2}\right] \tag{3.2.7}$$

[4]It is worth stressing that this model may be interpreted not only as comprising a single fluid with an exotic equation of state, but also as made of DM and scalar field DE or in the framework of modified Friedmann equations. For pedagogical reasons, we prefer the UDE interpretation even if the results do not depend on this assumption.

where $\mathbf{p}$ are the parameters characterizing the cosmological solution. The χ^2 merit function can be defined as :

$$\chi^2(\mathbf{p}) = \sum_{i=1}^{N} \left[\frac{y^{th}(z_i, \mathbf{p}) - y_i^{obs}}{\sigma_i} \right]^2 + \left[\frac{\mathcal{R}(\mathbf{p}) - 1.716}{0.062} \right]^2 + \left[\frac{\mathcal{A}(\mathbf{p}) - 0.469}{0.017} \right]^2 . \tag{3.2.8}$$

Terms entering Eq.(3.2.8) can be characterized as follows. For example, the dimensionless coordinate distances y to objects at redshifts z are considered in the first term. They are defined as :

$$y(z) = \int_0^z \frac{dz'}{E(z')} \tag{3.2.9}$$

where $E(z) = H(z)/H_0$ is the normalized Hubble parameter. This is the main quantity which allows to compare the theoretical results with data. The function y is related to the luminosity distance $D_L = (1+z)r(z)$. A sample of data on $y(z)$ for the 157 SNeIa is discussed in the Riess et al. [40] Gold dataset and 20 radio-galaxies are in Daly & Djorgovski [47]. The second term in Eq.(3.2.8) allows to extend the z-range to probe $y(z)$ up to the last scattering surface ($z \geq 1000$). The *shift parameter* [48; 49] $\mathcal{R} \equiv \sqrt{\Omega_M} y(z_{ls})$ can be determined from the CMBR anisotropy spectrum, where z_{ls} is the redshift of the last scattering surface which can be approximated as $z_{ls} = 1048\left(1 + 0.00124\omega_b^{-0.738}\right)\left(1 + g_1\omega_M^{g_2}\right)$ with $\omega_i = \Omega_i h^2$ (with $i = b, M$ for baryons and total matter respectively) and (g_1, g_2) given in Hu & Sugiyama [50]. The parameter ω_b is constrained by the baryogenesis calculations contrasted to the observed abundances of primordial elements. The third term in the function χ^2 takes into account the *acoustic peak* of the large scale correlation function at $100h^{-1}$ Mpc separation, detected by using 46748 luminous red galaxies (LRG) selected from the SDSS Main Sample [51; 52]. The parameter $\mathcal{A}$ depends on the dimensionless coordinate distance (and thus on the integrated expansion rate), on Ω_M and $E(z)$. This dependence removes some of the intrinsic degeneracies in distance fitting methods. Due to this reason, it is particularly interesting to include $\mathcal{A}$ as a further constraint on the model parameters using its measured value $\mathcal{A} = 0.469 \pm 0.017$ [51]. With the definition (3.2.7) of the likelihood function, the best fit model parameters are those that maximize $\mathcal{L}(\mathbf{p})$.

Using the method sketched above, the classes of models studied here can be constrained and selected by observations. However, most of the tests recently used to constrain cosmological parameters (such as the SNeIa Hubble diagram and the angular size - redshift) are essentially distance - based methods. The proposal of Dalal et al. [53] to use the lookback time to high redshift objects is thus particularly interesting since it relies on a completely different observable. The lookback time is defined as the difference between the present day age of the universe and its age at redshift z and may be computed as :

$$t_L(z, \mathbf{p}) = t_H \int_0^z \frac{dz'}{(1+z')E(z', \mathbf{p})} \tag{3.2.10}$$

where $t_H = 1/H_0 = 9.78h^{-1}$ Gyr is the Hubble time (with h the Hubble constant in units of 100 km s^{-1} Mpc^{-1}), and, as above, $E(z, \mathbf{p}) = H(z)/H_0$ is the dimensionless Hubble parameter and $\mathbf{p}$ the set of parameters characterizing the cosmological model. It is worth noting that, by definition, the lookback time is not sensible to the present day age of the universe t_0 so that it is (at least in principle) possible that a model fits well the data on the lookback time, but nonetheless it predicts a completely wrong value for t_0. This latter parameter can be evaluated from Eq.(3.2.10) by simply changing the upper integration limit from z to infinity. This shows that it is indeed a different quantity since it depends on the full evolution of the universe and not only on how the universe evolves from the redshift z to now. That is why this quantity can be explicitly introduced as a further constraint. In particular, taking into account the above procedures for distance and time measurements, one can reasonably constrain a given cosmological model. In any case, the main and obvious issue is to have at disposal sufficient and good quality data sets.

3.2.4 Discussion and the SKA perspective

Many rival theories have been proposed to solve the puzzle of DE ranging from a rolling scalar field to a unified picture where a single exotic fluid accounts for the whole dark sector (DM and DE). Moreover, modifications of the gravity action has also been advocated. The most widely used cosmological tests and, in particular the SNeIa Hubble diagram and the angular size - redshift relation, are essentially based on distance measurements to high redshift objects and are thus affected by similar systematic errors. Being affected by other kinds of observational problems, such methods could be considered as cross checks for the results obtained by the usual tests and they should represent complementary probes for cosmological models. The present age of the universe and the lookback time to some astrophysical source (e.g. galaxy clusters) can be used to build up a sort of *time diagram* of the universe in order to reconstruct its age evolution. Relying on stellar evolutionary codes, the estimate of the lookback time is related to a different astrophysics than the distance based methods and it is thus free from any problem connected with the evolution of standard candles (such as the SNeIa absolute magnitude and the intrinsic linear size of radio sources). Actually, this technique could be affected by its own systematics (such as, for instance, the degeneracy between age and metallicity), but comparing the results already obtained with those coming from distance based methods allows to strengthen the conclusions suggested by both techniques. In this way, we can obtain reliable values of cosmographic parameters. This can be considered an independent confirmation not only of the viability of the ΛCDM model, but also of the method. It is worth noticing that the ΛCDM scenario receives further support from this test and henceforth the cosmological constant Λ still remains the best candidate to explain the DE puzzle from an observational point of view. Nonetheless, the ΛCDM model is severely affected by conceptual problems so that it is worthwhile to look at alternative approaches, like considering models with dominant scalar field rolling down its potential. However, such a scheme does not still solve the coincidence problem and is plagued by the unidentified nature of the scalar field itself and the ignorance of its self-interaction potential. In Cardone et al. [45] and Capozziello et al. [46], phenomenological unified models have been proposed where a single fluid with a given energy density assigned by few parameters is able to fit both the SNeIa Hubble diagram and the angular size - redshift relation for ultracompact radio sources. Another possible approach to the cosmic acceleration is to consider DE and DM as signals of the breakdown of the Einstein General Relativity at some characteristic scale [54]. In this picture, the universe is still dominated by standard matter, but the Friedmann equations have to be modified as consequence of a different gravity action. This philosophy inspired curvature quintessence scenarios where an effective DE is related to the properties of the function $f(R)$ which replaces the Ricci scalar R in the gravity Lagrangian [55–57]. Having dealt with three different classes of models, it is worth asking what is the better one. Unfortunately, up to now, this is not possible on the basis of test results only. We have thus to conclude that this test alone is not able to discriminate among dark energy candidates. On the other hand, Sandvik et al. [58] claimed that UDE models are not viable because the growth of density perturbations will lead to matter power spectrum in disagreement with what is observed. This should be an evidence against the parametric density model. However, it is worth noting that Sandvik et al. explicitly consider the generalized Chaplygin gas model [59] which is characterized by a negative squared sound speed that seems to be the main cause of the anomalous growth of perturbations. This is in opposition to the parametric density model in which the speed is defined positive and so that argument should be at least reconsidered. In any case, from one hand we need some *"experimentum crucis"* capable of removing the degeneracy for a reasonably large redshift range and, from the theoretical viewpoint, we need a physically reliable cosmological model, emerging from some fundamental theory, without the conceptual shortcomings of ΛCDM. The Square Kilometer Array (SKA) radio-interferometer could result extremely important as a tool to remove the degeneracy of models

Dewdney et al. [60]. In fact, SKA radio data could contribute to define the energy spectrum of different sources and then contribute to the main shortcoming of today observational cosmology: defining standard candles or distance indicators capable of mapping large ranges of redshift. To detect furthest sources, namely high - z ones, it is necessary a huge sensitivity and SKA will have a sensitivity 50 times larger than the best current-day telescopes. Taking in account also the angular resolution, it will investigate in detail also the low and medium-z sources contributing to discriminate models at low and medium redshift. This approach could be extended to high-energy sources. Concerning this point, we believe it is important to investigate radio tails also for extremely energetic sources like gamma ray bursts in order to improve the Spectrum Energy Distributions (SEDs). In this way, the Hubble flow for DE models could result extremely ameliorated. It is worth stressing that widening the SEDs enables a good understanding about emission mechanisms, so entering into detail of source different zones. Furthermore, a program of proper motion studies of galaxies will provide a precise measurement of the local Hubble constant, H_0, as suggested by Torchinsky et al. [61]. Besides, the spectroscopic capabilities in ultra-wide fields of view allow SKA to make a billion galaxy redshift survey out to $z = 2$. Such an *all-sky survey* could be used to detect Baryonic Acoustic Oscillations in the galaxy distribution, leading directly to a fine measure of the EoS parameter w. Finally, SKA has a great advantage with respect to optical telescopes: it can simultaneously measure the sky positions and the redshifts by detecting the neutral hydrogen with 1.4 GHz emission. This fact eliminates the systematic errors which limit the optical surveys. Due to these reasons, SKA could be a formidable tool to discriminate among different DE models.

3.3 Probing the matter power spectrum at small scales

M. Viel

3.3.1 The importance of small scales

Measuring the clustering of matter at small scales is a primary scientific goal of present day cosmology. There are several scientific topics that highlight the importance of characterizing the properties of clustering in a non-linear and possibly high-redshift regime that will be probed by the SKA telescope.

First of all non-linearities develop differently in different cosmological models and constraining their behaviour both in redshift and in wavenumber (or real) space can allow to understand the relative importance between the clustering of matter inside and outside haloes, the coupling of long and short wavelengths modes, These goals are usually accomplished by comparing data with N-body/hydrodynamic results or with perturbation theories and halo models [62].

Secondly, the standard ΛCDM model which is based on a mixture of cold dark matter and a cosmological constant (or dark energy), has been found to have problems in the small scale regime: these tensions could be alleviated (or possibly solved) if the standard paradigm of structure formation is modified (for example using two dark matter components or a warm dark matter fluid [63]), or alternatively by modifying the distribution of baryons with some form of galactic feedback [64].

Finally, the intermediate and small-scale behaviour of matter is not fixed by Cosmic Microwave Background (CMB) experiments and measurements like the matter power spectrum r.m.s. amplitude at the scale of 8 Mpc/h (σ_8) rely on extrapolation of CMB data that must confront observations at those scales. The sinergy between small scale and large scale observable can allow to probe the long lever-arm of the the matter power with observables that sample different redshifts and are subject to different systematic errors, thus limiting significantly their importance. Probing small scales can thereby allow to disproof or confirm the model of structure formation or constraining the curvature by measuring the running spectral index and/or the neutrino mass fraction [65].

SKA will have a very high angular resolution (subarsecs) which will make possible to probe matter clustering down to scales that can be around few kpc (in physical units). When combined with its frequency resolution a tomographic study of matter clustering either via 21 cm brightness temperature power spectra or by using HI galaxies down to small scales and up to high redshifts in an unprobed regime could be made.

Among the different scientific questions, I will focus here on two specific topics: the impact that cosmological massive neutrinos and warm dark matter have on the matter power spectrum. In this field there is some expertise in the Italian Community both on the theoretical side, the modelling of non-linearities using analytical or numerical tools, and on the observational one, using large scale structure data in order to constrain cosmological parameters.

3.3.2 Cosmological Massive Neutrinos

The impact that massive neutrinos have in terms of non-linear matter power spectrum is shown in the left panel of Figure 3.3 by means of a full hydro-dynamic N-body simulation that follow the relevant physical processes for the cold dark matter component, for the baryons (e.g. star formation and gas cooling) and for the clustering properties of the neutrino fluid. The simulation also follows independently the neutral hydrogen content of any SPH particle within the cosmological volume, assumed to be in photoionization equilibrium with an Ultra-Violet background made by quasars and galaxies. These results have been obtained from a modification of the code GADGET-III that incorporate neutrino particles as a separate component [66]. From the Figure it is clear that the impact that massive neutrinos have in terms of matter power spectrum is both redshift and scale dependent and has distinctive signatures even at very small scales. Unveiling this effect is difficult, since we do not have access at the matter power spectrum but we use tracers of it: either galaxies, weak lensing shear power spectra, the 21cm brightness temperature or the Lyman$-\alpha$ forest. Most of the modelling is indeed devoted to exploiting the intimate relation between the matter power spectrum and these tracers: for example semi-anaylitical methods have been developed in order to model the sub-grid physics and galaxy properties; radiative transfer and astrophysical parameters are also important in order to predict the 21 cm temperature brightness signal; the Lyman$-\alpha$ forest simulations require to specify a thermal state for the Intergalactic Medium, etc. The present constraints on the total mass of neutrinos from cosmological data are around 0.3 eV (2σ upper limit) and are derived from a combination of CMB data and galaxy clustering (2dF, SDSS, CFHTLS, VIPERS data – see e.g. [82]). The recent constraints from CMB data in combination with BAO and SNe also points to a value around 0.3 eV, while there is an internal tension between the CMB Planck temperature data and lensing signal that relaxes the limit above to 0.83 eV [65]. It is thereby mandatory in order to detect the neutrino mass using cosmological data to reach an unprecedented precision in the modelling of the non-linear power spectrum at high redshift and small scales using as many observables as possible. Euclid constraints will also be very competitive in this respect but it is possible that they cannot discriminate between the two hierarchies (normal and inverted), when systematic effecst will be taken into account [68].

3.3.3 Warm or Cold Dark Matter?

The possibility of alleviating some small-scales discrepancies of the ΛCDM model by considering warm dark matter has been investigated in the past using different observables: the abundances of haloes or sub-haloes, weak lensing shear power spectra, the Lyman-α forest flux power spectrum. In the right panel of Figure 3.3 we show the ratio of the non-linear matter power spectrum for 3 WDM models that have different mass for a thermal relic. These results are taken from the simulations described in [70]. Each of these masses correspond to a different free-streaming length and to a different onset of the suppression of the WDM model w.r.t. the corresponding ΛCDM model. These

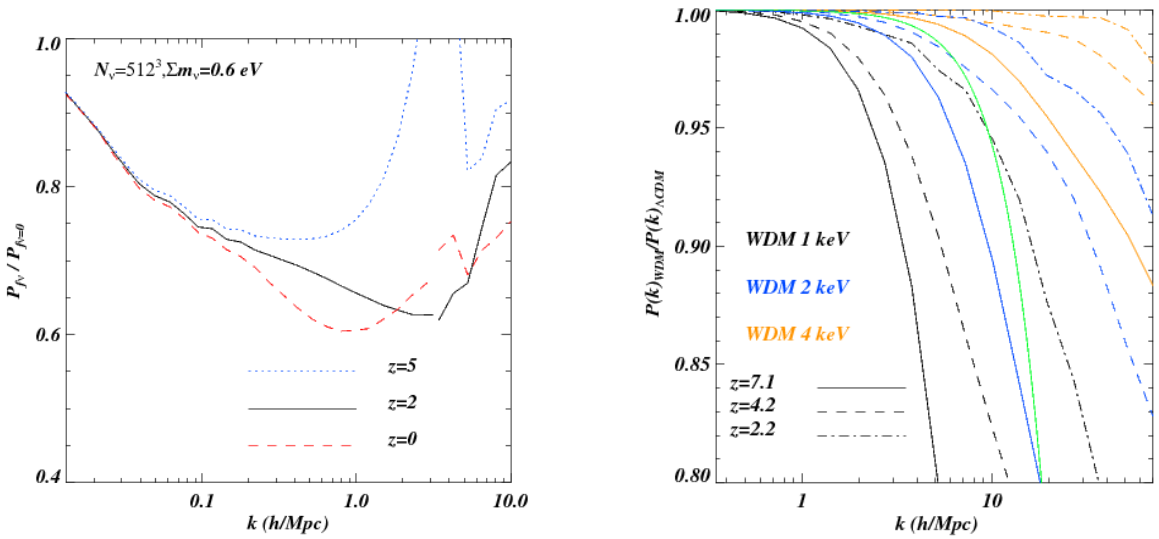

Figure 3.3. In the left panel we show the ratio of the non-linear matter power between a model in which neutrinos are massive with a mass $\Sigma m_\nu = 0.6$ eV and a model for which neutrinos are massles ($f_{\rm nu} = 0$). The models refer to three different redshift: $z = 0, 2, 5$, represented by the red dashed, black continouos and blue dotted curves, respectively. In the right panel we show the ratio of the non-linear matter power spectrum between WDM models of three different masses for a thermal relic (1 keV, 2 keV and 4 keV, shown as black, blue and orange curves respectively) at 3 different redshifts: $z = 2.2, 4.2, 7.1$ represented by the dot-dashed, dashed and continuous curves, respectively. The green thick curve in the right panel shows the linear suppression for a $m_{\rm WDM} = 4$ keV candidate, which is not ruled out by present data, but could be ruled out by SKA. In both panels it is clear the strong redshift and wavenumber dependence of the different models and the need to go beyond linear theory which stops at scales $k < 0.15\,h$/Mpc. The power spectrum has been computed in both cases by using Counts-In-Cells (CIC) interpolation on a mesh of 512^3 grid points.

models correspond to 50% suppression of power in the linear (redshift independent) matter power spectrum at scales $k = 6.9, 14.7, 32h$/Mpc, for $m_{\rm WDM} = 1, 2, 4$ keV, respectively. However, the non-linear signature is clearly redshift and scale dependent and shows that at high redshift is close to the linear behaviour and thereby more prominent. The suppression in the non-linear matter power could be probed in two different ways: by using the small scale clustering properties of HI selected galaxies and carefully assessing the relative importance of substructure at small scales in a WDM model; by using the 21 cm signal in the form of brightness temperature power spectrum and relying on a modelling of the relation between the two power spectra with a bias function that should be calibrated with hydrodynamic simulations $P_{\rm matter}(k, z) = b(k, z) \times P_{T_b}(k, z)$ Present day limits on $m_{\rm WDM}$ are around 1-2 keV (2σ lower limits) using either weak lensing or Lyman-α forest data: in the latter case the smallest scales probed is around 0.5 comoving Mpc/h ([71]). If SKA could constrain the matter power spectrum down to kpc scale it is envisaged that these limits could be improved by a factor ten, provided a proper knowledge of the astrophysical and modelling errors is done at these scales (see also [72]).

3.4 Cosmological Constraints from the Large Scale Structure

E. Branchini, L. Guzzo, M. Magliocchetti, G. de Zotti

Extragalactic radio sources have specific advantages as tracers of the density field and thus as clustering probes on the largest scales. One general advantage is that the radio selection is unaffected by

Galactic dust extinction, which in optically-selected catalogues may introduce spurious large-scale angular gradients due to its inhomogeneous distribution. In cosmological terms, this implies also the possibility to build all-sky catalogues that push much more into low galactic latitudes, which is a significant advantage for studies of large-scale cosmological dipoles (see e.g. [73–75]). Other cosmological advantages are more specific to each of the two kind of radio surveys one is considering (radio continuum or HI - 21 cm emission), which we shall be discussing in the following. The Square Kilometer Array has the potential to revolutionize cosmological studies using radio surveys of both kinds.

3.4.1 Radio Continuum Surveys

Due to their strong cosmological evolution, related to the evolution of Active Galactic Nuclei, radio sources identified in available all-sky radio surveys (down to a flux limit of $\sim$ 1 mJy), through their non-thermal continuum (synchrotron emission), are rare locally. This makes such surveys free from the profusion of local faint objects that dominate optically-selected galaxy samples. Hence the effect of large-scale structures at cosmological distances is detectable in the radio not only in the spatial but also in the angular correlation function, $w(\theta)$, not being strongly diluted by the projection of foreground sources.

The NRAO VLA Sky Survey at 1.4 GHz (NVSS; [76]) has provided us with the most extensive sky coverage available to date (82% of the sky to a completeness limit of about 3 mJy), with sufficient statistics to allow a determination of $w(\theta)$ on scales of up to several degrees [77; 78] has faced us with a puzzling result: the angular correlation function $w(\theta)$ is found to be positive up to very large ($\sim 10^\circ$) angular scales, which, for the median source redshift ($z_{\rm m} \simeq 1$), correspond to linear scales where the correlation function should be negative (see also the discussion in [79]). The excess large scale power is very difficult to account for in the framework of the standard hierarchical clustering scenario with Gaussian primordial perturbations. Proposed interpretations advocate either an evolution of the bias factor radically different from that found for optical QSOs [80; 81], in stark contrast with the similar evolution of the luminosity function, or a substantial non-Gaussian tail in the distribution of primordial perturbations [82]. Either possibility would have far-reaching implications, but first of all it is necessary to ascertain the reality of the excess large scale power, against the possibility that it comes from unexpected systematics. Deeper forthcoming all-sky surveys, like e.g. the EMU survey planned with ASKAP, will provide an assessment of the angular correlation function up to very large scales with a much better statistics and can also be exploited to compare the mapping of large scale structure provided by radio loud AGNs, that dominate above $S_{1.4\rm GHz} \simeq 0.5-1$ mJy, with that provided by star-forming galaxies and radio-quiet AGN that dominate below $S_{1.4\rm GHz} \simeq 0.05-0.1$ mJy (for more details on the nature of sub-mJy radio sources we refer to Sect. 4.2).

Other probes can be used to set constraints on cosmological models and parameters, in addition to the angular autocorrelation function, $w(\theta)$: the integrated Sachs-Wolfe effect (see Sect. 3.6.4) and two gravitational lensing effects known as cosmic magnification and shear [83; 84]. Here we just stress that the combined use of these probes greatly improves cosmological constraints, especially if complementary information from the 3D distribution of galaxies with measured HI 21 cm line is also available, as discussed in the next Section. Examples of such combined analysis of existing datasets already demonstrates the power of this multi-probe approach (see e.g. [85]).

3.4.2 HI 21 cm Redshift Surveys

It is when we come to 21 cm emission, however, that radio surveys, and SKA in particular, can have the most fundamental impact on our understanding of the cosmological model, providing a mean to

reconstruct the three-dimensional distribution of galaxies through massive redshift surveys.

The past three decades have seen galaxy redshift surveys emerge as one of the prime experimental means to test cosmology and the nature of galaxies. Measurements of large-scale galaxy clustering from these samples can directly test the values of the cosmological parameters regulating the formation and evolution of our Universe; on small scales, instead, they can probe the astrophysical properties of the sources producing the clustering signal, providing direct clues into the relationships between dark and baryonic matter. The largest redshift surveys over these years have been and are being performed using optical telescopes: 2dFGRS, SDSS, WiggleZ, BOSS, VIPERS [86–90] to mention the largest ones.

Radio observations in HI allow us to do this in an alternative and very effective way, easily pushing (with instruments like SKA) into the distant Universe. HI surveys provide in fact not only object detection, but also an estimate of its mass in neutral hydrogen and, most importantly, of the redshift of the galaxy. Once HI emission has been identified on the sky in a specific location, the observed wavelength of the 21 cm line provides the redshift of the corresponding galaxy and therefore an estimate of its distance. An extended blind HI survey of large areas of the sky is therefore fully complementary to the traditional spectroscopic redshift surveys to reconstruct the large-scale distribution of galaxies performed with optical telescopes. This technique has been pioneered with the Arecibo radio telescope, by the 21 cm surveys of Giovanelli & Haynes [91], who in the 1980's constructed what at the time was one of the largest existing surveys of galaxy redshifts, in the region dominated by the Perseus-Pisces supercluster.

Until recently, 21 cm surveys have seen only moderate improvement, with the main advances related to using the Parkes observatory and the refurbished Arecibo radio telescope to complete the HIPASS ($z_{med} \sim 0.01$) and the Alfalfa ($z_{med} \sim 0.026$) surveys consisting respectively of about 5,000 and 40,000 21 cm line measurements up to $z \sim 0.05$ [92; 93]. SKA promises to represent a quantum leap in this field, potentially leading to a half-sky survey of $\sim 3\,10^4$ galaxies per deg^2, totaling to $\sim 10^9$ objects down to $z \sim 1.5$ [94]. These are figures comparable or larger to those expected from the planned redshift survey of Euclid, the ESA cosmology mission due to launch in 2020 [95]. Euclid is expected to measure redshifts for $\sim 5 \times 10^7$ star-forming galaxies with $0.7 < z < 2.1$, using an optical slitless spectrograph. An SKA 21 cm redshift survey over $0 < z < 1.5$ would immediately represent a formidable complementary sample, with significant overlap in area and redshift and comparable or higher density, providing unique synergy and cross-check opportunities for both Euclid and SKA surveys.

The main cosmological driver of these redshift surveys is, in general, the measurement of the spatial clustering of galaxies, with the aim of extracting the crucial information contained in the amplitude, shape and spatial anisotropy of the galaxy power spectrum $P(k)$ (or its Fourier transform, the two-point correlation function). The shape of the power spectrum contains direct information on the overall mean density parameter of matter (dark plus baryonic), Ω_m. More in detail, the tiny wiggles in its shape produced by *Baryonic Acoustic Oscillations* in the pre-recombination photon-baryon plasma directly measure the baryon fraction. At the same time they provide a fundamental tool to probe the expansion history of the Universe. When transformed into real space, these waves in the power spectrum correspond to a well-defined spatial scale, imprinted into the large-scale distribution of galaxies at a physical separation that can be predicted from basic physics. This scale has been observed in redshift surveys around $\sim$ 110 h^{-1} Mpc, in comoving units, and provides us with a *standard ruler*, through which the angular diameter distance D_A and the Hubble parameter $H(z)$ can be obtained by matching its predicted and observed values. An all hempishere, SKA survey of 10^9 galaxies down to redshifts $z > 1$ can estimate the BAO scale with percent precision (e.g. [96]) within each of the $\sim$ 10 redshift bins of depth $\Delta z = 0.1$. Such measurements would be able constrain the

evolution of the equation of state of dark energy to a level comparable to Euclid (see [95]), but using a complementary data set with a very different selection function.

In addition to the power spectrum amplitude and shape, a fundamental source of cosmological information provided by a redshift survey is the *anisotropy* of the observed clustering, i.e. in the level of distortion introduced on the reconstructed distribution by angle-dependent phenomena. This is the case of the *redshit-space distortions* (RSD) generated on the observed galaxy maps and measured clustering statistics by the contribution of galaxy peculiar velocities to the measured redshift. The observed distortion on large scales is a measurement of the growth rate of structure, which is closely related to both the nature of dark energy and that of gravity. As suggested not long ago [97], measurements of RSD on cosmological scales represent one of the most promising probes for future redshift surveys, to understand the origin of cosmic acceleration. In particular, the measured growth rate can tell us whether dark energy or a modification of the laws of gravity are the most probable solutions.

21 cm -selected redshift surveys present specific advantages for measuring RSD. First, the magnitude of the distortion effect is inversely proportional to *galaxy bias b*. HI-selected galaxies are low bias objects, as HI emission traces neutral gas that is missing in high-bias objects like early-type galaxies that typically populate galaxy clusters. As such, for a given value of the growth rate the distortions signal is maximized using objects like HI-selected galaxies characterized by a low value of the bias parameter b [98; 99].

There is a second important advantage in using HI selected objects to trace redshift distortions. One of the current problems in estimating the growth rate, which depends on the large-scale linear component of the velocity field, from the observed RSD signal is how to properly model non-linear effects. By avoiding rich galaxy clusters, HI-selected sources minimize the impact of nonlinear effects and reduce the chance of systematic errors [100]. SKA measurements, therefore, should be intrinsically easier to model, and thus less affected by potential systematic effects that, at the moment, are known to plague simple estimators of redshift-space distortions.

In statistical terms, it is fairly straightforward to estimate the expected precision reachable on the growth rate measured within $\Delta z = 0.1$ bins by a half-sky SKA survey of of $\sim 10^9$ galaxies with $z_{MAX} > 1$. Again, one can forecast precision of 1-2 % in each redshift bin, with comparable errors on the growth index describing gravitational growth [100]. If one restricts to the framework of General Relativity, the combination of BAO and RSD measurements could bring precision on the evolution of the equation of state of dark energy $w(a) = w_0 + w_1(1 - a)$, where $a = 1/(1 + z)$, below 1% for w_0 and below 5% for w_1 [**?**].

Finally, although here we have focused on the full SKA, most of these considerations also apply to SKA pathfinders. The accuracy in the BAO and RSD measurements obtained with instruments like ASKAP and MeerKAT will parallel that obtained with ongoing optical surveys, like BOSS, that, in turn, can be regarded as Euclid pathfinders.

3.4.3 SKA Deep Fields

Clustering studies performed over deeper, limited-area radio–continuum surveys planned with SKA and SKA precursors (deep fields) will nicely complement those from the main all-sky surveys. The multi-wavelength coverage and the high resolution of the observations in such fields will in fact allow to distinguish up to the highest redshifts between star-forming sources and those mainly powered by an AGN. Clustering studies for these objects will then investigate the relationship between the large-scale structure traced by star-forming galaxies on the one hand and AGN of different type (e.g. FRI, FRII and most importantly radio-quiet AGN, see Sect 4.2) on the other, allowing to infer some of the properties of the galaxies which host these sources such as their dark matter content. This kind of analysis could for instance allow to discriminate amongst different formation and evolution scenarios

for different types of AGN. The inclusion of data-sets at different wavelengths will also permit to establish links between the dark matter content in galaxies and their star-forming activity and/or AGN power.

Even more interesting is the science that will be possible to carry out with SKA deep (redshifted) HI line surveys of selected fields. In fact, in this case, the evolution of the large-scale structure as traced by star-forming objects will be tracked directly as a function of cosmic ages beyond $z >> 2-3$. This will enable to study with unprecedented accuracy the time evolution of the relationship between the large-scale structure as traced by star-forming galaxies and the physical properties which shape these objects such as their star formation rate, metallicity or presence and relative importance of an AGN component. One of the main aim of this analysis will also be to state when, where and which processes gave way to the observational segregation phenomena which in the $z \lesssim 1$ Universe place star-forming galaxies in under-dense environments, while studies at different wavelengths find star-forming objects at higher redshifts to be hosted in much more densely populated fields (e.g. [101]).

In fact, the enormous number of sources detected in SKA HI surveys (both all-sky and deep fields) will allow clustering analysis on well-defined galaxy samples which cover the same range of physical parameters at different redshifts, therefore beating the various biases introduced by flux or magnitude limited surveys in smaller galaxy samples. The results can then be straightfowardly compared to those obtained with local samples such as the abovementioned HIPASS [92]), in order to provide the full assembly history of star-forming galaxies within their dark matter haloes from the local universe up to when this was just about 1 Gyr old.

3.5 Cosmology with Gamma–Ray Bursts: status, perspectives and SKA contribution

L. Amati, M. De Laurentis, M. Della Valle

Due to their huge energetic outputs, up to more than $\sim 10^{54}$ erg in terms of isotropic equivalent radiated energies, which are released in a few tens or hundreds of seconds , GRBs are the brightest cosmological sources in the Universe [see, e.g., 102–105, for reviews on the GRB phenomenon]. Therefore, they have been observed up to $z \sim 8-9$ [106; 107], well beyond the observing redshift range of SNe–Ia, limited to $z \sim 1.5$ [108]. In addition, GRBs emit most of their radiation as hard X–rays, thus they are marginally affected by uncertainties connected with correction for reddening. Unfortunately, GRB span not less than 6 orders of magnitude in terms of energy, therefore they cannot be used straightforwardly as standard candles. However, in recent years it has been shown [e.g., 109; 110] that the strong correlation between the photon energy at which the νF_ν spectrum peaks and the GRB radiated energy or luminosity ["Amati relation"; 111; 112] can be successfully used to measure cosmological parameters.

3.5.1 The $E_{p,i}$–intensity correlation in GRBs

The spectrum of GRBs is non thermal and can be empirically described by the so–called Band function, i.e., a smoothly broken power–law characterized by three parameters: the low–energy spectral index α, the high energy spectral index β and the "roll–over" energy E_0 [113]. After converting into νF_ν , i.e., the distribution of the emitted energy as a function of photon energy, the spectrum shows a peak; the photon energy at which this peak occurs is a characteristic quantity in GRB emission models and is called "peak energy", E_p . Every GRB for which it is possible to measure the redshift can be characterized by two key intrinsic properties: the total radiated energy (computed by integrating the spectrum in a standard 1–10000 keV energy band and assuming isotropic emission, E_{iso}) and the peak energy of the cosmological rest–frame νF_ν spectra of GRBs ($E_{p,i} = E_p \times (1 + z)$).

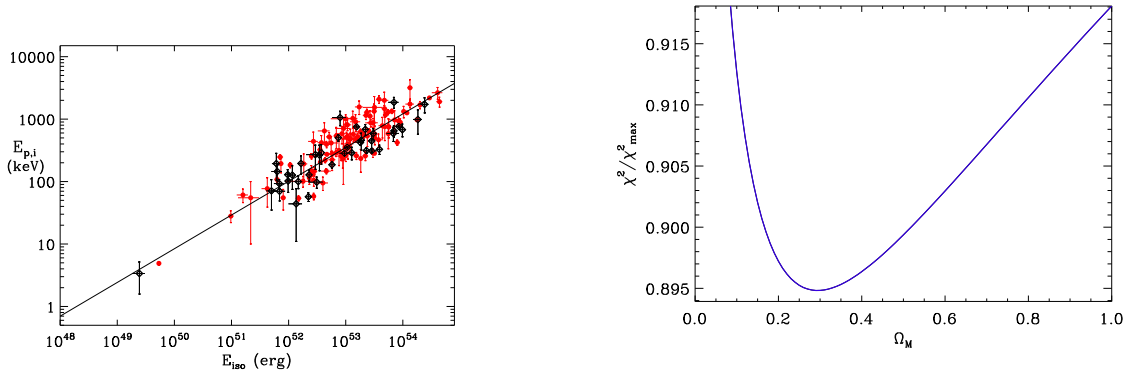

Figure 3.4. Left: the $E_{\rm p,i}$ – $E_{\rm iso}$ correlation in long GRBs (as of end 2009). The black line shows the best–fit power–law. Right: dispersion of the $E_{\rm p,i}$ – $E_{\rm iso}$ correlation of long GRBs, expressed in terms of fraction of χ^2/χ^2_{max}, as a function of the value of $\Omega_{\rm M}$ used to compute the $E_{\rm iso}$ values in a standard ΛCDM flat universe ([114]).

Table 3.1. Comparison of the confidence intervals on $\Omega_{\rm M}$ for a flat ΛCDM Universe obtained with the sample of 70 GRBs by Amati et al. [109], the sample of 120 GRBs available as of end 2009 ([114; 119]) and a simulated sample of 240 GRBs expected to be available within the next few years (see text), computed by adopting the same approach of Amati et al. ([109]) combined with the use of the likelihood function proposed by Reichart ([127]) (from Amati et al. [119]). In the last line we also show the results obtained by using the observed sample and assuming that the slope and normalization of the $E_{\rm p,i}$ – $E_{\rm iso}$correlation are known with a 10% accuracy based, e.g., on calibration against SNe–Ia, self–calibration with a large enough number of GRBs at similar redshift, a physical model.

GRB #	$\Omega_{\rm M}$		
	Best	(68%)	(90%)
70	0.27	0.09 – 0.65	0.05 – 0.89
120	0.29	0.14 – 0.57	0.10 – 0.79
240	0.29	0.17 – 0.45	0.13 – 0.65
120 + cal.	0.29	0.24 – 0.34	0.21 – 0.37

In 2002, based on a small sample of *Beppo*SAX GRBs with known redshift and spectral parameters, it was discovered that $E_{\rm p,i}$ is significantly correlated with $E_{\rm iso}$ [111]. This correlation, commonly called "Amati relation" within the GRB community, has the form

$$\log E_{\rm p,i}({\rm keV}) = m \log E_{\rm iso}(10^{52}{\rm erg}) + q$$

, with m~0.5 and q~2, and is characterized by an extra–Poissonian scatter normally distributed with a $\sigma_{\rm ext}$ of ~0.2 dex around the best–fit law. Subsequent observations with various detectors and spectrometers confirmed and extended the $E_{\rm p,i}$ – $E_{\rm iso}$ correlation, showing that it holds for all long GRBs and XRFs with well measured redshift and spectral parameters [109; 112; 118]. The distribution of long GRBs and XRFs in the $E_{\rm p,i}$ – $E_{\rm iso}$ plane as of end 2009 is shown in Fig. 3.4. The data, together with the power–law best–fitting the long GRBs points and its confidence region, have been taken from [109; 118; 119].

3.5.2 GRB cosmology through the $E_{\rm p,i}$-intensity correlation

Investigations into using GRBs as cosmological probes started in 2004, when it was found that the $E_{\rm p,i}$ – $E_{\rm iso}$ correlation tightened when $E_{\rm iso}$ was replaced with the collimation–corrected radiated energy $E_\gamma = (1 - \cos\theta_{jet}) \times E_{\rm iso}$ [120; 121]. This result was based on a small sub–sample of GRBs with known $E_{\rm p,i}$ and $E_{\rm iso}$ for which it was possible to infer the jet opening angle θ_{jet} from the "break time", $t_{\rm b}$, at which the decay index of the light curve of the optical afterglow sharply changes to a steeper one, under the assumption of a simple jet and afterglow model [122]. By exploiting the low scatter of the $E_{\rm p,i} - E_\gamma$ correlation and applying statistical methods accounting for the lack of calibration (so called "circularity problem"), it was possible to derive, within the "standard" ΛCDM cosmological model, estimates of $\Omega_{\rm M}$ and Ω_Λ consistent with the "concordance" values mostly coming from the analysis of Type Ia SNe and the CMB. A review of these methods and results is provided in Ghirlanda et al. (2006).

However, in the last years, the simple jet model assumed to compute θ_{jet} from the break time of the optical afterglow light curve has been questioned based on the observed different behavior of the X–ray afterglow light curves, which, in several cases, show no "jet–break" or show a break not simultaneous to the optical one [e.g., 124–126]. This makes the determination of E_γ, and thus the characterization and use of the $E_{\rm p,i} - E_\gamma$ correlation, less firm and, in any case, model dependent. Thus, it was investigated [109] the possibility to measure the cosmological parameters through the $E_{\rm p,i} - E_{\rm iso}$ correlation, which has the advantage, with respect to the $E_{\rm p,i} - E_\gamma$ correlation, of: i) allowing the use of a sample about four time larger; ii) being based on only two observables (the $E_{\rm p,i} - E_\gamma$ correlation requires, in addition to $E_{\rm iso}$ and $E_{\rm p,i}$, also t_b) and avoiding the model–dependent assumptions (jet model, afterglow model, density and profile of the circum–burst environment, efficiency of conversion of fireball kinetic energy into radiated energy) which affect the computation of E_γ.

Based on the sample of 70 long GRBs with known $E_{\rm p,i}$ and $E_{\rm iso}$, it was found that, after assuming a flat Universe, the χ^2 obtained by fitting the correlation with a simple power–law is a function of the value of $\Omega_{\rm M}$ assumed in the computation of $E_{\rm iso}$. In particular, as can be seen in Fig. 3.4, the function $\chi^2(\Omega_{\rm M})$ shows a minimum at $\Omega_{\rm M}$~0.25–0.30 at 99% c.l. This a very simple but relevant result: a) it shows that the $E_{\rm p,i} - E_{\rm iso}$ correlation can indeed be used to extract clues on the values of cosmological parameters; b) it provides evidence, independently of type Ia SNe, that $\Omega_{\rm M}$ is significantly smaller than 1. In Table 3.1, we show the 68% and 90% c.l. intervals for $\Omega_{\rm M}$ in a flat ΛCDM model derived with the 70 GRBs of Amati et al. ([109]), the 120 GRBs available as of end 2009 and a simulated sample of 240 GRBs expected to be available within a few years [114; 119]. These values were obtained with the same approach as Amati et al. ([109]) but using the likelihood function proposed by Reichart (2001), which has the advantage of not requiring the arbitrary choice of an indipendent variable among $E_{\rm p,i}$ and $E_{\rm iso}$ (see [119] for a discussion). As can be seen, by increasing from N_1 to N_2 the number of GRBs in the sample the accuracy of the estimate of $\Omega_{\rm M}$ improves by a factor of $\sim \sqrt{N_2/N_1}$, as expected for a method not significantly affected by systematics. This is confirmed also by the investigation of the contours in the $\Omega_{\rm M} - \Omega_\Lambda$ plane computed by following the same method as above but releasing the flat Universe assumption (Fig. 3.5). The accuracy of these measurements is still lower than obtained with SN data, but promising in view of the increasing number of GRBs with measured redshift (see Fig. 3.5) which will be allowed by the continuing simultaneous operation of *Swift*, *Fermi*/GBM, Konus–WIND and future GRB experiments (e.g., SVOM, UFFO).

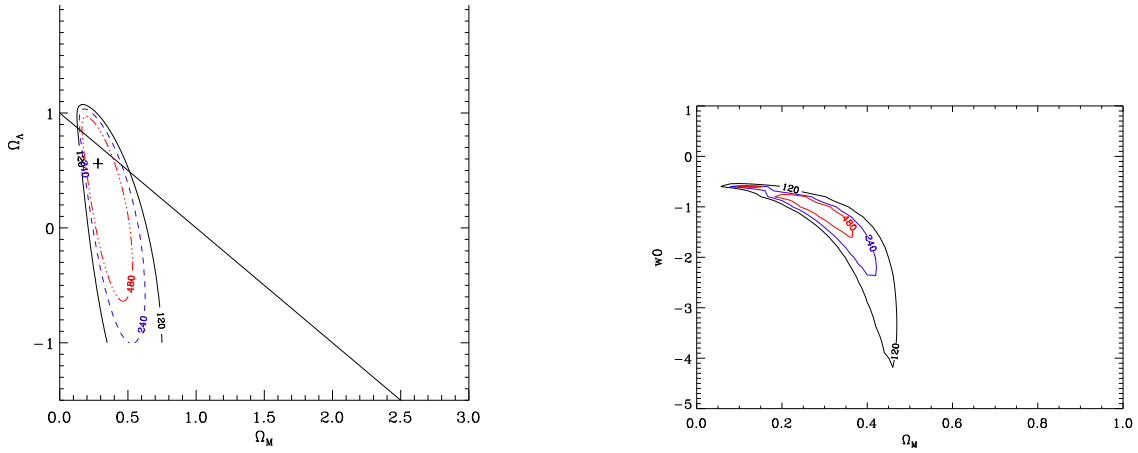

Figure 3.5. Left: 68% confidence level contour in the $\Omega_M - \Omega_\Lambda$ plane obtained by releasing the flat Universe assumption with the sample of 120 GRBs available as of end 2009 (black) compared to those expected in the next years with the increasing of GRBs in the sample (blue and red). Right: contours in the w0 - Ω_M plane obtained with the present and expected future samples by assuming that the slope and normalization of the $E_{p,i}$ – E_{iso}correlation are known with a 10% accuracy based, e.g., on calibration against SNe–Ia, self–calibration with a large enough number of GRBs at similar redshift, a physical model.

3.5.3 The SKA contribution

Radio observations of GRBs

In the *Swift* era, radio afterglow emission is being detected for about 30% accurately (< a few arcmin) localized GRBs, to be compared with ~93% in X–rays and ~75% in optical/NIR. Most measurements have been made with the VLA and EVLA, even though several detections were also provided by WSRT, ATCA, GMRT; a few by VLBA. The canonical long–duration GRB radio light curve at 8.5 GHz peaks at three to six days in the source rest frame, with a median peak luminosity of 10^{31} erg s^{-1} Hz^{-1}. The typical mean fluxes at 8.5 GHz in 5–10 days from the GRB range from ~100 to ~900 mJy. Peak fluxes may occasionally reach 10 mJy. See, e.g., [128] for a review.

The relevance of radio observations of GRBs consists in providing unique information about, e.g.: scintillation (fundamental probe of ultra–relativistic expansion of GRB sources), unbiased test of afterglow models w/r, e.g., to optical observations (dust extinction, contamination by SN and host galaxy light), properties of the circum–burst environment (and, hence, on the progenitors), late time non relativistic phase expansion (afterglow physics and determination of the blast-wave energy independent of the initial jet collimation), statistics of orphan afterglows (inference on maximum jet opening angle).

GRB physics and cosmology with SKA

The combination of high sensitivity, high angular resolution, short reaction time and broad band of SKA will allow to achieve important and partly unprecedented goals for GRB science through radio–observations. These include: measurement of GRB source size and expansion velocity through ISM scintillation; accurate location of GRBs in host galaxies; early radio afterglow: physics (reverse shock, transition from optically thick to optically thin synchrotron emission,etc.); estimate of kinetic energy and jet opening angle from SED fitting; measurement of host galaxy radio emission.

Concerning in particular GRB cosmology, the high sensitivity of SKA will allow accurate radio calorimetry for a large number of GRBs, the detection of very high–z GRBs (up to 10 ?), the study of

Star Forming Rate (SFR) evolution up to very high z, the detection and study of nearby (z <1) low-luminosity GRBs and local GRB/SNe. Also, the broad field of view will provide us with the detection of a significant number of orphan afterglows (for more details see Sect. 7.4), which will allow to set constraints on the distribution of GRB jet opening angles and, hence, of the energy budget.

3.5.4 Conclusions and synergies with high-energy forthcoming facilities

Given their huge radiated energies and redshift distribution extending from ~ 0.1 up to >9, GRBs are potentially a very powerful cosmological probe, complementary to other probes (e.g., SN Ia, clusters, BAO). The correlation between spectral peak photon energy, $E_{\rm p,i}$, and intensity ($E_{\rm iso}$, $L_{\rm iso}$, $L_{\rm p,iso}$) is one of the most robust and intriguing properties of GRBs and a promising tool for measuring cosmological parameters. Analysis in the last years (>2008) provide already evidence, independent on, e.g., SN Ia, that if we live in a flat ΛCDM universe, $\Omega_{\rm M}$ is < 1 at >99.9% c.l. and around $\Omega_{\rm M}$~0.3, consistent with the "standard". cosmology. The simultaneous operation of *Swift*, *Fermi*/GBM, Konus–WIND is allowing an increase of the useful sample (z + $E_{\rm p,i}$) at a rate of 15–20 GRB/year, providing an increasing accuracy in the estimate of cosmological parameters. Future GRB experiments and more investigations (physics, methods, calibration) will allow to go beyond SN Ia cosmology (e.g.,dark energy EOS). Radio observations by SKA will give a significant contribution by providing unique clues to the physics, energy budget and beaming angle of GRBs.

Radio follow up of GRBs by SKA and its precursors will depend on the prompt distribution of GRB alerts generated by forthcoming GRB detectors. After Swift, extended until 2015, the Space-based french–chinese multi-band astronomical Variable Object Monitor (SVOM - e.g. Schanne et al. 2010) will provide fast and accurate localization of GRBs. In the 2022-2024 time frame, the possible selection of the Large Observatory For X–ray Timing, LOFT [**?** **?**] among the four pre–selected missions for the ESA Cosmic Vision M3 opportunity, could extend the fundamental "service" of providing detection and prompt localization of GRBs for multiwavelength (Xray/Optical/Radio) studies.

Though GRB science is not one of its primary goals,no past, present or future (e.g., SVOM, UFFO) GRB experiment has such a combination of low energy threshold and high energy resolution (and wide FOV), which will make the LOFT/WFM unique also for GRB science. LOFT, possibly in combination with other GRB experiments flying at the same epoch, will give us useful and unique clues to some of the still open issues in the GRB research field, through: a) measurements of the prompt emission down to ~2 keV and ~arcmin localization with the Wide Field Monitor (WFM); b) measurements of the early afterglow emission with the Large Area Detector (LAD) [131]. In particular, the partly unprecedented characterization of the GRB X–ray prompt emission, joined with source location accurate enough for optical follow-up, by the WFM will allow to investigate the properties of the circum-burst environment, thus getting further clues on the nature of the progenitors, to provide more stringent tests for the emission mechanisms at play, to increase the detection rate of high–z GRBs w/r to previous missions, to shade light on the population of X–ray Flashes (XRFs) and sub-energetic events.

In combination with SKA and other telescopes operating in the >2020 time line, like e.g., LSST, CTA, gravitational wave / neutrino detectors, it will be possible to undertake multi–wavelength studies. In particular SKA and LOFT will allow to get unprecedented measurements of both the prompt X–ray and radio emission, which, joined together for those events detected by the two instruments, will provide unique clues to the physics, geometry and energetics of GRB emission. Under this respect, LOFT will complement and enhance the GRB science and cosmology that will be done by SKA also by providing directions were to promptly search for the radio afterglow, increasing, in particular, the number of high-z GRBs with energetics derived from radio calorimetry.

3.6 Synergy with CMB projects

C. Burigana, T. Trombetti, G. de Zotti, C. Baccigalupi, F. Finelli, A. Gruppuso, F. Perrotta, A. De Rosa

Although not specifically devoted to CMB studies, because of its high resolution and the limited high frequency coverage, the SKA extreme sensitivity and resolution may be fruitfully used to address several specific themes in synergy with current and future CMB projects. We identified (at least) eight relevant topics: (*i*) thermal and kinetic Sunyaev-Zel'dovich effect towards galaxy clusters; (*ii*) thermal Sunyaev-Zel'dovich effect at galaxy scale; (*iii*) contribution to future high precision CMB spectrum experiments; (*iv*) cross-correlation with CMB and other surveys, for the analysis of Integrated Sachs-Wolfe effect and constraining on dark energy; (*v*) non-Gaussianity from joint analyses of CMB and radiosources; (*vi*) free-free emission at different cosmic times; (*vii*) primordial magnetic fields; (*viii*) Galactic foreground studies aimed at component separation in future CMB experiments. Topics (*vii*) and (*viii*) will be discussed in Sect. 6.2.2 and Sect. 8.3, respectively.

3.6.1 Thermal and kinetic Sunyaev-Zeldovich effect towards galaxy clusters

The scattering of CMB photons from hot electrons in galaxies and clusters of galaxies produces a frequency dependent change in the CMB brightness. If the hot electron gas is globally at rest with respect to the observer only the thermal Sunyaev-Zeldovich (SZ) effect ([132]) (see also [133]) will be present; differently, a bulk peculiar motion, V_r, of the hot electron gas produces a kinetic SZ effect. In the Rayleigh-Jeans (RJ) region the first effect produces a decrement of the surface brightness, ΔI_{th}, towards the cluster. The second effect produces either a decrement or an increment, ΔI_k, depending on the direction of the cluster velocity with respect to the observer. Neglecting relativistic corrections:

$$\Delta I_{th} = I_0 y g(x) \;\; \text{and} \;\; \Delta I_k = -I_0 (V_r/c) \tau_e h(x)\,, \tag{3.6.1}$$

where $I_0 = (2h_P/c^2)(k_B T_{CMB}/h)^3$. Here $\tau_e = \int n_e \sigma_T dl$ and $y = \int (k_B T_e/m_e c^2) n_e \sigma_T dl$ are respectively the Thomson optical depth and the Comptonization parameter [134] integrated over the cluster along the line of sight, n_e being the electron density, $h(x) = x^4 e^x/(e^x-1)^2$, $g(x) = h(x)[x(e^x+1)/(e^x-1)-4]$, $x = h_P \nu/k_B T_{CMB}$ being a dimensionless photon frequency. The two effects have a different frequency dependence that in principle allows their separation through multi-frequency observations. SKA observations in the RJ regime (where $h(x) \sim g(x) \rightarrow x^2$) can be combined with millimetric observations (in particular $g(x) \simeq 0$ and $h(x)$ is maximum at ~ 217 GHz).

The identification of about one thousand of galaxy clusters with the X-ray Multi-Mirror (XMM)-*Newton*[5] and *Planck*[6] [135] European Space Agency (ESA) satellites is on-going, while observations of many thousands of clusters ($\sim 5 \times 10^5$) come from the Sloan Digital Sky Survey[7] (SDSS). The typical angular sizes of galaxy clusters range from $\sim$ arcmin to few tens of arcmin.

Although the major role on the study of the SZ effects towards galaxy clusters will be played by dedicated telescopes operating at $\simeq$ arcmin resolutions with frequency coverages up to $\simeq$ millimetric wavelengths, with the 50% of the SKA collecting area it will be possible to accurately map the SZ effect ([136]) of each considered cluster, particularly at moderately high redshifts, with an extremely precise subtraction of discrete radio sources. The combination with X-ray images, in particular with those proposed to ESA for the *Athena+*[8] (formerly XEUS, X-ray Evolving Universe Spectroscopy) satellite project, designed to reach $\sim$ arcsec resolution on a few arcmin FOV, will allow to accurately

[5] www.rssd.esa.int/xmm
[6] www.rssd.esa.int/planck
[7] www.sdss.org
[8] http://www.the-athena-x-ray-observatory.eu/

map the thermal and density structure of the gas in galaxy clusters. Also, remarkable will be the synergy with the optical and infrared (IR) surveys at $\sim$ arcsec resolution expected in about ten years from the ESA *Euclid*[9] satellite. Finally, we observe that SKA is planned to operate for many decades. This will make possible to accurately map in the radio the $\sim 10^6$ clusters that could be detected almost uniformly across the whole sky with a next generation of CMB ultra-precise mission (see Sect. 3.6.3).

The SKA sensitivity and resolution mainly depends on the used array collecting area. By considering a frequency band of $\simeq$ 4 GHz at 20 GHz, as an optimal high frequency goal, the whole instrument collecting area will allow to reach a (rms) sensitivity of $\simeq$ 40 nJy in one hour of integration with an angular resolution of $\simeq$ 1 mas (considering $\simeq$ 3000 km maximum baseline). By using only about 50% of the collecting area within $\simeq$ 5 km, the (rms) sensitivity in one hour of integration is $\simeq$ 80 nJy with a resolution of $\simeq 0.6''$.

It is also possible to study the SZ effect (both thermal and kinetic) from clusters in a statistical sense, namely through its contribution to the angular power spectrum, C_ℓ, of the CMB secondary anisotropies. This topic has been investigated in several papers (see, e.g., [137–142]). At sub-arcmin scales (i.e. at multipoles $\ell \gtrsim 10^4$) secondary anisotropies from thermal (more important at $\ell \lesssim$ few $\times 10^4$) and kinetic (more important at $\ell \gtrsim$ few $\times 10^4$) SZ effect dominate over CMB primary anisotropy whose power significantly decreases at multipoles $\ell \gtrsim 10^3$ because of photon diffusion (Silk damping effect [143]). Their angular power spectrum at $\ell \sim 10^4 - 10^5$ ($\approx 10^{-12} - 10^{-13}$ in terms of dimensionless $C_\ell \ell(2\ell + 1)/4\pi$) could be in principle investigated with the sensitivity achievable with SKA. On the other hand, at the SKA resolution and sensitivity the contribution to fluctuations from foreground sources (both diffuse radio emission, SZ effects, and free-free emitters) at galaxy scales probably dominates over the SZ effect from clusters. See Appendix A in [144] for further details.

3.6.2 Thermal Sunyaev-Zeldovich effect at galaxy scale

The proto-galactic gas is expected to have a large thermal energy content, leading to a detectable SZ signal, both when the protogalaxy collapses with the gas shock-heated to the virial temperature ([145; 146]), and in a later phase as the result of strong feedback from a flaring active nucleus (see, e.g., [147–152]). The astrophysical implications of these scenarios have been investigated by [153].

A fully ionized gas with a thermal energy density $\varepsilon_{\rm gas}$ within the virial radius, $R_{\rm vir}$, transfers to the CMB an amount $\Delta\varepsilon \simeq (\varepsilon_{\rm gas}/t_c)2(R_{\rm vir}/c)$ of thermal energy through Thomson scattering producing a Comptonization parameter ([134]) $y \simeq (1/4)\Delta\varepsilon/\varepsilon_{\rm CMB}$. Here $\varepsilon_{\rm CMB} = a_{BB}T^4_{\rm CMB} \simeq 4.2 \times 10^{-13}(1 + z)^4$ erg cm^{-3}, a_{BB} being the black-body constant and $T_{\rm CMB} = T_0(1 + z)$ the temperature of the CMB; t_c is the gas cooling time by Thomson scattering.

Assuming the binding energy ($E_{\rm b,gas} = M_{\rm gas}v^2_{\rm vir}$, $v_{\rm vir} = 162h^{1/3}(1 + z)^{1/2}(M_{\rm vir}/10^{12}M_\odot)^{1/3}$ km s^{-1}; see [154; 155]) to characterize the thermal energy content of the gas, $E_{\rm gas}$, the amplitude of the SZ dip in the RJ region can be written as:

$$|\Delta T|_{\rm RJ} = 2yT_{\rm CMB} \simeq 1.7\left(\frac{h}{0.5}\right)^2\left(\frac{1 + z_{\rm vir}}{3.5}\right)^3 \frac{M_{\rm gas}/M_{\rm vir}}{0.1}\frac{M_{\rm vir}}{10^{12}M_\odot}\frac{E_{\rm gas}}{E_{\rm b,gas}}\,\mu{\rm K}\,, \tag{3.6.2}$$

where h is the Hubble constant in units of 100 km s^{-1} Mpc^{-1} and $z_{\rm vir}$ is the virialization redshift.

This SZ effect shows up on small (typically sub-arcmin) angular scales, corresponding to an angular radius:

$$\theta_{SZ} \simeq 17''\left(\frac{E_{\rm BH}}{10^{62}}\right)^{1/4}\left(\frac{\varepsilon_{\rm BH}}{0.1}\right)^{-1/4}\left(\frac{1 + z_{\rm vir}}{3.5}\right)^{-3/2}\frac{d_A(2.5)}{d_A(z)}\,, \tag{3.6.3}$$

[9] www.rssd.esa.int/euclid

where $d_A(z)$ is the angular diameter distance.

This expression applies to quasar-driven blast-waves, that could inject into the ISM an amount of energy several times higher than the gas binding energy, thus producing larger, if much rarer, SZ signals. A black-hole (BH) accreting a mass $M_{\rm BH}$ with a mass to radiation conversion efficiency $\varepsilon_{\rm BH}$ releases an energy $E_{\rm BH} = \varepsilon_{\rm BH} M_{\rm BH} c^2$. We adopt the standard value for the efficiency $\varepsilon_{\rm BH} = 0.1$ and assume that a fraction $f_h = 0.1$ of the energy is fed in kinetic form and generates strong shocks turning it into heat. The re-assessment by [156] of the well known correlation between the BH mass and the stellar velocity dispersion and, following [151], an isothermal density profile of the galaxy have been adopted here.

The angular scales of these SZ signals from galaxies are of the order of $\approx 10''$, then of particular interest for a detailed mapping with the SKA and *Athena+* in the radio and X-ray, respectively. The probability of observing these SZ sources on a given sky field at a certain flux detection level and the corresponding fluctuations are mainly determined by the redshift dependent source number density $\phi_{\rm SZ}(S_{\rm SZ}, z)$ per unit interval of the SZ (decrement) flux $S_{\rm SZ}$. The lifetime of the considered SZ sources is crucial to determine their number density.

For quasar-driven blast-waves the lifetime of the active phase, $t_{\rm SZ}$, is approximately equal to the time for the shock to reach the outer boundary of the host galaxy. Assuming a self-similar blast-wave expanding in a medium with an isothermal density profile, $\rho \propto r^{-2}$, we have:

$$t_{\rm SZ} \simeq \frac{1.5 \times 10^8 {\rm yr} \left(E_{\rm BH}/10^{62} {\rm erg}\right)^{1/8}}{(h/0.5)^{3/2} \, (\varepsilon_{\rm BH}/0.1)^{5/8} \, (f_h/0.1)^{1/2} \, ((1+z)/3.5)^{9/4}} \, . \tag{3.6.4}$$

The evolving B-band luminosity function of quasars, $\phi(L_B, z)$, can be then adopted to derive the source number density $\phi_{\rm SZ}(S_{\rm SZ}, z) = \phi(L_B, z)(t_{\rm SZ}/t_{\rm q,opt})(dL_B/dS_{\rm SZ})$, where $L_B(S_{\rm SZ}, z)$ is the blue luminosity of a quasar at redshift z causing a (negative) SZ flux $S_{\rm SZ}$, and $t_{\rm q,opt}$ is the duration of the optically bright phase of the quasar evolution.

For the proto-galactic gas $t_{\rm SZ}$ should be replaced by the gas cooling time, $t_{\rm cool}$. Assuming that quasars can be used as effective signposts for massive spheroidal galaxies in their early evolutionary phases ([157]) and that they emit at the Eddington limit and using the relation by [158] between the mass of the dark-matter halo, $M_{\rm vir}$, and the mass of the central black-hole, $M_{\rm BH}/10^8 M_\odot \sim 0.1 (M_{\rm vir}/10^{12} M_\odot)^{1.65}$, the number density of sources with gas at virial temperature can be straightforwardly related to the quasar luminosity function $\phi(L_B, z)$.

In spite of the many uncertainties of these models, it is remarkable that the CMB fluctuations (dominated at small scales by the Poisson contribution) induced by the SZ effect of these source populations could contribute to the CMB anisotropy power at high multipoles (see Fig. 3.6, left panel, for a comparison with Cosmic Background Imager[10] (CBI) ([159]) and Berkeley Illinois Maryland Association[11] (BIMA) ([160]) data).

In general, a direct probe of these models and, possibly, their accurate knowledge through a precise high resolution imaging is highly interesting. Fig. 3.6, right panel, shows the number counts at 20 GHz predicted by these models: in a single SKA FOV about few $\times 10^2 - 10^3$ SZ sources with fluxes above $\sim$ 100 nJy could be then observed in few hours of integration. Given the typical source sizes, we expect a blend of sources in the SKA FOV at these sensitivity levels, while much shorter integration times, $\sim$ sec, on many FOV would allow to obtain much larger maps with a significant smaller number of resolved SZ sources per FOV. Both surveys on relatively wide sky areas and deep exposures on limited numbers of FOV are interesting and easily obtainable with SKA.

[10] http://www.astro.caltech.edu/ tjp/CBI/

[11] http://bima.astro.umd.edu/bima.html

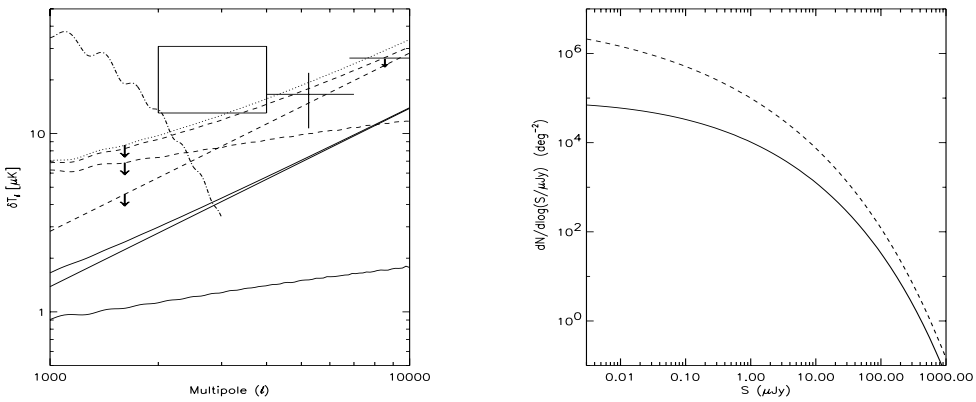

Figure 3.6. Left panel: angular power spectrum of SZ effects at 30 GHz compared to CMB primary fluctuation power spectrum and CBI (box) and BIMA (data points) measures. Solid lines represent clustering (bottom line), Poisson (middle line) and global (upper line) contributions from quasar driven blast-waves. Dashed lines represent clustering (bottom line at high ℓ), Poisson (middle line at high ℓ) and global (upper line) contributions from proto-galactic gas. The latter are actually upper limits since, because of the uncertainty in the cooling time, the extreme assumption that $t_{\rm cool} = t_{\rm exp}$ has been adopted in the computation. Dots refer to the overall contribution. Right panel: number count predictions at 20 GHz for SZ effects as function of the absolute value of the flux from proto-galactic gas heated at the virial temperature (dashes) assuming $M_{\rm gas}/M_{\rm vir} = 0.1$ and from quasar driven blast-waves (solid line). The exponential model for the evolving luminosity function of quasars is derived by [161] for an optical spectral index of quasars $\alpha = 0.5$ ($S_\nu \propto \nu^\alpha$). The parameters have been set at $\varepsilon_{\rm BH} = 0.1$, $f_h = 0.1$, $k_{\rm bol} = 10$, $t_{\rm q,opt} = 10^7$ yr. From [144].

A different scenario has been proposed by [162]. It involves hot gas winds powered by pair-instability supernovae (SN) explosions from the first generation of very massive stars at very low metallicity able to photoevaporate the gas in the halo potential. The SN remnants should then dissipate their energy in the intergalactic medium (IGM) and about 30-100% of their energy would be transferred to the CMB via Compton cooling. The resulting SZ effect from this sources is relevant in statistical sense. However, it is estimated to be too faint ($\approx$ few $\times 10^{-2}$ nJy) to be observable even by SKA.

3.6.3 SKA contribution to future CMB spectrum experiments

The current limits on CMB spectral distortions and the constraints on energy dissipation processes $|\Delta\varepsilon/\varepsilon_i| \lesssim 10^{-4}$ in the plasma ([163]) are mainly set by the National Aeronautics and Space Administration (NASA) COsmic Background Explorer[12] (COBE) / Far Infrared Absolute Spectrophotometer (FIRAS) experiment ([164; 165]). High accuracy CMB spectrum experiments from space, like the Diffuse Microwave Emission Survey (DIMES) ([166]; see also [167]) at $\lambda \gtrsim 1$ cm and FIRAS II ([168]) at $\lambda \lesssim 1$ cm, have been proposed to constrain (or probably detect) energy exchanges 10–100 times smaller than the FIRAS upper limits. In particular, experiments like DIMES may probe dissipation processes at early times ($z \gtrsim 10^5$) resulting in Bose-Einstein like distortions ([169–171]) and free-free distortions ([172]) possibly generated by heating (but, although disfavoured by NASA

[12] http://lambda.gsfc.nasa.gov/product/cobe/

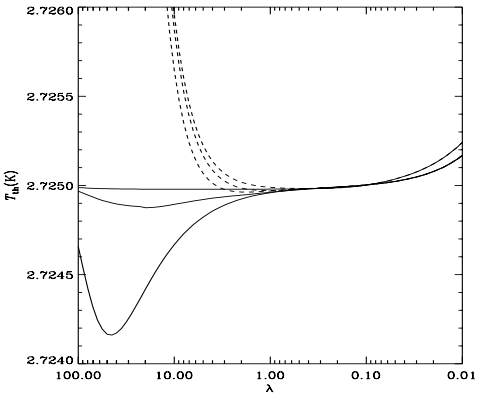

Figure 3.7. CMB distorted spectra as functions of the wavelength λ (in cm) in the presence of a late energy injection with $\Delta\varepsilon/\varepsilon_i \simeq 4y = 5 \times 10^{-6}$ plus an early/intermediate energy injection with $\Delta\varepsilon/\varepsilon_i = 5 \times 10^{-6}$ occurring at the "time" Comptonization parameter $y_h = 5, 1, 0.01$ (from the bottom to the top; in the figure the cases at $y_h = 5$ – when the relaxation to a Bose-Einstein modified spectrum with a dimensionless chemical potential given, in the limit of small distortions, by $\mu \simeq 1.4\Delta\varepsilon/\varepsilon_i$ is achieved – and at $y_h = 1$ are extremely similar at short wavelengths; solid lines) and plus a free-free distortion with $y_B = 10^{-6}$ (dashes). y_h is defined by y below Eq. (3.6.1) but with $dl = cdt$ and $T_e = T_{CMB}$ when the integral is computed from the time of the energy injection to the current time.

Wilkinson Microwave Anisotropy Probe[13] (WMAP) data, in principle also by cooling ([173])) mechanisms at late epochs ($z \lesssim 10^4$), before or after the recombination era ([174]). These perspectives have been recently renewed in the context of a new CMB space mission like the Primordial Inflation Explorer (PIXIE) ([175]) proposed to NASA, combining high accuracy polarization and spectrum measures at $\sim$ degree resolution, or even in the possible inclusion of spectrum measures in the context of a polarization dedicated CMB space mission, of high sensitivity and up to arcmin resolution, like the Cosmic Origins Explorer[14] (COrE) proposed to ESA ([176]) and its evolutions, e.g. PRISM[15] proposed in the context of the call for the definition of the L2 and L3 missions in the ESA Science Programme (see [177]). Typical distorted spectra ([178]; see also [179; 180]) are shown in Fig. 3.7. To firmly observe such small distortions the Galactic and extragalactic foreground contribution should be accurately modelled and subtracted.

Accurate radio source counts at 1.4 GHz have been presented in [181] and a recent estimation of radio source background can be found in [182]. On the other hand, the very faint tail of radio source counts is essentially unexplored and their contribution to the radio background at very low brightness temperature is not accurately known. For illustration, by assuming differential source number counts, $N(S)$, given by $\log N(S)/\Delta N_0 \sim a \log S + b$, with $\Delta N_0 \sim 150 S^{-2.5}$ sr^{-1} Jy^{-1} (S in Jy) ([183]), for $a \sim 0.4 - 0.6$ and $b \sim -(0.5 - 1)$, we find a contribution to the radio background at 5 GHz from sources between $\sim$ 1 nJy and $\sim$ 1μJy between few tens of μK and few mK. These signals are clearly negligible compared to the accuracy of current CMB spectrum experiments, in particular at $\lambda \gtrsim 1$ cm, but are significant at the accuracy level on CMB distortion parameters potentially achiev-

[13] http://lambda.gsfc.nasa.gov/product/map/current/
[14] http://www.core-mission.org/
[15] http://www.prism-mission.org/

able with future experiments. This effect is small compared to the Galactic radio emission, whose accurate knowledge currently represents the major astrophysical problem in CMB spectrum experiments, but, differently from Galactic emission, it is isotropic at the angular scales of few degrees and can not be then subtracted from the CMB monopole temperature on the basis of its angular correlation properties. With accurate absolute measures on a wide frequency coverage a fit including both CMB distorted spectra and astrophysical contributions can be searched (see [163] for an application to FIRAS data) but a direct radio background estimate from precise number counts will certainly improve the robustness of this kind of analyses.

The relevance of this problem emerged in the detection by the NASA Absolute Radiometer for Cosmology, Astrophysics, and Diffuse Emission[16] (ARCADE) 2 of an excess in the CMB absolute temperature at 3.3 GHz ([184; 185]) possibly explained by a contribution by very faint sources as a possible explanation of this signal. [186] concluded that, if the radio background is at the level reported, a majority of the total surface brightness would have to be produced by ordinary star-forming galaxies above redshift 1 characterized by an evolving radio–far-infrared correlation, which changes towards the radio loud with redshift. Analyzing dedicated radio observations with the Karl G. Jansky Very Large Array[17], [187] arrived to the result that, if discrete sources dominate the bright extragalactic background reported by ARCADE 2 at 3.3 GHz, they cannot be located in or near galaxies and most are fainter than 0.03 μJy at 1.4 GHz.

Although the 3.3 GHz excess and its interpretations are controversial, this underlines how crucial is the precise estimation of very faint source counts for the exploitation of precise CMB spectrum measures. The SKA sensitivity at 20 GHz will allow the detection (to 5σ) of sources down to a flux level of $\simeq$ 200 nJy ($\simeq 60, 20, 6$ nJy) in 1 (10, 10^2, 10^3) hour(s) of integration over the $\simeq$ 1 mas (FWHM) resolution element; similar numbers (from $\simeq$ 250 to 8 nJy in an integration time from 1 to 10^3 hours, respectively) but on a resolution element about 10 times larger will be reached at $\approx$ GHz frequencies by using a frequency bandwidth of about 25%. Therefore, the SKA accurate determination of source number counts down to very faint fluxes can directly help the solution of one fundamental problem of the future generation of CMB spectrum space experiments at $\lambda \gtrsim 1$ cm.

3.6.4 Cross-correlation with CMB and other surveys: integrated Sachs-Wolfe effect and constraints on dark energy

High accuracy CMB surveys, like that available in next years by *Planck*, are designed to cover a high sky fraction if not the whole sky. The SKA is mainly designed to achieve very faint fluxes on limited sky fields. On the other hand, the sensitivity of the SKA (SKA2_mid_dish in particular, but also SKA precursors) is so high on typical FoVs of $\sim$ degree side at frequencies around one GHz, that it is reasonable to think to cover a significant sky fraction (thousands of square degrees) with unprecedented sensitivity accumulating some months of integration. This opens the possibility of carrying out improved cross-correlation analyses with CMB surveys, but also with surveys in other frequency bands.

The integrated Sachs-Wolfe (ISW) effect results from the line of sight integral in the Sachs Wolfe equation [188]. It arises when CMB photons streaming across the Universe interact with the time evolving gravitational potential wells associated with the foreground large scale structure (LSS). The potential evolution leads to a net change of the photon energies as they pass through them. ISW is a linear effect depending the cosmological model, since it requires a change in equation of state of the cosmic fluid. The evolution of the gravitational potential is related to the matter linear density

[16] http://asd.gsfc.nasa.gov/archive/arcade/
[17] http://www.nrao.edu/pr/2012/jansky/

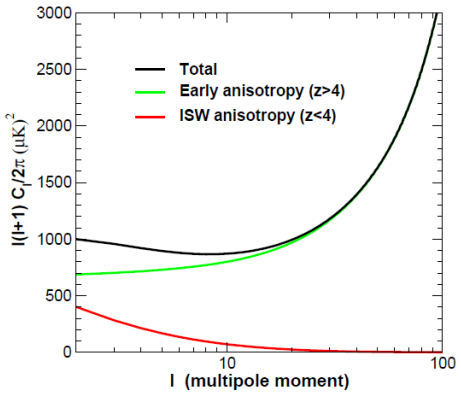

Figure 3.8. The auto-correlation function for the ISW effect in a ΛCDM model. From [189].

perturbations; in the matter dominated regime, the growth of matter perturbation is proportional to the scale factor. This balances the dilution of matter due to the cosmic expansion and makes negligible the gravitational potential variations. Such change happens instead at early times, when the Universe goes from being radiation dominated to matter dominated (*early ISW*), and at late times, as the dark energy (or curvature) takes over from the matter (*late ISW*). The ISW contribution to the CMB anisotropy in a direction $\hat{n}$ on the sky is approximately given by

$$\Delta^{ISW}(\hat{n}) \approx -2 \int_{\text{Last Scattering}}^{\text{Today}} d\eta \, \dot{\Phi}[r\hat{n}, \eta] \,, \tag{3.6.5}$$

where Φ is the Newtonian potential, the dot denotes a derivative wrt the conformal time η, and $r(\eta)$ is the proper distance.

Unlike the early ISW, the late ISW is virtually uncorrelated with the CMB anisotropies generated at last scattering: the typical auto-correlation function for the ISW is shown in Fig. 3.8. Direct detection of (late)ISW is difficult because of its small amplitude and because it is only dominant on super-horizon (i.e. large) scales, where cosmic variance is large. However, it is possible to isolate the late ISW generated at low redshifts through the cross-correlation of the CMB maps with LSS surveys. Indeed, when CMB photons cross a time-varying potential, they become slightly hotter or colder: statistically, we expect a tiny correlation of hot spots in the CMB with large scale structure, an effect which expected to be less than 1 μK, orders of magnitude smaller than the CMB correlations [189; 190].

Several measurements have been performed to detect the ISW signal: positive cross-correlations were measured using galaxy data from the Sloan Digital Sky Survey (SDSS) and WMAP [191–195]. Other successful attempts were based, [196], on APM galaxies, [197], using the 2MASS survey, [198; 199] using radio data and [200; 201] in which correlations were found with the hard X-ray background. Besides, [197; 202; 203] used infrared galaxy samples to characterize the ISW signal. The typical ISW significance of the detections is currently quite low, around 2-3 σ. Detecting the cross-correlation of CMB with LSS requires a good CMB map on large scales and a galaxy distribution map, deep enough, and covering a large fraction of the sky, f_{sky}, to reduce the noise of the uncorrelated early CMB map, being the signal to noise $\propto f_{sky}^{1/2}$.

Our group has been working on the characterization and exploitation of the ISW from CMB-LSS cross-correlation for what concerns the statistical of the early Universe, by developing a set

of estimators [204] capable of taking into account the features of the redshift surveys considered. [205] considered the correlation of WMAP7 CMB data with the radio sources in the NRAO Very Large Array Sky Survey (NVSS) and its implications concerning the statistics of cosmological perturbations. [206] investigated the role of foreground removal from CMB anisotropies in this context, resulting in an update of results including auto and cross-correlation spectra in [207]. [208] recently cross-correlated WMAP 7-yr maps with NRAO NVSS and constrained dark energy content through dedicated data analysis methods. The Quadratic Maximum Likelihood (QML) estimator [209] is well suited for such analysis. Given a CMB map in temperature and a galaxy survey $\mathbf{x} = (\mathbf{T}, \mathbf{G})$ (vector in pixel space), QML provides an estimate of the angular power spectrum $\hat{C}_\ell^X$ - with X being one of TT, TG, GG [18]. QML is optimal (i.e. unbiased and minimum variance), as essential when the signal-to-noise ratio is pretty low as for the ISW effect. It is computationally demanding but can be applied at the relatively low resolution, i.e. for large scales, where (late) ISW effect appears and even for incomplete sky coverage surveys, being a pixel based method.

Based on Cosmic Microwave Background (CMB) maps from the 2013 data release, the *Planck* Collaboration already presented a detection of the ISW effect with a significance ranging from 2 to $4\,\sigma$, depending on which method is used [210]. Three separate approaches have been explored, providing results compatible with previous works based on WMAP data but with a better foreground cleaning thanks to the broader frequency coverage. The correlation of the CMB with the *Planck* reconstructed gravitational lensing potential, using the lensing-induced bispectrum between the low-ℓ and high-ℓ temperature anisotropies, has been investigated for the first time. The correlation between lensing and the ISW effect has a significance close to $2.5\,\sigma$. The cross-correlation with tracers of large-scale structure, based on a combination of radio (NVSS) and optical (SDSS) data, yields around $3\,\sigma$ significance. Finally, aperture photometry on stacked CMB fields at the locations of known large-scale structures have been used, providing and confirming, over a broader spectral range, a $4\,\sigma$ signal when using a previously explored catalogue, but showing strong discrepancies in amplitude and scale compared to expectations.

SKA may play a crucial role in improving the current large scale dataset. Following the analysis of [96], the requirement to have a negligible shot noise in the galaxy power spectrum is obtained if $\beta\ FOV\ T_0 > 10\,\mathrm{deg}^2\mathrm{yr}$, where β is the receiver bandwidth, T_0 is the survey duration and FOV indicates the telescope field of view, which, for $SKA1_{mid}$ and $SKA2_{low}$ is, respectively, 1 deg^2 and 200 deg^2. It is foreseen that a 1-yr SKA survey will contain $> 10^9 (f_{sky}/0.5)$ HI galaxies in a redshift range $0 < z < 1.5$. This makes the combination of SKA and *Planck* data a powerful tool for investigating the ISW correlation, offering the opportunity to achieve an independent measurement of the effect and increasing the confidence level in the detection from the present, marginal evidence. We also plan to extend our exploitation for constraining the statistics of primordial perturbations and the dark energy dynamics.

[18] This estimator is given by $\hat{C}_\ell^X = \sum_{\ell' X'} (F^{-1})_{\ell\ell'}^{XX'} \left[\mathbf{x}^t \mathbf{E}_{\ell'}^{X'} \mathbf{x} - tr(\mathbf{N}\mathbf{E}_{\ell'}^{X'})\right]$, where the $F_{\ell\ell'}^{XX'}$ is the Fisher matrix defined as $F_{\ell\ell'}^{XX'} = \frac{1}{2} tr\left[\mathbf{C}^{-1} \frac{\partial \mathbf{C}}{\partial C_\ell^X} \mathbf{C}^{-1} \frac{\partial \mathbf{C}}{\partial C_{\ell'}^{X'}}\right]$, and the $\mathbf{E}$ matrix is given by $\mathbf{E}_\ell^X = \frac{1}{2}\mathbf{C}^{-1} \frac{\partial \mathbf{C}}{\partial C_\ell^X} \mathbf{C}^{-1}$, $\mathbf{C} = \mathbf{S}(C_\ell^X) + \mathbf{N}$ being the total global covariance matrix including the signal $\mathbf{S}$ and noise $\mathbf{N}$ contributions. C_ℓ^X is called the fiducial theoretical power spectrum. Although an initial assumption is needed for this fiducial power spectrum, the QML method provides unbiased estimates of the power spectrum of the map regardless of this initial guess $\langle \hat{C}_\ell^X \rangle = C_\ell^X$. Here the average is taken over the ensemble of realizations based on the input spectrum C_ℓ^X. The assumed fiducial power spectrum can impact the error estimates, but, in practice, starting near to the true result makes this effect negligible. The QML method is also optimal, since it can provide the smallest error bars allowed by the Fisher-Cramer-Rao inequality, $\langle \Delta\hat{C}_\ell^X \Delta\hat{C}_{\ell'}^{X'} \rangle = (F^{-1})_{\ell\ell'}^{XX'}$, where $\Delta\hat{C}_{\ell'}^{X'} = \hat{C}_\ell^X - \langle \hat{C}_\ell^X \rangle$, and the averages, as above, are over an ensemble of realizations.

3.6.5 Non-Gaussianity from joint analyses of CMB and radiosources

Statistical analyses of the extragalactic source distribution in the sky can be applied to test cosmological models. In this context, the possibility of probing the Gaussianity of primordial perturbations appears particularly promising. Primordial perturbations at the origin of the large scale structure (LSS) may leave their imprint in the form of small deviations from a Gaussian distribution. Different kinds of configurations, such as the so-called local type, equilateral, enfolded, orthogonal, have been predicted ([211; 212]). For example, the local type of deviation from Gaussianity is parameterized by a constant dimensionless parameter f_{NL} (see, e.g., [213–215]) $\Phi = \phi + f_{NL}(\phi^2 - < \phi^2 >)$, where Φ denotes Bardeen's gauge-invariant potential (evaluated deep in the matter era in the CMB convention) and ϕ is a Gaussian random field. Extragalactic radio sources are particularly interesting as tracers of the LSS. They span in fact large volumes extending out to substantial redshifts. The radio sources from the NRAO VLA Sky Survey[19] (NVSS), the quasar catalogue of SDSS Release Six (SDSS DR6 QSOs) and the MegaZ-LRG (DR7), the final SDSS II Luminous Red Galaxy (LRG) photometric redshift survey, have been recently analyzed by [207]. A global analysis of the constraints on the amplitude of primordial non-Gaussianity by the angular power spectra obtained from extragalactic radio sources (mapped by these surveys) and, moreover, from their cross-correlation power spectra with the WMAP CMB temperature map allowed to set limits on $f_{NL} = 48 \pm 20$, $f_{NL} = 50 \pm 265$ and $f_{NL} = 183 \pm 95$ at 68% confidence level for local, equilateral and enfolded templates, respectively, that have found almost stable with respect to potential systematic errors and analysis details ([207]). Such tests of non–Gaussianity would have profound implications for inflationary mechanisms – as single-field slow roll, multifields, curvaton (local type) – and for models which effects on the halo clustering can be described by the equilateral template (related to higher-order derivative type non-Gaussianity) and by the enfolded template (related to modified initial state or higher-derivative interactions). *Planck* data already set strong limits on the non-Gaussianity parameter f_{NL}, namely $f_{NL} = 2.7 \pm 5.8$, $f_{NL} = -42 \pm 75$ and $f_{NL} = -25 \pm 39$ at 68% confidence level for local, equilateral and orthogonal configurations [216], significantly constraining or ruling out many classes of inflationary models. We expect in principle a significant progress in this topic from the combination of high accuracy and deep extragalactic source surveys achievable with SKA and the CMB maps provided by *Planck*, at least for the local configuration, and from the future CMB missions mentioned above.

3.6.6 Free-free emissions

Projects like the SKA and the Atacama Large Millimeter Array (ALMA; [217]) will be able, for the first time, to trace in detail the distribution of neutral hydrogen before reionization (through the 21-cm line; see e.g. [218]) and the neutral-to-ionized Universe transition state at the time of reionization (ALMA could see the first galaxies emerging at that epoch). Reionization affects the CMB both in anisotropies at large and small scales and in the spectrum. A particular way to look at this stage is based on the analysis of free-free signal. Free-free emission produces both global and localized spectral distortion of the CMB. We will discuss later on specific models and/or in a defined simulation context for haloes formation and evolution.

A robust lower limit to the global averaged free-free distortion signal expected from the diffuse ionized IGM in a given cosmological reionization scenario can be derived from fundamental arguments.

The CMB brightness temperature, T_{br}, under the combined effect of Comptonization, resulting into a decrement of signal at long wavelengths as described in Sect. 3.6.1, and free-free process can

[19] http://www.cv.nrao.edu/nvss/

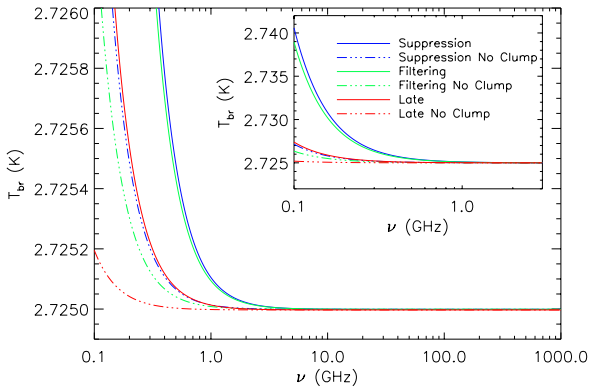

Figure 3.9. Minimal free-free distortion signal in terms of brightness temperature computed from combining Boltzmann and free-free CMB distortion numerical codes produced by the two astrophysical reionization histories and a phenomenological model (see text for details). CMB temperature distortions induced by free-free accounting for the clumping factor are found to be $\sim$ 10 times larger than the ones derived neglecting IGM density contrast. The inset shows better the signal at low frequencies and reports the meaning of the different lines.

be well approximated by $(T_{br} - T_{CMB}\phi_i)/T_{CMB} \simeq y_B/x^2 - 2y\phi_i$ where x is the dimensionless photon frequency, $y = (1/4)\Delta\varepsilon/\varepsilon_i$ is the Comptonization parameter related to the global energy released in the plasma, $\phi(z) = T_e(z)/T_{CMB}(z)$ and $\phi_i = \phi(z_i) = (1 + \Delta\epsilon/\varepsilon_i)^{-1/4} \simeq 1 - y$ is the ratio between equilibrium matter temperature and radiation temperature at the beginning of the heating process (i.e. at z_i or t_i), and y_B is the free-free distortion parameter. For an homogeneous ionized medium $y_B(x,t) = \int_{t_i}^{t}(\phi - \phi_i)\phi^{-3/2}g_B(x,\phi)K_{0B}dt$, where g_B is the Gaunt factor weighted over ionized atoms and $K_{0B}(z) \simeq (8\pi/3)e^6h^2n_e^{free}(n_H^+ + n_{He}^+ + 4n_{He}^{++})\phi^{7/2}/[m(6\pi mkT_e)^{1/2}(kT_e)^3]$ defines the bremsstrahlung rate in a H and He plasma [219]. The density of free electrons and ionized atoms is associated to the reionization history. [220] presented lower limit approximations for the free-free distortion parameter computed under the homogeneous medium approximation for realistic astrophysical reionization scenarios based on two different radiative feedback assumptions (the so-called *filtering* and *suppression* models) in the range of $\sim 5 \times 10^{-10} - 10^{-9}$. The structure formation process is well far from homogeneity. Given the dependence of free-free emission on the square of the baryon density, the bremsstrahlung rate should be amplified by a factor $\simeq 1 + \sigma^2$, where σ^2 is the matter distribution variance, $\sigma^2 \gg 1$ at moderate and low redshifts. Thus, coupling Boltzmann codes for the matter variance evaluation with a dedicated code for the free-free distortion including the correct time and frequency dependence of Gaunt factor [221], the above estimates turns to be $\sim$ 34 or 22 times larger for the two cases, respectively. We exploited also a reionization phenomenological model (called *late* model) by [222], as revisited in section 4 of [223] with parameters given by their equation (4).

As shown in Fig. 3.9, where signals from both free-free distortion and Comptonization decrement are included, the expected excess is at ~mK level at decimeter wavelengths, a target clearly accessible to the SKA sensitivity. To firmly detect this signal it is necessary to accurately observe the diffuse background level; this could be an issue for SKA, which is designed for other purposes, calling for a dedicated data analysis approach.

Going to specific models, we can distinguish between more extreme scenarios involving ionized haloes at high redshifts (and implying larger signals) and moderate scenarios relying on cluster cosmological evolution.

Possible free-free signal at high redshifts

The observation of diffuse gas and Population III objects in thermal bremsstrahlung as a direct probe of these quantities has been investigated by [224]. A natural way to distinguish between free-free distortion by ionized halos rather than by diffuse ionized IGM is represented by observations at high resolution of dedicated sky areas and by the fluctuations in the free-free background. In the model by [224] halos collapse and form a starburst lasting $t_o = 10^7$ yr, then recombine and no longer contribute to the free-free background. By adopting a Press-Schechter model ([225; 226]) for the number density of collapsed halos per mass interval, dn_{PS}/dM, [224] exploited the expression by [227] for the collapse rate of halos per mass interval per unit comoving volume to compute the comoving number density of ionized halos in a given flux interval as a function of redshift given the expected flux from a halo of mass M at redshift z, $S = S(M, z)$, and the starburst duration, t_o. Adopting a cut-off mass for a halo to be ionized of $M_* = 10^8(1 + z/10)^{-3/2} M_\odot$ (the critical mass needed to attain a virial temperature of 10^4 K to excite atomic hydrogen cooling), [224] computed the number counts of sources above the flux limit S_c from the zeroth moment of the intensity distribution moments due to sources above a redshift $z_{\rm min}$.

The relation $\dot{N}_{\rm recomb} = \alpha_B \langle n_e^2 \rangle V \approx (1 - f_{esc}) \dot{N}_{\rm ion}$, between the production rate of recombination line photons, $\dot{N}_{\rm recomb}$, and the production rate of ionizing photons, $\dot{N}_{\rm ion}$, (here α_B is the recombination coefficient and f_{esc} ($\approx$ some%) is the escape fraction for ionizing photons) implies that the source luminosities in Hα and free-free emission ($\propto n_e^2 V$) are proportional to the production rate of ionizing photons. Over a wide range of nebulosity conditions ([228]), given the free-free volume emissivity ([229]) in the case of an approximate mild temperature dependence with a power law, $\varepsilon_\nu = 3.2 \times 10^{-39} n_e^2 (T/10^4 K)^{-0.35}$ erg s^{-1} cm^{-3} Hz^{-1} , it is found $L_\nu^{ff} = 1.2 \times 10^{27} (\dot{N}_{\rm ion}/10^{53} {\rm ph\ s^{-1}})$erg s^{-1} Hz^{-1} . Assuming the starburst model of [230] [224] derived a production rate of ionizing photons as a function of halo mass $\dot{N}_{\rm ion}(M) = 2 \times 10^{53}\ (f_{star}/0.17)\ (M/10^9 M_\odot)$ ph s^{-1} , which specifies the above free-free ionized halo luminosity. The corresponding flux is then:

$$S_{\rm ff} = \frac{L_\nu^{\rm ff}}{4\pi d_L^2}(1+z) \approx 2.5 \left(\frac{1+z}{10}\right)^{-1} \frac{\rm M}{10^9 {\rm M}_\odot} \left(\frac{\rm T}{10^4\ {\rm K}}\right)^{-0.35} {\rm nJy}\,. \tag{3.6.6}$$

Clearly, SKA will allow to detect only bright sources with deep exposures. The ionized halo number counts can be calculated from Eq. (17). The result by [224] is reported in Fig. 3.10: SKA should be able to detect $\sim 10^4$ individual free-free emission sources with $z > 5$ in 1 square degree above a source detection threshold of 70 nJy. The redshift information from the Balmer line emission detectable by the Next Generation Space Telescope[20] (NGST) can be used to discriminate ionized halos from other classes of radio sources.

Ionized halos may contribute to the temperature fluctuations. In particular, the Poisson contribution is predicted to be larger (smaller) than the clustering one at scales smaller (larger) than $\sim 30''$ ([224]), but, likely, both are dominated by the radio source contribution.

The integrated emission from ionized halos produces a global CMB spectral distortion, $\Delta T_{ff} = c^2 \langle S \rangle / 2 k_B \nu^2$, that can be computed from the mean sky averaged signal $\langle S \rangle$. By using Eq. (17) (since no point source removal is feasible at degree scales) with $z_{\rm min}$ and $S_c = 0$, [224] found a free-free distortion $\Delta T_{ff} = 3.4 \times 10^{-3}$ K at 2 GHz, corresponding to a free-free distortion parameter $y_B \simeq 1.5 \times 10^{-6}$, well within the observational capability of a DIMES like project ([166; 174]).

[20] www.nas.edu/bpa2/tier3text/ngst.htm

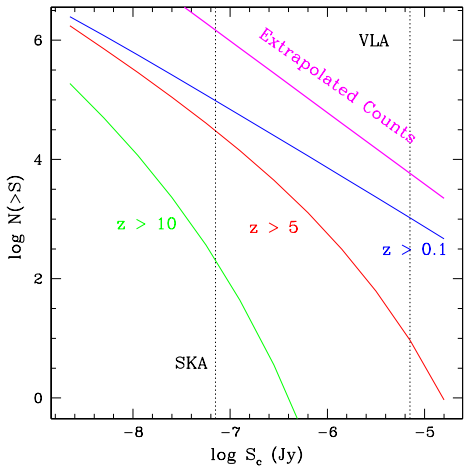

Figure 3.10. Number of sources which may be detected in the 1° by SKA, as a function of the threshold flux S_c. Realistic limiting fluxes for point source detection are shown. The extrapolated source counts from [231] are also shown. From [224].

Free-free signal at moderate redshifts

Focusing on the post reionization era, [232] studied with analytical models and simulations the regime of more massive haloes and the free-free radio emission from ionized gas in clusters and groups of galaxies. The cooling time is notably larger for massive haloes and highly non-linear phenomena like radiative cooling can be more easily ignored.

Combining a halo gas distribution model, as the β-model, with the haloes abundance as function of mass and redshift, it is possible to compute the mean free-free signal in a solid angle, function of redshift and/or mass. The data integration in the redshift-mass space ($z \in (0, 7)$, $M \in (10^8, 10^{16}) M_\odot$) estimates the mean free-free signal from all these haloes. This prediction falls below that by [224] because of the model higher haloes temperature. Fixing $T = 10^4$ K like in [224], the model predicts more signal than in [224] according to according to the fact that all haloes are ionized while in [224] only a fraction of them were *active*.

Fig. 3.11, top left panel, shows the free-free signal for various mass bins, as function of redshift. The smaller but more abundant haloes give a larger signal. Smaller haloes have about the same abundance at all redshifts so their average free-free contribution shows a slow redshift dependence. Note how the simulation predicts significantly less average signal than the analytical model, as direct consequence of the simulation resolution lack not able to capture the contribution from the smallest haloes. This prediction, however, should be taken with care since haloes are assumed to be ionized at all times and the gas temperature corresponds to the virial temperature of the halo. In small systems, the cooling time is short and the gas can cool down significantly, become neutral and form stars. The assumptions are only valid for the most massive haloes (groups and clusters) and the model predictions are robust only in that regime.

Fig. 3.11, top right panel, shows more explicitly the dependency of the average free-free distortion with the mass range for different redshift intervals. Again, smaller haloes contribute more to the average signal than massive ones at all redshifts (see also [233]).

Cooling and star formation plays a critical role in determining the actual contribution of galaxy-sized haloes ($M < 10^{12} h^{-1} M_\odot$) to the CMB temperature distortion. On one hand, the ionized gas

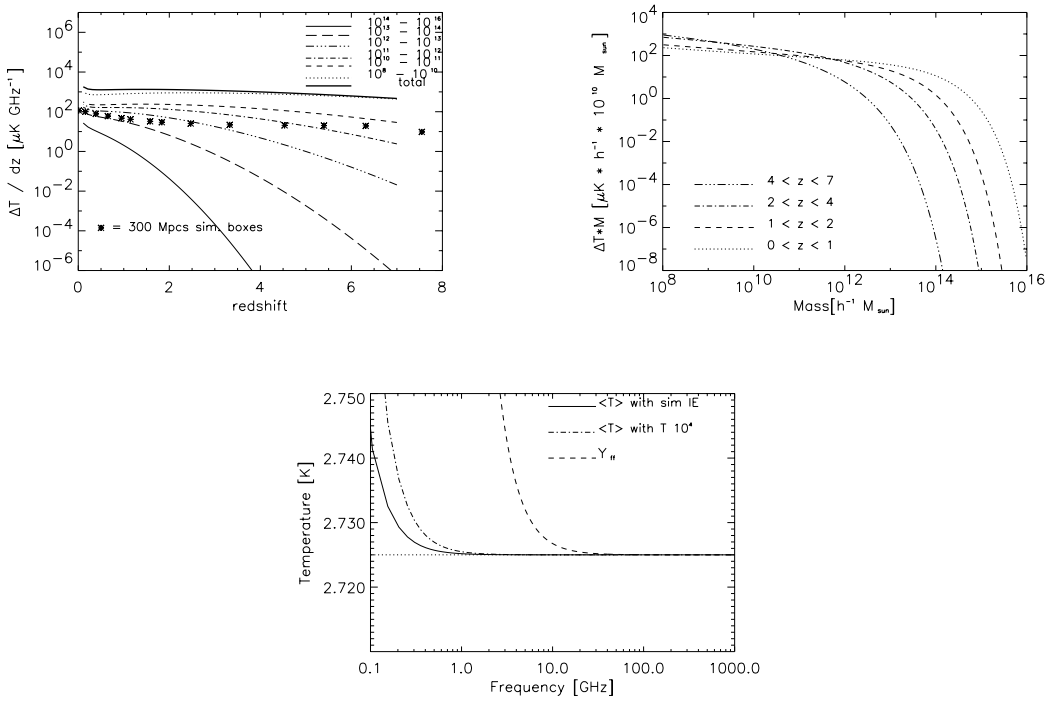

Figure 3.11. Top left panel: free-free signal for different mass intervals as a function of redshift and for $\nu = 1$ GHz. The points represent the distortion ΔT computed from a cosmological simulation of 300 Mpc. The minimum mass resolved in the simulation at $z = 1.57$ is $M_{\rm min,sim} = 1.14 \times 10^{11}$ and the maximum mass is $M_{\rm max,sim} = 8.21 \times 10^{13}$. Top right panel: free-free signal as a function of the halo mass and for different redshift intervals. Bottom panel: free-free emission distortion from the 300 h^{-1} Mpc simulation. The emission is computed from 20 snapshots within the interval $0 < z < 7$. The field of view covers 2.7 degrees. The solid line shows the distortion in the case where the emissivity has been computed with the temperature derived from the simulation. The dash-dotted line corresponds to the case where the temperature for all particles has been fixed to 10^4 K. The dashed line shows the observational upper limit constraints (95% CL) from [237]. From [232]. Note the substantial agreement of the solid line with the results displayed in the inset of Fig. 3.9 for the astrophysical models, in spite of the different computational approaches.

temperature will be about 10^4 K and its density considerably higher than predicted by the β-model. This could boost the expected free-free signal by a large factor (see [224]).

Numerical N-body simulations based on the GADGET-2 code [234] (a combination of Particle Mesh Refinement algorithm and TreeSPH method by [235]) have been used by [232] to compute the distribution of electron density, its temperature and lastly the free-free signal which can be projected into sky maps, evolving from $z = 49$ until $z = 0$ in a cosmological volume with 512^3 dark matter particles and 512^3 gas particles distributed in a box of side $\simeq 300h^{-1}$ Mpc[21].

Each snapshot (the output result in GADGET-2 terminology) is analyzed independently from the others. In order to identify haloes and sub-haloes in the simulations, the authors run the MPI+OpenMP

[21]The force smoothing parameters has been set to 1/30 of the inter particle distance, and corresponds to 20 Kpc for the $300h^{-1}$ Mpc simulation. Initial conditions (at $z = 49$) have been generated with the code 2LPT ([236]) based on a second-order Lagrangian perturbation theory. A concordance model with cosmological parameters $\Omega_\Lambda = 0.73$, $\Omega_{\rm M} = 0.27$, $\Omega_{\rm b} = 0.039$, $\Omega_{\rm K} = 0$, $\sigma_8 = 0.79$, $h = H_0/(100\ {\rm Km\ s^{-1}Mpc^{-1}}) = 0.72$ has been assumed.

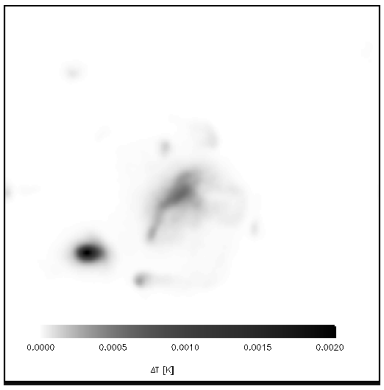

Figure 3.12. Free-free distortion for a massive halo ($M = 6.6 \times 10^{14} h^{-1} M_\odot$) at redshift $z = 0.15$. The greyscale shows the distortion in K and at 1 GHz. The field of view is $\approx 40'$. The total flux in this region is $S_{\rm ff} = 2.83 \times 10^{-5}$ Jy. From [232].

hybrid halo finder AHF[22]. The inside haloes mass only span between $M \approx 10^{11} h^{-1} M_\odot$ and $M \approx 10^{14} h^{-1} M_\odot$. Low mass haloes are not present due to resolution limit. On the high end mass, the limited simulated volume prevents the formation of most massive clusters in simulation.

For each gas particle in the volume, free-free luminosity is computed assuming an electron density nearly constant over the particle volume. After the flux per particle is computed, these are projected along the line of sight into a pixelized 2D map. In order to compare the induced frequency dependent CMB temperature distortion, a mean flux, $\bar{S}_{\rm ff}$, is extracted from the projected maps and then converted into temperature $\Delta T(\nu) = c\bar{S}_{\rm ff}/(2k_{\rm b}\nu^2)$.

Fig. 3.11, bottom panel, shows the corresponding upper limit CMB temperature distortion induced by free-free emission (solid line: mean temperature distortion of the projected map in the sky from simulation; dot-dashed line: result found assuming a constant temperature of $T = 10^4$ K for all particles (see [224]). Since the signal strength depends inversely on the temperature, the lower the gas temperature, the higher the signal. The average free-free distortion predicted from a 300 h^{-1} Mpc N-Body simulation is well below the current observational constraint (*dashed* line). A much lower temperature for the gas (10^4 K) does not change the effect too much because of the weak dependency of the free-free distortion with the temperature[23].

Free-free signal from an individual halo

Finally, we focus on the signal expected from an individual halo. It can be explored comparing the prediction from the β-model with the result obtained from the numerical simulation. The most massive cluster has been extracted from a high resolution simulations (50 h^{-1} Mpc box, $M_{\rm gas} = 0.8 \times 10^7 h^{-1} M_\odot$ per particle) in order to compare its free-free flux with an analytical model. The redshift of the simulation is $z = 1.6$ but the same conclusions can be extracted at other redshifts. It is however interesting to explore the high redshift regime since the free-free signal could be potentially useful to detect clusters in their earlier stages of formation and before the gas is too hot to be seen through X-rays. In this sense, the free-free emission could extend the actual X-ray science in clusters

[22] AMIGA halo finder, to be downloaded freely from http://www.popia.ft.uam.es/AMIGA

[23] Note that the simulated signal is also significantly smaller than the analytical model one. The most likely reason is that the simulation does not include small mass haloes that give most of the signal in the analytical case. These results can be compared with those from the $50h^{-1}$ simulation that has much higher resolution. For example, considering a single slice of 50 h^{-1} Mpc at redshift 1.57 in both cases: in the bigger box the average ΔT is $\Delta T \approx 10^{-6}$ K at 1 GHz while in the smaller box $\Delta T \approx 5 \times 10^{-6}$ K also at 1 GHz.

to the range of the radio waves. Similarly, the same cluster could be seen through the SZ effect but its detection will be harder if the cluster is not hot enough. On the contrary, a lower temperature in the cluster makes the free-free signal stronger.

For the simulation case, [232] find $S_{\rm ff} = 3.67 \times 10^{-9}$ Jy, while the β-model predicts a larger flux $S_{\rm ff} = 2.80 \times 10^{-8}$ Jy (a factor 7.5 larger). In terms of ΔT, the maximum temperature distortion is about a few μK (at 1 GHz) at the center of the cluster, that is, within reach of future planed experiments like SKA. According to [144], SKA could reach a sensitivity limit of 40 nJy in one hour of integration and with an angular resolution of 1 milliarcsecond in the 4-20 GHz band. More massive and denser clusters would produce an even stronger signal making the study of free-free emission in clusters at radio frequencies an interesting and useful way to study the intracluster medium. Fig. 3.12 shows a map of the free-free signal at 1 GHz in an area containing a more massive cluster at redshift $z = 0.15$ extracted from the 300 Mpc simulation. In this case, the free-free distortion is of the order of 1 mK in the cluster regions (while, at higher frequencies, the temperature distortion decreases as $\simeq \nu^{-2}$, being of only $\approx 1\mu$K at 30 GHz).

4 Galaxy Formation and Evolution

4.1 Theoretical Background

G. De Lucia, S. Borgani

Understanding how galaxies form and the physics that drive their evolution has been a long-standing problem in modern astrophysics. Current models of galaxy formation find their seeds in the pioneering work by White & Rees [238] who proposed that galaxies form when gas condenses at the centre of dark matter haloes, following the radiative cooling of baryons. This leads to the formation of a neutral hydrogen reservoir in which denser regions can cool further and form molecular clouds where, in turn, star formation takes place. Therefore, gas provides the basic fuel for galaxy formation, with neutral gas (HI) representing the source of the material that will eventually form stars and molecular gas (usually traced by CO) probing the environments in which stars are currently forming.

Many other physical processes that are believed to play a crucial role in driving galaxy evolution, affect significantly the gas components of galaxies: at high redshift and for small dark matter potential wells, the infalling gas is shock heated to high temperatures but cools so rapidly that it is not able to maintain the pressure needed to support a quasi-static hot atmosphere [239; 240]. In this regime of gas accretion - the so-called cold accretion mode - the star formation rate of galaxies is expected to be directly proportional to the gas accretion rate. Galactic winds induced by supernovae explosions can eject significant amounts of gas from galaxies [e.g. 241, and references therein], and have a large impact on the chemical enrichment of the intergalactic and intra-cluster medium [242; 243]. At the centre of relatively massive haloes, jets from radio-loud AGNs are believed play a crucial role in preventing gas from cooling and forming stars. The conditions under which black holes produce jets are not well understood, but there is clear observational evidence that radio-emitting jets play a role in regulating gas cooling in nearby clusters [see 244, and references therein]. Direct and important constraints on all of the above mentioned physical processes can come through observations of gas content for a large number of galaxies, and over a large redshift range. This is something that only SKA will be able to achieve.

Besides providing key information on the physical processes regulating galaxy formation and evolution, radio surveys represent also powerful tools to constrain cosmological models and the dark content of the Universe. This is achieved through both the study of the large–scale distribution of galaxies, as traced by radio continuum [e.g. 245] and HI redshift surveys [e.g. **?**], and the study of the HI-bearing galaxy population through the HI-line velocity width. As for the former, we refer to Sect. 3.4 (see Chapter 3), devoted to the study of the large–scale galaxy distribution with radio surveys. For the latter, we remind that the analysis of the Arecibo `ALFALFA` survey [e.g. 247] indicates a substantial deficit of galaxies with velocity width $w \simeq 50$ km s^{-1} with respect to predictions of a standard Cold Dark Matter (CDM) model [246]. If confirmed, this result could indicate a that Warm Dark Matter (WDM) model, in which DM particles have a non–negligible free streaming scale, could be responsible for the reduced number density of small haloes hosting galaxies with low HI-line velocity width. Thanks to its sensitivity, SKA will provide very stringent constraints on the

"coldness" of DM.

4.1.1 Numerical Simulations/Theorectical Models: Italian Expertise

As mentioned above, the formation and the evolution of the baryonic components of galaxies is regulated by a number of non-linear processes operating on vastly different scales. These processes combine in a complex network of actions, back-reactions and self-regulation that is very difficult to model. Different approaches have been developed to link the observed properties of luminous galaxies to the dark matter haloes in which they reside. The two most widely used techniques to model galaxy formation in a cosmological context are semi-analytic models of galaxy formation (SAMs) and hydrodynamical simulations.

Modern SAMs take advantage of high-resolution N-body simulations to specify the location of galaxies, and invoke simple, but physically and observationally motivated prescriptions to describe processes such as cooling, star formation, supernovae and AGN feedback, etc. [for a review, see 248]. Since N-body simulations can handle very large numbers of particles, SAMs can access a very large dynamic range of mass and spatial resolution, at small computational cost. In addition, they allow a fast exploration of the parameter space and an efficient investigation of the influence of specific physical assumptions. One second approach is to use hydrodynamic simulations which provide an explicit description of gas dynamics [e.g. 249, and references therein]. These simulations are, however, still limited by relatively low mass and spatial resolution, and by computational times that are still highly prohibitive for high resolution simulations of galaxies throughout cosmological volumes. These studies also require an adequate handling of 'sub-grid' physics to properly take into account the huge range of scales of the different physical processes involved.

The Italian community possesses wide expertise with both approaches. In particular, Italian researchers are among the main developers of two independent SAMs that have been successfully coupled to either large cosmological simulations including dark matter substructures [250, and references therein] or to merger trees obtained using an algorithm that is based on Lagrangian perturbation theory [251, and references therein]. Substantial work has been carried out in the past few years to compare different specific predictions from these models [252–255], and ongoing work is being devoted to update or extend the modelling of different specific physical processes. Like most of the available SAMs, the two models mentioned above treat the interstellar medium (ISM) of galaxies as a single star-forming phase. This can be broken into atomic and molecular hydrogen either using empirical relations [256; 257], or by including a self-consistent treatment of the ISM and star formation [258; 259]. In particular, the latter models mentioned implemented two ways to estimate the partition between H_2 and HI: (i) an empirical relation that relates the molecular-to-atomic surface density ratio to the hydrostatic pressure within the disc [260] and (ii) a theoretical model that estimates the abundance of molecular gas from the balance between the dissociating radiation flux and the formation of molecules on the surface of dust grains [261]. Similar prescriptions can be easily implemented in the models available to the Italian community. In addition, the models mentioned above neglect or consider only in part the relatively strong dependency on metallicity of the transition between atomic and molecular gas. Finally, both models use a simplified treatment of chemican enrichment based on the instantaneous recycling approximation, i.e. the models neglect the finite lifetimes of stars and their dependency on stellar mass. In contrast, the model by De Lucia & Blaizot [250] has been recently updated to include a more sophisticated and self-consistent chemical model that is able to follow the abundances of individual elements and that accounts for the dependency of stellar lifetime on stellar mass (De Lucia et al., in preparation). Taking advantage of these new prescriptions, the modelling of the transition from HI to H_2 can be carried out in a self-consistent way.

The Italian community also includes a very active group of researchers working on hydrodynamical cosmological simulations. Italian researchers have been the first to include a self-consistent chemical enrichment model in the framework of simulations carried out using smoothed particle hydrodynamics [243]. In addition, Italian researchers have recently developed a new subresolution model for star formation and feedback [262] that computes the cold gas molecular fraction using the phenomenological relation between this fraction and the external disc pressure [260]. The prescription used in this model for star formation is not based on imposing the Schmidt-Kennicutt relation, that is instead naturally reproduced in the framework of the proposed scheme. The new model also reproduces the basic properties of the interstellar medium in disc galaxies, the surface densities of cold and molecular gas, of stars and of star formation rate, the vertical velocity dispersion of cold clouds and the flows connected to the galactic fountains. The scheme also provides efficient stellar feedback without the need to include a model for kinetic energy feedback. Recent work based on this model [263] has shown that stellar feedback strongly affects the termodynamical state of the gas accreting onto galaxies. In particular, an efficient thermal feedback would produce significant amounts of 'warm' gas (with temperature between 2×10^5 K and 10^6 K) accreting onto galaxies at high redshift, with important consequences on the observability of gas flows infalling onto high redshift galaxies. Finally, work is ongoing to quantify the flows of metals and masses determined by the proposed scheme. These data will be used to implement a new stellar feedback scheme in the semi-analytic models available to the community so as to test the validity of the proposed scheme on scales different than those tested so far with hydrodynamical simulations. Stellar feedback is expected to have a strong impact on the distribution of different baryonic components [264]. SKA and its precursors will put strong constraints on these models.

As for the cosmological applications of the SKA surveys, the Italian community has large expertise in carrying out cosmological N–body simulations for non–standard DM models. Interfacing large simulations of WDM [e.g. 265] with the above described semi–analytical models of galaxy formation would offer the possibility of comparing in detail observations of HI-line velocity width to theoretical predictions with the purpose of placing stringent constraints on the free–streaming scale of the DM particles.

Thanks to the complementary expertise in models of galaxy formation and numerical simulations of large-scale structure formation, members of the Italian community are also involved, within the Euclid collaboration, in the generation of large mock catalogues. These catalogues, extracted from large cosmological simulations, represent a very useful tool for developing complex software pipelines to analyse the statistical properties (e.g. correlation functions and power spectra) of the galaxy distribution [e.g. 266]. At the same time, mock catalogues are also used to quantify the impact of different survey selection functions and/or observational biases through a detailed comparison between observations and model predictions. Numerical methods based on Lagrangian Perturbation Theory (LPT) [e.g. 267; 268], interfaced with SAM and Halo Occupation Distribution (HOD) models [e.g. 269], will provide a flexible and efficient tool to genetate mock SKA galaxy surveys.

4.2 Radio-Continuum Studies

I. Prandoni, G. de Zotti, L. Hunt, M. Magliocchetti, P. Tozzi, Z.-Y. Cai, M. Negrello

The problem to understand the formation and evolution of galaxy populations has been addressed in the past by using optical and near-infrared surveys, culminating in the first attempts to determine the integrated star-formation history (SFH) of the Universe [e.g., 270; 271]. However, these early attempts and many later ones have been hampered by the large uncertainties in the corrections for dust extinction, necessary to measure star-formation rate (SFR) from rest-frame ultraviolet (UV) or Hα

fluxes [e.g., 272; 274; 444]; such corrections can be as large as a factor of 20 or more [e.g., 275; 276]. The problem is compounded because the obscuration itself has been found to depend on galaxy mass (more massive galaxies are more obscured) and on SFR (higher SFR means more obscuration [277; 278]). Because of this complexity, much of the effort devoted to the study of galaxy formation and evolution has been dedicated to the calibration and correction of different SFR tracers at different rest-wavelength regimes. Infrared (IR) measurements are one way around this problem, and recent *Spitzer* and *Herschel* deep surveys have made considerable advances in tracing dust emission and SFR to $z \sim 2$ [e.g., 279; 280]. However, the limited spatial resolution of these diffraction-limited telescopes mandates radio follow-up to precisely locate the objects within the large IR beams. The radio continuum is a powerful and unbiased tracer of SFR [e.g., 281], but current sensitivities require stacking analyses to examine galaxy populations at high redshift [282; 283]. In the following we will discuss how the spatial resolution, field-of-view, and sensitivity of SKA will revolutionize tracing SFR in star-forming galaxies via the radio continuum.

To reliably interpret the integrated SFH over cosmic time, we need to break it down, and independently track the star formation activity assembling stellar mass in the rotationally- and pressure-supported structural components of galaxies (disks and spheroids or bulges), as well as the variation of these processes with redshift, galaxy mass and environment. Early attempts to do this, using high-resolution ($\sim$ 100−mas) optical imaging from *Hubble Space Telescope* (HST), suggested that the strong increase seen in the integrated star formation rate in the Universe out to $z \sim 1$ is driven by increasing activity in disk galaxies [e.g., 284]. More recent studies, based on high-resolution HST surveys (e.g., CANDELS), confirm that massive galaxies at $1 < z < 3$ are increasingly disk-dominated with increasing redshift [285; 286]. Although nearby disk galaxies are actively forming stars and spheroid- or bulge-dominated systems are more quiescent, a significant fraction of the most quiescent galaxies at $1 < z < 3$ have disk-like morphology. Nevertheless, the relations that give rise to the Hubble sequence of morphology in galaxies at $z = 0$ already seem to be in place at $z \sim 2$ [287].

Current theoretical models of galaxy formation and evolution ([e.g., 288–290]) are able to crudely reproduce the properties of present-day galaxies as well as some of their characteristics at earlier times - such as the evolution of the SFR, peaking at $z \sim 2-3$ ([e.g., 292; 464]). A key ingredient of modern galaxy formation models is feedback from supernovae and from active nuclei ([e.g., 293–295]) found to be ubiquitous in the centers of spheroidal components of galaxies (see [296] for a comprehensive review). Feedback effects have a crucial role in shaping both the high-mass, high-luminosity and low-mass, low-luminosity tails of the galaxy distribution. Supernova feedback quenches the star formation in small halos, making the low-luminosity portion of the galaxy luminosity function flatter than the mass function of dark matter halos. On the other hand, the AGN feedback quenches the star formation in the most massive galaxies, causing the luminosity function to sink down, at high luminosities, much faster than the halo mass function. AGN feedback may also explain the observed relationship between the masses of super-massive black holes (SMBHs) and those of the pressure-supported spheroids hosting them [e.g., 297–299]. Indeed, the peak of QSO activity has been established at $z \sim 2-3$ [e.g., 300; 301], i.e., at the same epochs as the peak of star formation activity [271; 464]. Although it is not yet clear whether SMBH growth occurred mainly through galaxy mergers or efficient gas accretion [e.g., 302–305], or primarily in Compton-thick, obscured environments, a significant fraction of Compton-thick AGN at $z \sim 2-3$ is necessary to explain the cosmic X-ray background [306], as well as the local SMBH mass function [304]. Moreover, observational evidence of an obscured, embedded AGN population at $z \gtrsim 2$ is mounting [307–310].

Hence, an essential step in testing galaxy formation theories is a better assessment of the importance of embedded AGN activity in star-forming galaxies. We need to identify the contribution of obscured accretion activity in bolometric surveys and quantify its impact on the evolution of star

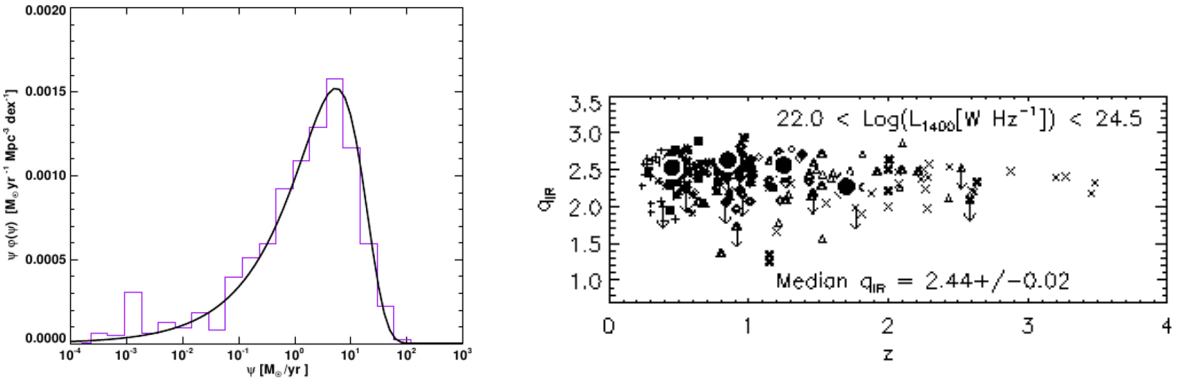

Figure 4.1. *Left:* The SFR density function as a function of SFR for the Local Universe. The integral under the curve gives the total SFR volume density at $z \sim 0$. The plot shows a 'characteristic SFR' at $z = 0$ of $\sim 9\,M_\odot\,yr^{-1}$ [Figure from 311]. *Right:* q_{IR} versus redshift for galaxies in the radio-selected sample of [314]. Filled circles show values of q_{IR} for another sample, selected at 24 μm. Figure from [314].

formation. In other words, we need to identify and separately trace the total (obscured and unobscured) star formation in individual high-redshift galaxies, the related nuclear activity, and any star formation occurring on larger scales within a disk. Only by doing this we will be able to obtain a bolometrically complete census of star formation and the growth of galaxies and their SMBHs. However, observations have provided little input into this (predominantly theoretical) scenario and as a result, much uncertainty remains about the rate of build-up of the stellar populations in galaxies over cosmic time, the distribution of newly formed stars among different structural components, including clumps, and the role of mergers or secular processes in driving this growth. The lack of observational constraints arises from current facilities's lack of sensitivity, dust-penetrating power and resolution needed for an unbiased census of the total number of new stars being formed in galaxies at high redshifts, their integrated SFR density and distribution within the galaxies, and the role of AGN activity in this growth. A complete census of both star formation and AGN galaxy activity is missing at high redshifts, where dust extinction and gas obscuration by circumnuclear material are thought to play a major role. Hence there is an urgent need to exploit a sensitive, dust-insensitive tracer of star formation, to obtain a spatially-resolved view of galaxy formation which can identify and disentangle the various physical processes driving the evolution of galaxies. We will outline how SKA can meet this challenge.

4.2.1 The Star Formation History

The radio continuum is an optimum tracer of star formation because of its capacity to penetrate significant dust obscuration. As discussed below, the only caveat is that the conversion from non-thermal radio emission to SFR does not change significantly with redshift. Typical SFRs in star-forming galaxies at $z \sim 0$ are shown in Fig. 4.1 where the left panel reports the SFR volume density measured in the Local Universe [311]. In the Local Universe, the most likely place for a star to form is in a galaxy with a SFR $\sim 9\,M_\odot\,yr^{-1}$. The integral of the curve gives the total SFR density at $z \sim 0$, and the integral of the curve to the right of the peak shows that *locally* roughly 20% of the SF is occurring in 'starbursts', with SFR $\gtrsim 9\,M_\odot\,yr^{-1}$. However, this fraction is highly debated, both in the Local Universe, and at $z \gtrsim 2$ where starbursts host from $\lesssim 10\%$ (less than locally) to $\gtrsim 50\%$ of the star-formation activity [312; 313].

Much of the discrepancy among these estimates arises from different definitions of starbursts at different redshifts, and of how SFRs in different galaxy populations are determined. Sensitive radio–

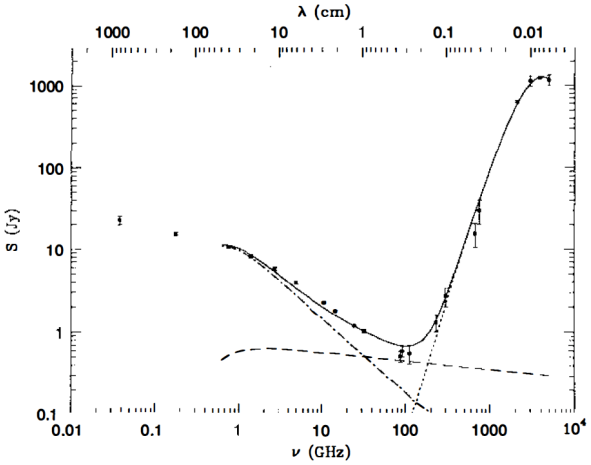

Figure 4.2. The observed radio/FIR spectrum of M82 is the sum (solid line) of synchrotron (dot-dash line), free-free (dashed line), and dust (dotted line) components. The H II regions in this bright starburst galaxy start to become opaque below $\nu \sim 1$ GHz, reducing both the free-free and synchrotron flux densities. The free-free component is largest only in the poorly observed frequency range 30–200 GHz. Thermal re-radiation from $T \sim 45$ K dust with opacity proportional to $\nu^{1.5}$ swamps the radio emission at higher frequencies. Lower abscissa: frequency (GHz). Upper abscissa: wavelength (cm). Ordinate: flux density (Jy). Figure from [281].

continuum studies will provide a unique and reliable tool to trace star-forming galaxies from the local Universe out to $z \sim 5$, down to very modest SFRs.

Much of the power of the radio continuum derives from the very tight correlation between the far-infrared (FIR) and radio luminosities of ordinary and star-forming galaxies [281; 315–317; 356]. Following [315] this is usually expressed as

$$L_{1.4\mathrm{GHz}} = 10^{-q_{\mathrm{IR}}} \frac{L_{\mathrm{IR}}}{3.75 \times 10^{12}\,\mathrm{Hz}} \quad , \tag{4.2.1}$$

where $L_{1.4\mathrm{GHz}}$, in W Hz^{-1}, is the monochromatic luminosity at 1.4 GHz. Defining L_{IR} as the total luminosity between 8 and 1000 μm (a choice somewhat different from L_{FIR}(42.5–122.5 μm) used by [315]) [314] and [319] find $q_{\mathrm{IR}} \simeq 2.4$.

This simple relationship holds over a very wide range of luminosities from normal, radio-quiet spirals to ultra-luminous IR galaxies (ULIRGs). Surveys with the *Spitzer* [318] and *Herschel* [314; 319] satellites have demonstrated that the IR-radio correlation not only is independent of galaxy type and luminosity, but also appears not to change significantly as we move back into the epoch of galaxy formation (see, e.g., Fig. 4.1, right). If so, there are interesting implications for the study of galaxy formation and evolution. Since the IR luminosity is an excellent tracer of the star formation rate (SFR), the tight IR/radio correlation implies that we can use radio observations alone to measure the SFR up to high redshifts and thus to reconstruct the cosmic star formation history. A first attempt in this direction was made by [320]. Emission associated with AGN activity yields much higher radio to IR luminosity ratios than implied by eq. (4.2.1), so to measure SFRs from radio luminosities care must be taken to exclude the AGN-related component. This can be largely achieved using a variety of indicators, as further discussed below.

The radio–IR correlation is based on radio synchrotron emission, which is however an indirect tracer of star formation because of spatial diffusion over 100 Myr timescales. A much more direct tracer is radio free–free emission [281; 321; 322]. For star–forming galaxies near the apparent peak epoch in the star formation rate density (SFRD) at $z \sim 2-3$, the emission observed at e.g. 10 GHz arises at a rest-frame frequency of 30−40 GHz, probing the regime where free-free emission begins to dominate over synchrotron (see Fig. 4.2). Thus sensitive observations at radio frequencies >1.4 GHz,

along with parallel deep observations at 1.4 GHz, will allow the identification and separation of free–free and synchrotron emission components in high-redshift star–forming galaxies [e.g., 323]. This will provide a unique and powerful tracer of SFR at high redshift to assess the evolution of the SFRD and to calibrate and test less reliable tracers such as rest-frame UV or Hα.

Importantly, sensitive observations at centimetre wavelengths with long baseline ($>$ 100 km) interferometers enable accurate determination of source position; this is not possible with the large beams of diffraction-limited IR satellites such as *Spitzer* and *Herschel* or ground-based sub-millimetre surveys. SKA will also be able to probe star formation activity on scales of 50 – 2000 mas within the high-redshift population. These angular scales correspond to spatial resolutions spanning sub-kpc to 10's of kpc at $z > 1$, ideally suited for mapping the distribution of star formation within these systems. With SKA, we can investigate whether star formation occurs predominantly in clumps [324; 325], in diffuse massive disks [e.g., 326; 327], or in compact nuclear bursts [328].

4.2.2 The Black Hole Cosmic Accretion History

One of the most fundamental issues in understanding the role of AGN in galaxy formation and evolution is the need to measure accurately the cosmic evolution of AGN activity and the super-massive black hole (SMBH) accretion history of the Universe, and to compare it with the build-up of the stellar populations of galaxies. In other words we need to understand whether black holes and their host galaxies grow coevally, or whether one precedes the other. Much of the growth of black holes is believed to occur in an obscured phase, and these obscured AGN are difficult to identify. Even the deepest current X-ray observations do not detect the most heavily absorbed sources which Cosmic X-ray Background synthesis models predict to exist in abundance [e.g. 306], implying that much high-z quasar activity has yet to be detected directly.

Radio–continuum surveys are traditionally recognized as very powerful in probing radio-loud AGNs up to very high-redshift, which however constitute only a small fraction ($\sim$ 10%) of the overall AGN population. Nevertheless recent multi-wavelength studies of deep radio fields, have shown that a significant fraction (30 – 50%) of the AGNs detected in these fields are characterized by low radio/optical (and radio/IR) ratios, as compared with classical radio-loud AGNs ([see e.g. 329; 330]. This is a first direct evidence of 'radio-quiet' AGNs being present at μJy flux levels (see also Fig. 4.3, left). Such result supports theoretical modeling [331; 332] and follow-up observational work [333; 334] indicating that 'radio-quiet' AGNs are not necessarily radio silent, paradoxically opening the perspective of studying the entire AGN population, including the radio-quiet component, at radio wavelengths. In other words, deep radio surveys offer an alternative route to identifying distant AGN, in a manner which is unbiased by dust and gas absorption at other wavelengths. Combined with multi–wavelength datasets to separate source populations, the relative contribution of radio-quiet AGN to the faint radio source population can be determined. This will enable investigation of the dependence of the fraction of obscured AGN on luminosity and cosmic epoch, and thus the history of SMBH accretion in the Universe to be determined.

4.2.3 The Role of AGN Feedback in Galaxy Evolution

AGN activity – ie. black-hole growth – occurs in at least two different modes, each of which may have an associated feedback effect [e.g. 335]:

(i) a fast accretion mode [e.g. 336], also known as 'quasar mode'; this radiatively–efficient accretion mode is mostly associated with (radio–quiet) quasars and/or high-luminosity radio galaxies, and may be important in curtailing star formation at high redshifts and setting up the tight relationship between black hole and bulge masses observed in the nearby Universe [e.g. 297].

(ii) a radiatively–inefficient slow accretion mode [e.g. 337],Bower2006, also known as 'radio mode', the observational manifestation of which is low-luminosity radio galaxies; this mode is thought to be responsible for preventing strong cooling flows in galaxy clusters [e.g. 338].

Thanks to their ability to probe the overall AGN population, future deep large-area radio surveys, can be used to assess both accretion modes, and to identify and quantify the physical processes involved in 'AGN feedback'. Of particular importance is the role of radiatively–inefficient accretion mode in galaxy evolution. Significant progress towards this end has been made in recent years, through studies in the local Universe, but to fully quantify the effect of AGN it is necessary to extend such studies back to earlier cosmic epochs where the AGN and star-formation activity of the Universe peaked. The population of low–excitation (typically low–power) radio-loud AGNs (the numerically dominant population), show little evidence for radiative emission from an accretion disk, and the bulk of the accretion power is channelled into the expanding radio jets [e.g. 339; 340]. These sources are distinct from the high–excitation (quasar–like) radio-AGN in their luminosity function, Eddington accretion ratios, host galaxy properties, and possibly cosmic evolution [at a given radio luminosity; e.g. 341]. Their radio jets pump energy into their environments, inflating cavities in the surrounding inter-galactic and intra-cluster medium.

The role of the fast and slow accretion modes accretion modes appears to be strongly influenced by the environment (e.g. Tasse et al. 2008; Falder et al. 2010) while the presence or absence of a radio-loud AGN appears to be a strong function of the stellar mass of the host galaxy [e.g. 342; 343]. The time–averaged energetic output associated with recurrent radio source activity may indeed be sufficient to control the rate of growth of massive galaxies. However, sensitivity limits of current large-area radio surveys mean that these low luminosity sources are only observed in the nearby Universe. Hence several questions remain unanswered: how does the relation between galaxy mass and radio-AGN fraction (the radio source duty cycle) evolve with redshift; out to which redshift does the radio-AGN heating continue to balance cooling; what is the differential evolution of the radiatively efficient and inefficient accretion modes [see e.g. 341]; what drives these processes. This is key information for any attempt to incorporate kinetic feedback from radio-loud AGN in models of galaxy, group and cluster formation and evolution (see § 6.1.5 for more details), and are key questions for the next generation radio arrays. Large-area surveys are required in order to study a sufficient volume to include the full range of galaxy environments, given the very important role that large-scale environment can play in the evolution of galaxies (see § **??** for more details).

4.2.4 Separating Star Formation from AGN Activity in Radio Sources

As illustrated in the previous sections, large deep radio–continuum surveys provide a powerful, obscuration independent, tool for measuring *both* star formation and AGN activity in high-redshift galaxies, hence tracing the apparently simultaneous development of the stellar populations and the black hole growth in the first massive galaxies. However, this requires that radio sources triggered by star formation can be reliably separated from those triggered by nuclear activity.

This is a recognized issue for deep radio surveys, and a variety of diagnostic tools, have been developed to distinguish star formation from AGN activity in radio sources. Such tools are mainly based on multi-wavelength/band analysis of the source properties, demonstrating the strong synergies existing between future deep radio surveys and deep surveys that will be undertaken at other wavelengths. In particular the radio–IR ratio (see e.g. eq. 4.2.1), proves to be very effective in separating radio-loud AGNs from star-forming galaxies; radio morphology and radio spectral index studies allows to distinguish extended AGN-driven steep-spectrum radio-galaxies characterized by 10's–100's kpc-scale jets and/or lobes from flat-spectrum core-dominated radio–AGNs [e.g. 344–347]. Other

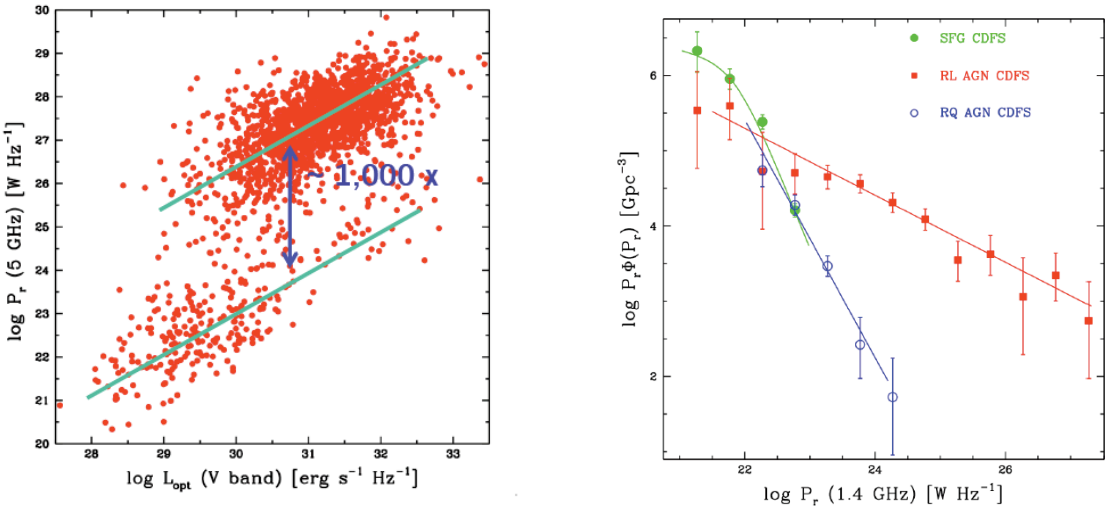

Figure 4.3. *Left panel:* Radio luminosity (5 GHz) against optical luminosity (V-band) for a radio source sample from the CDF South field, showing the 1000× jump in radio/optical luminosity ratio between star-forming galaxies (and radio-quiet AGN) and radio-loud AGNs. *Right panel:* Radio luminosity function for the different classes of sources in the same sample: radio-loud AGNs (red), star-forming galaxies (green), radio-quiet AGNs (blue). Figures from [330].

tools to distinguish between radio–loud AGN and star-forming galaxies include the classical analysis of optical line ratios [e.g. 348]; radio polarization and variability [e.g. 349].

However, recent studies have shown that radio–quiet AGN share many properties with star-forming galaxies: they have similar radio luminosities (10^{22-24} W Hz^{-1}) and similar optical– and infrared–radio flux ratios (see Fig. 4.3, left). In addition radio-quiet AGNs are typically characterised by Seyfert-2-like optical spectra, which are often difficult to distinguish from those of star-forming galaxies [see e.g. 329]. This makes it difficult to separate radio-quiet AGNs from star-forming galaxies, even with multi-wavelength information, although the availability of IRAC colors and/or X-ray data can help [329; 330; 350; 351]. In addition, there is growing recognition that many galaxies are not simply 'star-forming' or 'AGN' but include a significant contribution from both. Seyfert 2 galaxies are a well-established example in the local Universe [see e.g. 352], but recent studies indicate that composite AGN/SF systems may constitute a significant fraction of the galaxy population at high redshifts [see e.g. 307; 309; 353]. This means that a simple classification into AGN or SF galaxy can be inadequate, and that the contribution to the galaxy luminosity from both AGN and SF activity must be assessed, so to measure the relative contributions from underlying physical properties such as black hole and galaxy mass, star-formation rate, environment, etc. Only once star-forming galaxies and AGN are reliably separated, and the starburst and AGN fractional contribution to individual sources are determined, it is possible to derive results such as luminosity functions and relative contributions by type to the source counts.

Techniques based on optical/IR Spectral Energy Distribution (SED) fitting algorithms, including both a starburst and an AGN component, have been used to recognize embedded low-luminosity AGNs in radio sources dominated by star-formation [see e.g. 354], and viceversa. This, however, does not necessarily tell us about the dominant physical process responsible for the radio emission itself. As pointed out by [330], sources classified as radio-quiet AGN (based on their properties at other wavebands) can be described by a radio luminosity function, which is very similar to that obtained for star-forming radio sources (see Fig. 4.3, right panel), strongly suggesting that the radio

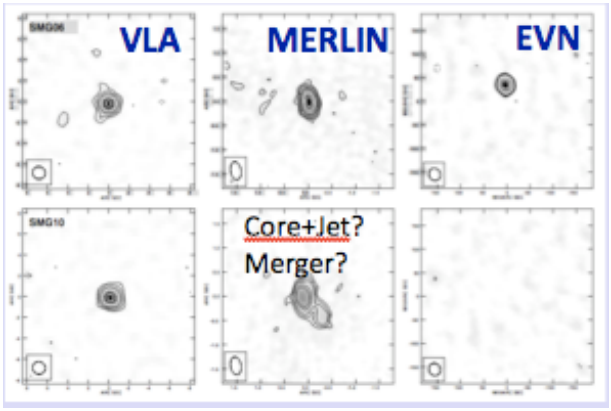

Figure 4.4. Radio emission at 1.4 GHz on arcsec scale (VLA, left), on 200 mas scale (MERLIN, middle) and mas scale (EVN, right) for two galaxies in the HDF North field, at $z \sim 2.7$ (top panels) and at $z \sim 1.2$ (bottom panels) respectively. An AGN core is detected in the upper object at VLBI scale, while no VLBI detection is found for the other, supporting a merger scenario, over a jet+core one. Figure from [363].

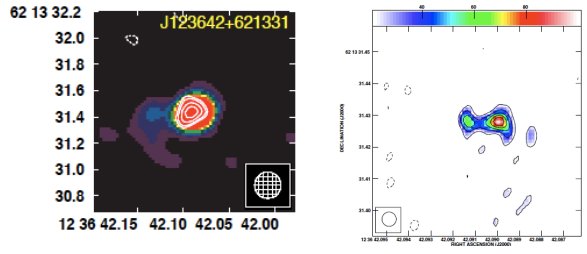

Figure 4.5. *Left panel:* Radio emission on 200 mas scale at 1.4 GHz (colors) and 5 GHz (white contours) for an ultraluminous galaxy at $z \sim 4.4$ in the GOODS-N region. Figure from [361]. *Right panel:* VLBI–scale 1.6 GHz radio emission (both colors and contours) from the same galaxy. Figure from [358].

emission in such AGNs is actually triggered by star formation. In other words, a very careful analysis of the radio properties is needed in order to assess whether the radio emission in individual objects is due to star formation, AGN activity, or both. One of the most direct ways to pinpoint embedded radio–AGN cores in galaxies is the detection of high surface brightness ($T > 10^7$ K) radio emission through high resolution – VLBI-like – observations. In order to reliably separate radio structures on several scales, from AGN core/inner jets (<< 1 kpc) to nuclear/disk starbursts (≥ 1 kpc) in high redshift ($z > 1$) galaxies, sub-μJy imaging sensitivity together with milli-arcsec resolution is clearly crucial [see e.g. 355–358]. Figures 4.4 and 4.5 show examples of the powerfulness of this technique. In Figure 4.4 two intermediate/high redshift galaxies in the HDF North have been observed at 1.4 GHz from arcsec to mas scales. At VLBI scale an AGN core is detected in the first galaxy, while no VLBI detection is found for the second, supporting a merger scenario, over a core+jet one. This implies that in this object star formation processes are at work. Figure 4.5 shows a distant ($z \sim 4.4$) ultra-luminous infrared galaxy identified in the GOODS-N region, and interpreted as a dusty star-forming galaxy with an embedded weak AGN [359]. Such galaxy was observed at 1.4 GHz with the MERLIN+VLA interferometers. The 1.4 GHz radio emission (Figure 4.5, left) shows both diffuse and compact sub-arcsec radio structures, indicating the possible presence of coexisting star formation and AGN activity [360]. Compact emission was later detected through eMERLIN 5 GHz observations (see white radio contours in Figure 4.5 left; [361]), further supporting the presence of a weak embedded AGN core at its center. Deep, higher-resolution 1.6 GHz global VLBI observations (baselines > 1000 km) removed all doubts, resolving the compact emission detected at 5 GHz in a jet+core structure (Figure 4.5, right; [358]). The separation between the jet and the AGN core is about 70 pc. This may be an example of a high redshift ultra luminous infrared galaxy in which the high star-formation rate and the efficiency are enhanced by AGN jet activity [e.g. 362]. Future extensive deep high-resolution surveys will allow us to systematically apply this technique to much larger high-redshift source samples.

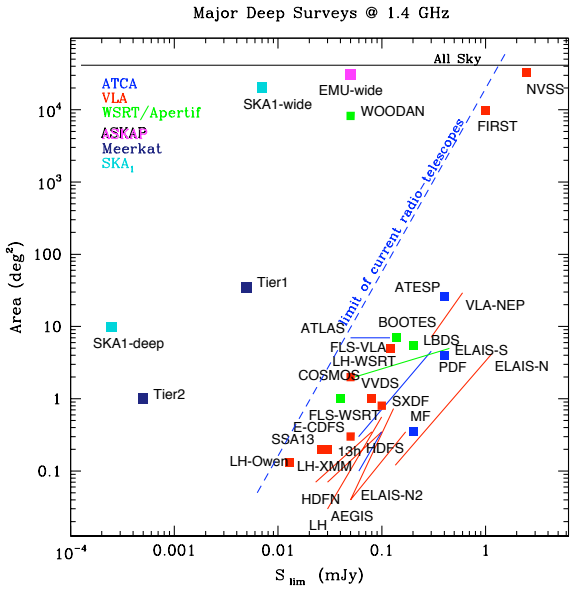

Figure 4.6. Comparison of existing and planned deep 1.4 GHz radio surveys. The horizontal axis shows the 5σ sensitivity, and the vertical axis shows the sky coverage. The diagonal dashed line shows the approximate envelope of existing surveys, which is largely determined by the availability of telescope time. The squares to the left of the diagonal line represent the new radio surveys planned with the two SKA precursors (ASKAP and Meerkat), with the APERTIF upgrade of the Westerbork (WSRT) radio telescope, and two possible surveys for SKA Phase 1 (Huynh, private comunication). Figure adapted from [1].

4.2.5 The role of future deep radio–continuum surveys: the pathway to SKA

The new generation of radio interferometers, from SKA pathfinders and precursors to SKA in its two implementation phases, will allow us to observationally address the several open questions discussed above in incremental steps. In the lead-up to the SKA, several next-generation radio telescopes and upgrades are coming on line around the world, including APERTIF (The Netherlands), eMERLIN (UK), EVLA (USA), e-EVN (based in Europe), LOFAR (The Netherlands), MWA (Australia), and the two SKA precursors: ASKAP (Australia) and Meerkat (South Africa). Large and or deep continuum surveys are being planned for many of these telescopes. Most of these surveys have multiple science goals (see Chapter 2 for more details), but they have one goal in common, which is to survey the radio continuum emission from galaxies, in order to understand the formation and evolution of galaxies over cosmic time, and the cosmological parameters and large-scale structures that drive it.

In particular, future deep high-resolution centimetric radio continuum observations will provide the temperature and dust-obscuration-insensitive tool required to resolve and measure the massive SF and nuclear activity in high-redshift galaxies, and so track the growth of their stellar populations and of the SMBH at their center. Combined observations at two or more radio frequencies will provide the opportunity to spectrally and morphologically identify embedded AGN activity in galaxy populations. This is critical for two reasons. Firstly, it allows us to remove the contribution from obscured accretion activity from the radio SFRD as a function of redshift and so ensure we trace the true global evolution of SF in the Universe [e.g. 320]. Secondly, by mapping the relative frequency of starburst and AGN activity within galaxies as a function of redshift we can test the role of AGN feedback in controlling SF within galaxies. Including high-frequency ($\geq$ 5 GHz) observations will provide the first measurements of the evolution of the SFRD in the Universe using the best measure of SFR: the free-free radio emission. Probing radio emission on several scales (e.g. from 10 mas to 2 arcsec) will yield a statistically-robust measurement of the distribution of SF within galaxies at the era of their peak activity, to determine the nature of the structures in which these stars are forming (disk, clumps or bulge). Such observations will also trace the relationship between SF and AGN feedback at this critical juncture, when the characteristics of massive galaxies may be defined, providing the essential observational constraints on the input physics needed to refine current cosmological simulations of

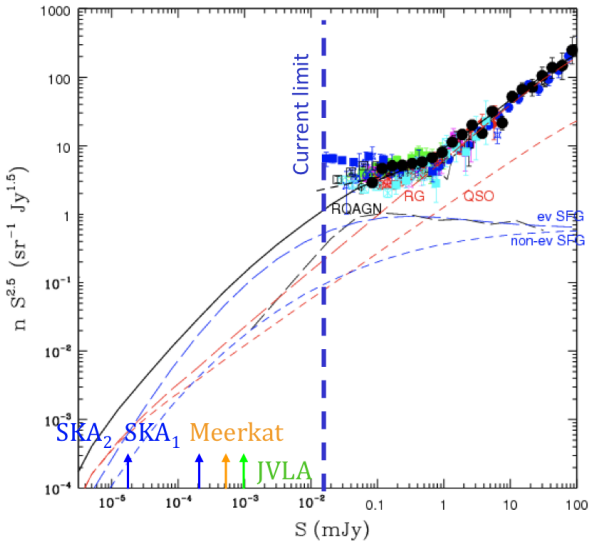

Figure 4.7. Comparison of existing 1.4 GHz source number counts with the modeling of the faint ($sub-mJy$) radio population proposed by Wilman et al. (2008): star-forming galaxies (blue dashed lines), radio-loud AGNs (red dashed lines), radio-quiet AGNs (black dashed line). The black solid line is the sum of all models, while the vertical blue dashed line indicate the flux limit of current deep surveys. Also indicated are the flux limits that will be reached by JVLA and Meerkat, and by SKA in its two implementation phases (SKA1 and SKA2).

galaxy evolution.

Such kind of studies will be possible down to ~ 1 μJy sensitivities on limited areas of the sky with the upgrades of current telescopes (JVLA, eMERLIN), will be extended to much larger areas and/or deeper sensitivities with the SKA precursors (ASKAP and MeerKat), and will further explore the sub-μJy sensitivity regime with SKA Phase 1 (SKA1) and SKA Phase 2 (SKA2).

The predicted sensitivities and areas for the major 1.4 GHz future surveys are shown in Figure 4.6, together with existing 1.4 GHz continuum radio surveys. The largest existing radio survey, shown in the top right, is the wide but shallow NRAO VLA Sky Survey (NVSS) (Condon et al. 1998). The most sensitive existing radio survey (~ 10 μJy flux density limit) is the deep but narrow Lockman Hole observation [364] in the lower left. All current surveys are bounded by a diagonal line that roughly marks the limit of available telescope time of current-generation radio telescopes. The region to the left of this line is currently unexplored, and this area of observational phase space presumably contains as many potential new discoveries as the region to the right. In particular it will be possible to constrain the current modeling of the composite faint (sub-mJy) radio population, as shown in Fig. 4.7, where the source counts derived from current deep radio surveys are compared to the modeling scenario proposed by [332]. In such a scenario the faint radio population is modeled in several components, including star-forming galaxies, radio-loud AGNs and a radio-quiet AGN component, in which the radio emission is inferred from the hard X-ray emission properties of X-ray selected AGN samples.

An example of the radio luminosity functions [based on modeling by 332] that will be derived for both star-forming galaxies and AGN combining the planned ASKAP and Meerkat 1.4 GHz surveys is shown in Fig. 4.8. It is clear that the brightest (Arp220-like) starbursts will be traced out to redshift ~ 5, while MW-like galaxies ($\sim 10^{21.5}$ W Hz^{-1}) will be probed up to $z \sim 0.5-1$. In addition, the local star-forming galaxy luminosity function will be probed down to 10^{19} W Hz^{-1}. On the other hand, the combination of ASKAP and Meerkat surveys will trace the low-power ($> 10^{23}$ W Hz^{-1}) component of the radio-loud AGN population up to the highest redshifts ($z \sim 4-5$) and will be able to trace the radio-quiet AGN component ($\sim 10^{22}$ W Hz^{-1}) up to $z \sim 1-2$.

As illustrated in Fig. 4.9, the much deeper samples that will be made available by the SKA will allow us to trace (modest) starbursts ($SFR \sim 1-10$ M$_\odot$ yr^{-1}) such as those in the Local Universe

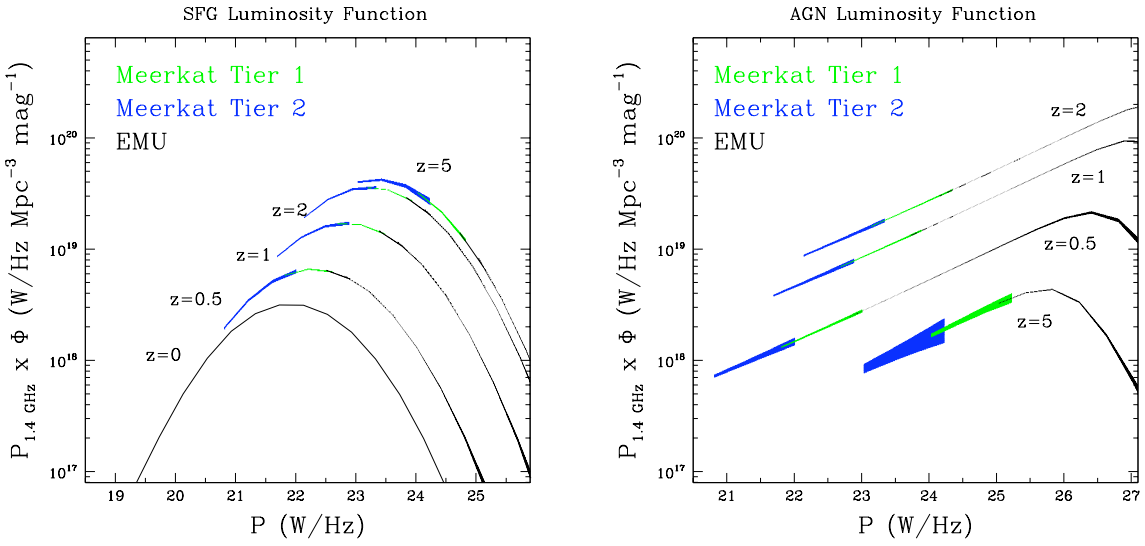

Figure 4.8. Luminosity function at different redshifts that can be obtained from the combination of ASKAP and MeerKat deep surveys for star-forming galaxies (left panel) and AGNs (right panel). Based on Wilman et al. (2008) modeling. Figures from [1].

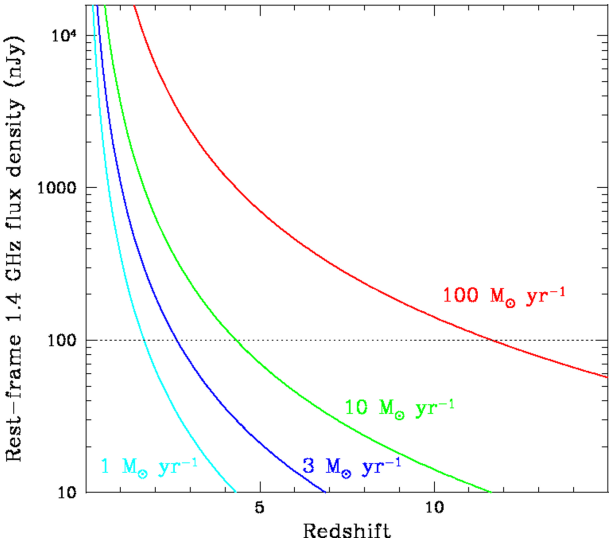

Figure 4.9. Rest-frame 1.4 GHz flux density for a given SFR as a function of redshift, assuming a non-thermal origin for the radio emission. The full SKA 8-hr 3σ limit of 0.1 μJy is shown as a horizontal dotted line.

(see Fig. 4.1, left panel) out to $z \gtrsim 5$. With an 8-hr integration, full SKA (SKA2) images at 1.4 GHz and higher frequencies (up to 10 GHz) will probe SFRs at $z \sim 3$ equivalent to those in the 400-orbit *HST* Ultra-Deep Field at rest-frame UV wavelengths [365]. However, the SKA field-of-view will be $\sim$1 deg^2, dwarfing the 202×202 arcsec^2 *HST* field.

Another interesting perspective for future deep radio surveys regards the possibility to shed light on the physical processes responsible for the radio emission in radio-quiet AGNs, which are currently matter of debate. As pointed out earlier, [332] propose a model where the radio emission has a non-thermal AGN-related origin, while the multi-wavelength data analyzed by [330] (see Fig. 4.3) suggest that the radio emission in radio-quiet AGNs is closely related to star formation. On the other hand, the detection of compact, high brightness temperature cores in several (mostly local) radio-quiet AGNs hits at a possible coexistence of two components, one non evolving and AGN related, and one

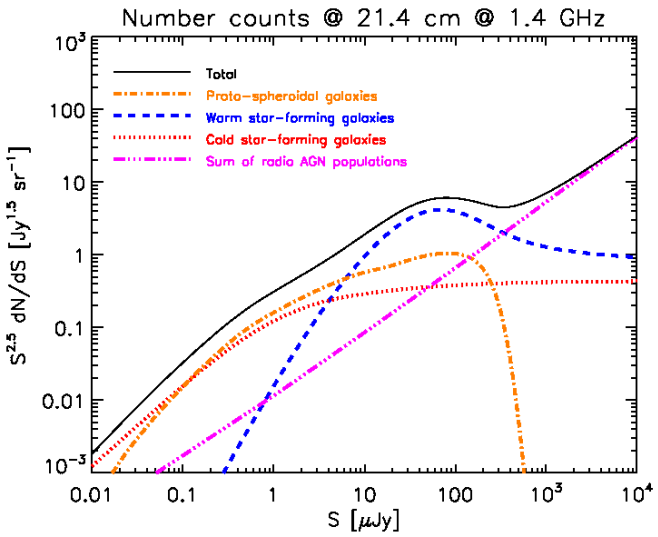

Figure 4.10. Contributions of different populations of star-forming galaxies and of radio-loud AGNs to the (sub)-mJy source counts at 1.4 GHz as modeled by Cai et al. (in prep). The various source components are indicated in the legenda. Warm and cold star-forming galaxies refer to starbursts and normal spirals (plus irregulars) respectively. Radio-loud AGNs are modeled following [81]. Here the radio-quiet AGN component is not included and is replaced by a proto-spheroidal galaxy population, caught in its active star-formation phase. Figure from [366, in prep.]

evolving and related to star formation.

A different model (see Fig. 4.10), not including a radio-quiet AGN component, is proposed by [366, in prep.] to explain the steepening of the source counts at sub-mJy flux densities. This model accurately fits the multi-frequency counts, luminosity functions and redshift distributions of star-forming galaxies, extrapolated to radio frequencies exploiting the IR/radio correlation (dotted and dashed lines), and of radio-loud AGNs (triple dot-dashed line, modeled following [81]). In this model the radio-quiet AGN component is replaced by a population of proto-spheroidal galaxies caught in their active star-formation phase (see dot-dashed line). The proto-spheroidal galaxy component is expected to account for most of the Cosmic Infrared Background (CIB) at wavelengths $\geq 350\,\mu$m [290]. If so, while *Herschel* can directly resolve only a minor fraction of the CIB ($\sim$ 15%, 11% and 5% at 250 μm, 350 μm and 500 μm, respectively ([367]), the SKA will detect the sources of essentially all of it. As shown in Fig. 4.9, at z = 2–3, where the cosmic star formation rate peaks, the SKA can detect galaxies with SFRs down to a few $M_\odot\,\mathrm{yr}^{-1}$, well below the SFRs of the most active star formers in the universe which are found to have SFR $\simeq$ 100–200 $M_\odot\,\mathrm{yr}^{-1}$.

Only combining high sensitivity and high (mas) spatial resolution it is possible to disentangle among the various scenarios proposed to explain the sub-mJy radio source counts, with particular respect to the radio-quiet AGN component. Studies in this direction will be undertaken in the next future with e-MERLIN, through dedicated surveys reaching μJy sensitivities on spatial scales of 50-100 mas (see e.g. Guidetti et al. 2013). Sub-μJy sensitivities will be routinely reached by SKA on similar spatial scales, as baselines up to $\sim$ 100 km (SKA1) and $\sim$ 200 km (SKA2) will be incrementally implemented, according to the current design. However, as shown in Figs. 4.4 and 4.5, only VLBI-like observations allow to securely pinpoint AGN cores in sources at cosmological redshifts. This calls for 10$\times$ longer baselines ($\geq$ 1000 km) for the SKA.

4.3 Line Studies

G. Cresci, F. Fraternali, L. Hunt, A. Marconi, A. Wolter, A. Capetti, F. Gastaldello, F. Mannucci, N. Menci, P. Tozzi, G. Trinchieri, V. Casasola, D. Vergani

4.3.1 The Evolving Gas Content of Galaxies and the Onset of the Hubble Sequence

Various lines of evidence suggest that the *total* baryonic gas mass fraction changes with redshift in a similar way to the SFRD [368]. Normal star-forming galaxies at $z \gtrsim 1$ are from 3 to 30 times more gas rich than their local counterparts [e.g., 369]. However, these numbers are derived from observations of the molecular component only. In fact, outside the Local Universe, there are no direct measurements of the HI content of galaxies out to $z \sim 1$ and beyond. Since stars are thought to form from molecular gas [although see 370], this makes it a problem to verify observationally at high redshift how gas transforms from the atomic to the molecular phase [e.g., 371; 372]. In ~ 12 hr, SKA will be able to trace HI masses of $3 \times 10^9\,M_\odot$ out to $z \sim 1$, and $3 \times 10^{10}\,M_\odot$ out to $z \sim 2.5$ (at system temperatures that vary from 54 to 70 K and taking into account the Galactic foreground emission). We can thus much better constrain the physics behind star formation and the observed evolution of gas content in galaxies.

The HI mass function in the Local Universe depends on Hubble type [e.g., 373]. Since atomic gas is associated with the galaxy disk component in the nearby Universe, SKA high-resolution HI imaging of galaxy populations out to $z \sim 1-2$ should help constrain morphological transformation and the buildup of stellar mass in disks and spheroids. This means that a (rotationally-supported) disk component can be constrained by comparing a galaxy's HI content with other galaxy properties.

With a deep HI survey of ~30 days of integration time, a typical L_* galaxy (with an HI mass of $\sim 6 \times 10^9\,M_\odot$) can be traced to $z \gtrsim 2.5$. Out to $z \sim 0.3$, a few times 10^4 galaxies will be resolved in HI so that rotation curves, mass distributions, and gas fractions can be derived. By comparing high-redshift survey fields tuned to various redshifted HI frequencies, we can start to better understand how galaxies of the various classes (rotation-supported disks, or pressure-dominated spheroids) interact at various redshifts. This could be a first step to pinning down the epoch of the origin of the Hubble sequence.

4.3.2 Probing the SMBH - galaxy coevolution in AGN with HI based mass estimates

As discussed in Sect. 4.2, one of the most striking achievements in the last decade has been the realization that supermassive black holes (BH; $M_{BH} \sim 10^6 - 10^{10}\,M_\odot$) are key actors in the formation and evolution of galaxies. This important fact is based on three seminal discoveries: the detection of supermassive black holes in the nuclei of nearby galaxies, the discovery that their masses are strictly correlated with the structural parameters of the host spheroids or galaxies in the case of ellipticals [374–376] and that they were grown through efficient accretion during bright AGN phases [377]. In order to be established, M_{BH}-host galaxy correlations require a physical mechanism linking the pc-scale region surrounding the BH with the kpc-scale galaxy. Thus, the physical mechanism triggering the gas accretion onto the SMBH is thought to be linked to global quantities characterizing the host galaxy (like star formation rate and stellar mass), possibly stabilized by a feedback mechanism. Such a feedback from the actively accreting BH, i.e. the AGN, is also thought to contribute to the apparent anti-hierarchical growth of galaxies and supermassive black holes, the low fraction of baryons condensed into stars and the low number density of massive galaxies observed [378–382]. The resulting *coevolution* of supermassive black holes and their host galaxies is currently a key ingredient for understanding galaxy evolution: at the beginning there is plenty of cold gas and, due to frequent mergers and interactions, star formation and balck hole accretion proceed at very fast rates. This

phase of rapid growth in stellar and black hole mass is embedded in a gas and dust rich environment and therefore can only be studied at FIR-radio wavelength (e.g. [383; 384]). When the BH reaches a sizeable mass ($M_{BH} \sim 10^7 - 10^8\ M_\odot$), the Eddington limited AGN output is powerful enough to expel gas from the host galaxy (e.g. [385; 386] and references therein). This feedback process gradually reduces BH growth and star formation. At the end most of the gas has been expelled and an unobscured type 1 AGN shines in a generally passive galaxy. With almost no gas left, BH growth and SF can occur only through gas and dust in stellar winds and/or accretion of pristine gas. Perturbations of external origin, such as galaxy collisions, mergers, and mass accretion ([387]), or of internal origin due to density waves, such as spirals or bars, and their gravity torques (e.g. [388; 389]), but also more localized phenomena, such as nested nuclear bars (e.g. [390]) and warped nuclear disks (e.g. [391; 392]) can destabilize gas and make it available for BH accretion or star formation.

Although the coevolution picture is an attractive one, there are currently many open problems (see, e.g., [393]).

- What process brings the gas into the bulge? Is it mergers, secular processes, cold and/or hot accretion?
- What process determines the fraction of gas transformed into stars and accreted onto the BH? Why the ratio of cosmic SFR and BH accretion rate is ~ 1000?
- What process is responsible for AGN feedback (if any) and what is the magnitude of this effect on the host galaxy?
- What comes first, the BH, the galaxy (stars) or are they co-eval?

These open issues can be addressed by SKA in combination with other observatories already operating or which will operate in the 2020 and beyond time frame (es. ALMA, Euclid, E-ELT).

The italian community has played a key role in the study of the coevolution between BHs and their host galaxies. To cite but a few, from the observational point of view, it has contributed to the detection of supermassive black holes in nearby galaxies [394–399], to the study of the correlation with the host galaxy properties [374; 376; 400–403], and to their redshift evolution [404–409], to the determination of the cosmological evolution of the AGN population through X-ray surveys and to the study the connection between AGN activity and star formation [377; 384; 410–418] and to the discovery of the first evidences for AGN feedback in action [419–423]. From the theoretical point of view, the italian community has also been extremely active creating state of the art models of galaxy evolution which take into account the feedback of accreting black holes and follow their coevolution with galaxies [378; 382; 424–426] and which have been extensively used to explain apparent discrepancies in the observational determinations of the cosmological evolution of the BH-galaxy relations [427].

SKA and its precursors will be among of the most powerful observatories for the study of the way supermassive black holes are fueled and of the BH-galaxy coevolution, allowing determinations of the galaxy star formation rates (SFR), through the radio continuum emission and measurements of kinematics and gas content through the HI 21cm line. Although much progress has been made on both theoretical and observational fronts in the last decade, the relationship of black hole growth with galaxy formation and evolution is still far from being completely understood.

The local $M_{BH} - galaxy$ relation

Currently, the $M_{BH} - galaxy$ relation is limited to ~ 60 BH mass measurements based on spatially resolved stellar or gas kinematics (fig. 4.11, left panel). To detect the presence of a BH and measure

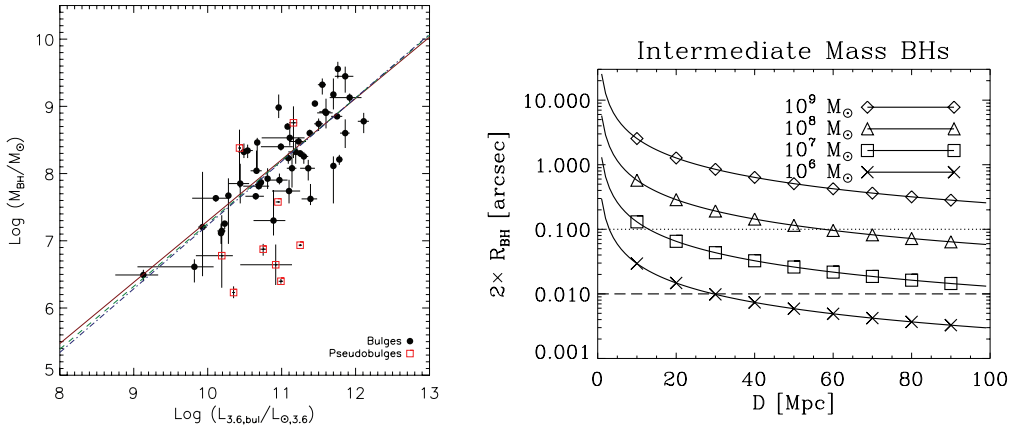

Figure 4.11. Left: The local relation between BH mass and luminosity of the host spheroid from [402]. The red squares denote pseudobulges. Right: the angular size of the BH sphere of influence as a function of distance and BH mass. The dotted ad dashed lines denote a spatial resolution of 0.1″ and 0.01″; $2 \times R_{BH}$ must be larger than the spatial resolution for a BH mass measurement to be possible.

its mass, it is necessary to resolve the gravitational sphere of influence of the BH defined as

$$R_{BH} = \frac{G\,M_{BH}}{\sigma^2} = 10.7\,pc \left(\frac{M_{BH}}{10^8\,M_\odot}\right)\left(\frac{\sigma}{200\,km\,s^{-1}}\right)^{-2}$$
$$= 0.11'' \left(\frac{M_{BH}}{10^8\,M_\odot}\right)\left(\frac{\sigma}{200\,km\,s^{-1}}\right)^{-2}\left(\frac{D}{20\,Mpc}\right)^{-1}$$

where σ is the average velocity dispersion of the star in the bulge, and D is the galaxy distance. It is clear that to observe a $10^8\,M_\odot$ BH at a distance of 20 Mpc a spatial resolution of $2 \times 0.11''$ (FWHM) is required.

The study of the HI 21cm line will also allow to determine the kinematics of the neutral gas. In very nearby galaxies, (e.g. $D < 100$ Mpc) it will be possible to directly estimate BH masses by studying the kinematics of HI emission from circumnuclear material, like that in the AGN obscuring torus. Such masses will allow to study M_{BH}-galaxy relations in the local universe with an unprecedented number of objects, thus allowing to study these relations in different morphological galaxy types. In figure 4.11 (right), we plot the radius of the BH sphere of influence as a function of galaxy distance and BH mass; for a BH to be detectable $2 \times R_{BH}$ must be larger than the spatial resolution. For instance, a spatial resolution of 0.1″ will allow to detect BH masses $10^8 - 10^9\,M_\odot$ up to $\sim$ 100 Mpc.

At high redshift, it will not be possible to spatially resolve the kinematics of the circumnuclear material and the challenge will then be to spatially resolve the kinematics of the whole galaxy. For instance, 0.1″ correspond to $\sim 10pc$ at 20 Mpc and to 1 kpc at $z \sim 3$. The BH mass in type 1 AGN can then be estimated from optical-NIR spectra using virial relations (e.g. [428]) and the study of galaxy kinematics at 10kpc-scales will allow to determine the dynamical mass of the host galaxies and of the associated dark matter haloes. There are indications that dynamical mass estimates for the host galaxies are less biased than the stellar mass estimates currently adopted [429]. This will allow to study the cosmological evolution of the relation between BH, host galaxy and dark halo masses discovered in the local universe [400; 403]. To study the dynamics of the host galaxy, a resolution of 0.1-1 kpc is required. Sizes of 0.1 kpc are always resolved if the resolution is 0.01″, and with a resolution of 0.1″ we will always resolve 1 kpc scales.

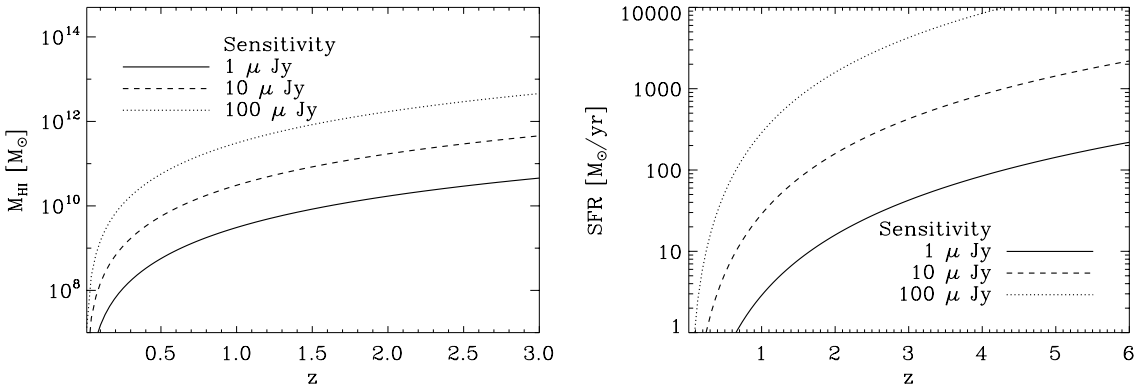

Figure 4.12. Left: Minimum detectable HI mass as a function of redshift and equivalent sensitivity in continuum. A line width of 300 km/s has been assumed. Right: minimum measurable SFR as a function of redshift and flux sensitivity at 1.4 GHz.

In conclusion, in the local universe it will be possible to greatly enlarge the local sample of galaxies with BH mass determinations, while at high redshift it will be possible to measure the dynamical masses of the galaxies and their host halos.

The evolution of AGN activity, Star Formation and Gas Content

The SFR can be directly estimated from the radio continuum emission. Excluding radio loud AGN, which constitute only $\sim$ 10% of the AGN population, radio continuum emission is dominated by free-free emission in star forming regions and can therefore be used to estimate SFRs (see, e.g, [430] and references therein). A more accurate SFR determination which can single out AGN emission can be performed by combining SKA observations with submm and X-ray observations like those that can be obtained by ALMA and by future X-ray surveying missions.

The total HI gas content can be directly estimated from the 21cm luminosity ((see, e.g, [281] and references therein). The total content in neutral atomic gas can be related to the molecular gas content (commonly traced by CO lines thanks to ALMA, but also with SKA at higher redshifts), the BH masses (estimated from optical spectroscopy of the broad emission lines in type 1 AGN), the SF and AGN accretion rates, thus sheding light on the relation between gas consumption, BH and stellar growth.

Assuming that SKA will be sensitive down to 0.4 GHz, the HI line at 1.43 GHz will be observable up to redshift $z \sim 2.5$. The total HI mass can be estimated from the HI line flux as $M_{HI} = 2.35 \times 10^5\, M_\odot\, (D^2_{Mpc}\, F)$, where D_{Mpc} is the luminosity distance in Mpc and F is the integrated line flux in Jy km s^{-1}. For a given line width Δv, the equivalent continuum flux is simply $F/\Delta v$. In figure 4.12 we plot the minimum detectable HI mass for a given sensitivity of 1, 10 and 100 μJy, assuming a line width of 300 km/s. Lower line widths will only increase the mass sensitivity. Clearly, it will be possible to detect HI masses down to $10^{10}\, M_\odot$ up to a redshift $z \sim 2$.

A similar plot can be obtained for the star formation rate. Using the relation by [430], $SFR = 5.5 \times 10^{-22} L_{1.4\,GHz}\, M_\odot/yr$ (with $L_{1.4\,GHz}$ in W/Hz), it is possible to estimate the minimum SFR measurable as a function of redshift for a given continuum sensitivity at 1.4 GHz (rest frame). With a 1 μJy sensitivity it is possible to measure down to 10 $M_\odot/yr$ up to $z \sim 2$ and down to 100 $M_\odot/yr$ up to $z \sim 6$.

In conclusion, it will be possible to measure the gas content and star formation rates with high

sensitivities ($M_{HI} > 10^{10}\,M_{\odot}$, $SFR > 10\,M_{\odot}/yr$), up to a redshift of $z \sim 2$ with a flux sensitivity of $1\mu Jy$.

4.3.3 Probing the interplay between cold gas and metallicity at high-z with SKA

Gas metallicity is regulated by a complex interplay between star formation, infall of metal-poor gas and outflow of enriched material. The discovery of a relation between stellar mass $M_{\star}$ and metallicity ([431–435]), with more massive galaxies showing higher metallicities, has been a fundamental step in this field. However, the origin of this relation is debated, and many different explanations have been proposed, including ejection of metal-enriched gas (e.g., [434; 436; 437]), "downsizing", i.e., a systematic dependence of the efficiency of star formation with galaxy mass (e.g., [438–440]), variation of the IMF with galaxy mass ([441]), and infall of metal-poor gas ([442; 443]). The mass-metallicity relation (MZ) has been studied at high redshift by e.g. [444] at $z \sim 2.2$ and by Maiolino et al. ([445]) and by Mannucci et al ([446]) at $z = 3 - 4$, finding a strong and monotonic evolution, with metallicity decreasing with redshift at a given mass. Recently the Italian community provided an important step forward the field. Mannucci et al. ([447]) and Cresci et al. ([448]) showed that the scatter in the MZ relation shows a correlation with the star formation rate (SFR), especially for lower mass galaxies, with more active galaxies showing lower gas metallicities. In fact, the MZ is just the projection of a more fundamental relation between Stellar Mass, Metallicity and a third parameter, the Star Formation Rate (SFR). The introduction of the so-called Fundamental Metallicity Relation (FMR) results in a significant reduction of residual metallicity scatter to ~ 0.05 dex i.e., about 12% and a factor 3 lower than the Mass-Metallicity relation. Interestingly, high redshift galaxies up to $z \sim 2.5$, are found to follow the same FMR defined by local SDSS galaxies, with no indication of evolution. This suggests that the FMR is produced by a complex interplay between metal production and gas cycle (accretion, outflow and consumption). Moreover, these mechanisms seem to regulate the overall evolution of galaxies both in the local and high-z Universe, with higher star-formation activity at high-z being triggered by the larger amount of infalling gas.

If this scenario is correct, an even tighter relation is expected between stellar mass, metallicity and gas content in galaxies. However, direct measurements of the gas content (both molecular and atomic) in galaxies are still sparse.

A first test of a Gas Fundamental Metallicity Relation (GFMR) was done by Hughes et al. ([449]), using HI 21 cm line observations of a pilot sample of 260 local late type spirals. They confirmed that, at fixed stellar mass, galaxies with lower gas fractions typically also possess higher oxygen abundances, but their sample was still too small to draw firm conclusions on the scatter of the relation. Moreover, observations of cold gas at higher redshift are still beyond the capabilities of current radio facilities. Although existing or upcoming projects, such as LUCI@LBT, KMOS@VLT, E-ELT, JWST and the Euclid satellite, will provide stellar masses and gas-phase metallicity for several thousands of galaxies at 1.5<z<3.5, the HI content of these objects is the critical missing ingredient.

The advent of SKA will therefore open a new window for the observation of atomic gas in MilkyWay-like galaxies up to redshift 1-2, allowing for the first time to study the GFMR for a statistically significant sample of galaxies both in the local and in the high-z universe, and to understand the evolution of cold gas content in galaxies and its interplay with metals, dust and star formation rate in shaping the evolution of galaxies.

As detailed in the previous Section and shown in figure 4.12, with SKA it will be possible to measure the HI gas mass and SFR to extend the Fundamental Metallicity Relation up to very high redshifts ($z \sim 6$), at least for the most massive objects. It will then be possible to verify at which redshift the FMR starts to evolve.

4.3.4 Dynamics of galaxies and dark matter

The kinematics of the galactic discs studied with HI observations is the prime probe to trace the distribution of dark matter in galaxies and its relation to the baryonic matter. The neutral gas extends further out with respect to stars and other gaseous components and allows us to probe the flat parts of the galactic rotation curves, which are crucial to determine the dark matter content. To date, this information is available only for local galaxies. One of the most distant galaxies for which a rotation curve has been traced in HI is Malin 1, located at at $z = 0.08$, which corresponds to 1.1 Gyr of lookback time [470]. Malin 1 has a huge (100-kpc radius) HI disk and thus it is possible to resolve the disk in a few resolution elements with the VLA. Smaller and/or more distant galaxies cannot be studied in HI with the current facilities. Rotation curves at higher redshift are successfully traced using optical emission lines [e.g. 458] and molecular gas [e.g. 453]. However, both these tracers allow us to probe only the inner parts of the galaxies. The Square Kilometer Array will revolutionize this field by detecting and studying rotation curves of thousands of galaxies out to $z = 1$ and beyond.

We will observe galaxies throughout the Hubble time down to column densities of 10^{-17} cm^{-2}, and study the very edges of disks also for distant objects despite the cosmological dimming. At present, the only information about HI beyond $z = 0.2$ comes from the study of the Damped Lyman α systems, which show that galaxies in the past had similar column densities and HI masses as local galaxies [488]. This makes us confident that when SKA, and to some extent its pathfinders, will open their eyes on the intermediate-z and high-z Universe we will be able to trace rotation curves like we do now for local galaxies. Having all these data requires handling them efficiently and reliably by automatically fitting datacubes to derive physical properties of the gas and of the galactic potentials. Tracing the distribution of dark matter in distant galaxies is of paramount importance to understand the processes of galaxy assembly. One key diagnostic is the evolution of galactic scaling relations and in particular the Tully-Fisher, which is a fundamental test for any model of galaxy formation and evolution [463; 487]. SKA will be able to greatly extend the HI measures and give a strong constraint to rotation curves.

4.3.5 Gas around galaxies and gas accretion

Galaxies are not isolated systems as they continuously interact and exchange material with the environment where they live [486]. Understanding when and how gas is transferred to galaxies from the intergalactic medium is a major challenge of current cosmological models. Disk galaxies must collect fresh gas to feed their star formation throughout the whole Hubble time. The evidence for gas accretion comes from the calculation of gas depletion times [468], the study of the star formation histories [477] and the chemical evolution models of the Milky Way [454; 483]. Indirect determinations of the gas accretion rate show that it should follow quite closely the star formation rate (SFR) in every galaxy [461; 465]. Despite expectations, there is very little evidence for gas accretion taking place in local galaxies, mostly because it is very difficult to observe directly [480]. In the Milky Way, a recent determination of the accretion rate from high velocity clouds led to only 0.08 $M_\odot$ yr^{-1} [479], more than an order of magnitude below the SFR ($1 - 3\ M_\odot$ yr^{-1}, [455]). HI studies of local galaxies provide very similar estimates [482].

A possibility is that the current facilities allow us to detect only the tip of the iceberg of the accretion. At the moment the deepest HI observations of nearby disk galaxies reach column densities slightly below 10^{19} atoms cm^{-2} and typical masses for HI clouds of $\sim 10^6 M_\odot$ [476; 478]. Fig. 4.13 shows three observations of the same galaxy: NGC 891 obtained in the last thirty years with the Westerbork Synthesis Radio Telescope. The improvement in sensitivity from $\sim 1 \times 10^{21}$ cm^{-1} (left panel) [481] to $\sim 1 \times 10^{19}$ cm^{-1} (right panel) [476] has brought to light a completely different picture of this galaxy in HI. A very extended low-column-density HI halo had been unveiled already in 1997

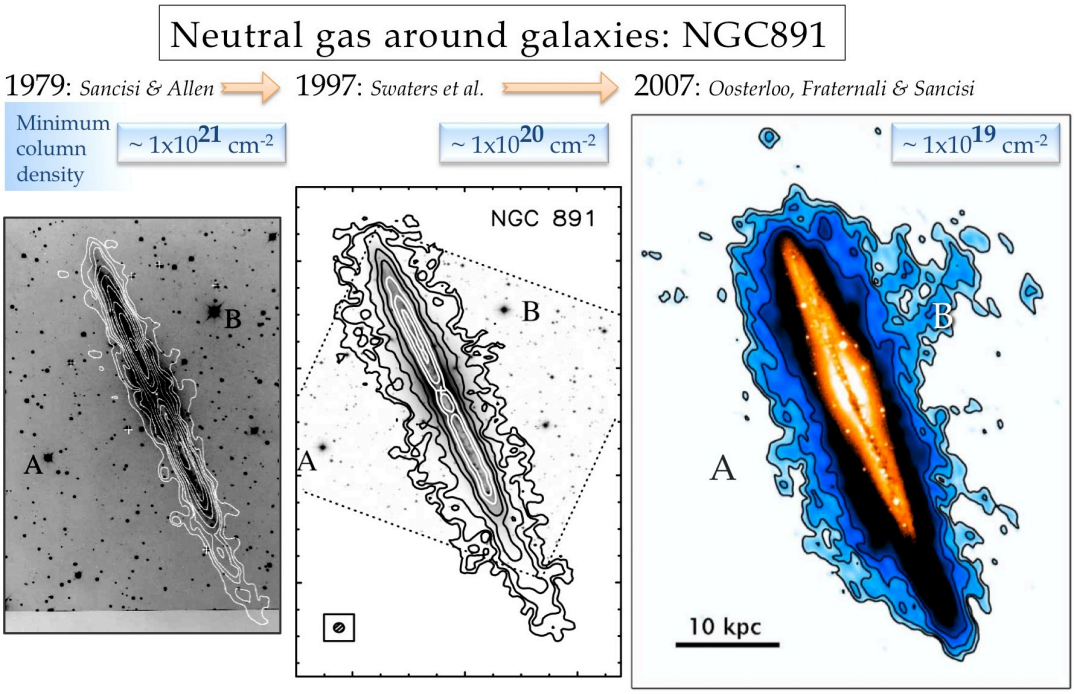

Figure 4.13. Three generations of neutral hydrogen observations of the edge-on spiral galaxy NGC 891, obtained with the Westerbork Synthesis Radio Telescope in 1979 (left panel), 1997 (middle panel) and 2007 (right panel). The improvement of only one order of magnitude between each observations brought first to the discovery of the HI halo (middle panel) and then to the realization that this halo comprises almost 30% of the HI mass of the gas and hosts gas filaments extending up to more than 20 kpc from the disk (right panel). SKA will go down two more orders of magnitude in column density, we can only wonder what we will find.

(middle panel) [485]. However, the new data show the remarkable extent of this halo up to 8 – 10 kpc everywhere above the disk of NGC 891, and with a long filament reaching up 20 kpc. Most of this gas is likely to be produced by stellar feedback from the disk [460] but a fraction could come from accretion, e.g., the filament. Clouds and filaments at similar column densities are observed also around other galaxies [e.g. 459]. Below these densities we cannot go with the available instruments.

Given the dramatic difference made by two orders of magnitude in column density shown in Fig. 4.13 it is difficult to anticipate what SKA will be able to see going down to a sensitivity of a few $\times 10^{16}$ cm^{-2}. We will obtain the full picture of HI around galaxies, characterize the properties of the HI halos, and derive precise estimates of gas accretion. Competing models are now proposed to solve the long-standing problem of sustainability of star formation in disks. Cosmology predicts that large nearby galaxies should be surrounded by hot coronae that contain a significant fraction of the so-called missing baryons [452; 456]. Hydrodynamical simulations suggest that these coronae should be, under certain conditions, thermally unstable and cool to form clouds [467] but these instabilities have been challenged by other theoretical work [451]. Some recent cosmological simulations show *cold* filaments penetrating the hot coronae and reaching the disks to feed star formation [457]. Finally, galactic fountain models predict that coronae are polluted and cooled by stellar feedback from the galactic disks [460; 473]. All these models make clear predictions of what the circumgalactic medium should look like at column densities below the current detection limits, and it very likely that SKA

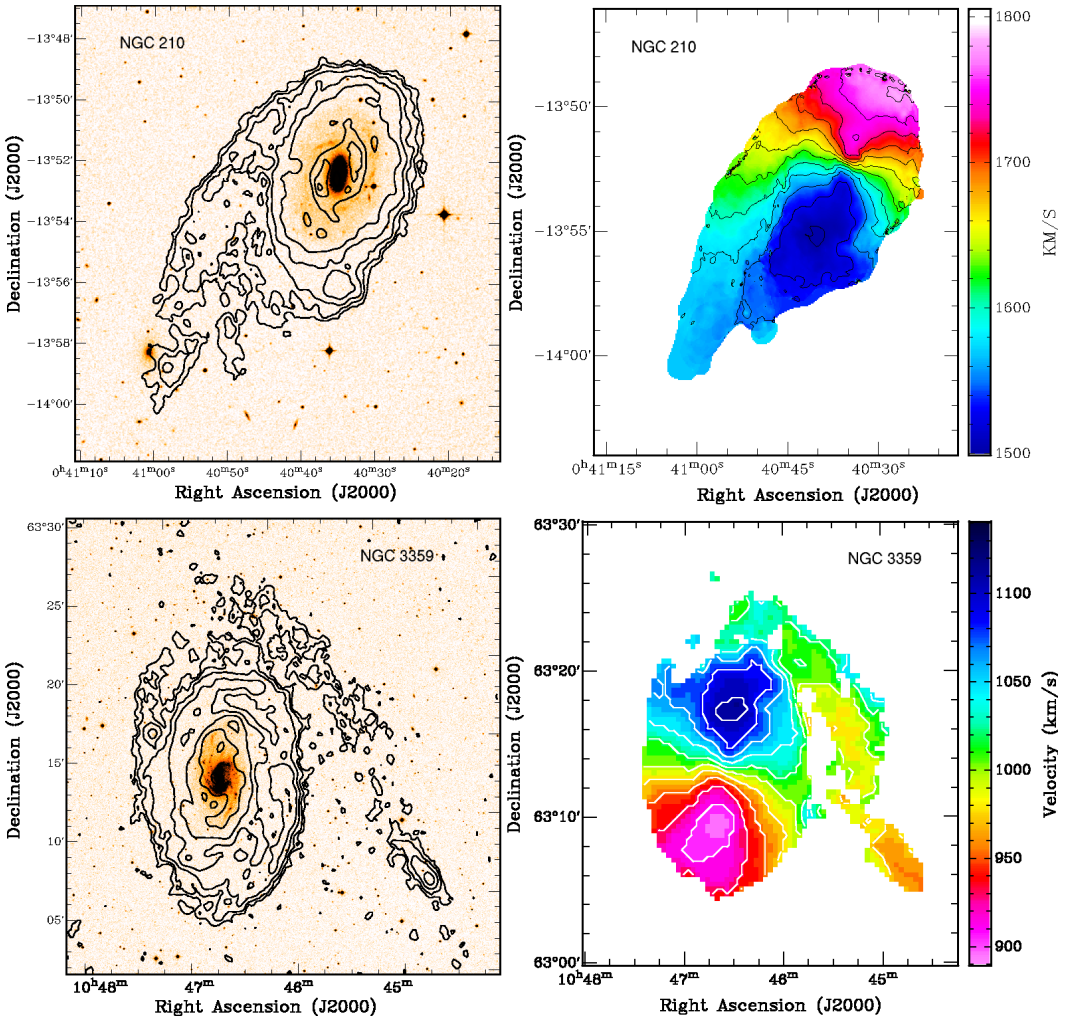

Figure 4.14. Neutral hydrogen observations of two nearby galaxies undergoing a minor merger with a gaseous companion. The contours in the left panel show the HI density distribution superposed on the optical image. For NGC 210 (top left panel) the levels are 5, 10, 20, 50, 100, 200×10^{19}cm^{-2}, for NGC 3359 (bottom left panel) they are 10, 20, 50, 100, 200, 400×10^{19}cm^{-2}. The right panels show the velocity fields. From Sancisi et al. [482].

will finally tell us how gas accretion into galaxies takes place.

4.3.6 Dwarf Galaxies and Mergers

Our hierarchical cosmology predicts that structures form largely through the merging of smaller objects. In this scheme, galaxies like the Milky Way may have experienced a few major mergers, especially in the early Universe accompanied by a very large number of minor mergers down to the present epoch [484]. Minor mergers can also bring gas and contribute to the gas accretion [482]. Quantifying the effect of minor mergers in galaxy evolution is crucial to constrain the models and understand the build up of mass in galaxies. Until now, all studies made use of optical surveys and estimated the merger rate measuring the population of galaxy pairs. The results are however in disagreement as the estimated rates differ by more than an order of magnitude between the different works [e.g. 472]. Moreover, the evolution with redshift appears ill determined; some authors find no-

evolution [466] other find strong evolution [471]. Studying these phenomena in HI brings two main advantages with respect to optical surveys. First, it immediately provides the kinematic information without the need of a follow up; moreover the kinematics is traced in very high detail and it can be used to reconstruct the dynamics of the interaction [450]. Second, the interaction between galaxies produces tidal features that are clearly visible in HI observations and do not require particularly deep observations like in optical [474]. Example of such features are shown in Fig. 4.14, taken from Sancisi et al. [482], where one can appreciate the disturbance in the gas distribution (left) and kinematics (right) of a couple of nearby minor mergers.

In this context, SKA and its pathfinders will be ideal instruments to study galaxy pairs and interactions as a function of galaxy types and redshifts. The combination of high-resolution, high sensitivity and large field of view will allow SKA to detect about 10^4 galaxies per square degree at $z \sim 1$ and estimate the merger rate with gas-rich galaxies to a very high precision. The results will be contrasted with the predictions of cosmological simulations [e.g. 469]. This will bring tremendous insights on the accumulation of mass into galaxies and the role of mergers in the formation and evolution of galaxies. Mergers are also considered to be crucial for triggering starbursts in galaxies and this is likely to have been very important in the past [464]. Unfortunately until now, the lack of information in HI at intermediate and high redshift has completely hampered the possibility of testing the relation between mergers and the starbusting phenomenon. SKA will also fill this gap.

4.3.7 HI in Ellipticals and Groups

The formation and mass assembly history of early-type galaxies (ETGs) is not fully understood in the context of the general topic of galaxy formation. The current understanding favours a hierarchical model in which present day structures form by merging, either dissipative (gas rich) or dissipationless ("dry") [494; 502]. A monolithic collapse [510] is instead favoured by the evidence for a costant comoving density of ellipticals up to z~2 [513], in which galaxies assembled their baryonic mass at an early time in a gaseous form and passively evolve until today after a single dominant episode of star formation.

The environment also plays a role in the assembly of galaxies and in governing their final outcome, as witnessed by the morphology-density relation and the associated truncation of star formation [496]. There is growing evidence that much of the modification of galaxies actually takes place in galaxy groups [493] with a variety of physical mechanisms, both gravitational, such as mergers and tidal interactions, and hydrodynamical, like gas stripping due to the ram pressure of the ambient gas. Mergers and tidal interactions dominate in small galaxy groups [490]. Recent simulations and observations show that starvation and ram pressure can be moderately effective at stripping gas from some galaxies in X-ray emitting compact groups [503; 509] in which the final fate is believed to be the coalescence of their brightest members into a field elliptical galaxy, with timescales depending on the dark matter content and distribution [e.g. 489].

A well traveled path to tackle the problem of galaxy formation and evolution is to extend observations to the highest possible redshift, in order to constrain the number of galaxies already assembled and link it with time and environment. A powerful alternative is to observe our nearby universe at different wavelengths, including the 21cm line, e.g. [475] to understand what kind of signature galaxies have inherited from the formation mechanism. X-rays have shown to be a powerful observing window in which it is possible to probe directly the amount and morphology of the hot ISM, which can be used as a tracer of their evolutionary stage.

The link between the stellar evolution and the hot gas is still elusive, as is clearly visible in the large scatter in the L_B–L_X relation for the hot gas for ETGs of similar morphological and environmental properties [e.g. 492; 495; 506; 507]. Attempts at pinpointing the fundamental parameters that

need to be considered have found that, in general, core, old, rounder E galaxies are more likely to have a detectable hot ISM than core-less, young, flattened objects, although the amount they are able to retain covers a considerable spread [see also 497]. In particular, we see a trend for young post merger galaxies to be underluminous, compared with typical mature Es into which they are expected to evolve [491; 498; 508; 511; 512].

Dynamical modeling require late-type spiral progenitors [501], which produced HI-rich tidal tails expected to fall back to the main body of the galaxy in about 3 Gyr. Es formed through merging of spirals might possess a reservoir of cold gas which is otherwise missing. An attempt to verify the hypothesis that the presence of HI is related to a recent merger event and anti-correlated with high X-ray–luminosity gas did not yield a compelling result. In a sample of isolated ellipticals [517] most of the galaxies with secure detection of hot X-ray emitting gas have only upper limits in HI, while the objects for which cold gas is present are actually upper limits for the hot gas. This is consistent with the above scenario, however the paucity of data does not allow us to draw conclusions at this time. If true, this would help explaining the L_X/L_K spread in terms of different evolutionary paths.

Many observational studies highlight the importance of HI features for our understanding of environmental effects. HI observations would be crucial to verify if this process is tenable for the construction of ellipticals. Is the cold gas mostly associated with low X-ray luminosity objects? Is it regularly distributed or concentrated in e.g. tidal features? The HI gas should bear trace of the process: in particular the extent and the spatial distribution could reveal the presence of a component much larger than the resulting optical galaxy. A disturbed velocity field would be a tell-tale signature of merging. On the theoretical side recent numerical simulations [515] studied the evolution of a disc galaxy within the global field of a group environment, showing that significant disk transformation occur and that more massive galaxies suffer more tidal stripping because of dynamical friction.

In groups, the information provided by HI observations, such as velocity, mass and HI distribution gives crucial constraints for theoretical predictions of different environmental mechanisms [516] and could provide the identification of the perturber and the dynamic of the encounter.

Spiral galaxies are less common within dense environments and they tend to be deficient in HI; this deficiency itself correlates with the projected local galaxy density [500]. Historically, studies of the impact of the environment on galaxy properties have been focusing on galaxy clusters, while most of the galaxies reside in groups. A key to elucidate the origin of the morphology-density relation is therefore the study of the processes, both gravitational and hydrodynamical, acting on galaxies within groups.

Neutral hydrogen distributions revealing ongoing tidal interaction, galaxy merging and gas stripping are particularly common in groups of galaxies [e.g. 504; 514]. The observation of these processes in action suggests that the morphology and gas content of galaxies can undergo substantial evolution inside a group. HI is an excellent tracer of tidal/gravitational interactions interactions and often shows evidence for these gravitational disturbances when optical observations of the same source appear undisturbed. And it is the only signature present when hydrodynamical interactions such as ram pressure stripping are taking place. From an observational point of view the main challenge is that the stripped gas can diffuse quickly in the group medium (in about a group crossing time). It therefore reaches low column densities, requiring high sensitivity, and spreads over large areas, requiring observations over a large field. SKA and its pathfinders will be ideal instruments to carry on these studies. Probing the variety of HI features across the all range of density environments in groups, from spiral only groups with no detectable intra-group medium (with upper limits on the X-ray emission) to X-ray luminous groups will allow to gauge the relevance of tidal and ram pressure stripping [e.g. 499]. A signature of the influence of the group tidal field on the disc galaxy acting as perturber is given by the cold fronts, most likely induced by minor mergers that produce a disturbance

on the gas in the core of the main object, displace it from the center of the potential well, and decouple it from the underlying dark matter halo through ram pressure [sloshing cold fronts in the X-ray gas, e.g. 462; 505]. Characterization of HI features in groups with X-ray signatures of recent gravitational interactions of galaxies with the group potential will allow to further contrain the mechanisms of HI removal.

Understanding group processes is important to understand galaxy properties over a broad range of large-scale environment densities, as groups are the building blocks of clusters and pre-processing in groups may be important to shape the properties of galaxies at the present epoch. Our knowledge of the mechanisms of galaxy formation would be greatly enhanced by extending both the depth of observations for local galaxies, for which it is important to reach very low levels of HI density, and the number of objects that can be detecte at cosmological distances. SKA will enable both.

5 AGN physics

5.1 Relativistic jets with SKA

A. Wolter, F. Tavecchio, G. Bonnoli, M.Giroletti, S. Turriziani, A. Tramacere, I. Donnarumma, L. Costamante

Besides the core science items, the SKA is expected to dramatically improve our knowledge in the field of structure and dynamics of extragalactic relativistic jets, allowing us to image the full extent of jet radio emission, to characterize the polarization and to track the evolution of emission features down the jet (e.g. [518]). Particularly important for several topics will be the synergy with the forthcoming Cherenkov Telescope Array (CTA), planned to start observations in 2016-2017, and with LOFT.

Among the most relevant topics we can put in evidence:

- *Jet dynamics*: SKA will ensure the possibility to unravel with high accuracy the global dynamics of jets. In particular it will allow us to probe the velocity field of the jet (through the tracking of moving knots and jet brightness profiles) and its changes along the flow, with important consequences on our understanding of jet dynamics. An important related aspect is the precise characterization of the possible "stratification" of the jet, with the presence of a fast core and a slow layer, as already found in nearby jets of few TeV-emitting BL Lac (e.g. [519]). Advances in these topics, contrasted with the results of numerical simulations, will provide unique ingredients to theoretical models of jets production and dynamics and will give direct support to emission models of high-energy emitting blazars (e.g. [520]).

- *Magnetic field structure*: the precise polarization measurements possible with SKA will permit to map the detailed structure of the magnetic fields in the jet (e.g. [521; 522]), allowing us to investigate the dynamical role of the magnetic field and its effects in the jet collimation. This will be particularly relevant at small (< pc) scales, where the jet behavior is believed to be dominated by the magnetic field dynamics. Polarization is also an essential tool to explore the structure of shocks, marking the site of the interaction with the external material or the internal collision of portions of the flow moving at different speeds.

- *Particle acceleration*: the coupling of the high-resolution and high-sensitivity radio data with high-energy (X-rays, gamma-rays) observations will allow us to deeply investigate all topics related to the acceleration of relativistic particles in the jet. In particular, the radio data will provide accurate information on shock structure and dynamics which, coupled to the information on the particle evolution, effectively probed by high-energy observations, will give us a clearer understanding of the mechanisms at the base of acceleration processes. In turn, these information could be relevant to enlighten the mystery of the sources of ultra-high energy cosmic rays.

- *Jet and extended structures*: the impressive sensitivity of SKA will allow us to map with unprecedented detail the structure of jets at large (> 1 pc) scales. Particularly important issues are the study of the global dynamics of jets (speed, stability) and the investigation of the extended structures (hot spots, lobes, knees in curved jets). These latter topics also relevant for the study of the jet/environment interaction and the possible role in the AGN/galaxy and AGN/cluster feedback.

A particularly illuminating example of the potentiality offered by the SKA capabilities in synergy with high-energy observatories (in particular CTA) is offered by the jet in the nearby radiogalaxy M87.

Studies of the jet in M87 already showed that TeV flares are accompanied by changes of the radio structure of the inner (sub-pc scale[523]) jet, although the precise causal chain is still unclear (do the structural changes trigger the TeV emission or viceversa?). Among the hot topics that will be possible to solve there is the precise location of the high-energy emitting region. Current studies depict a rather confusing scenario, with possible emission regions ranging from the black hole magnetosphere to knots in the pc-scale jet. The possibility offered by SKA to map in detail the magnetic field structure of the jet and the motion of plasma features will provide invaluable information on this issue and on the details of the particle acceleration processes resulting in the emission of high energy gamma-rays.

The jet in M87 is however so remarkable mostly because of its proximity. Several other sources of comparable intrinsic luminosity exist in the Universe, and the SKA sensitivity will allow us to observe them with great accuracy. In particular, structures as the peculiar knot HST-1, which is in the range 1-10 mJy at $\sim$ 1 GHz, will be easily detectable with SKA1_mid within a radius of at least 100 Mpc, within observing times of a few minutes. To most effectively resolve such structure out to such distances, a resolution of about 0.1 arcsec would be ideal, and it can be approached with the longest baselines in SKA1_mid. An extension to even longer baselines as planned for the SKA phase 2 will improve accordingly.

The studies in the field of relativistic jets are based on a fertile sinergy between multifrequency studies in the high-energy (X ray, HE and VHE gamma ray) domain, and high resolution radio observations. A case of special interest for Italy would be the LOFT satellite.

The Large Area Detector (LAD) aboard LOFT [130] will provide tight observational constraints on jet dynamics (item 1 above). Indeed, thanks to its large area, the LAD will allow for monitoring the X-ray emission of TeV BL-Lacs providing unprecedented temporal sampling (<100 s). This temporal resolution will grant detection if the ultra-rapid variability observed at TeV for PKS 2155-304 [524] and Mrk 501 [525] is present at X-ray energies too. The measurement of the existence of rapid temporal lags between these two spectral bands is instrumental in probing and constraining the stratification of the jets. Moreover, the wide field-of-view of the Wide Field Monitor (WFM) aboard LOFT (nearly 1/3 of the whole sky) will provide long term histories of large numbers of sources with a sensitivity in the 2-50 keV band of nearly 2 mCrab/day at 5-σ (see [130] for details). These long-term data will enable us to relate X-ray states to events at radio wavelengths. The observation and quantification of possible lags between these two bands will make possible to understand if the radio behaviour is more compatible with the cooling time scales of high energy electrons emitting at X-ray energies, or with the propagation and expansion of the flaring region along the jet. This sinergy will provide crucial information to pin down the physical location of the emission region, and to characterize the jet structure and composition via broadband energy spectra modeling.

Thanks to its large sensitivity, broad energy range and pointing flexibility, the LOFT/LAD can

play a crucial role in the context of particle acceleration studies as well, providing a high spectral accuracy measure of the X-ray SED of TeV BL-Lacs. This in turn will allow us to accurately trace at high energies the shape of the underlying emitting particle distribution, so as to probe the presence of a stochastic component in the acceleration and to assess its competition with the first order process. In addition, it will allow to disentangle acceleration dominated states, from states at the equilibrium [526].

5.2 Radio emission from Low Luminosity radio-AGNs

M. Giroletti, F. Panessa

It is now well established that there are massive black holes at the center of galaxies. Most of these black holes go through phases of activity during their evolution - in the form of accretion of gas and in some cases of the formation of a relativistic jet visible in the radio. However, the duty cycle of such phenomenon is currently not well constrained, although it is a fundamental piece of information for galaxy evolution models. Even during their phase of radio quiescence, however, most Active Galactic Nuclei (AGN) are not radio silent and radio observations could be a fundamental tool to probe the physics of the accretion flow and to detect low luminosity and/or obscured AGNs. Both these goals can not be reached with the sensitivity of the present arrays but SKA could radically change this status.

Here we focus on the so-called Low Luminosity AGN (LLAGN), generally associated with late-type galaxies. Such AGNs have typical radio luminosities of 10^{19-21} W Hz^{-1} [e.g. 527; 528] and can be studied only in the local Universe with present radio facilities. Such weak radio-AGN are typically associated to Seyfert 2/LINERS optical spectra and do not produce the typical large-scale radio features (jets and lobes) of classical radio-loud AGNs. Still, they are also distinct from the so-called radio-quiet quasar-like AGNs traditionally studied at optical/IR or X-ray bands, characterized by radiatively-efficient accretion (see discussion in Sect. 4.2.2). Compact radio emission from a number of LLAGNs has been attributed to free-free emission/absorption or advection-dominated accretion flow [ADAF, 529] processes [530; 531], as well as to a combination of a compact radio jet with an ADAF [532] or a standard accretion thin disk [533]. Critical observational parameters to constrain such models include total intensity and polarized flux density, size, spectral index, and variability. In turn, these quantities can be used to estimate the luminosity, the brightness temperature, the energy distribution of the radiating particles, the magnetic field, and the energy density. However, such measurements are at present possible only for a few very bright and very nearby sources, which might be not representative of the whole population. Indeed, recent results from a VLBI survey of a sample of local LLAGN reveal that compact (milliarcsecond scale) radio emission is rather common but the large uncertainty on the observational parameters can not unambiguously discern among physical processes, even with the use of the most sensitive existing arrays, like the EVN [534–536].

5.2.1 The role of SKA

A continuum observation in the 1–3 GHz frequency range including also long ($\sim$ 100 km) baselines, like the one offered by the SKA1_mid configuration will be ideal to dramatically improve our current knowledge. With about one hour integration, and assuming 250 15-m dishes, a sensitivity of 1μJy can be reached over the whole band, with a resolution of $\sim$ 100 mas. Current limits for non detected sources are one to two magnitudes higher; it will thus be effectively possible to reveal many more sources in the local Universe than today, as well as nuclei comparable to those we study now but in galaxies about 10 times more distant. These two improvements will likely provide an increase of the

population of detected LLAGNs by a factor 10^3. It is also expected that the fraction of radio detected LLAGNs will approach 100% in volume limited samples, thus suggesting that radio surveys with the SKA will become an efficient tool to search for faint (intrinsically weak) AGNs.

In terms of the physics of the detected sources, the SKA will also provide some fundamental information. Polarized emission is expected in synchrotron sources at a level of $\sim$ 10%. This will be easily detectable in the brightest cases, and will be a crucial test of the emission mechanisms. Similarly, variability studies are now limited by the large uncertainties on the measured flux density. With the high signal-to-noise flux density measurements provided by SKA, it will be much easier to monitor the variability, which in turn can constrain the compactness of the emission region and can also be compared with multi-wavelength coordinated observations (e.g. in the X-ray band). Finally, spectral index will be constrained over a relatively large frequency band, and this will already allow us to put some constraints on the physical mechanisms. An extension to higher frequencies and longer baselines as expected in Phase2 will eventually seal the deal on the classification.

5.3 Nuclear radio emission from quiescent galaxies

A. Capetti

It is now clear that the mass of supermassive black holes (SMBH) residing at the center of all massive galaxies correlates with the properties of the host, in particular with bulge mass and stellar velocity dispersion [542; 543]. The interstellar medium (ISM) at the galaxy's center is expected to accrete onto the SMBHs at a rate governed by its global physical state, but the processes that set the accretion level are still poorly understood. When the mass accretion rate is sufficiently high, the dissipation of gravitational energy, radiated in various bands of the electromagnetic spectrum, leads to the presence of an active galactic nucleus (AGN), in one of the various and complex manifestation of this phenomenon. While these types of objects have been addressed in the previous sections, here we focus on objects with least accretion rates.

Indeed, a minimal level of accretion is always expected, even in quiescent galaxies. Spherical accretion, as described by [540], can be considered as a fiducial low level of ISM accretion onto a SMBH. This idea is strengthened by the observations that show that a link exists between the Bondi accretion rate (estimated from the temperature and density of the hot ISM phase derived from X-ray observations) and the level of radio emission in low luminosity radio-galaxies [537; 538]. This trend extends down to very faint active nuclei, characterized by extremely low accretion rates, $\sim 10^{-4}$ solar masses per year [546].

At the lowest level of accretion the standard signatures of an AGN are unobservable due to the contamination of the host galaxy. For example, the X-ray emission from the nucleus is overwhelmed by the diffuse hot gas and by various classes of active stars, from X-ray binaries to cataclysmic variables [544]. Similarly, the characteristic presence of nuclear emission lines is swamped by gas photoionized by hot evolved stars [539; 545]. The limited spatial resolution of the images that can be obtained over most of the spectrum hampers our ability to detect the emission associated with extremely low accreting SMBHs.

This is not the case of radio observations that can reach a resolution of the order of the milliarcsec, corresponding to $\sim$ 0.1 pc at a distance of 20 Mpc. Over this small volume the host contribution is negligible. Furthermore, the presence of radio emission is naturally expected in the close SMBHs environment, characterized by relativistic gravitational fields and magnetic fields. This is confirmed by the SMBH at the center of the Galaxy, which, despite its low mass and extremely low bolometric luminosity, is clearly seen in the radio domain with a characteristic flux level of $\sim$ 1 Jy (e.g. Yusef-Zadeh et al. 547).

Currently, the study of radio emission in quiescent galaxies is limited by sensitivity. A recent VLA survey targeted a complete sample of 63 elliptical galaxies in Virgo [541]. Giant E-galaxies (with a stellar mass exceeding 10^{11} $M_{\odot}$) have been generally detected above the flux limit of 0.1 mJy at a frequency of 8.4 GHz. Nonetheless, two giant Es failed to be detected at a luminosity threshold of $\sim 5 \times 10^{18}$ W/Hz, despite the fact that they host a SMBH with an estimated mass of $\sim 10^8$ solar masses. Furthermore, only 4 out the 51 less massive galaxies show the presence of a radio core. This level of incompleteness clearly prevents to draw any conclusion on the process of accretion in these objects. The situation is even less clear about the radio nuclear emission in other type of hosts, such as in spirals. In these objects the need to remove the large scale contamination to the nucleus requires higher spatial resolution images (on the mas scale) which are currently even more limited in flux threshold.

How can we expect to improve the census of the radio emission from quiescent galaxies with SKA? By scaling the radio flux of Sgr A to a distance of 10 Mpc we obtain a level of emission within the range accessible to SKA observations. Indeed, the sensitivity limit of the SKA1_mid configuration already reaches $\sim 1\mu$Jy in one hour of integration, about two orders of magnitude better with respect to the currently available instruments and at a spatial resolution sufficient to remove the host contamination. Information on variability, spectral shape, and polarization will also prove to be extremely important to constraint the emission and accretion processes in the detected sources.

Beside the study of accretion processes, the detection of non thermal radio emission from the nucleus of a quiescent galaxy represents a unique tool to establish the presence of a SMBH. This is particularly important for low mass galaxies, whose fraction of occupation by SMBHs is an essential ingredient for models of SMBH growth and galaxy evolution.

5.4 The life cycle of radio AGN

M. Murgia, P. Parma

Dying radio galaxies represent an interesting, but still largely unexplored, stage of the active galactic nuclei evolution. During their active stage, which may last several 10^7 years, these strong synchrotron radio sources associated with elliptical galaxies are supplied with energy from active galactic nuclei via plasma beams or jets. Due to the continuous accumulation of new particles, the total spectra of the active radio sources are usually well approximated by a power law over a wide range of frequencies. The injection of energy also sustains the growth of these radio sources which is governed by the balance between the internal pressure in the radio lobes and the pressure in the hot X-ray emitting external medium in which they must expand. At some point, however, the activity in the nuclei stops or falls to such a low level that the plasma out flow can no longer be sustained and the radio source is expected to undergo a period of fading (dying phase) before it disappears completely. In the dying phase, radio core, well-defined jets and compact hot-spots will disappear because they are the structures produced by continuing activity. On the other hand, the radio lobes may still remain detectable for a long time if they are subject only to radiative losses of the relativistic electrons. The first example of such sources is B2 0924+30 and was illustrated by [548]. It is also possible that radio galaxies may be active intermittently or even that jets flicker before eventually going off completely. In this scenario, one expects to observe fossil radio plasma remaining from an earlier active epoch, along with newly restarting jets in the core of the host galaxy. Dying sources are rarely observed at frequencies > 1 GHz. In fact, in the absence of fresh particle injection, the high-frequency radio spectrum develops an exponential cutoff. At this point, the adiabatic expansion of the radio lobes will concur to shift this spectral break to lower frequencies and the source will disappear quickly. Note that only few percent of the radio sources in the B2 and 3C samples have the characteristics of a dying

radio galaxy. On the other hand, if the source expansion is somehow reduced, or even stopped, there is still the chance to detect the fossil radio lobe, at least at low frequency. For the reasons mentioned above, low-frequency selected samples are particularly well-suited to search for these elusive fossil radio sources (see e.g. [549]). Indeed, we may expect the existence of a large population of dying radio sources that have been missed from the current surveys because of very steep spectra. These sources are very faint at centimeter wavelengths but should still be visible at frequency $\lesssim 100$ MHz.

5.4.1 The Role of SKA

Due to its unprecedented sensitivity and angular resolution the SKA represents the ideal instruments to discover and to understand in detail these elusive objects. Both resolution and sensitivity are necessary to study in detail the radio morphology and spectrum along the lobes of these faint sources in order to determine whether they are really de-energized objects or restarting radio sources. Based on our calculations (see e.g. [550]), we expect that extreme dying sources are characterized by a rather uniform and steep spectral index distribution, in contrast with active galaxies where we usually observe strong spectral index gradients (i.e. we can distinguish the flat spectrum regions like cores, jets, or hot-spots, where the electrons are injected/accelerated from the steep spectrum regions like lobes and tails, where the electrons age). Moreover, determining the exact fraction of restarting sources could give important clues on the relation existing between the accretion of matter on the black hole at the center of the host galaxy and the formation of the radio jet. It is important to stress that the angular resolution is of paramount importance in order to achieve the above goals. The expected typical angular size of dying sources is less than 1 arcminute (100 kpc at a redshift of $z = 0.1$, see e.g. Fig. 5.1). Indeed, we will need arcsecond resolution even at the lowest radio frequencies. In this context, the combination of high sensitivity and resolution of the SKA will play a crucial role. Furthermore, we want to estimate the main physical parameters, like internal energy and age, of these dying sources. To do this we will need to model the observed radio spectra in conjunction with the properties of the X-ray emitting gas in which these sources expand. Again, radio images at arcsecond resolution are needed in order to match the resolution of the X-ray satellites like Chandra or XMM. In fact, most dying sources we found so far are associated to a diffuse X-ray emission. In many cases the association is with a known cluster of galaxies. This suggests that the presence of a particularly dense gaseous environment may prevent the adiabatic expansion of the fading radio lobes or even that the AGN feedback and duty cycle are strictly related phenomena in galaxy clusters (see [551]). Finally, it is worthwhile to mention that on the long run the dying source in clusters will be likely disrupted by the turbulent gas motions and their relativistic electrons and magnetic field will finally enrich the non-thermal component in the surrounding medium. These magnetic fields, if released in the intra-cluster medium by these radio sources at high-redshifts, can be a spread over Mpc scales and amplified to the level observed in the local Universe by galaxy cluster mergers (see e.g. [552] and references therein).

Dying sources currently represent only a few percent of the population of radio sources in classical samples. However, if the dying phase lasts long enough before the source get disrupted (or completely regenerated by the onset of a new active phase), we could expect to observe a significant number of dying sources as active ones, provided we have the necessary sensitivity to detect the faint fading radio emission. In Fig. 5.1 we present an example drawn from the real case of the dying radio source WNB 1734+6407 at the center of the cooling-core cluster Abell 2276 at a redshift of z =0.106 (see [550], [551]). From the modeling of the observed radio spectrum we derived that the source has been active for about $t_{\rm ON} \simeq$60 Myr while the dying phase is lasting for $t_{\rm OFF} \simeq$ 26 Myr so that the total source's age is about $t_s \simeq$86 Myr. The de-energized radio lobes are detached from the host galaxy and are fading rapidly. We forecast the passive radiative evolution of the radio spectrum and we compare

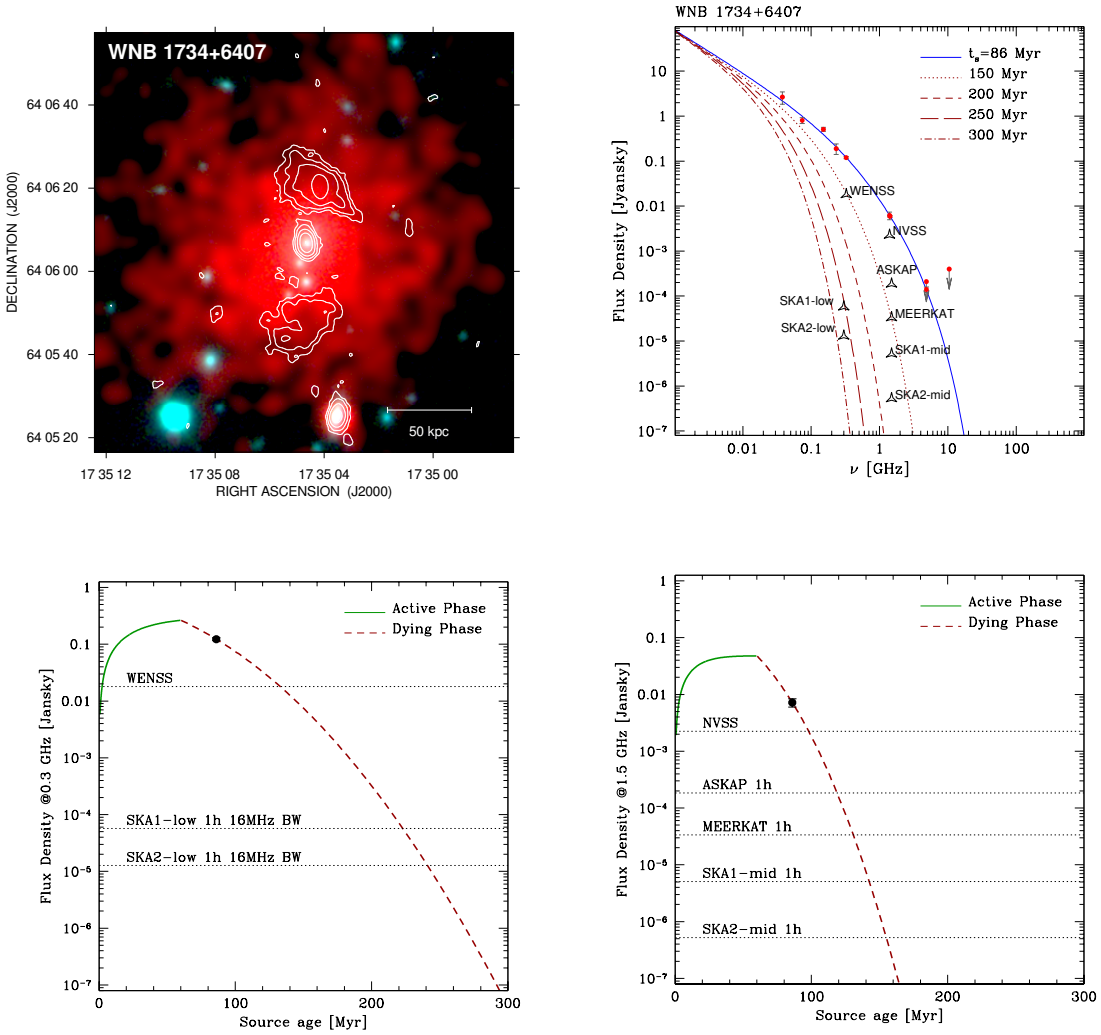

Figure 5.1. The dying radio source WNB 1734+6407 at the centre of the cooling-core cluster Abell 2276 at a redshift $z = 0.106$ (see [551]). The top-left panel show the VLA radio contours at 1.4 GHz overimposed to the X-ray image obtained with the Chandra satellite (red) and the optical image from the SDSS (blue). The radio spectrum of the source is shown in the top-right panel. From the fit of the observed data points (continuous line) a total source age of 86 Myr is derived. The radio source spent about 30% of its age in the dying phase. The dotted lines represent the passive radiative evolution of the radio spectrum compared with the sensitivity limits of the current radio survey WENSS and NVSS (in which the source has been discovered), those of the SKA precursors ASKAP and MEERKAT, and finally with the SKA phase 1 and 2. Bottom panels show the presumed evolution of the flux density at 0.3 GHz (bottom-left) and 1.5 GHz (bottom-right) as a function of time in comparison with the sensitivities of current surveys, SKA precursors, and SKA phase 1 & 2.

our expectations with the sensitivity limits of the current and future radio survey. In particular, we plot the sensitivity limits of the WENSS, in which the source was originally discovered, and the NVSS. In addition, we plot the expected sensitivities of the SKA precursors ASKAP and MEERKAT and then those of the SKA phase 1 and 2. Our calculation show that the source will disappear from both the

WENSS and the NVSS at an age of 150 Myr. In fact, the comparatively shallow sensitivities of these surveys limit our capability to observe the duration of the dying phase to $t_{\rm OFF}/t_s \lesssim 50\%$. This in part explains why extreme dying sources are hardly detectable in the present all-sky surveys. The spectral cut-off is so sharp that in the GHz regime such a dying source would be difficult to detect also with the improved sensitivities of MEERKAT, ASKAP, and even with that of the SKA-mid phase 1. The expected flux density at 1.5 GHz at $t_s = 150$ Myr is as low as 1μJy, achiavable only with the SKA-mid phase 2 configuration. The situation is radically different at low frequencies. Due to its ultra-steep radio spectrum, the dying source would be potentially detectable at 0.3 GHz by both SKA-low phase 1 & 2 up to an age of ~250 Myr. In conclusion, future all-sky SKA-low surveys will be fundamental to discover a large number of dying sources if sensitivities of a few 10 μJy will be reached. These sensitivity levels require arcsecond resolution to limit confusion noise as much as possible. At higher frequencies the sensitivity of SKA-mid phase 2 is necessary due to the extremely steep spectra of these radio sources.

5.5 Probing AGNs with Water (Mega)Masers

A. Tarchi, P. Castangia

In Active Galactic Nuclei (AGN) an enormous quantity of energy and angular momentum is released in a relatively small volume making of these objects exceptional laboratories to study physical processes in environments with extreme densities and temperatures. The widely accepted Unified Model of active galactic nuclei (e.g., [553], [569]) implies, in their very centres, the presence of a supermassive black hole (with masses ranging from 10^6 to 10^9 solar masses) surrounded by a parsec-scale accretion disk. The emission from the disk is particularly intense at ultraviolet (UV) and soft X-ray wavelengths. The accretion disk is then surrounded by a torus (or a thick disk) of atomic and molecular gas, with a size of 1-100 pc, that obscures the optical and UV emission along certain directions. Therefore, the object appears as either a type 1 or type 2 AGN depending on the line of sight. In type 1 AGN, the observer views the accretion disk and black hole through the hole in the torus, while in type 2 AGN the direct view of these nuclear components is obscured by the torus. The amount of radio loudness in each object (thus, if it is classified as a radio-quiet or radio-loud AGN) and its membership to an individual radio class of AGN (e.g., QSO, FR I, BL Lac, etc...) are instead also ascribable to the host galaxy type and/or to intrinsic properties of the nuclear components of the AGN (spin, mass, and accretion rate of the black hole, the relativistic jet power and orientation, etc...; see, e.g., [569]).

Studies of the central regions of AGN are complicated by the extremely small scales and complex structures of the nuclear components. In addition, particularly in type 2 AGN, the inner regions are often obscured at optical and UV wavelengths. Observations at infrared (IR, the band where most of the nuclear radiation absorbed by the torus is re-emitted), X-ray, and radio frequencies can, however, access these obscured regions. In particular, at radio wavelengths, water and OH maser studies are a unique tool for investigating the structure and kinematics of the gas close to and around the nuclear engines of AGN.

When water masers are associated with accretion disks in AGN, through Very Long baseline Interferometry (VLBI) and single-dish monitoring studies in the radio, they can be used to map nuclear accretion disks and provide a calibration of the cosmic distance scale (for NGC 4258: [565], [561]; for UGC 3789: [555]). Furthermore, by modelling and analysing the keplerian rotation curve of the accretion disks, as derived from the aforementioned maser studies, mass estimates of the nuclear engine can be obtained (e.g., [563]). H_2O masers currently provide the most precise method to determine black hole masses in external galaxies, especially in the case of type 2 AGN, where other

methods, such as those based on optical broad lines emission, cannot be used. Measuring black hole masses in AGN, allow to estimate Eddington luminosities and accretion efficiencies. In addition, this studies are extremely relevant to probe the low mass end of the $M_{BH} - \sigma^*$ relation, so far, almost uniquely derived for elliptical galaxies with larger BH masses (e.g., [558])

Water maser emission can also be associated with radio jets, produced by either the interaction between the radio jet and an encroaching molecular cloud or by the amplification of the radio continuum from the jet from excited water molecules in a foreground cloud. Detailed studies of these masers allow to derive relevant physical quantities of the jet material, like its velocity and density (e.g., [567]).

A third class of AGN-associated water masers is named 'outflow-masers'. Presently, however, there is only one case that has been thoroughly investigated, the nearby Seyfert 2 galaxy Circinus ([559]). VLBI maps of the water emission from this galaxy have shown the potential of this kind of sources to trace wide-angle nuclear outflows up to few parsecs from the central engine.

So far, most of these kind of studies have been performed on radio-quiet AGN in the local Universe ($z < 0.05$), mainly because of the limited sensitivity and angular resolution of available radiotelescopes. However, the discovery of a water maser in the gravitational lens MG J0414+0534 at z=2.64 ([562]), paves the way to the study of H_2O masers at high redshifts. Indeed, using the magnification provided by the foreground gravitational lens to increase the observed flux density and the angular extent of any water maser in the background, it is in principle possible to map parsec-scale accretion disks in distant AGN, also with current instrumentation. Furthermore, this discovery suggests that the space density of luminous water masers was larger at high redshift than in the local Universe ([562]). The detection of H_2O masers at cosmological distances ($z > 1$) would allow us to study the nuclear environment around powerful radio sources, to investigate the physical conditions of the gas in the inner parsecs of quasars, and to measure their black hole masses not only in the local but also in the early Universe. Nonetheless, systematic searches for unmagnified water masers require a significant improvement in instrument sensitivity. Nicely, the next generation of radio telescopes, such as the EVLA and the SKA, will provide such an improvement and will allow deep and/or wide-field surveys to be performed in frequency ranges suitable to detect maser sources at cosmologically-relevant distances. But how promising, in terms of detection rates, can be the outcome of blind surveys with these telescopes? And which are the specific requirements, already planned for, or to be likely implemented in these facilities, to achieve successful results, in particular, w.r.t. high-resolution followups of the detected masers?

5.5.1 The role of SKA

Sensitivity requirements

Following the detection of the maser in the gravitational lens MG J0414+0534 at z=2.64 ([562]), [564] (hereafter M11) performed a search for water maser emission in a small sample of (five) dusty, gravitationally lensed quasars and star-forming galaxies at redshifts between 2.3 and 2.9. Despite no new confident detection was found, this study allowed to update the water maser luminosity function (LF) derived by [560] and [554] at high redshift. In particular, M11 demonstrates that there must be some evolution in the LF at moderate redshifts, thus motivating high-sensitivity blind surveys for the water maser transition at high z. Recent results from the *Herschel* space observatory [566] also suggests that high-z ultra-luminous infrared galaxies tend to be very strong emitters in water vapour, reinforcing the motivation to search for H_2O masers at cosmological distances. Following the line of reasoning in M11 (therefore, also considering all the reported assumptions and caveats), by parametrizing the evolution of the LF with redshift, i.e. $(1 + z)^m$, with the parameter m equal to 0, 4 or 8, to account for a no, moderate, and strong evolution, respectively, the number of water maser

galaxies found in pointed and/or blind surveys for a certain survey detection limit can be predicted. Indeed, this has been done by M11 for two conceptual blocks of the MeerKAT and SKA particularly suitable to perform pointed and/or blind surveys of redshifted water maser lines. The number of expected masers have been computed for all three evolutionary parameter of the luminosity function (m = 0,4,8) and for different area covered in the surveys, i.e., single pointing, 100 pointings, and, in the SKA case only, for a quarter-sky survey (M11; their Table 4). By summarizing the main outcome of such a computation, it can be first noticeably said that the potential for the SKA and its precursors to find many more water masers up to cosmological distances is granted. This is particularly true if the evolution with redshift of the LF, with m=4 (the numbers reported below are for this case) or higher, is confirmed.

In particular, the sensitivity of MeerKAT makes this telescope more suitable for targeted searches (rather than blind surveys) to detect masers out to redshift 1-2 with luminosities of a few thousands solar luminosities. In the MeerKAT case, the specifications assumed/required are that: i) the frontend system can cover a frequency range of 10-14 GHz, with a 4-GHz simultaneous bandwidth; ii) the collecting area is equivalent to $\sim$ 80×12-m antennas; iii) the aperture efficiency and system equivalent flux density (SEFD) of order 0.7 and 13 Jy, respectively.

The sensitivity and field of view of the SKA is instead particularly promising to detect a large number of new high-z water maser sources performing blind surveys. While in the optimal case of a quarter-sky survey, thus by investing a total integration time of $\sim$ 3000 hours (5 s per pointing), M11 predicts the extremely intriguing chance to detect more than 20000 water maser galaxies out to redshift 3, also less extensive searches, 100(×30-h) pointings or even 1(×3000-h), would already yield between $\sim$ 1000 and $\sim$ 4000 detections out to redshift of 4.5. In the SKA case discussed, the specifications assumed/required are that: i) the frontend system can cover a frequency range of 4-10 GHz, reachable with a possible frequency setup of 3×2-GHz simultaneous bandwidths; ii) the collecting area is equivalent to $\sim$ 2000×15-m antennas; iii) the aperture efficiency and system equivalent flux density (SEFD) of order 0.7 and $\sim$ 0.35 Jy, respectively.

Spatial resolution requirements

In the previous section, the feasibility for MeerKAT and the SKA to detect new water maser sources has been described, also from the quantitative point of view. Together with the statistical importance that a large number of new detections will necessarily bring, however, each source also represents a goldmine of information, as those mentioned in the first paragraphs of this section. Indeed, a number of relevant details can be already inferred from the spatially-unresolved spectra of the water maser emission alone, like hints on the nature of the maser nature (e.g., as accretion-disk or jet/outflow maser), and, in the case of disk-masers, rough estimates of the accretion disk rotation velocity and size, thus the black-hole mass. However, in order to fully exploit the potential offered by maser studies (in particular to determine precise black-hole mass and distance estimates of the host galaxies, etc...) high spatial resolution imaging capabilities are required to map the distribution of the water maser spots. While the prototypical disk-maser case is that in NGC 4258 whose accretion disk has a subparsec scale size, more and more disk-maser sources are now under investigation, especially in the framework of the Megamaser Cosmology Project (see, e.g., [556]), and, in some cases, a disk size of the order of 1 pc have been also observed (in addition, possibly, larger accretion disks are expected in radiogalaxies were more massive black-holes are present; [568]). Then, in order to resolve a 1-pc structure at z=1, at 11 GHz (the frequency at which the water maser line is Doppler-shifted), baselines of $\sim 10^5$ km are required. Consequently, only maser sources (much) closer than z=1, masing structures with larger extent, or gravitationally-lensed maser galaxies (for such a case, see [562] and [557]), will take full profit of interferometric studies with earth-based antennas only. For these studies, a network

of radiotelescopes is then recommended that combines the SKA or MeerKAT arrays (possibly used in phased mode) with a number of antennas (or other suitable arrays, e.g., the ATCA, KVN, or VERA) at relatively-large distances to provide the necessary baseline lengths (few thousands of km). Instead, as shown before, in the case of water masers at cosmological distances, only space VLBI (presently represented by RadioAstron) may grant the necessary resolution for detailed studies of the emission.

6 Galaxy Clusters and Magnetic Fields

6.1 Galaxy Clusters, Cosmic Web, and Particle Acceleration Mechanisms

G. Brunetti, L. Feretti, F. Govoni, P. Tozzi, R. Cassano, M. Gitti, P. Mazzotta, T. Venturi, S. Ettori

6.1.1 Introduction

Clusters of galaxies and the filaments that connect them are the largest structures in the present universe in which the gravitational force due to the matter overdensity overcomes the expansion of the universe [570]. Massive clusters have typical total masses of the order of $10^{15} M_{\odot}$, mostly in the form of dark matter ($\sim$ 70-80% of the total mass), while baryonic matter is in the form of galaxies (few %) and especially in the form of a hot (T $\sim 10^8$ K) and tenuous ($n_{gas} \sim 10^{-2} - 10^{-4}$cm^{-3}) gas (15-20%), the intra-cluster-medium (ICM). Diffuse synchrotron radio emission associated with the ICM is observed in an increasing number of galaxy clusters [571]. This radio emission demonstrates that the thermal ICM plasma is mixed with non-thermal components. Such components are large-scale magnetic fields and relativistic particles in the cluster volume. They have the potential to affect the dynamics and thermodynamics of the ICM. Radio observations play a series of path-finding roles in the study of galaxy clusters and large scale structures because the radio emission is uniquely sensitive to the turbulence and shock structures of large scale environments. The existence of non-thermal components in clusters raises important questions :

- are cosmic rays and magnetic fields common in the ICM ?
- which is the origin and evolution of these components ?
- what is the energy budget in the form of non-thermal components in the ICM ?
- which is their impact on the micro-physics and dynamics of the ICM ?

The interactions between relativistic radio jets from the central galaxy and the surrounding ICM has also an impact on the dynamics and evolution of galaxy clusters [572]. In recent years such interactions have been unambiguously shown thanks to spectacular images where radio emission is observed to fill the cavities in the X-ray emitting ICM. This phenomenon is widespread and is critical to understand the physics of the inner regions of galaxy clusters and the properties of the central BCG.

Future observations with the new generation of radio telescopes, such as LOFAR, ASKAP, and MeerKaT, combined with complementary data in the X-ray and γ-ray bands, will aim at important steps in the field. In particular the study of non-thermal emission in galaxy clusters constitutes important Science Key Projects for all these SKA pathfinders. These radio telescopes will also allow to probe the evolution of the AGN feedback in clusters up to high redshift, at the epoch where clusters

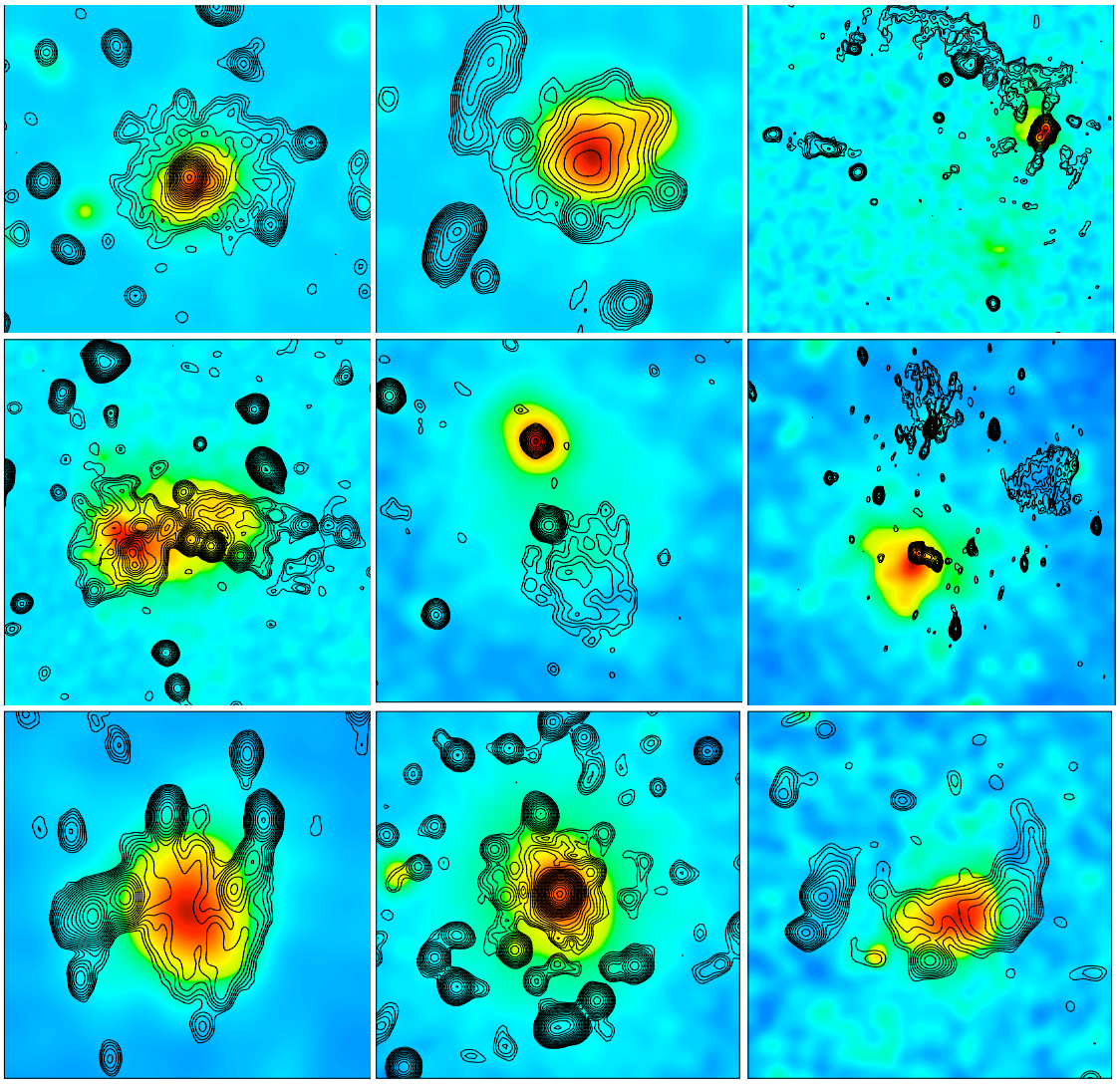

Figure 6.1. Collection of clusters [571] showing several types of radio emission, shown in contours, overlaid onto the X-ray emission, shown in colors. Clusters are (from left to right and from top to bottom) A 2219 (halo), A 2744 (halo + relic), A 115 (relic), A 754 (complex, halo plus relic), A 1664 (relic), A 548b (relic), A 520 (halo), A 2029 (mini-halo), RXCJ1314.4-2515 (halo plus double relics).

virialize, providing a complete picture of the feedback phenomenon and its impact on the physics of the large scale structure of the Universe.

However, although their fundamental role, the SKA pathfinders are still limited in terms of sensitivity, spatial resolution and polarization capabilities and they will not allow to address some of the most critical questions. In addition future studies with these radio telescopes are expected to rise new, unpredictable, fundamental questions that await for the SKA.

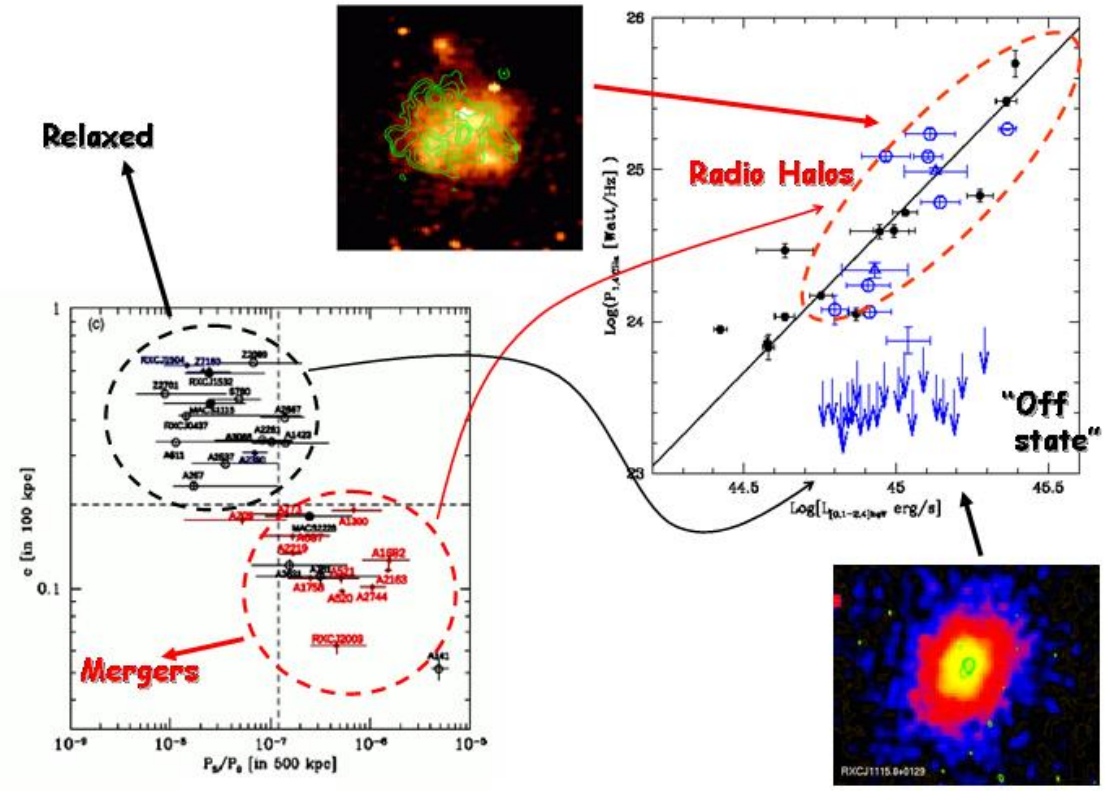

Figure 6.2. Left panel: Plot of the cluster concentation parameter vs the power ratio, showing a clear separation between merger and relaxed systems. Right panel: Radio Halos are detected in merging clusters and their power is correlated with the cluster X-ray Luminosity. Clusters with no evidence of Mpc-scale diffuse radio emission at the sensitivity level of present observations are relaxed systems.

6.1.2 Physics of diffuse radio emission from galaxy clusters

Relativistic electrons and magnetic fields are very well traced in the ICM of several tens of galaxy clusters through their diffuse radio emission. Diffuse sources are typically grouped in halos, relics and mini-halos, according to their location and polarization properties (see Figure 6.1). Giant radio halos are Mpc-scale roundish sources located at the cluster center and appear morphologically connected to the X-ray emitting (thermal) gas of the hosting clusters, while radio relics are elongated sources located in cluster peripheral regions. A clear difference between halos and relics is in their polarization properties with relics being strongly polarized. Mini-halos are centrally located sources, they extend on scales similar to (smaller than) the cores of the hosting clusters and are always hosted in relaxed cool-core systems. All diffuse radio sources in clusters have steep radio spectra in common, $F(\nu) \propto \nu^{-\alpha}$ with $\alpha > 1$. The detailed knowledge of their spectral properties is critical to fully understand the physics of the emitting electrons, their diffusion, evolution and acceleration. The electrons responsible for the radio emission on large, Mpc, scales open to investigate the nature of particle acceleration mechanisms in galaxy clusters. In fact, local acceleration or injection is likely to be necessary to account for observed electrons, since their energy-loss lifetimes are quite brief, in contrast to protons of similar energies [573].

One of the milestone understanding in the last decade is that the presence of radio halos and relics is connected with the dynamical activity of the hosting systems (see e.g. [574; 575]). There is consensus on the observational fact that halos and relics are preferentially generated in massive merging systems (see Figure 6.2). It suggests that halos and relics trace the hierarchical cluster assembly and probe the dissipation of gravitational energy into cosmic rays acceleration and magnetic fields amplification during mergers [576; 577]. In particular, the polarization and morphological properties of radio relics suggest a connection with large scale shocks that cross the ICM during mergers and may accelerate or reaccelerate to GeV energies the emitting electrons. On the other hand, there are reasons to believe that radio halos trace gigantic turbulent regions in the ICM, where relativistic electrons can be reaccelerated through scattering with MHD turbulence and/or injected by way of inelastic collisions between trapped cosmic ray protons and thermal protons [578].

The spectrum of radio halos and relics provides fundamental information on their origin. Nowadays only a handful of halos and relics have good spectral information due to the lack of adequate sensitivity of present observations and to the difficulty to combine observations at different frequencies and with different radio telescopes [579; 580]. The SKA pathfinders will have unprecedented sensitivities to diffuse emission on clusters scales and will measure the spectrum of these sources over a large frequency range. It will allow to explore correlations between the spectral shape of radio halos and the thermal and dynamical properties of the hosting systems, and to measure with great accuracy spectral steepenings and spectral variations in both halos and relics.

The polarization properties and the brightness distribution [581–583] of radio halos and relics are important probes of their physics (see Sect. 6.2). Previous studies discovered point-to-point correlations between the synchrotron and X-ray brightness in clusters with radio halos (e.g. [584]). More recently a correlation between the y-parameter and the radio brightness in the Coma cluster has been discovered by combining SZ (Planck) and radio data [585]. All these correlations pin-point a direct connection between the thermal plasma and the relativistic matter that is still poorly understood by present theoretical models. Important progresses in this direction are expected from high-resolution and high-sensitivity studies of the brightness distribution of radio halos and relics. Substantial variations of the magnetic field intensity and spatial diffusion of the relativistic electrons occur on scales of several kpc. Sensitive observations of the brightness distribution of halos and relics that resolve these scales can extract unique information on the physics of acceleration of the relativistic particles and on their interplay with the mechanisms of amplification of the magnetic fields. In this respect, it is indubitable that the measure of the power spectrum of the synchrotron-brightness fluctuations in several nearby radio halos and relics, combined with their polarization properties and with the X-ray emission properties of the ICM on the same scales will allow a tremendous step in our understanding of the physics of relativistic plasma in these systems. The incoming SKA pathfinders will not have the combination of sensitivity and spatial resolution that are required to perform these studies and consequently the SKA will be the first radio telescope that will enter into this unexplored observational regime. In many radio halos the majority of the flux is coming from the external, low brightness, regions. For reference, the average radio brightness of the Coma halo at 1 GHz is $\sim 0.1\mu$Jy per square arcsecond [586], that is only 3-4 times above the confusion noise. Due to the steep spectrum, at higher frequencies the halo-surface brightness becomes closer to the confusion noise, while at substantially lower frequencies brightness fluctuations induced by ghost plasma from dying AGNs and old radio lobes may be difficult to separate from those intrinsic to the radio halo emission. This makes the GHz frequency-range the most suitable to perform these studies for nearby radio halos. Given the properties of the Coma radio halo at this frequency, observations with about 5 arcsec resolution, rms $=1\mu$Jy/beam and a good uv-coverage down to very short baselines, $\sim 0.05 - 0.1k\lambda$, are required to derive high signal-to-noise measurements of the brightness fluctuations on scales of several kpc. With

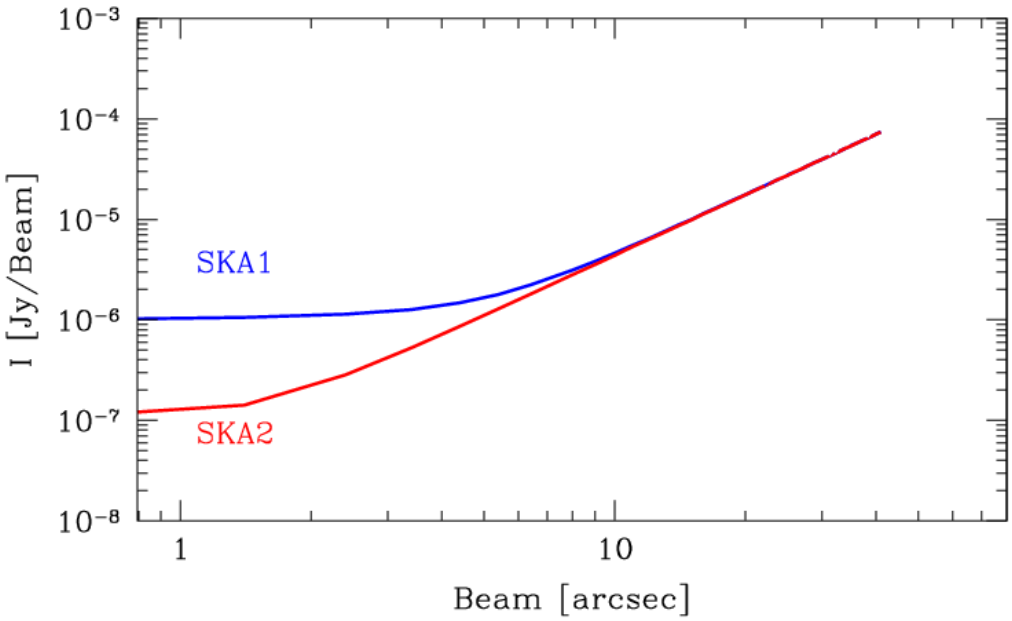

Figure 6.3. Sensitivity achievable with SKA Phase-1 and SKA Phase-2 as a function of the resolution at 1.4 GHz, for 1 hour of integration time, and a bandwidth of 1 GHz. The solid thick lines indicate the 1-σ sensitivity limit obtained taking into account both the sensitivity reached for 1 hour of exposure time and the confusion limit.

SKA Phase-1 we expect to reach a rms=1μJy/beam (with a beam of about 5 arcsec) with about one hour of integration time. In Figure 6.3, we show, up to a resolution of 40″, the sensitivity achievable with SKA Phase-1 and SKA Phase-2 at 1.4 GHz for 1 hour of integration time and a bandwidth of 1 GHz.

6.1.3 How many halos await discovery ?

The very low surface radio brightness of halos and relics, combined with their steep radio synchrotron spectra, make their detection difficult. Pioneering studies using Arecibo and the NVSS and WENSS radio surveys suggested that radio halos and relics are not common in galaxy clusters [588–590]. More recently the GMRT Radio Halo Survey provided the first statistical radio follow up with sensitive observations of a large complete sample of galaxy clusters selected in the X-rays [591; 592]. This survey allows a first meaningful separation between clusters hosting radio halos and those without evidence of diffuse synchrotron emission (see Figure 6.2) and provides a first tentative evidence that the occurrence of radio halos increases with the mass of the hosting clusters [593]. To date, radio searches for diffuse emission have largely concentrated on rich, X-ray luminous, clusters. This is partly due to the fact that according to the correlation that is observed between the radio and the X-ray luminosity radio halos in less X-ray luminous clusters are expected very faint. A few cases of radio halos in poor clusters have been detected so far [594; 595], but these halos are over-luminous in radio by an order of magnitude with respect to what is expected from the extrapolation of the observed radio-X correlation. The knowledge of radio halos properties is also limited in redshift, up to z=0.3-0.4, with only a few halos discovered at higher redshift [eg. 587]. The next generation of radio telescopes, like LOFAR and ASKAP, will survey the sky with sensitivities better than those of the

GMRT Radio Halo Survey and should allow to investigate the process of formation of radio halos in a slightly wider range of cluster masses and redshifts.

The next generation of radio surveys at low radio frequencies (e.g. with the LOw Frequency ARray, LOFAR) may also unveil radio halos with very steep spectra that are difficult to detect with present radio surveys at higher frequencies. This is predicted by theoretical frameworks for the origin of radio halos based on turbulent acceleration [596; 597]. According to this scenario radio halos visible in present radio surveys are those generated in connection with the most energetic merger events in the universe; namely, during collisions between massive sub-clusters. On the other hand, radio halos with much steeper synchrotron spectra should be generated during less energetic and more common merger events, thus constituting a large population of halos that is presently invisible. However additional mechanisms may contribute to the acceleration of cosmic ray electrons in radio-halo regions, such as CRp-p collisions or Fermi-I–type acceleration in regions of fast magnetic reconnection [598]. These mechanisms may accelerate electrons to very high energies producing power-law synchrotron-spectra extending to very high frequencies with a slope substantially flatter, $\alpha \sim 1$. In the next few years the combination of surveys at different frequencies, such as LOFAR and ASKAP/EMU, will provide a unique chance to better constrain the role of these different mechanisms and their interplay [599; 600]. As an example, Figure 6.4 shows model expectations for the number of giant radio halos in ASKAP/EMU and WSRT/WODAN surveys, and the expected increase of the number of detectable halos with respect to present surveys (see caption).

Given the complexity of the scenario of the origin of relativistic particles in radio halos, constraints on the "off state" radio halos are extremely important. "Off state" in radio halos evolution is defined as the stage where the radio luminosity generated in galaxy clusters is below the region of present upper limits in the radio – X-ray diagram (see Figures 6.2 and 6.4). Different models predict corresponding different levels of radio emission in "off state" clusters, depending on the mechanisms responsible for the generation/acceleration of relativistic electrons and on their connection with clusters dynamics and evolution [576; 601–605]. Brown et al. [606] reported a tentative evidence for the detection of "off state" emission in galaxy clusters by means of the stacking of clusters fields from the SUMSS survey. ASKAP/EMU and WSRT/WODAN will provide a meaningful investigation of the level of the "off-state" of galaxy clusters based on an "all sky" survey that will improve present constraints. These surveys will start to probe the “off state” of galaxy clusters, but this will be limited to low redshifts, $z \leq 0.3 - 0.4$ (Fig. 6.4), thus a much better sensitivity is necessary. The minimum brightness that can be detected is limited by the confusion noise [607],

$$\sigma_c(\mu\mathrm{Jy}) \sim 25(\frac{\theta_1}{25})(\frac{\theta_2}{25})\nu_{GHz}^{-0.7} \tag{6.1.1}$$

where $(\theta/25)$ is the beam FWHM in units of 25 arcsec. Using eq.11 in [599], it can be shown that the minimum radio luminosity (in W/Hz) of radio halos detectable in a survey at confusion limit is :

$$P_{1.4,min} \sim 10^{20}(\frac{\theta_b}{10})(\frac{D_A}{Mpc})\frac{R}{Mpc}(1+z)^4 \ \mathrm{W/Hz} \tag{6.1.2}$$

where $\theta_b/10$ is the beam size in units of 10 arcsec, and D_A, z, and R are the angular distance, redshift and radius of radio halos. Surveys with the SKA1 and SKA2 will be limited by the confusion noise assuming 10 and 4 arcsec resolution, respectively (Fig. 6.3). Under these assuptions, Figure 6.4 shows the minimum radio luminosities of radio halos that can be detected with the SKA at 1.4 GHz (see caption). Interestingly, at redshift $z \leq 0.4 - 0.5$, the SKA will probe the entire range of radio luminosities that are expected in current theoretical models for the evolution of radio halos [eg. 604],

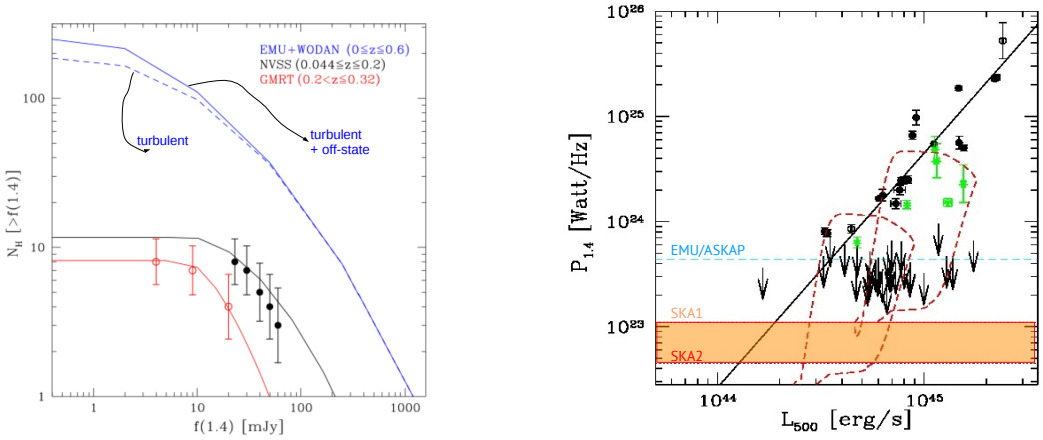

Figure 6.4. (LEFT) Number of Mpc-scale radio halos in EMU and WODAN surveys predicted from turbulent acceleration models of merging clusters (dashed line) and considering also "off-state" radio halos in more relaxed systems (solid lines) [from 599]. In the same plot we also show the number of radio halos in the GMRT survey and NVSS compared with model expectations. (RIGHT) A comparison between the distribution of galaxy clusters in the radio power vs X-ray luminosity (within R_{500}) plane and the evolutionary track (red dashed line) of clusters during a merger phase extracted from simulations that include turbulent reacceleration [604]. Orizonthal (magenta–dashed) line give the minimum luminosity of giant radio halos at redshift 0.4 that can be detected by the ASKAP/EMU survey (assuming 20 arcsec resolution, [from 599]), while the orange region gives the minimum luminosity of radio halos at redshift 0.4 that can be detected by SKA (top: SKA1 with 10 arcsec resolution, bottom: SKA2 with 4 arcsec resolution). Upper-limits are from the GMRT radio halo survey (z=0.2-0.35) and green points mark radio halos with ultra-steep spectrum.

thus providing crucial constraints to their origin. In addition, if we assume the radio–X-ray correlation in Figure 6.4, the SKA is expected to detect radio halos hosted in galaxy clusters with lower X-ray luminosity, down to $\sim 10^{44}$erg s^{-1}, at redshift $z \leq 0.5$, and to probe halos in more massive systems up to very high redshift, $z \sim 1 - 1.5$ (from eq.6.1.2 using $P_{1.4,min} \sim 10^{24}$W/Hz).

6.1.4 Constraints on CRs and Dark Matter physics

A fairly natural consequence of our present theoretical view of cosmic rays in galaxy clusters is that relativistic protons should be the dominant non-thermal particles component in the ICM, and that their properties trace the history of the complex interplay between particle acceleration and advection processes that take place in galaxy clusters from their formation epoch (e.g. [573] and references therein). The most direct approach to constrain the energy content of relativistic protons in galaxy clusters consists in the observation of the clusters gamma ray emission from the decay of the neutral pions that originate during proton-proton collisions in the ICM. The recent advent of the orbiting Fermi-LAT observatory greatly improved the detection prospects thanks to its unprecedented sensitivity at MeV/GeV energies. However, after about four years of observations no firm detection of galaxy clusters has been obtained, and only upper limits to the gamma-ray emission from nearby clusters have been derived ([608]). Assuming that cosmic ray protons follow the spatial distribution of the thermal ICM, these limits can be applied to constrain the ratio of the energy densities of CRs and thermal ICM to < 0.05, with a weak dependence on the spectrum of CRs. Less stringent limits are obtained in the case of flatter spatial distribution of the CRp component.
Even more stringent limits have been derived from deep, pointed observations at energies >100 GeV with ground-based Cherenkov telescopes (HESS, MAGIC, VERITAS). These limits however depend

on the (unknown) spectral shape of the proton-energy distribution and on the spatial distribution of cosmic ray protons in the clusters.

Radio observations of galaxy clusters can also be used to obtain limits on the ratio between cosmic rays and thermal energy density in the ICM [609; 610]. The majority of galaxy clusters do not host diffuse radio halos at the sensitivity level of present observations (Sect. 6.1.3). For undetected clusters, radio upper limits to the cluster-scale emission constrain the combination of magnetic field and secondary electrons energy densities in the ICM, and thus the energy budget in the form of primary cosmic ray protons. Present upper limits to the energy content of cosmic rays in the central regions of galaxy clusters are reported in Figure 6.5. For relatively strong magnetic fields the limits obtained from radio observations of "off-state" clusters are the most stringent. Assuming typical magnetic field strengths inferred from the analysis of Faraday Rotation Measures, constraints from radio observations and from gamma-ray upper limits from FERMI-LAT limit the ratio of the cosmic rays and thermal energy densities to a few percent level.

The SKA sensitivity to cluster-scale diffuse emission will be more than 10 time better than that of present radio telescopes. It will allow to obtain unprecedented upper limits to the cosmic rays energy content in galaxy clusters in case of non-detection of cluster-scale diffuse emission. The non detection of synchrotron radio emission generated by secondary electrons at this faint level will indicate that the energy density of cosmic rays is surprisingly below 0.1% of the thermal energy density of the ICM (Figure 6.5), implying a complete change of the present paradigm of acceleration and dynamics of cosmic rays in these systems.

Recent searches for Dark Matter annihilation in galaxy clusters have largely focused on indirect detections through gamma–ray emission [see 611–614]. Among the best motivated candidates for Dark Matter are weakly interacting massive particles, WIMPs. In this case gamma-rays are expected from the decay of neutral pions produced in the hadronization of strongly-interacting particles produced in the WIMP annihilation, and/or from the emission of secondary electrons and positrons (injected from the decay of particles produced in the annihilation process). Annihilation of Dark Matter in galaxy clusters can result in the production of stable Standard Model particles including electrons and positrons that, in a magnetised medium, also generate synchrotron radiation in the radio band. Similarly to the case of cosmic rays in galaxy clusters, radio upper limits to cluster-scale (core-scale) radio emission allow to constrain Dark Matter annihilation in these systems. Recently, using a sample of nearby galaxy clusters, Storm et al. [615] derived limits on the annihilation cross section from radio observations that are a factor ~ 3 better than limits derived from the non-detection of clusters in the gamma-ray band. Interestingly, in the most optimistic case of sub-structure models (using sub-structures from [616]) the derived limits already reach below the thermal relic cross section $< \sigma v >= 3 \times 10^{-26} \mathrm{cm}^3 \mathrm{s}^{-1}$ for masses of Dark Matter particles $m_\chi < 400$ GeV. As in the case of cosmic rays, a limitation of these studies comes from the uncertainties in the magnetic field models for galaxy clusters, with limits becoming progressively less stringent for weaker magnetic fields. However, radio observations with the SKA will overcome these limitations, thanks to the very large effective area, providing stringent limits even in the case of relatively weak ICM magnetic fields. If we assume conventional values (a few μG) for the ICM fields, SKA observations should provide the deepest constraints on Dark Matter in cluster-scale environments. In the case of non-detection of synchrotron emission from the cores of nearby clusters, limits derived with the SKA will reach below the thermal relic cross section for Dark Matter masses $m_\chi < 100$ GeV even under the conservative assumption of NFW profile for the spatial distribution of Dark Matter. Interestingly, these limits will be more than 10 times deeper assuming optimistic substructure models, such as profiles from [616], reaching below the thermal relic cross section for particles with masses $m_\chi <$ many TeV. In this respect SKA observations will constrain the region of Dark Matter (WIMP) parameters that is

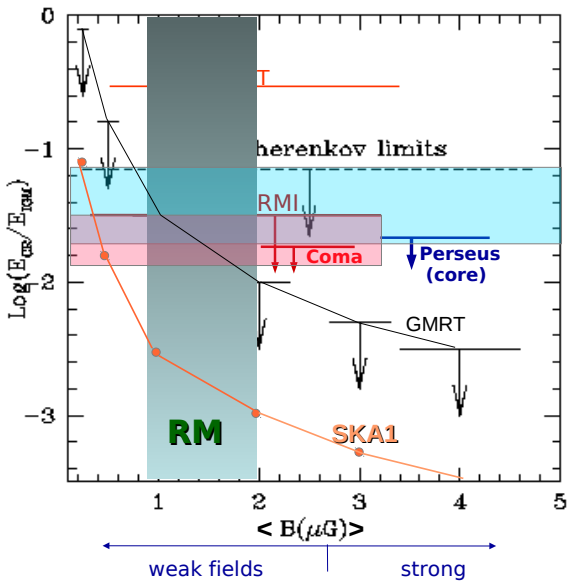

Figure 6.5. A compilation of limits to the radio of cosmic rays and thermal energy densities in galaxy clusters obtained from gamma-ray observations (blue region: Cherenkov, red region: Fermi-LAT) and from GMRT radio observations (black-arrows). The vertical region marks the reference range of values of magnetic fields in the central Mpc region in galaxy clusters (from Rotation Measures, Section 6.2). The orange line marks the sensitivity level that can be obtained using observations with the SKA1.

still allowed by the LHC experiment.

6.1.5 Radio-mode feedback in clusters of galaxies

X-ray observations show that the inferred cooling time of the ICM in the dense, central regions of relaxed galaxy clusters is typically much shorter than the dynamical time of the cluster, implying the presence of a cooling flow [617]. However, the minimum temperature in the center is only a factor of ~ 3 lower than the ambient temperature [see 618], therefore the gas does not appear to cool massively to low temperatures. These properties force one to consider complex non-gravitational physical processes in order to provide smoothly distributed heating on scales of about 100 kpc and stop the cooling process.

In the last ten years, the combination of deep images in the X-ray and radio bands have shown in the most spectacular way that such a process is provided by the radio feedback from the central radio galaxy through the relativistic radio jets interacting with the surrounding ICM [see 572, and references therein]. In Figure 6.6 we show clear examples of radio lobes filling the cavities in the ICM in a group (left panel) and in a massive cluster (right panel). These radio images show the presence of a significant non thermal component in the ICM and of a large-scale magnetic field of the order of $1\mu G$. This non-thermal component is directly injected by the radio AGN in the BCG, and must be distinguished from the diffuse radio emission in halos. In the radio-feedback bubbles, instead, thermal and non-thermal components are spatially separated, since the former has been pushed away by the relativistic jets [571; 621; 622].

The study of cavities in the ICM inflated by relativistic electrons has been the subject of several studies aimed at understanding the energetics of the feedback processes, and the mechanism by which the mechanical energy is transferred to the ICM. The energetics can be estimated thanks to the en-

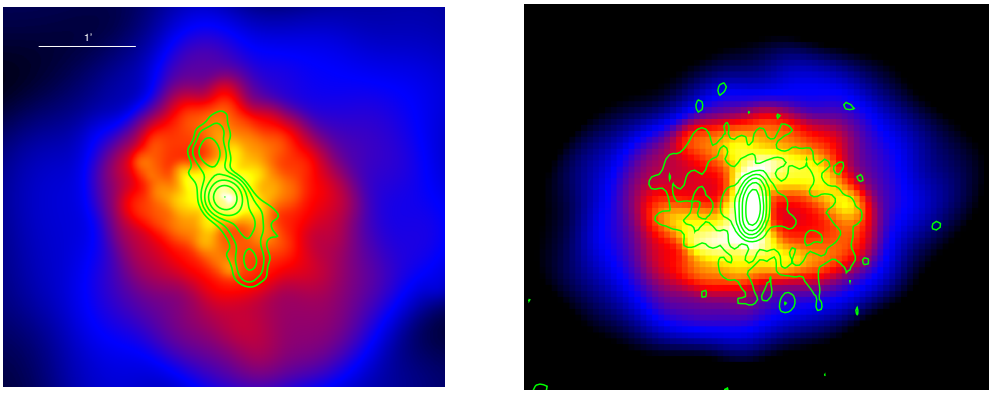

Figure 6.6. Left panel: X-ray image of the galaxy group HCG 62 at $z = 0.0137$ [619] with superimposed GMRT radio contours at 610 MHz. Right panel: X-ray image of the Galaxy cluster RBS 797 at $z = 0.35$ [620] with superimposed VLA radio contours at 1.4 GHz. In both cases large cavities in the ICM are observed to be coincident with the radio lobes.

thalpy ($4P \times V$ for relativistic plasma) of the bubbles [see 623; 624], while the heating mechanism is still strongly debated. This mechanism is important also because it is thought to be the same responsible of the heating of the gas at galactic scales, efficiently quenching the star formation processes and therefore setting the stellar mass scales and colors for massive galaxies [625]. This process is actually observed in the central radio galaxy in cool core clusters [see 626; 627].

At present, the study of the radio-mode feedback in clusters is limited to $z < 0.7$ and for very few cases [628], while virialized cluster are currently detected up to redshifts of 1.6 or larger. Therefore, there is a wide redshift range where the feedback mechanism is still unexplored. We also know that cool cores undergo some negative evolution with the redshift, which is also expected on the present knowledge of cool core formation. Basically, at higher redshift less time is available for the cluster to reach the dynamical equilibrium and develop a cool core. However, recent studies show that they are already present and well developed at high redshift $z \sim 1$, suggesting that cool core formation is occurring on a short time-scale [see 629; 630]. Since the association of radio AGN and cool core is ubiquitous [631], we expect to be able to trace the feedback activity in clusters, and therefore study the interplay between thermal and non-thermal plasma in the central regions of galaxy clusters, up to the highest redshift where clusters are found. In addition, polarisation studies will allow to constrain the coherent scales/topology of the magnetic field in these bubbles/lobes and most important the properties of the magnetic field at the boundaries of relativistic bubbles/lobes, where they interact with the thermal ICM. The combination of polarisation and high spatial resolution will constrain the mixing of thermal and non-thermal plasma, quantify the energetics of the bubbles, the viscosity of the ICM and the amplification of the magnetic field. Finally, strong radio sources can be the beacon of massive protoclusters at redshift 2 and larger [see, e.g., 632]. Therefore, radio selection of clusters and protocluster may be an efficient method to find the progenitor of massive clusters at $z > 2$, where the red sequence of the cluster galaxies is not fully established yet, and the ICM is not shining in the X-ray band, indicating an uncomplete virialization.

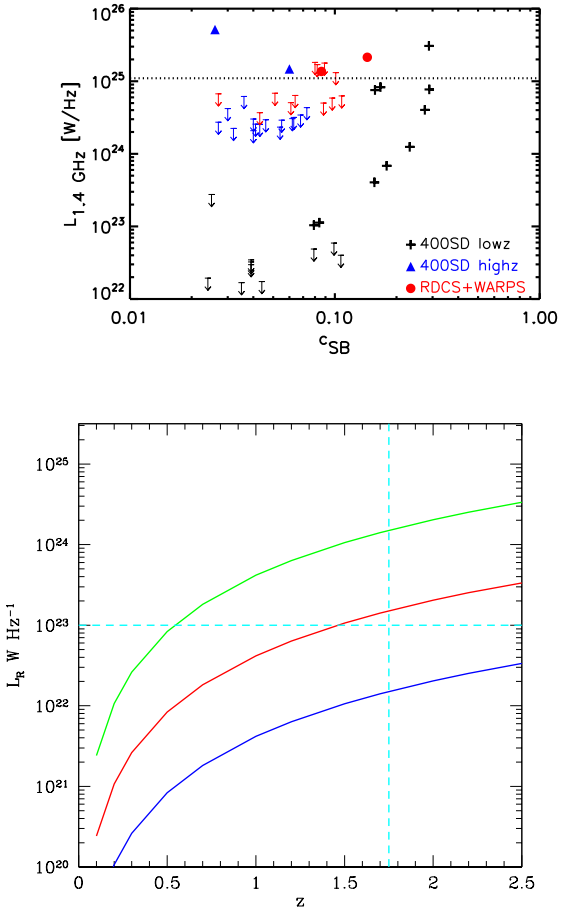

Figure 6.7. Top panel: relation between the radio luminosity of sources in close proximity to the cluster cores, $L_{1.4}$ GHz, and the surface brightness concentration, C_{SB}. Arrows refer to upper limits of non-detections. The dotted line at 1.1×10^{25} W Hz^{-1} marks the luminosity limit at $z = 1$ for NVSS sources, corresponding to the flux limit of 2.5 mJy [from 629]. Bottom panel: radio power at 1.4 GHz detectable with a sensitivity of 1-10-100 μJy as a function of redshift. The vertical dashed line shows the highest redshift where virialized, X-ray emitting clusters are currently detected, while the horizontal dashed line shows the minimum radio luminosity measured in a radio galaxy hosting a cool core in local clusters.

To summarize, the radio feedback in clusters of galaxies is a scientific case key to the physics of the ICM, the evolution of the cosmic large scale structures, and the identification of protocluster at very high redshift. Radio astronomy in the era of SKA and its pathfinders can be the main scientific driver in these fields.

Tracing the feedback in galaxy clusters in the radio band consists in detecting the presence of radio AGN in the central galaxy, measuring its total power and, if possible, resolve the radio emission in the radio lobes filling the cavities in the ICM. These studies have been shown to be very succesfull for local targets, where deep radio and X-ray data are both available, but becomes increasingly difficult at higher redshifts. Recently, a few studies focused on high-redshift clusters and on the evolution of their properties with cosmic time. In particular, it has been realized that the evolution of the cool-core phenomenon is mirrored by the evolution of the feedback processes itself. A simple correlation of the radio power and the cool core strength (quantified through the

concentration parameter C_{SB}) has been shown for low and medium redshift clusters, see Figure 6.7, top panel [629]. It is observed that the luminosity of radio galaxies in the center of cool core cluster have radio powers ranging from $\sim 10^{23}$ to 10^{25} W Hz^{-1}, typical of FRI galaxies. An ongoing EVLA program (PI P. Tozzi) is being carried out by an italian research group, targeting the large majority of the high redshift clusters with X-ray data known to date to extend this relation up to $z \sim 1$.

From a simple visual inspection of Figure 6.7, top panel, we conclude that we need to detect every radio galaxy at least down to 10^{23} W Hz^{-1} (at 1.4 GHz) in order to explore the same dynamical range at high redshift. In the bottom panel of Figure 6.7 we show the radio power in unresolved sources corresponding to a detection limit of 100, 10 and 1 μJy from top (green line) to bottom (blue line). We find that sources above 10^{23} W Hz^{-1} can be detected up to redshift $z \sim 1.7$ (the largest redshift where virialized galaxy clusters are currently found) with a sensitivity of 10 μJy per beam. Assuming a detection threshold at 5 σ, 10 μJy corresponds to an rms noise of 2 μJy per beam. This can be achieved with 200 hours[1] with ASKAP (36 antennas of 12m diameter, assuming a bandwidth of 300 MHz), but only 16 hours with MEERKAT (64 antennas of 13.5m diameter, assuming a bandwidth of 700 MHz). Therefore, with SKA pathfinders it would still take a significant amount of time to follow up a large sample of high-z ($z > 1$) clusters (100 clusters with X-ray detection at $z > 1$ is a realistic number expected from of all the present-day X-ray facilities across their lifetime). On the other hand, it would take about half an hour with SKA 1 (250 antennas of 15m diameter), and about 20 seconds with SKA 2 (2500 antennas of 15m diameter). Clearly SKA will open an unprecedented window on the exploration of cosmic feedback at any redshift in massive clusters and will be able to strongly constrain the duty cycle of radio galaxies in the cluster center. If we consider radio power observed in small groups of galaxies, we need to extend the dynamic range down to few $\times 10^{21}$ W Hz^{-1}. This implies detection limits about 50 times lower, corresponding to 40 nJy per beam. This can be achieved with 15 hours with SKA 2.

Another relevant aspect is to detect and resolve the radio lobes produced by the relativistic electrons which are responsible of the cavities in the ICM. If we use as a reference the bubble size in the two objects shown in Figure 6.6, we can straightforwardly compute the typical angular size of the bubbles as a function of the redshift. For the group HCG 62 ($z = 0.0137$) the average bubble size (assuming a roughly spherical shape) is 20 kpc, while for the cluster RBS797 ($z = 0.35$) the size is about 70 kpc. If we focus on targets at $z > 1$ the angular size turns out to be about 2.5 and 8 arcsec, respectively, with a weak dependence on the redshift. We therefore assume that an angular resolution of about 1 arcsec will be sufficient to resolve the radio lobes both in groups and clusters (in massive clusters, also a resolution of ~ 4 arcsec would be sufficient).

To derive a realistic detection criterion, we assume the total measured radio power at 1.4 GHz in HCG 62 and RBS797, which is 2.7×10^{21} W Hz^{-1} and 7.4×10^{24} W Hz^{-1}, respectively, with a spectral index $\alpha \sim 1$. For these values, the radio flux density per resolution element as a function of redshift is plotted in Figure 6.8 for a beam of 1 (solid line) and 2 (dashed line) arcsec. Clearly, the detection of extended radio emission appears to be within reach of SKA 2 even in the case of the weak radio lobes expected in small groups of galaxies.

Our preliminary feasibility study shows that the radio feedback will be unveiled practically at any level up to $z \sim 1.7$, a redshift where virialized clusters are currently detected in the X-ray band. When SKA 2 will be fully operational, the knowledge of distant galaxy clusters will be largely but unpredictably changed. A large number of optically and IR selected clusters will be available thanks to the forthcoming surveys of the EUCLID satellite, of the LSST project, and, most important, of future Sunyaev Zeldovich surveys which directly probe the ICM and therefore can be directly

[1]Exposure times here and in the following have been obtained through the exposure time calculator http://www-astro.physics.ox.ac.uk/hrk/SKA_EXPOSURE.html

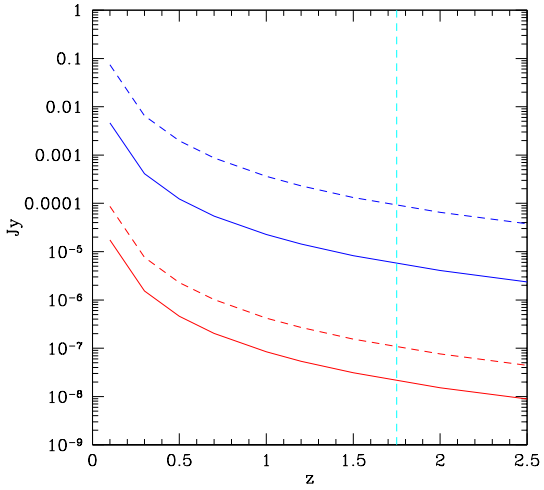

Figure 6.8. Flux density per beam with a resolution of 1 arcsec (solid lines) and 2 arcsec (dashed lines) expected for radio lobes analogous to those observed in the cluster RBS797 (red lines) and the group HCG 62 (blue lines).

combined with the radio data to search for cavities. The future of X-ray astronomy is more uncertain at the time of writing (2013) due to the difficult task constituted by the realization of a Super-Chandra satellite, providing at the same time arcsec resolution, large effective area (a few m^2) and a large field of view. Clearly, deep and highly resolved X-ray data will be crucial to fully understand the properties of the ICM on a wide redshift range, and hence to put on more solid basis the mass proxies derived from the X-ray observations of the ICM. In this field, as in many others, the advent of SKA will provide access to incredibly deep and high quality data, which are hardly matched by any planned of foreseen facility in other wavebands.

6.1.6 Synergies with Athena+

Athena+ (http://www.the-athena-x-ray-observatory.eu/) is an X-ray observatory to be proposed as a large mission for the ESA science program. It will incorporate a single telescope with a fixed focal length (12 m) and two interchangeable instruments in the focal plane (WFI and X-IFU). The X-ray Integral Field Unit (X-IFU) will cover the 0.3 to 10 keV energy range with unprecedented 2.5 energy resolution (at 6 keV) over a 5 arcmin circular field of view. The Wide Field Imager (WFI) will provide a large field of view (>40 arcmin diameter) and excellent spatial resolution (5 arcsec HEW) over the 0.1 to 12 keV energy range, simultaneously with spectrally and time-resolved photon detection. Athena+ will have the unique capabilities, in terms of collecting area and spectral resolution, to answer the most outstanding questions on how the feedback operates in gravitationally-bound structures and which is the inter-relation in the evolution of AGNs, galaxies and large-scale structures. Complementary data from present (LOFAR) and future (SKA and relative pathfinders) radio surveys will be essential to reveal the populations of (i) the radio cluster galaxies at low and moderate luminosity out to the highest redshifts and (ii) the extended emission connected to the non-thermal component of the energy budget in galaxy clusters. The evolution of radio jets will be mapped in X-rays though the

detection of the shocked gas around expanding radio lobes. X-IFU's spectral resolution will enable direct measurement of the shock expansion speeds in nearby systems. With X-IFU, it will be also possible to measure the broadening and displacement of the emission lines in X-ray spectra allowing to map the total kinetic energy stored in the bulk motions and the properties of the ICM velocity field at different spatial scales (e.g. [633]). These observations will provide a completely new window on the processes responsible for the assembly of galaxy clusters. Turbulent and shocked regions, generated during cluster formation (e.g. [634]) and potentially associated to the sources of diffuse synchrotron radio emission (e.g. [571]), will be mapped routinely. The X-ray morphology, temperature and density of the thermal gas will be estimated permitting to characterize the physical and dynamical state of the ICM and its connection to radio halos and relics (e.g. [575]). At high redshift, the contamination of the inverse Compton emission from radio photons to the total X-ray emission will be evaluated through a joint modelling of the thermal and non-thermal components of the X-ray spectrum. Athena+ observations of the hot plasma, the most significant baryonic mass component of clusters, combined with high-sensitivity radio observations (e.g. SKA), high angular resolution SZ millimetric observations (e.g. GBT, IRAM, SRT), observations of the cold baryons in galaxies (e.g. from JWST, ALMA, and E-ELT) and of the dark matter via lensing data (LSST, Pan-starrs, Euclid) will provide, for the first time, the details needed for a sufficiently critical comparison with theory. The major breakthrough of a detailed understanding of structure formation and evolution on cluster scales will probably come from simulation-assisted interpretation and modelling of these new generation observational data.

6.2 Magnetic Fields

F. Govoni, V. Vacca, M. Murgia, L. Feretti, F. Finelli, G. Giovannini, D. Guidetti, G. Brunetti, D. Paoletti

6.2.1 Introduction

The presence of magnetic fields in extragalactic astronomical objects has been unambiguously revealed. They have been detected in galaxies, galaxy groups, galaxy clusters, and recently even along filaments, in the large scale structure of the Universe. Indeed, the detection of synchrotron radiation in cosmological filaments connecting rich galaxy clusters suggests that magnetic fields are present over scales as large as $\simeq 5$ Mpc e.g. [635].

Much of what is known about magnetic fields in the Universe comes from sensitive radio observations. This is because extragalactic radio emission is mainly due to synchrotron radiation which is a direct probe of relativistic electrons gyrating around magnetic field lines. The observed intensity of the synchrotron emission is related to the field strength, while the fraction of polarized emission is related to the field's degree of ordering. Moreover, Faraday rotation is related on the magneto-ionic medium along the line of sight, so that magnetic fields properties can be derived through the analysis of polarized radio sources.

Determining magnetic field strength and structure in the interstellar medium, in the intracluster medium, at the boundary of galaxy clusters, in the bridges which join clusters, or in the filamentary cosmic web, is important for answering fundamental questions about structure formation and the origins of cosmic magnetism. Magnetic fields control the cosmic ray motion, contribute to the energy budget and can strongly affect the energy transfer, the dynamic and evolution of all the above mentioned systems. Understanding the magnetic Universe is a major challenge in modern astrophysics, for this reason 'Cosmic Magnetism' has been acknowledge as a key science project of the SKA.

Despite of their importance, our knowledge about magnetic fields is still poor and numerous open questions remain unanswered. What are the magnetic field strength and structure? How did

magnetic fields form? How did they evolve and how are they maintained? These are all questions we can hope to address with the unique capabilities of the SKA through deep observations.

6.2.2 Primordial magnetic fields vs seed magnetic fields

Large scale magnetic fields of the order of few μG observed in galaxies and galaxy clusters may be the product of the amplification, during structure formation, of primordial magnetic seeds [636]. Several models of early universe predict the generation of primordial magnetic fields (hereafter PMF), either during inflation or during cosmological phase transitions (see [637] for a review).

PMF have an impact on cosmic observables and therefore it is possible to constrain their characteristics through cosmological observations. The impact of PMF on Big Bang nucleosynthesis constrain their amplitude at the μG level [638].

Tighter constraints at the nG level come from CMB temperature power spectrum [639–641] and bispectrum [642–646].

PMF have also an impact on structure formation. The presence of an extra component of anisotropic stress carried by the PMF and the Lorentz force induced on baryons modifies the evolution of matter perturbations and has an impact on the small scale matter power spectrum and on structure formation and early evolution. This impact has been studied through magnetohydrodynamics N-body numerical simulations [647] but the field is still at early stages of development especially concerning the analytical non/linear treatments.

In the recent years, data from the Gamma ray observatory FERMI have added new intriguing observations in the context of cosmological magnetic fields which might be interpreted as a *lower* bound for the amplitude for primordial one. The data on gamma ray cascades from Blazars show a lack of photons which is compatible with diffuse extra-galactic magnetic fields in the intracluster medium (voids) with a lower bounds of the order of $10^{-15} - 10^{-16}$ G[648–650]. If this lower bound for PMF will be confirmed, SKA can perform crucial measurements towards the probe of the generation mechanism.

Current CMB constraints on PMF are dominated by the accuracy in the temperature anisotropies measurement. PMF impact on CMB anisotropies is at high multipoles ($\ell \gtrsim 1500$) and is not suppressed by the Silk damping: recent measurements from WMAP combined with SPT and Planck have been crucial in disentangling a PMF contribution from high-ℓ foreground and secondary anisotropies (see [639]). SKA measurement of very high-ℓ multipoles can improve these bounds on PMF as well as the characterization of foreground and secondary anisotropies beyond the Silk damping tail.

There are great expectations from the measurement of CMB polarization anisotropies. PMF contribution to CMB anisotropies is generated either at the last-scattering surface or by Faraday rotation of the intervening magnetic fields of the stochastic background with the characteristic frequency dependence $\propto \nu^{-4}$ [651]. The smoking gun of the Faraday rotation from a stochastic background of PMF is a B-polarization signal at very high-ℓ multipoles, $\ell \sim 10^4$. SKA bands can target such signal. CMB polarization is not only a complementary probe to temperature anisotropies but can be crucial to determine the nature of the stochastic background: if PMF are generated with a non-vanishing helicity parity-odd correlators, such as Temperature-B mode polarization and E mode-B mode polarization are expected to be non-zero at high multipoles.

6.2.3 Intracluster Magnetic Fields

Several observational evidences indicate that Mpc-scale magnetic fields are present in the intracluster medium. The most important evidences are:
1) the existence of extended synchrotron sources diffuse in the intracluster medium like halos and relics e.g. [589];

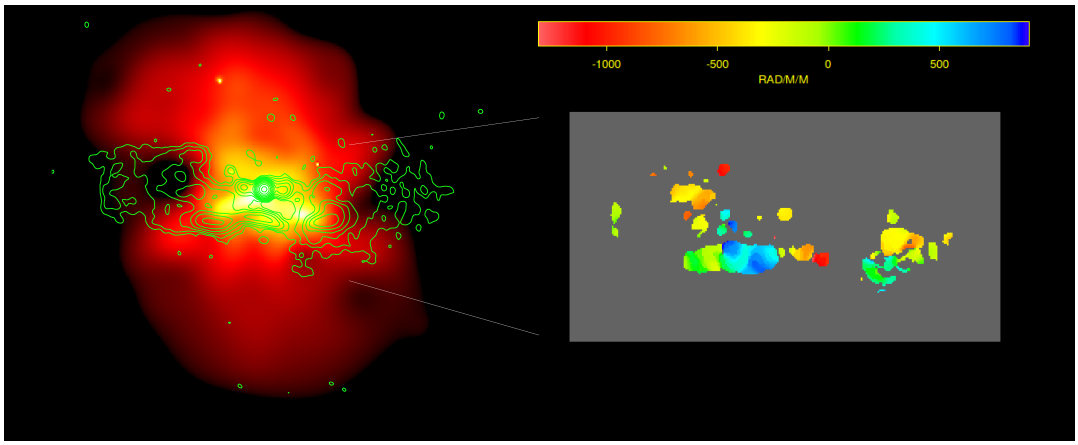

Figure 6.9. Left panel: Chandra X-ray image of the galaxy cluster A2199 with VLA radio contours of 3C338 overlaid. Pronounced X-ray cavities can be identified in correspondence of the radio galaxy lobes. Right panel: rotation measure image of 3C338. Taken from Vacca et al.(2012) [661] .

2) the excess of the Faraday Rotation Measure (RM) from sources behind or inside galaxy clusters with respect to field radio sources e.g. [652];
3) the systematic decrease of the sources polarized emission observed toward the center of many galaxy clusters is also interpreted as a consequence of the Faraday rotation originating in the intracluster medium [653].

These studies (see e.g. [571; 654–656] for reviews) reveal magnetic field strengths with values of a few μG at the center of merging galaxy clusters and up to tens of μG at the center of relaxed cooling core clusters. The magnetic field intensity is likely to decrease with the distance from the cluster center. Moreover, intracluster magnetic fields appear fluctuating both in strength and structure over a range of scales between few kpc and Mpc.

There is a general agreement on the fact that primordial magnetic fields have been amplified to the observed levels by the merger events occurring during the formation of galaxy clusters (see e.g. the review [657]). Cosmological magnetohydrodynamical cluster simulations predict that during major merger events, considerable amount of energy is injected at large spatial scales. As the cluster relaxes, the turbulent motions are dissipated on smaller and smaller scales. Indeed, we may expect that the magnetic field power spectrum depends on cluster dynamics. However, a good knowledge of the magnetic field power spectrum is still limited to a few nearby galaxy clusters, and a number of topics related to the intracluster magnetic fields such as their possible evolution with redshift and dynamical state of the cluster, and their interplay with the thermal intracluster medium, have not been investigated in detail yet.

Our base of knowledge on cluster magnetic fields will be greatly enhanced by SKA which will permit to study the details of total intensity and polarization of radio halos and the rotation measure of radio galaxies in a large number of galaxy clusters. The high-sensitivity, low instrumental polarization contribution, large-bandwidth, and large field of view of SKA will allow high-accuracy investigations of the intracluster magnetic fields in the central regions of galaxy clusters, as well as in the outskirts, where the magnetic fields are weaker. In addition, SKA will permit to investigate cluster magnetic fields at high redshift. Studying the cosmological evolution of fields in clusters might lead to the origin of magnetism and constraint the mechanism of their amplification.

Faraday rotation effect

Small-scale cluster magnetic fields are studied through detailed rotation measure images of radio galaxies located within or behind galaxy clusters e.g.[582; 658–660]. The presence of a magnetized plasma between an observer and a radio source changes the properties of the incoming polarized emission. In particular, as it passes through the magnetized plasma, the polarized synchrotron radiation undergoes the following rotation of the plane of polarization:

$$\Psi_{Obs}(\lambda) = \Psi_{Int} + \lambda^2 \times RM \tag{6.2.1}$$

where $\Psi_{Obs}(\lambda)$ is the observed polarization angle at a wavelength λ and Ψ_{Int} is the intrinsic polarization angle. The rotation measure RM is related to the plasma thermal electron density, n_e, and magnetic field along the line-of-sight, $B_{\parallel}$, by the equation:

$$RM[rad/m^2] = 812 \int_0^{L[kpc]} n_e[cm^{-3}] B_{\parallel}[\mu G] \mathrm{d}l. \tag{6.2.2}$$

Therefore, information on the intracluster magnetic fields can be obtained, in conjunction with X-ray observations of the hot gas, through the analysis of the rotation measure of radio galaxies in the background or in the galaxy clusters themselves. To date, detailed RM images are available just for few radio galaxies in few clusters. An example [661] of rotation measure image is shown in Figure 6.9. The best case is the Coma cluster [662], where the polarimetric properties of 7 radio galaxies have been analyzed. In general, the RM distributions seen across the radio galaxies present patchy structures. The observed RM fluctuations indicate that the intracluster magnetic field is not regularly ordered but turbulent on scales ranging from tens of kpc to $\lesssim$ 100 pc. Moreover, Guidetti et al. [663] have shown rotation measure images for sources located in a range of environments (from small group to rich cluster core) with peculiar banded patterns across the radio lobes, implying that the magnetic fields responsible for the Faraday rotation are anisotropic. This work has demonstrated unequivocally for the first time that interaction between radio galaxies and their immediate environments strongly affect the magnetisation of the intracluster medium making the scenario significantly more complicated than was apparent from earlier work. A further RM component may stem from thermal material mixed with the synchrotron emitting plasma [664; 665]. This is a point widely debated and is of primary importance also to understand the pressure balance and dynamics of radio galaxies in their environment. Therefore, RM measurements probe the complex topology of the cluster magnetic field and indeed dedicated software tools and semi-analytical approach have been developed to constrain the magnetic field power spectrum parameters on the basis of the RM images [581; 666–668]. In order to uniquely separate external from possible internal Faraday rotation, more sensitive and higher resolution radio observations of a larger number of sources are required.

The sensitivities of the current facilities limit the RM studies to a few radio galaxies per cluster. The SKA will have the potential of measuring the RM toward a large number of sources by deriving a detailed description of the strength, structure, and radial decrease of cluster magnetic fields. In particular, Krause et al. [669] found that the full SKA aperture array would be able to make very detailed magnetic field structure measurements of clusters with more than 100 background sources per cluster up to a redshift of 0.5 and more than 1000 background sources per cluster for nearby clusters. In high redshift clusters, SKA could constrain the power law index for the magnetic field evolution to better than Δm=0.4, if the magnetic field in clusters should follow $B \propto (1+z)^m$.

Bogdanović et al. [670] evaluated the effects of two different physical mechanisms on the Faraday RM of a magnetized cooling-core cluster, in the context of the planned capabilities of the JVLA

and SKA. They compared a theoretical scenario in which conduction-driven MHD instabilities dominate the dynamics of the ICM, to a scenario in which magnetic field topology is defined by turbulent motions. Within the bounds of their models they found that the two mechanisms can produce strikingly different RM patterns and that future polarimetric measurements, that can be achieved in longer exposures with JVLA and relatively short exposures with SKA, will have sufficient sensitivity to discriminate between them.

In conclusion, the SKA would be able to detect RM from 100-1000 radio sources per cluster with a high spatial resolution. The capabilities of SKA will give the possibility to significantly improve the present knowledge about intracluster magnetic fields giving the opportunity to extend the study of the magnetic field structure on a range of scales never explored so far.

Polarization of cluster diffuse radio sources

Large-scale cluster magnetic fields are studied through radio halos, permeating the cluster center, and relics at the cluster periphery. These cluster synchrotron sources are diffuse in the intracluster medium and extend on up to Mpc scales, revealing that magnetic fields are spread over large volumes of space. Under the assumption that radio halos and relics are on the minimum energy condition and hence their magnetic energy density is comparable to the energy density in relativistic electrons, it is found that the volume-averaged magnetic field is of the order of $\sim 0.1-1\ \mu$G.

Radio relics are typically strongly polarized e.g. [671; 672], with fractional polarizations up to 30 -50%. The detection of polarized emission from radio halos has been shown to be extremely important to constrain the magnetic field power spectrum at the cluster center [581–583]. However, detecting this polarized signal is a very hard task with the current radio facilities and so far only a few radio halos have been imaged in polarization [673–675].

In preparation for SKA, several next-generation radio telescopes and upgrades are being constructed around the world. Among them, APERTIF, ASKAP, LOFAR, Meerkat, and JVLA all offer the chance to explore the polarization properties of cluster diffuse emission. Deep polarization sky surveys are being planned for many of these telescopes. The survey WODAN (Westerbork Observations of the Deep APERTIF Northern-Sky [9]) will use APERTIF to explore at 1.4 GHz the northern sky. This survey will provide a spatial resolution of $\simeq 15''$ and a sensitivity of about 10μJy/beam. Similar performances will be reached in the southern sky with ASKAP through the polarization survey POSSUM (POlarization Sky Survey of the Universe's Magnetism). These surveys may play an important role in the study of non-thermal cluster physics through the analysis of polarized radio halos.

It is possible to predict the expected polarized level of radio halo synchrotron emission to compare with the sensitivity level expected for SKA, its precursors, and its pathfinders. Figure 6.10 shows an example of polarized emission in two mock radio halos, representative for halos of strong and intermediate radio power. The images have been obtained by using the cosmological magnetohydrodynamical cluster simulations by Xu et al. [677]. The polarized halo emission is at 1.4 GHz, with a bandwidth of 300 MHz, and a spatial resolution of $\simeq 15''$. The top panel of Figure 6.10 shows the radio halos as they would appear in an ideal observation, neglecting the noise effects. The bottom panel of Figure 6.10 shows how the clusters polarization will appear in observations whose sensitivities are in line with that expected for future sky surveys conducted at 1.4 GHz in preparation for SKA. The figure shows that the resolution and sensitivity values expected to be obtained in future sky surveys performed at 1.4 GHz with the SKA precursors and pathfinders (like APERTIF and ASKAP) are very promising to detect the polarized emission of the most powerful ($L_{1.4GHz} \simeq 2.5\times10^{25}$ Watt/Hz) radio halos, while halos of intermediate luminosity ($L_{1.4GHz} \simeq 2\times10^{24}$ Watt/Hz) will be hardly detectable.

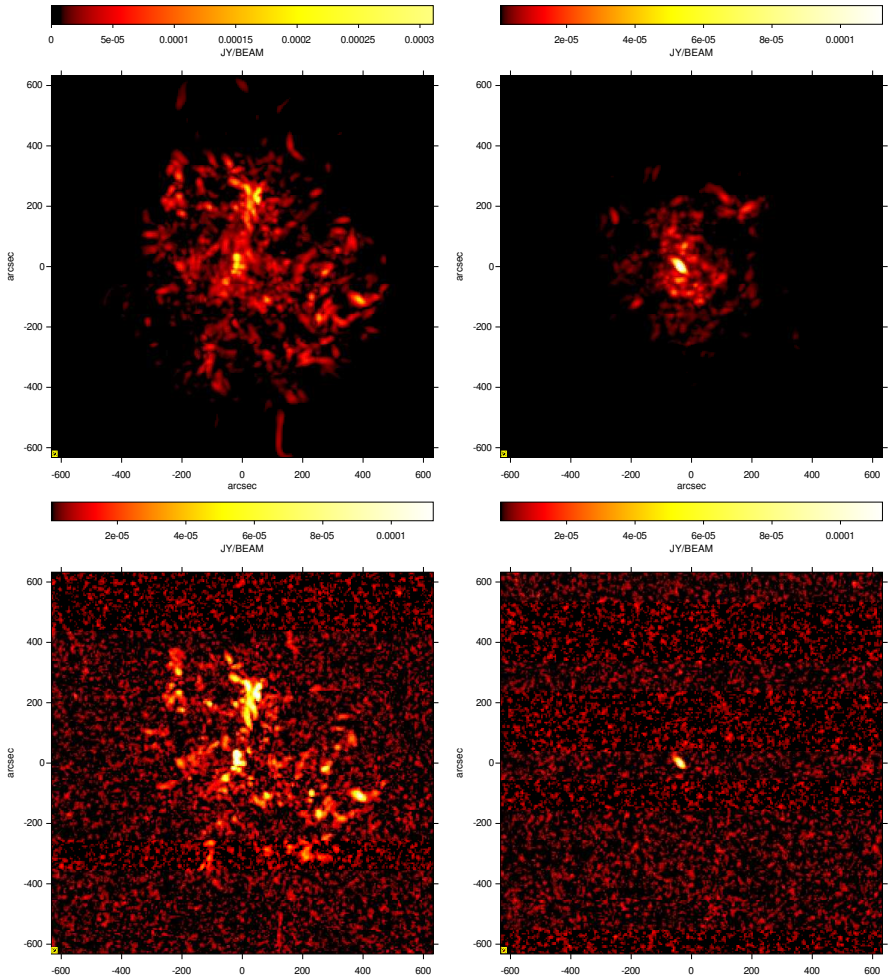

Figure 6.10. Top: example (taken from [676]) of two mock radio halos obtained by using the cosmological magnetohydrodynamical cluster simulations by Xu et al. (2012). Simulations are performed in polarization at 1.4 GHz with a bandwidth of 300 MHz and a spatial resolution of $\simeq 15''$. Left and right panels refer to simulated clusters with radio power in total intensity of $P_{1.4GHz} \simeq 2.5 \times 10^{25}$ and $P_{1.4GHz} \simeq 2 \times 10^{24}$, respectively. Top: polarization of the radio halos in an ideal observation, neglecting the noise effects. Bottom: polarization of the radio halos in observations whose sensitivities are in line with that expected for future sky surveys conducted at 1.4 GHz in preparation for SKA with SKA precursors and pathfinders.

In order to detect polarized signal in this kind of radio halos at a resolution of $15''$, future instruments like SKA should reach a polarization sensitivity of about 1 μJy/beam.

7 Stellar Astronomy

7.1 Stellar Radio Emission in the SKA Era

G. Umana, C. Trigilio, C. Buemi and P. Leto

In the last few years, radio surveys have provided a large number of unexpected discoveries, revealing different populations of radio emitting objects, a very gold mine for successive, more focussed radio studies. Unfortunately, up to now, very few stars were found in large radio surveys and nearly all known radio stars have been detected by targeted observations directed at small samples of stars thought likely to be radio emitter. This approach has been proven to be quite productive but it is biased against discovering unknown, unexpected, or intrinsically rare objects, preventing a good knowledge of radio stars at the sub-mJy level. As consequence, at the moment, it is quite difficult to provide a trustworthy forecast on what can be the real potentiality of the near all sky, deep ($\sim 1 - 10\,\mu$Jy) surveys planned with the SKA and its pathfinders in the field of stellar radio astronomy.

The improvement of the observational capabilities have lead to the discovery of radio emission in a broad variety of stellar objects from all stages of stellar evolution. Radio stars emit a tiny fraction of their total luminosity in the radio band. For example, the quiet Sun has a radio luminosity which is only 10^{-12} its bolometric luminosity. Nevertheless, in many cases, radio observations of stars and stellar systems have revealed astrophysical phenomena, not detectable by other means, that play a fundamental role in our understanding of stellar evolution and of physical processes that operates in stellar atmospheres.

Generally, the brightest stellar radio emission appears to be associated with magnetically-induced phenomena, such as stellar flares, related to the presence of a strong and/or variable stellar magnetic field (high brightness temperature) or with enhanced mass-loss (large emitting surface).

Much of our knowledge on microwave emission from radio stars comes from the study of active stars and binary systems as a large fraction of them have been found to be strong radio sources. The radio flux arises from the interaction between the stellar magnetic field with mildly relativistic particles, i. e. gyrosynchrotron emission. The same emission mechanism is at the origin of radio emission from pre-main sequence (PMS) stars and X-ray binaries. Non-thermal radio emission also originates from shocks of colliding winds in massive binaries and from Pulsar. There is a growing evidence that radio flares can occur also as narrow band, rapid, intense and highly polarized (up to 100 %) radio bursts, that are observed especially at low frequency (<1.5 GHz). For their extreme characteristics, this kind of radio flares have generally been interpreted as result of coherent emission mechanisms, such as the Electron Cyclotron Maser Emission (ECME). Coherent burst emission has been observed in different classes of stellar objects, RS CVns, flares stars, Brown Dwarfs (BD), Chemically Peculiar Stars (CPs), all having as common ingredient a strong and also, but not necessarily, variable magnetic field and a source of energetic particles. Thermal emission (bremsstrahlung emission) is expected from winds associated to Wolf-Rayet (WR) and OB stars, shells surrounding Planetary Nebulae (PN) and Novae and jets from symbiotic stars and class 0 PMS stars.

Two areas of stellar radio emission will particularly benefit from high sensitive radio observa-

tions: the study of non-thermal stellar flares in active stars and binary systems and of the coherent events.

7.1.1 Stellar Coronae: the solar-stellar connection

In the Sun, according to the evaporation model [678], beams of fast electrons travel down magnetic fields and deposit their energy in the chromosphere, whereupon heated plasma expands into coronal magnetic flux tubes. This hot plasma then cools radiatively and through conduction. The solar model can be used in trying to understand the energetics and location of flares in active stars. Various theoretical mechanisms for this have been proposed, but more observations are needed to check ideas, in particular, the sought non-thermal electron population in the impulsive phase of flares. This is relevant to the power-law index of the electron energy distribution and its lower energy bound [679] used in microwave data analysis.

Until now, targeted observations of well known radio stars have constituted the best approach to investigate their radio emission mechanisms (e.g. flare development, spectral and polarisation evolution, emission mechanism, etc.). Deep radio measurements would significantly enlarge the known stellar radio emitting database, free from selection effects, allowing new insights into the physics of active stellar systems and plasma processes. Systematic, deep surveys will enable the detection of serendipitous flaring activity and hence to to derive a typical behaviour (occurrence rate, variation amplitude, etc.) from a statistical study of a larger source population. Moreover, detailed studies of a large number of stellar coronae will be possible, allowing us to understand the nature of energy release in the upper atmospheres of stars of different mass and age and to investigate the correlation between radio and X-ray emission and thus to to study the occurrence of the Neupert effect in stellar coronae [680].

Cool star radio emission processes naturally lead to multi-wavelength type follow-up observing campaigns. High sensitive radio observations would allow also to check on long-lived centers of surface activity, whose signature is the presence of a persistent broadband maculation effects in particular stars. It will be possible to explore the relationship of electron energization to such centers of activity, pointing out the existence of possible magnetic cycles also in the radio. Because of the lifetimes of particular stellar activity centers, radio observations were often able to be followed in observations at other wavelengths, even when not exactly co-incident in time.

7.1.2 Coherent events

Deep radio observations, such those that SKA and its pathfinder will provide, will offer the best opportunity yet to determine how common coherent radio emission is from stellar and sub-stellar systems. The detection of coherent emission on large sample of different kinds of star will have immense implications for our understanding of both stellar magnetic activity and the dynamo mechanism generating magnetic fields in fully convective stars and brown dwarfs [681; 682].

Coherent emission observed in binary systems and active stars and in UCD stars shares several characteristics with that observed in CP stars [683], since both require a large scale magnetosphere, and are similar to the low frequency coherent radio emission observed from the magnetised planets in our solar system [684].

If coherent emission is present in many radio active stars, with the same characteristics, it will constitute an excellent diagnostic for star magnetospheres, and a powerful probe of magnetic field topology. In the case of UCDs the study of ECM instability provides the only potential probe into magnetic field strengths for late-M, L and T dwarfs.

More observations of wider samples of active stars are also necessary to establish the percentage of active stars and binary systems that show coherent emission, time-scales of its variability and how

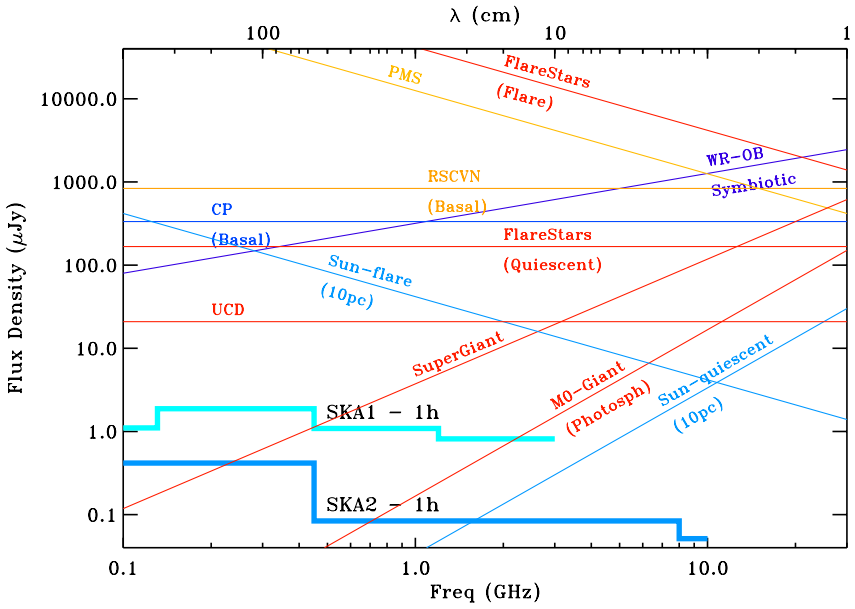

Figure 7.1. Typical radio spectrum of several classes of radio emitting stars. Fluxes have been derived from the radio luminosity assuming a distance as appropriate for each type of radio stars. Detection limits for SKA1 and SKA2 have been computed for one hour integration time. See text for explanation.

this is related with basic physical parameters of the stars. Follow-ups of the detected sample would allow to point-out any similarities between ECME from single stars and binary systems and thus to disentangle between possible cause for the population inversion which drives the ECME events [685].

In one CP star (CU Vir) the coherent emission is stable on a time-scale of years, and has been used to time the rotation of the star, revealing a likely change of its period [686; 687]. The discovery of other similar radio lighthouses will enable high precision studies of the rotation period, and thus angular momentum evolution, in different classes of star.

7.1.3 Radio stars detection forecast

We don't have a statistics on radio emission for each obvious classes of stars surveyed for radio emission. We have only indications, as all information collected so far come from small samples biased versus some kind of peculiarities observed in other spectra regimes. In Fig 1, schematic continuum radio spectra of several classes of radio emitting stars are drawn. Fluxes have been derived assuming a typical radio luminosity [686; 688–690; 692], and a typical distance for each different types of radio stars: 10 pc for flares stars and late M-L, 100 pc for active binary systems, 1 kpc for supergiants, OB and WR, 500 pc for CP stars. The spectral and sensitive characteristics of SKA, in both phases SKA1 and SKA2, have been also drawn. It is evident that, with SKA1, in one our of integration time, all the WR, OB and stars and Symbiotic systems of the Galaxy can be detected, while CP, PMS, RSCVn and supergiants could be seen up to the distance of the Galactic Center

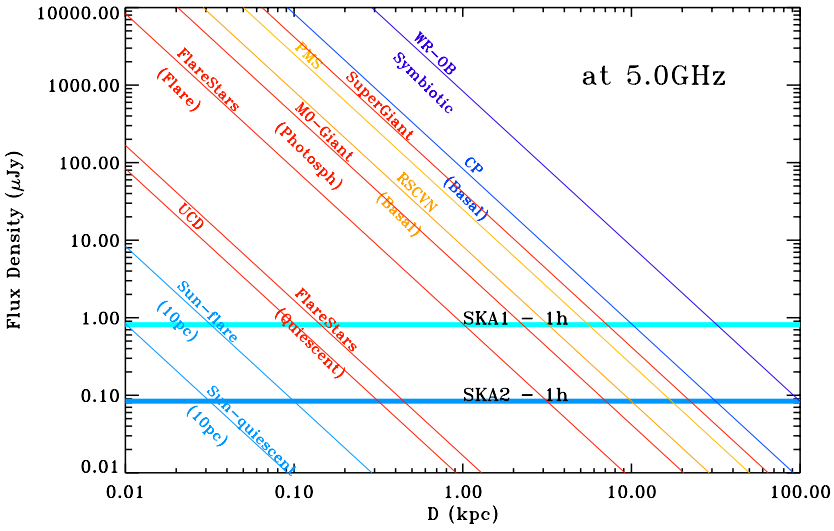

Figure 7.2. Typical flux density at 5 GHz for each class of radio star as a function of the distance. The sensitivity limits foreseen for SKA1 and SKA2 in one our integration time (sky blue and blue lines) show the maximum distance of detection.

(GC). With the same integration time, SKA2 will be able to detect almost all the above classes in the Galaxy, and probably in the nearby galaxies, RG photospheres up to the GC, Flare stars and UCD within several hundreds pc, and "a quiescent Sun" at 10 pc (Fig. 2).

7.2 Pulsar astrophysics with SKA

A. Possenti

7.2.1 Summary

The use of the pulsars for carrying on *strong field tests of gravity theories*, and experiments of fundamental physics represents one of the key science projects of SKA. In these brief notes, it will be given a summary of the exciting perspectives of these experiments as well as of other possible applications of SKA in the fields of the pulsar research for which there exists a strong interest – and there will be an expected large involvement – of the italian community, and of the pulsar group based in Cagliari, in particular.

7.2.2 Setting the scene

There are probably no other astronomical objects whose discovery and subsequent studies provides insights in such a rich variety of physics and astrophysics than the radio pulsars, i.e. rapidly-spinning and highly-magnetized neutron stars (NSs). As they rotate, they emit directional beams of radio waves, appearing as pulses when Earth lies in the direction of these emissions. In fact, thanks to

their clock-like signal (recorded and interpreted with a technique called *timing*), they have been exploited as unique tools for performing experiments ranging [693] from relativistic gravity to modern cosmology, from the physics of super-dense matter to the study of super-fluid and super-conducting materials, from plasma physics to stellar cluster dynamics, from the evolution of binary systems to the detection of gravitational waves, from the investigation of the shape of the Galactic magnetic field to the mapping of the distribution of electrons in the Milky Way. The italian astrophysical community has played a significant role in these fields of research over the last three decades, being part of (and in some cases leading) some of the most fruitful and/or promising pulsar experiments ever (the surveys at Parkes, the timing of the unique Double Pulsar, the European Pulsar Timing Array project, etc).

After having summarized (§ 7.2.3) the expected capabilities of SKA in the framework of the observations of pulsars, in § 7.2.4 it will be reported on the new exciting perspectives opened by SKA in some of the fields of the pulsar research for which there is a large interest and there will be an expected large involvement of the already well-positioned italian radio pulsar community.

7.2.3 SKA performances for pulsar observations

The advent of SKA will completely revolutionize both the main branches of the pulsar research, namely the *search* for new radio pulsars and their subsequent investigation with the already mentioned (see § 7.2.2) *timing* technique.

As far as the searches for new pulsars are concerned, SKA will exploit an unprecedented sensitivity, combined with a rather large field-of-view. Simulations suggest that this will translate in more than one order of magnitude increase in the number of known pulsars. Starting from the current 2200 sources, calculations [694] predict that the pulsar catalog will be eventually filled with 20000-30000 objects. They will basically include all the pulsars in the portion of the Milky Way visible from SKA, as well as many objects belonging to other nearby Galaxies. Also, the number of the known recycled pulsars (often found in binaries) will reach about 3000-4000 vs the $\sim$ 350 discovered so far [695]. The latter figure is very interesting, since the rapid spinning and the remarkable rotational stability of most of the recycled pulsars (the fastest of which are also dubbed millisecond pulsars, MSPs) can lead to many of the physical applications mentioned in the previous section. E.g. the availability of $\sim$ 100 relativistic binaries (vs the current handful of objects) will be extremely beneficial to the studies of strong field gravity and of fundamental physics.

An even larger factor of improvement is expected from the use of SKA for the timing of the pulsars. In this case the simulations predict that the precision in the determination of the Time of Arrival of the pulses could be up to $\sim$ 100 better than that of the best available apparatuses to date [696] .

The estimates above hold for the fully developed Phase 2 of SKA (reference configurations *SKA2_mid_dish* and *AIP_PAF*), with a typical sensitivity of order 10^4 m^2/K and operating in the frequency range 0.5-3 GHz. Of course, those figures must be scaled down for the Phase 1 (namely that referenced in this white book as *SKA1_mid*), for which a typical expected sensitivity is of order 10^3 m^2/K: e.g. simulations [694] indicate a total number of pulsar discoveries in the range 7000-14000 for Phase 1.

7.2.4 Pulsar science with SKA

Tests of General Relativity in binary pulsars

The radio pulsars can be regarded as clocks, the orbit of which can be tracked down with an accuracy depending on the "quality" of the clock. This is particularly interesting when the pulsar is orbiting

another compact object in a close-enough orbit. In this case, the large deformation of the space-time produced by the two massive stars in the system, as well as the occurrence of a very high orbital velocity, can lead to strong relativistic effects. If the pulsar signal is strong and the geometry and orientation of the orbit is favorable, these effects can be directly measured and, in turn, a direct comparison between the observations and the predictions of the various theories of gravity can be carried on. As to date, the best tests of general relativity result from the observations of the Double Pulsar [697] (which the italian community is deeply involved in and for which the non radiative prediction of general relativity are tested at 0.05% level [698]), whereas PSR J1738+0333 [699] is the best target for constraining a large class of alternative gravity theories. It is important to highlight that the aforementioned tests are sensitive to *strong field effects* and investigating these effects is not an academic question. In fact, on one hand *(i)* there exist alternative gravity theories which would pass all the Solar System (weak-field limit) tests, but would be violated as soon as extreme conditions (strong-field limit) are reached [700]; on another hand *(ii)* extreme conditions are certainly those at which any long sought unified model for interactions applies.

In this perspective, SKA will provide the discovery of many tens of additional relativistic binaries (some of them likely more suitable than the already known binaries for performing the tests described above) and will strongly improve the timing analysis of all the known sources [701], leading to probe relativistic effects of higher order, with particular emphasis on those related with the spin of the neutron star(s) (e.g. [702]).

Investigating the properties of the black holes

Completely new and intriguing perspectives will be opened by the discovery of pulsars orbiting a black-hole (BH), the long sought and still missing holy grail of the modern pulsar science. They are expected to be very rare in term of percentage over the whole Galactic pulsar population, but at least two - and maybe three - families of pulsar-BH binaries should likely result from the very large sample of SKA discoveries: i.e. some pulsars, or millisecond pulsars, with a stellar mass BH companion, few slowly rotating pulsars orbiting Sgr A* (i.e. the super massive BH at the center of the Milky Way) and perhaps some MSP orbiting a intermediate mass BH in a globular cluster [703–705].

The subsequent *timing* observations of these objects will provide plenty of unprecedented information on the BH properties, leading not only to a measurement of the mass of the black hole M_{BH}, but also, if the BH rotates significantly, of its angular momentum S_{BH} and its quadrupole moment Q_{BH}. That will allow one to experimentally test both the so-called Cosmic Censorship Conjecture, and the No-Hair Theorem [696; 706; 707]. The first claims that any singularity in the space–time (like that occurring at the center of a BH) must be hidden behind a event horizon, i.e. out of reach for any observation. The second theorem states that any BH can be described only by its mass, angular momentum and electric charge, the latter not being usually relevant in an astrophysical context. Recent simulations [706] show that, with SKA, the value M_{BH} for Sgr A* will be easily measured with better than 0.001% precision, and, if Sgr A* is rotating, the value of S_{BH} with better than 0.1% precision and the value of Q_{BH} with $\sim 1\%$ precision.

In summary, the observation of a pulsar-BH binary with SKA will lead to a unique series of experiments, where the descriptions of the BH given by general relativity and by alternate theories of gravity will be directly compared to the observations and then eventually discriminated.

Gravitational Wave astrophysics

The so-called *Pulsar Timing Arrays* (PTAs) are based on the consideration of the Earth and a millisecond pulsar (MSP) as a pair of test masses in the space-time metric; the passage of a gravitational wave (GW) perturbs the metric and is then expected to leave a signature on the observed Times of Arrival

of the pulses from the MSP. The size of the effect is very small and is proportional to the amplitude of the characteristic strain of the GW. The correlation between the data of many Earth-MSP pairs [708] distributed throughout the sky (thus forming a PTA) is required to remove spurious effects. Given the typical total timespan (from few years to some decades) and the rate of occurrence (typically once or twice a month) of the timing observations, the PTA are most sensitive to gravitational waves with periods above 1 year (i.e. frequency below 10 nHz), and therefore probe the nanoHertz gravitational waves sky, thus being nicely complementary to the other experiments aimed to a direct detection of gravitational waves, operating in other GW frequency bands.

The most suitable target for the current PTAs is the stochastic background – or better saying *foreground* – of gravitational waves produced by coalescing super-massive BH binaries in the early stage of assembling of the galaxies in the universe, i.e. at red-shift $z \sim 1$. Also single powerful (in GW) and relatively close coalescing supermassive BH binaries could be observed by present PTAs, although at a less level of likelihood. In fact, the capabilities of the current PTAs (in some of which the italian community is significantly involved) are rapidly approaching a suitable level for a detection. It is expected that the very high sensitivity of SKA will not only warrant a detection, but will give the chance of using the properties of the observed GWs for constraining the alternate gravity theories (e.g. by studying the mass and the spin of the gravitons, [709]), as well as for characterizing the parameters of the massive black hole binary systems (e.g. [710]), i.e. for performing unprecedented experiments of GW astrophysics.

Constraints to the Equation of State of nuclear matter

It's well known that the maximum mass M_{max} of a neutron star (NS), as well as the most rapid spin period P_{lim} that that can attain depend on the Equation of State (EoS) for the nuclear matter which the NS is composed of (e.g. [711]). Thus, observing a very rapidly spinning MSP or a very "heavy" pulsar in a binary system provides a powerful test for discriminating between the various tens of EoS proposed so far. On the basis of the $\sim$ 350 MSPs and $\sim$ 250 binary pulsars discovered to date [695; 712], the observed limiting values are $P_{lim} = 1.40$ ms and $M_{max} = 1.97 \pm 0.04\ M_{\odot}$. These values led to exclude some proposed EoS, but the vast majority of them are still acceptable. Interestingly enough, there are indications for the occurrence of NS masses higher than the M_{max} above (up to $\sim 3\ M_{\odot}$) in a subclass of the binary pulsars – the so called ultra-close black-widow systems, containing a MSP and a ultra-light companion often found in the verge of being disrupted by the impinging energetic pulsar flux. The confirmation of the existence of a $\sim 3\ M_{\odot}$ NS will exclude most of the EoS.

In this context, the impact of SKA will be twofold: on one side it will provide a factor ~ 10 increase in the known sample, which will likely lead to discover pulsars with more extreme rotational rates or masses than the current record holders. On another side, the pulsar timing capabilities of SKA will open the possibility of observing at least two relativistic effects in the most promising binaries, thus permitting to firmly confirm (or to reject) the case for $\sim 3\ M_{\odot}$ NS masses.

Moreover, for the most relativistic double neutron star systems (like the Double Pulsar or even more relativistic binaries to be discovered during the surveys performed with SKA), the timing observations with SKA might be able to simultaneously provide a determination of both the mass and the moment of inertia (hence its radius) of a given pulsar. That will translate in the survival of a very small number of EoS (e.g. [713]), finally addressing one of most important and long standing issues in the neutron star physics.

Studies of the ISM and the Galactic magnetic field

The vast majority of the pulsars discovered by SKA will belong to the Milky Way and will represent an array of clocks distributed almost everywhere in the Galaxy. From monitoring their emission at various radio frequencies in the SKA bands it will be possible to careful study the effects of the interstellar medium (ISM) on the pulsar signal and, from those, derive the physical properties of the ISM along few tens thousands lines of sight. In particular, from the observation of the dispersion, scintillation, scattering and the Faraday rotation of the pulsar signals, as well as their variations with time, it will be possible to investigate not only the Galactic magnetic field and/or the distribution of the ionized component (and the composition) of the ISM, but also the so-called *interstellar weather*, accounting for the mutual interactions between the different constituents of ISM.

It is interesting to note that the aforementioned mapping of the properties of the ISM will be largely improved by the availability of a independent determinations of the pulsar distances, which will be inferred from the accurate parallaxes provided by SKA (via imaging and/or timing observations) for about ten thousands pulsars [714].

Globular cluster dynamics

Despite the large difference in total mass (a factor larger than 10^3) between the Disk of the Galaxy and the system of the Galactic Globular Clusters (GGCs), the latter contains $\sim 40\%$ of the entire known population of MSPs. Part of this discrepancy can be ascribed to a observational bias: almost all the GGCs have been searched for MSPs for much longer integration times than most of the locations in the Galactic Disk. However, it is commonly believed that a more fundamental explanation calls for the occurrence of two formations channels for the MSPs in globular clusters (GCs). One channel is the evolution in a primordial binary via the so-called recycling process [715], alike the case of the MSPs in the Galactic Disk. On the contrary, the second channel is unique to the GCs and results from 3-(or 4-) body dynamical interactions in the ultra-dense stellar environment of a GC core, which can sustain the formation of various kinds of binaries which are later suitable for the spin-up of the embedded NS (e.g. [716]), thus forming a new MSP. Since the GCs are old (and almost relaxed) stellar systems, the MSPs – which are more massive than the typical GC stars – are expected to segregate in the central GC core.

Given the hypothesis above, the study of the total number, binary fraction (e.g. isolated vs binary), location in the GC and distribution among the various possible types of companion may be potentially able to unveil both the current dynamical status and the previous dynamical evolution of a GC. Indeed, the role of the dynamical mechanisms in the formation of MSPs is reflected in the tendency for the GCs with the largest predicted rate Γ of dynamical interactions (in turn depending on the central density and the radius of the core of the GC) to contain a higher number of known pulsars. However, there are few remarkable counter–examples, i.e. GCs with a very high value of the parameter Γ and no associated pulsar, or, on the other side, rather loose GCs with associated pulsars. As a matter of fact, up to now there is no satisfactorily theory for predicting the pulsar content of a GC on the basis of the GC internal parameters and/or history.

Part of the difficulties are due to hard-to-quantify observational biases which can play a significant role in preventing the discovery of MSPs in any given GC. Thus the comparison between the pulsar content in various GCs may not mirror the intrinsic properties of the pulsar population.

Given its unprecedented sensitivity, a dedicated survey with SKA will allow one to go much deeper than now in searching MSPs in GCs and to probe the pulsar luminosity function in a uniform and unbiased way for a majority of the GCs. In other words, for a large subgroup of all the GCs, a deep SKA survey will likely lead to catalog their entire population of potentially visible MSPs

(i.e. those MSPs the radio beam of which sweeps the line-of-sight to the Earth) at least down to a conventionally chosen but unform (very low) pulsar luminosity.

Furthermore, the expected high quality of the timing for most the MSPs discovered in GC may provide the possibility of tracking down the peculiar motions of the MSPs within the core of their associated GC. For GCs with many pulsars in the core, this will open the possibility to reconstruct the shape of the gravitational potential well in the central region of the cluster, and thus maybe to unveil the presence of dark massive bodies in the GC center, like stellar mass BHs or Intermediate Mass BH (IMBH). This would be a very important result, since no evidence of the presence of these kinds of BH in a GC has been collected so far.

In effect, if IMBHs are common in the GC centers, one can also predict the ejection of several rapidly moving MSPs from the GGC system into the Galactic halo, as a consequence of dynamical encounters between the MSPs and the IMBHs. Simulations ([717]) indicate that this population of fast halo MSPs could be revealed by a SKA survey at high Galactic latitudes. These fast moving MSPs would provide a strong, albeit indirect, evidence of the presence of a substantial population of IMBHs in GCs.

7.3 Supernovae and GRB-Supernovae

M. Della Valle

7.3.1 Introduction

Supernovae (SNe) come into two basic types: 1. thermonuclaer Supernovae (SNe-Ia) which are caused by the explosion of a massive (near Chandra limit) white dwarf in a binary system. Their optical spectra are characterized by the lack of H lines and the presence of a strong absorption at 6150 Å , which is the signature of Si II; 2. Core-Collapse (CC) Supernovae, which mark the end of the life of massive stars ($> 12 M_{\odot}$). They come into three flavors: i) SNe-II, which show H lines with different strengths often flanked by P-Cyg profiles. SNe-II present a wide range of spectral and photometric properties and there is consensus that much of this variety is due to the mass of the H envelope of the progenitors at the time of the explosion; ii) SNe-Ib are characterized by the lack of both H lines and Si II absorptions, and by the presence of conspicuous He emission lines; iii) SNe-Ic show no, or only very weak, Si II absorptions and He I lines. SNe-Ib/c progenitors are massive stars ($> 20 M_{\odot}$) possibly in binary systems (e.g. [723]), which undergo the collapse of their cores after they have lost the respective H or He envelopes, via strong stellar wind or transfer to a binary companion via Roche overflow. Finally we point out the existence of a tiny subclass of SNe-Ic, $\sim 0.4-3\%$ of Ib/c events ([724]), which are characterized by a high kinetic content, about 10^{52} erg of energy associated with the SN ejecta, 10 times larger than observed in "standard" CC-events. Their progenitors appear to belong to the massive wing of SNe-Ibc, likely $M \sim 1-40 M_{\odot}$ ([734]) and are associated with long duration Gamma-ray Bursts (GRBs). As the SN ejecta plough through the circumburst material (CBM) a forward shock is driven into the CBM and a reverse shock is driven into the expanding ejecta. These shocks can either amplify the magnetic field and accelerate particles to relativistic energies, producing synchrotron emission. Therefore only Supernovae surrounded by a dense CBM, are able to produce radio emission detectable with current technology. So far only type II, SNe-Ib/c and SNe associated with long duration Gamma-ray Bursts have been detected at radio wavelengths ([736]), while SNe-Ia have never been observed in the radio ([731]).

7.3.2 SN Radio Observations

The importance of SN radio observations will be illustrated by the following qualitative sketch. The SN blastwave moves through the circumstellar medium (CSM) at about 10,000 km/s, which is

roughly 10^3 times faster than the stellar wind velocity, responsible for shaping the density profile of the circumburst medium. Therefore SN radio observations can be considered actual "time-machine" where one year of radio monitoring can sample thousands years of stellar wind mass loss history of the progenitor star. For example the CSM density around a massive progenitor star is expected to decrease as an inverse power of the radius $\rho \sim r^{-2}$. On the other hand radio observations of SN 1993J and SN 1980K have found different trend $\rho \sim r^{-1.6}$ ([725]) and a steep decline in the flux density occurring at about 5000 days past maximum ([730]), respectively. These radio observations can be used in synergy with optical data to understand the final stages of stellar evolution, particularly: i) the role played by strong episodes of mass loss occurring a few years of months before the SN explosions (e.g. [732]; [729]; ii) the "strange" behavior of some GRBs, like 081007 ([737]). NIR data of GRB 081007 suggest that the expansion and interaction of SN shells is occurring in a medium with density profile more typical of homogenous $\rho \sim r^0$ ISM rather than stellar wind$\rho \sim r^{-2}$ medium, as expected, because of the association of this GRB with SN 2008hw and therefore with a massive stellar progenitor.

Sub milliarcsecond resolution imaging of nearby SNe, observed within the "Virgo circle", can be used to compute the distance of the parent galaxies, through accurate radio-parallaxes. Radio imaging show relatively symmetric expansion of the blastwave into the CSM, so after computing the expansion speed and the deceleration there are sufficient data to allow independent distance estimates.

7.3.3 The impact of SKA

One of the main strong point of SKA will be the greatly increase of the sensitivity. Currently only the radio-brightest SNe are detected, and this fact explains because for only $\sim 10\%$ of the discovered core-collapse SNe it is possible to make the radio "lightcurves" with the accuracy needed to study the history of the progenitor star. As an obvious consequences of the increasing sensitivity of SKA, it will be possible to study a larger number of SNe (from current 2 radio detections/yr up to 50 detections/year with SKA) and to follow-up each of them for a longer time. Here below, we briefly sketch out a few science cases, which will greatly benefit from the coming into operation of SKA.

a) SNe-Ia: Despite SNe-Ia are used for 'precision cosmology' the nature of the progenitor system (double-degenerate or single- degenerate) is still unknown (e.g.[727]). No SNe-Ia have been detected so far in the radio, then implying a very low density for any possible circumstellar material established by the progenitor system before explosion. Current upper limits to a steady mass-loss rate for individual SN systems, based on the radio upper limit measuremants, are as low as $\sim 3 \times 10^{-8} M_{\odot} yr^{-1}$ for the best case, but more likely $\sim 10^{-7} M_{\odot} yr^{-1}$ ([731]). This situation is certainly due to sensitivity limitations and there have been predictions ([718]; [733]; [720]; [726]) that radio emission from Ia may lie not far below the detection limits reported above. It should persist the lack of radio detection up to M(dot) $\sim 10^{-10} M_{\odot} yr^{-1}$ (or below), this scenario would argue against the single degenerate system as type Ia progenitor.

b) SNe-II: Radio observations of SNe-II are strongly biased due to large differences in the radio lumninosity of CC- SNe. SN 1987A and SN 1993J could be detected in radio because they were nearby. 'Standard' events, like SN 1980K (10^{26} erg s^{-1} Hz^{-1} at 6 cm) can be observed to Virgo distance. The ultra luminous 1988Z-like ($\sim 10^{28}$ erg s^{-1} Hz^{-1} at 6 cm) objects up to 100 Mpc. With an improved sensitivity level of 1 μJy, one can detect the brightest of radio SNe, such as the Type IIn SN 1988Z at the cosmologically interesting distance of $z = 1$ ([736]). The possibility to sample such a huge volume of universe will allow, on one side, to obtain a more complete 'census' of SN remnants, and one the other side, to monitor in 'real time' the

apparence of new radio Supernovae, then allowing a measurement of SN rate which will be independent of classical measurement (e.g. [721]).

c) GRBs associated with SNe: It is well known that a significant fraction of long duration GRBs are associated with SNe-Ibc (e.g. [722]). The narrowness of the relativistic jets (4-5^o up to 20^o), which give rise to γ-ray and X-ray bursts, implies that most GRB outbursts are missed. The more isotropic radio emission coupled with the SKA sensitivity will increase dramatically the number of direct detections of the 'relativistic' SNe associated with long durations GRBs ([735]). This approach will yield an independent measurement of the frequency of occurrence of 'local' low-luminosity GRBs, currently affected by un uncertainty of a factor $\sim$ 100 ([724])

d) GRBs produced by merger of collapsed stellar remnants: Recently [728] have suggested that mergers between neutron stars (NS-NS mergers) can launch subrelativistic outflows. The interaction with the CSM can produce radio-flares with peak emission at 1.4GHz that persists at μJy level for days/weeks at $z < 1$. The transient RT 19870422 ([719]) might be the prototype of these kind of radio-sources. SKA could help to find an array of binary systems, such RT 19870422, that could be used to search for gravitational waves in synergy with LIGO-VIRGO GWs detectors.

7.4 Gamma Ray Bursts

G. Ghirlanda, S. Campana, S. Covino, P. D'Avanzo, G. Ghisellini, A. Melandri, R. Salvaterra, G. Tagliaferri, A. Wolter

Gamma Ray Bursts (GRB) consist of a transient (0.1-100s) prompt emission of γ and X-ray photons accompanied by a long lasting afterglow (AG) emission in the X–ray, Optical/NIR and radio band. GRBs have been detected up to very high redshift (z = 8.2, [738]) and they release a huge amount of energy ($10^{49} - 10^{51}$ erg, considering their typical collimation angle of $\sim$5° - e.g. [739]). GRBs come into two flavors: long events (with duration > 2 sec) and short bursts (with duration < 2 sec). While long bursts are typically found in star forming host galaxies and few of them have been associated with a supernova of type Ibc, short GRBs are hosted in galaxies of different morphologies with no SN associated (e.g. [740]).

The "standard model" attributes GRBs to the formation of stellar mass black holes, either through the core collapse of a massive star (for long–duration GRBs - [741; 742]) or through the merger of two compact objects (for short GRBs - [743]). The GRB emission is thought to be produced by shock dissipation in a relativistic jetlike flow. While the prompt emission comes from shocks developing inside the relativistic flow (internal shocks - [744]), the afterglow emission is thought to arise from the external shock [745] running into the interstellar medium. Synchrotron and inverse Compton emission should be the radiation mechanisms of shock-accelerated electrons. The "standard model" of GRBs has still some major **open issues** (e.g. [746]) related to the jet dynamics, structure and composition, to the physics of the relativistic shock and to the total jet power. In a wider cosmological context it is debated whether GRBs can be tracers of the cosmic star formation, probes of the formation of the primordial stars and tools to constrain the cosmological parameters.

7.4.1 The present status of radio observations of GRBs

Although the afterglows of GRBs have been discovered since 16 years, the study GRBs at radio frequencies is still poor compared to the wealth of informations available at other wavelengths (X-ray and Optical/NIR). Radio follow–up campaigns consist in most cases in single epoch (between 0.1 and 300 days) and single frequency (mostly at $\sim$8.4GHz) observations. The current detection rate

is ∼30% and both upper limits and detections (open triangles and filled red circles in Fig.7.3) have flux densities of 100–200 μJy [747]. The low detection rate of GRB emission at radio frequencies is mainly due the sensitivity limits of the currently available radio facilities. Sensitivities at μJy levels are required to detect and follow the radio afterglow emission from early to very late times.

Despite their paucity, observations of GRBs in the radio band have proved some fundamental properties of these sources: (1) radio scintillation (GRB 970508 – [748]) showed that the outflow is relativistic; (2) the late time (∼100d) flattening of the light curve (GRB 980703 and 000418 – [749]) has been interpreted as the jet becoming non–relativistic; (3) late time (100–450d after the burst) radio calorimetry (GRB 030329 – [750], GRB 970508, 980703 – [751]) set some constraints on the total kinetic power of the jet; (4) the afterglow spectrum, obtained by combining Optical and radio data, supports the synchrotron origin of the radiation emitted during the afterglow phase; (5) radio monitoring of local SN Ibc put some constraints on the GRB/SN association (e.g. [752; 753]); (6) the detection of a few GRB hosts [754–756] in the radio band provided an estimate the host unobscured star formation rate.

One practical advantage of radio observations of GRB afterglows with respect to Optical observations, is that the radio emission peaks on timescales of few days and generally keeps bright up to several tens of days after the burst. Therefore, radio observations can be planned without the extreme rapidity which is needed for optical observations.

7.4.2 GRB detectability by SKA

At early times (few days post the burst) the radio afterglow emission is suppressed by synchrotron self–absorption until (due to the expansion) the emitting region becomes optically thin and the flux peaks (typically around 10 days with a flux density of ∼100 μJy). After the peak the flux decreases as $\propto t^{-2}$ until the outflow becomes non relativistic (at about 100 days with a flux density - e.g. at 8.5GHz - of ∼ few μJy). These timescales and flux levels are only indicative because they depend on several GRB parameters: the kinetic energy E_k driving the jet expansion into the interstellar medium with density n, the jet opening angle θ_{jet} and the microphysical parameters at the shock front (namely the electron energy distribution index p and the fraction ϵ_e and ϵ_B of the shock energy shared between electrons and magnetic field respectively).

Fig.7.3 shows (open grey circles) the expected peak flux densities at 8.5GHz for reasonable assumptions on the parameters distributions of the GRB population (Ghirlanda et al. 2012). Simulated bursts reproduce the presently detected GRBs (red circles) and extend down to sub–μJy fluxes, i.e. below the current upper limits "stripe" (open triangles) which is representative of the current radio facilities sensitivity limits. The comparison with the expected MeerKAT (dashed line) and full SKA (SKA phase 2 - dot–dashed line) continuum sensitivities[1] shows that ∼70% and almost 100% of the burst population can be detected by MeerKAT and SKA2 [757].

7.4.3 Early time radio observations

These radio observations (before and around the peak of the light curve - Fig.7.3) can probe different aspects of the jet physics. Polarization measurements before the peak could reveal the effects of Faraday rotation or conversion (e.g. [758]), depending on the plasma parameters, providing some constraints on the shock microphysical parameters or revealing the possible presence of a population of thermal electrons in addition to the shocked non–thermal one (e.g. [759]). Observations in the optically thin phase ($\nu > \nu_a$ where ν_a is the self absorption frequency) should provide linear and

[1] We considered 71 dishes of 13.5m and 2GHz bandwidth for MeerKAT and 2500 dishes of 15m and 4GHz bandwidth for SKA2 and a 1h exposure in both cases.

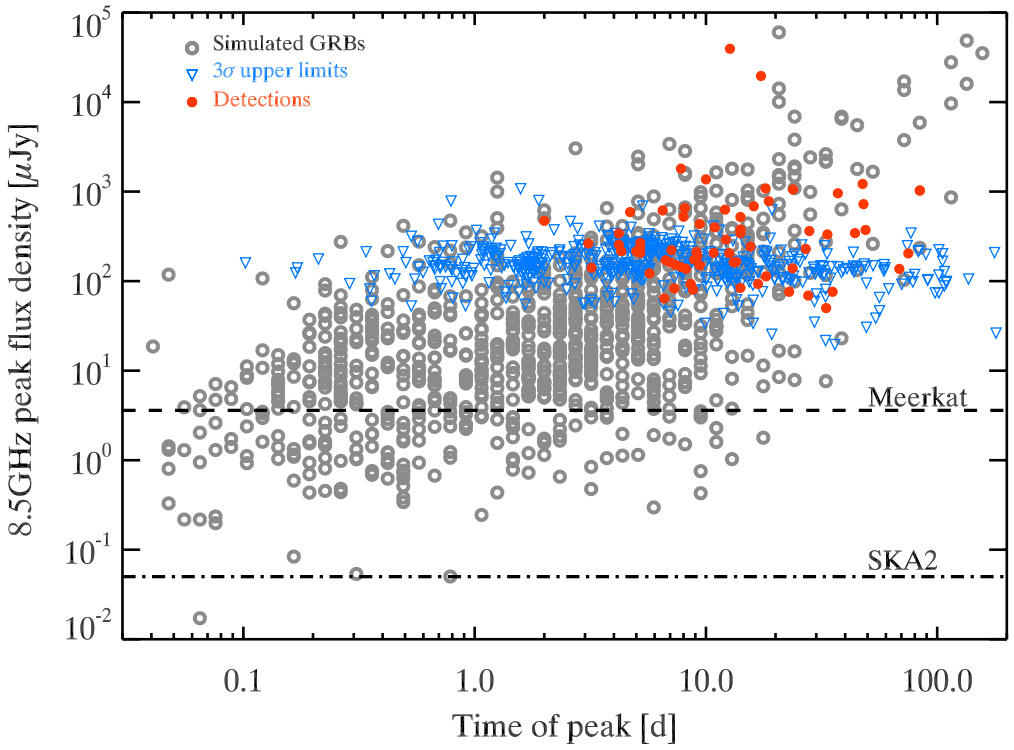

Figure 7.3. Peak flux of the afterglow light curve at 8.5GHz versus time of the peak (in the observer frame). GRBs observed at radio frequencies in the last 16 years (adapted from [747]) are shown by the blue triangles (upper limits) and by the filled red circles (detections - corresponding to a detection rate of ~30%). The peak fluxes of the radio afterglow light curve for a population of simulated GRBs are shown by the open grey circles [757].

circular polarization measurements at the same level to what has been observed in the optical [760; 761] but, thanks to the relatively high brightness of the radio afterglow, for a large sample of GRBs thus allowing to study the possible dependence of the polarization level on other GRB parameters (e.g. the global energetic or the geometry of the outflow).

At the shock front both a forward shock (FS) , propagating into the interstellar medium, and a reverse shock(RS), traveling through the expanding outflow, should form. The RS has been detected only in a few bursts in the Optical band [762] but tentative detections have also been claimed in the radio band [747] contrary to what predicted by the standard model (Ioka & Meszaros 2005). Monitoring of the radio light curve at early times between 0.1 and 10 days should reveal the presence of the peaks of the RS and of the FS. If detected, the RS peak would allow us to constrain some of its presently unknown parameters (e.g. ϵ_B/ϵ_e).

7.4.4 Observations around the trans–relativistic transition

The standard afterglow model predicts that the outflow should become non–relativistic (NR) at $t_{NR} \sim 275(1+z)E_{k,53}^{1/3}n^{-1/3}$ [764]. Across t_{NR} the light curve flattens with a temporal decay index variation $\Delta\alpha = (21-5p)/10$ where p is the slope of the electron energy distribution at the shock front. $\Delta\alpha \simeq 1$ was found in a couple of GRBs [749]. However, also a steepening of the light curve around t_{NR} is

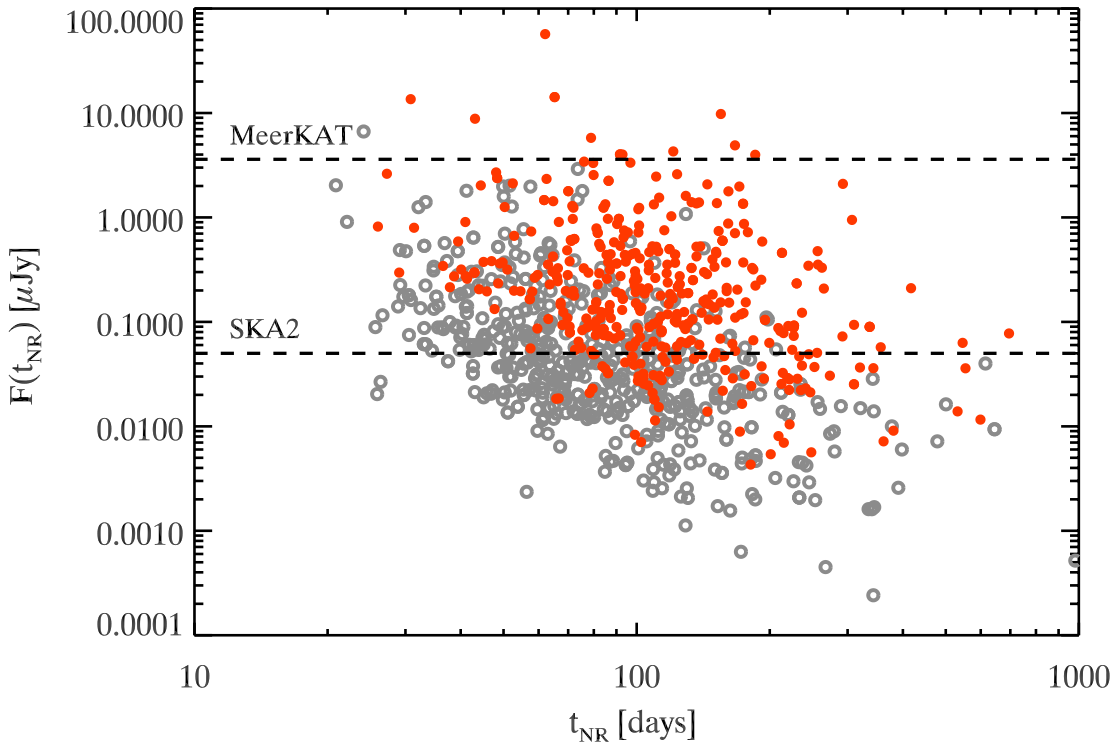

Figure 7.4. Flux at the time of the transition to the sub relativistic jet expansion phase versus time of occurrence of this transition. Bursts in which the afterglow flux is larger than the typical flux of the host galaxy are shown by the filled (red) dots, while bursts whose flux is dominated by the host galaxy at the corresponding time are shown by the open (grey) circles.

possible (i.e. for a steep electron energy distributions $p > 5$). If the interstellar medium has a wind density profile (e.g density scaling as $n \propto R^{-2}$ – expected if the progenitor WR star underwent intense mass loss before its collapse), t_{NR} should happen later (with a different $\Delta\alpha$). The detection of the NR transition in the radio band would provide an independent diagnostic of the ISM structure (either constant density or wind). If early time (few days after the burst) observations in the Optical/NIR provide an estimate the jet opening angle θ_{jet} and late time radio observations provide E_k, the detection of the trans–relativistic transition would constrain the ISM density n or of the wind velocity and mass loss rate of the progenitor WR star.

Fig.7.4 shows the flux F_{NR} at the time of the trans–relativistic transition t_{NR} derived for the simulated GRB population. Red circles are those bursts whose flux at t_{NR} is still dominated by the afterglow, the host galaxy being at least a factor 2 dimmer (assuming a typical host radio spectrum $\nu^{-0.6}$ and a star formation rate of 5 $M_\odot$ yr^{-1}). While MeerKAT will be able to monitor the afterglow emission only in ~15% of the bursts, with SKA2 at least half of the population of GRBs detected at earlier times (Fig.7.3) will be monitored across t_{NR}, i.e. typically between 10 and 500 days.

7.4.5 "Radio calorimetry"

Radio calorimetry is a powerful tool to derive the total energy of GRBs. This requires deep radio observations after t_{NR} when the jet is non–relativistic. Optical afterglow observations of about 30

long GRBs showed that the true GRB energies are clustered around $E_\gamma \sim 10^{51}$ erg [739; 765; 766]. Assuming a unique efficiency of conversion of kinetic energy to radiation ($\eta \sim$20%) this would imply a typical kinetic energy of $\sim 5 \times 10^{51}$ erg. Some nearby long GRBs have much lower energies and appear to be quasi-isotropic [753]. Radio calorimetry through the study of the afterglow emission during the non–relativistic phase, possibly accounting for radiative losses during the relativistic one, provided an estimate of the total kinetic energy in a few GRBs [739; 750; 751]. The unique advantage offered by radio observations at $t \gg t_{NR}$ is that the estimate of E_k is independent from θ_{jet} and from η. As a return, the comparison of E_k with the prompt emission energy gives a unique estimate of the radiative efficiency η. Fig.7.4 shows that in order to perform radio afterglow observations in the non–reltivistic phase the full SKA2 sensitivity is required.

One immediate consequence of radio calorimetry for a large sample of GRBs will be the testing the possible use of GRB as standard candles. One method[2] to use GRBs to constrain the cosmological parameters [767] relies the collimation corrected energy $E_\gamma = \theta_{jet}^2 E_{iso}$ (where E_{iso} is the isotropic equivalent energy derived from the prompt emission radiation). The estimate of $\theta_{jet} \propto E_k^{-1/8}$ is subject, among other uncertainties, to the lack of E_k for most GRBs (i.e. it is substituted by $E_k = E_{iso}/\eta$, assuming a unique efficiency for GRBs). Radio calorimetry will instead provide E_k allowing to test the possible use of GRBs for cosmology through the $E_p - E_\gamma$ correlation.

7.4.6 Extremely late radio observations

When the afterglow emission has faded below the host galaxy flux (hundreds of days past the explosion), radio observations will reveal the properties of the GRB host population and of the burst environment and will allow us to use GRBs to trace the cosmic star formation history up to very high redshifts. A first systematic study of GRB hosts galaxies at radio frequencies [769] provided only upper limits of 10–100 μJy. More recently, the search for radio host emission in 20 GRBs at redshift $z < 1$ [770] provided only few detections. Despite the small detection rates, these studies indicate that the host star formation rates derived from the radio, which have the advantage of probing the unobscured SFR of these hosts, are $\ll$100 $M_\odot$ yr^{-1} (except for one case of an ULRIG). Current estimates of the SFR from radio observations, however, suffer of an uncertainty between 20% and 40% due to the unknown host radio spectrum, which will be secured by multifrequency observations by SKA. Assuming a typical SFR and a typical spectrum we expect that the host galaxies should have typical fluxes between 0.01 and 0.5 μJy and they should be observed when the afterglow has faded below these flux levels (at $\gg$100 days) so to catch only the host emission. We estimate that SKA will be able to detect ~60% of the hosts (according to our assumptions) while only a small fraction (<5%) of hosts will be observable with MeerKAT.

Radio hosts observations will shed light on the class of dark GRBs (~20–30%) i.e. bursts that are not detected in the Optical band. These bursts are most likely the dust obscured population of GRBs and their properties are still highly unexplored. Of fundamental importance will be the measure of their hosts SFR from radio observations to be compared with the values derived for the optically "bright" bursts.

7.4.7 "Orphan" GRB radio afterglows

Due to the collimated nature of GRBs with typical half opening angles of $\theta_{jet} \sim 5^\circ - 10^\circ$, for each GRB pointing to the Earth (and detected in the γ–ray band) there are $\sim \theta^{-2}$ events pointing in all other directions. These off–axis bursts, viewed at angles $\theta_{view} > \theta_{jet}$, are undetected in the γ–ray band but

[2] Alternative methods have proposed to use correlations based only on prompt emission (i.e. γ–ray) observables [109; 768]. These methods do not require radio observations.

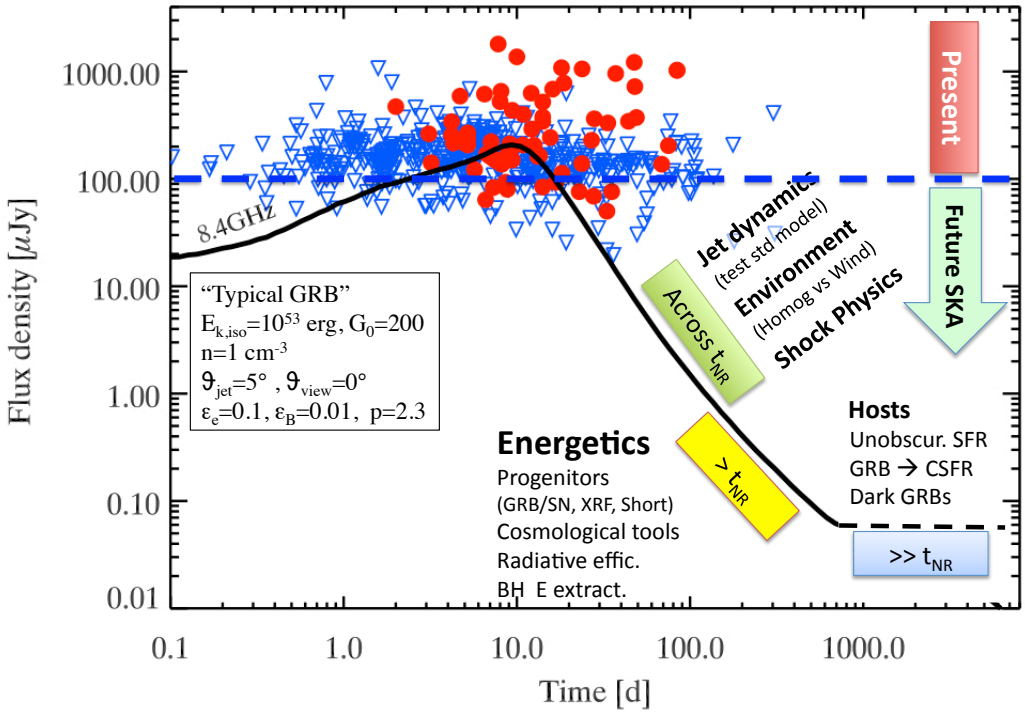

Figure 7.5. The impact of future radio observations on GRB science. A typical radio afterglow light curve (at 8.5GHz) for a GRB with parameters shown in the box is shown by the solid black line. The current detections and upper limits are shown by the filled red circles and open blue triangles, respectively. The blue dashed line represents schematically the current sensitivity limit and the different scientific goals that can be reached by future SKA observations are reported.

can show up as "orphan" GRBs at Optical and radio wavelengths when, during the afterglow, their bulk Lorentz factor $\Gamma \sim 1/\theta_{view}$. Radio surveys could detect several orphan GRBs whose number count would constrain the average burst jet opening angle (the rate of orphan afterglows to detected GRBs being proportional to $\sim 2/\theta^2_{jet}$). While optical surveys might be limited by the low fluxes of these transients, radio surveys have the advantage that the radio afterglow emission becomes bright on relatively long timescales. It will be however challenging to distinguish genuine GRB orphan radio afterglows from other transients (e.g. flaring AGN or radio supernovae).

7.4.8 Exploring the early universe through radio GRB observations

First, massive metal free stars (PopIII) are believed to play a major role in the first stages of evolution of the early Universe providing: i) large amount of ionizing photons; ii) the first metals and iii) the seed of intermediate and super-massive black holes. It has been recently proposed [775–777] that GRBs could in principle arise from the last stages of evolution of very massive ($M > 100\ M_{\odot}$) PopIII stars. The detection of such an event represents one way (possibly the only one) for the direct

detection of these, otherwise elusive, first stars. From a theoretical perspective, PopIII GRBs should be characterized by a long smooth prompt emission with energetics of $\sim 10^{54}$ erg (if powered by the neutrino flux from the accretion disk) up to extreme energetics of $\sim 10^{57}$ erg (if powered by the spin energy of a massive black hole - [777]). The medium in which they explode could also be peculiar as $n \propto (1+z)^4$ [772] even though other studies suggest that the ISM density could be independent from z [773]. In order to test the detectability of PopIII GRBs we considered a wide range of parameters with $E_{k,iso} = 10^{54-57}$ erg and $n = 1 - 10^3$ cm^{-3}. For hyper energetic GRBs the peak flux at 5 GHz can reach even 10 mJy at extremely late times (> 1000 days) while the lower energy burst are expected to have peak fluxes ~ 100 μJy at 100 days, still well above the sensitivity of MeerKAT and SKA (see Fig. 1,2). Radio observations can allow us to measure several physical parameters of the burst (E_k, n, η, etc.) providing clues about the peculiar nature of PopIII stars and their circumburst medium. Moreover, radio observations of energetic PopIII GRBs can allow us to extend the study the IGM at extremely high redshift (in principle even at $z = 20$) through the detection of the 21cm absorption due to the neutral hydrogen along the line-of-sight [774]. The study of the 21cm forest overimposed on the radio afterglow can be used to constrain the reionization history and the possible incidence of mini-halos and protodisks in primordial galaxies [778; 779]. These studies require background sources as bright as 2-10 mJy, as expected in the case of the most extreme GRBs powered by PopIII stars [777].

7.4.9 Conclusions

Fig. 7.5 shows schematically the power of radio observations of GRB afterglows to study different aspects of these sources. We show as an example the 8.5GHz radio light curve of a typical bursts (parameters are reported on the plot) at $z = 2$. The present sensitivity limit for a typical observation with current radio facilities is shown by the dashed (blue) line. Radio observations around the time of the transition to the non–relativistic phase can provide unique probes of the jet and shock physics, observations past the non–relativistic transition can probe the environment properties of GRBs and allow to estimate the GRB energetics through radio calorimentry. Very late time observations can provide a unique view of the host galaxy properties.

All these fundamental topics will be covered by SKA thanks to its unprecedented sensitivity and its broad band coverage. The study of GRB radio emission needs to be complemented with all other available informations on the prompt gamma-ray emission and on the afterglow emission in the X-ray and in the NIR/Optical. The italian GRB community has a strong worldwide reputation both from the theoretical and observational point of view. The presence of the italian Swift team at OA Brera ensures a unique connection with the prompt, X-ray and Optical informations. This team has also a leading role in coordinating the italian GRB follow-up activities in the NIR/optical band in close collaboration with researchers of other Institutes. The expertise on the global energetics of GRBs, on their afterglow properties and on the radiation mechanism(s) acting in these sources, developed in the last few years (through direct multi-frequency data analysis and hydrodynamical-radiative codes) motivates us to concentrate also on the radio emission of GRBs to understand, test and discover what, since now, has only been imagined, taking advantage of the unique capability of the SKA experiment.

7.5 Radio investigation of Ultra-Luminous X-ray Sources

A. Wolter, L. Zampieri

Ultra Luminous X-ray sources (ULXs) are point-like, off-nuclear X-ray sources with inferred luminosity (if assumed to be isotropic) in excess of the Eddington limit for spherical accretion onto a 10 $M_\odot$ compact object (see, e.g., [780], for a review).

By this empirical definition, ULXs may encompass extreme examples of high-mass and low-mass X-ray binaries, recent supernovae, and perhaps intermediate-mass black holes (IMBH), the missing link between stellar-mass and supermassive BH.

Several different scenarios have been suggested to explain these sources, from stellar mass black holes with super-Eddington [781] or beamed [782; 783] X-ray emission, which would give the possibility of observing a jetted object, like a micro-quasar or an X-ray Binary (XRB) in a high or transition state, to sub-Eddington intermediate-mass (100-1000 $M_\odot$) black holes, [784–787]. In a few cases, emission nebulae have been found that are apparently associated with the ULX [788; 789]. A few early-type stars are found in optical images at the ULX position, that might be the mass donors in the binary system [e.g. 790–794]. Based on the X-ray spectral shape, namely a steep power-law index or, equivalently, a cool plasma temperature, about 20% of the ULX candidates are potentially supernovae [795]. However, in most cases there is no discrete optical counterpart to the ULX.

In spiral galaxies, the number of ULXs has been found to be correlated with the galaxy's global star formation rate, suggesting that they are mostly high-mass X-ray binaries [HMXBs; 795–797]. This is consistent with studies that show good correlations of the star formation rate of a galaxy with its global hard X-ray luminosity [798; 799] and with the number of HMXBs [800; 801].

A few X-ray point sources in distant galaxies have extreme luminosities: $L_X \geq 10^{41} erg/s$ [HyperLuminous X-ray sources, HLX: 802–806]. Such extreme luminosities (and, at least in the case of HLX-1, also the X-ray spectra [807]) can be easily explained by accretion onto an intermediate-mass black hole. Black holes with lower masses would need unreasonable beaming and/or super-Eddington luminosities to produce such luminosities [796; 808]

We see then that, despite the impressive advancements occurred in recent years, the existence of ULXs represents still a theoretical challenge in modern Astrophysics. If accretion is deemed to be the main source of the observed luminosity, the nature of the compact objects hosted in these sources is still a very intriguing issue.

In this respect, the radio band would give a solid opportunity of discriminating between different models, for both the spatial and spectral capabilities. Extended objects, like SNR and large HII regions are easily identified. The spectral shape can distinguish between a steep, thin synchrotron emission, and the flat, blazar like, emission from a jet pointed in our direction. As a bonus, the extinction by the interstellar medium is not an issue, in contrast to other wavebands. Furthermore, by assuming the emission is due to accretion and that ULXs are in a sub-Eddington regime, similar to Galactic XRBs and AGNs, the radio detection allows us to locate the ULXs in the fundamental plane of sub-Eddington accreting black holes [cf. 809–812] as defined by a correlation between radio core (L_R) and X-ray (L_X) luminosity and black hole mass, M_{BH}, $\log L_R = 0.6 \log L_X + 0.78 \log M_{BH} + 7.33$. This could be one of the most viable option of determining the mass of the ULXs.

Currently, very few observations have been performed up to now, due to the faintness of the sources and the sensitivity limits of the current telescopes. Typically observed ULXs have luminosities in the radio band of the order $L_R = 10^{34-36}$ erg/s, one to three orders of magnitude lower than radio supernovae [813]. The radio to X-ray flux follows roughly a linear correlation, albeit with a large scatter, similar to that derived for interacting supernovae [814], but the distribution of radio Luminosities is lower than about 3 orders of magnitude and this supports the hypothesis the most ULXs are not supernovae. The detected sources are mostly closer than 15 Mpc. One notable exception is the radio counterpart of HLX-1 at 95 Mpc, which has, in any case, a faint flux of 50 μJy [815] and was targeted just because it is a very special object. Two famous nebulae have been studied in the radio, Holmberg II X-1 and IC 342 X-1 [816]: their radio spectra is consistent with optically thin synchrotron emission; the radio nebulae can be compared with optical results an allow an estimate of the energetic of the systems; if the compact component in IC 342 X-1 is identified with a jet, then the

use of "fundamental plane" of accreting BH implies an upper limit to the mass of the BH at around a thousand $M_\odot$.

The study of the timing properties of ULXs represent a promising way to better understand their nature by comparison with the properties of BH binaries (BHB). Different states observed in BHB and transient are probably associated with different accretion regimes as measured by the relation between aperiodic variability and intensity [817; 818]. This type of relations can be used as a good tracer of the different accretion regimes in Galactic sources. (Quasi)-simultaneous monitoring of the flux and short-timescale variability in the radio and X-rays of bright ULXs would provide for the first time the opportunity to characterize the accretion states and transitions in these sources, in a way similar to what has been recently done for Galactic BH binaries. In this respect, potentially important synergies are envisaged between SKA and the Large Observatory For X-ray Timing (LOFT) [129]. This is an X-ray spectral-timing mission for the study of collapsed objects in our Galaxy and of the brightest supermassive black holes in Active Galactic Nuclei, and has been selected by ESA as one of the four Cosmic Vision M3 candidate missions to undergo an assessment phase. Persistent ULXs can be observed simultaneously with SKA and the LOFT Large Area Detector, jointly monitoring their radio/X-ray variability, while transient sources could be followed up after being triggered by the LOFT Wide Field Monitor.

To summarize: with radio data we can measure the total energy content if the ULX is embedded in a nebula; we can measure the mass in case a jet can be identified. A high spatial resolution allows both the identification of extended objects, like SNR, and the clear-cut association to the X-ray source. Timing studies can give us insight of the accretion states. The current observational limits are much more stringent in the radio than in the X-ray band and therefore only a very small number of ULXs has radio data. The SKA and precursors will allow both to reach larger distances and fainter sources.

7.6 Tidal Disruption Events: Synergies between SKA and LOFT

I. Donnarumma, E.M. Rossi, L. Stella, M. Feroci

Since the late 80s, it has been suggested that stars torn apart by the gravitational field of a supermassive black hole (SMBH) may be observed as flares from Earth ([819]; [820]). These are called tidal disruption events (TDEs). The flares would be caused by the sudden accretion of the star debris, which would feed the SMBH at an ever decreasing rate which follows $\dot{M} \propto t^{-5/3}$. The detection of these flares would thus deliver important astrophysical information. On the one hand, they allow us to detect otherwise quiescent SMBHs and estimate their masses. This would inform theory of galaxy-SMBHs cosmological coevolution. On the other, they constitute a unique opportunity to study the – highly theoretically uncertain – formation of an accretion disc and its continuous transition through different accretion states, as the accretion rate decreases. We can in principle observe a disc which transits from an initial super-Eddington phase, lasting several months, passing through a *s*lim and later a *t*hin disc regime, and ending its life, years later, in a radiative *i*nefficient state. The super-Eddington phase –which occurs only for SMBH masses $< 10^7$ $M_\odot$ is highly uncertain, but it may be associated with a copious radiative driven wind, which thermally emits $\sim 10^{41} - 10^{43}$ erg s^{-1}, mainly at optica frequencies. The disc luminosity ($\sim 10^{45} - 10^{46}$ erg s^{-1}), instead, peaks in soft X-rays. Finally, of paramount theoretical importance would also be the possibility to investigate the formation and evolution of an associated jet, powered by this sudden accretion. There is no specific theory for the jet emission from TDEs. Astronomers mainly borrow theory developed for blazars and/or γ-ray bursts. In general, non thermal emission in X-rays and radio is the jet signature.

Handful of candidate TDEs ($\sim$ 10) have been detected so far, particularly in ROSAT All sky survey ([821], [822]) and GALEX Deep Imaging Survey ([823], [824]; [825]). These "soft" events are

generally associated with the disc and wind thermal emission. The presence of a bright optical flare in the initial super-Eddington months makes optical surveys a useful tool for discovery. Significant advances in optical transient surveys are expected to be achieved by the Panoramic Survey Telescope and Response System (Pan-STARRS) and LSST (Large Synoptic Survey Telescope). The former may detect 10-100 events ([826]). *Thousands* of candidates could be, instead, detected by LSST, with its 6-band (0.3 – 1.1 micron) wide-field deep astronomical survey of over 20000 square degrees of the southern sky, using an 8.4-meter ground-based telescope.

More recently, two candidates TDEs were triggered by the BAT instrument on board of SWIFT ([827], [828]). A multi-frequency follow-up from radio to γ-rays revealed a new class of TDEs, where we are likely observing the non-thermal emission from a relativistic jet, responsible for the hard X-ray spectrum ($\Gamma \sim 1.6$) and the increasing radio activity ([831]), detected a few days after the trigger. Given the lack of statistics and of a solid theoretical framework for the non-thermal emission, we will assume the behavior of the best studied event, Swift J1644+57, as a prototype for the following estimates of the detection capability of both SKA and future X-ray observatories.

Swift J1644+57 (see Figure 7.6) was hosted by a star forming galaxy at $z = 0.354$. Its X-ray peak luminosity $\sim 3 \times 10^{48}$ erg s^{-1} was reached after a couple of days form the trigger, and it persisted at the level of $> 10^{45}$ erg s^{-1} for about 1 year. During its decay, the X-ray emission was approximately described by a $t^{-5/3}$ temporal law, the same as that expected from the fallback of stellar debris (see top panel in Figure 7.6). Variability at optical wavelength within the host was not detected, while transient emission was seen in infrared, becoming stronger at longer wavelengths, especially at millimeter and radio wavelengths. Radio (1.4. and 4.8 GHz) observations from Westerbork Synthesis Radio Telescope (WSRT) showed a bright source (Figure 7.6, bottom panel). [829] reported EVLA observations of the radio transient coincident with the hosting galaxy, providing an estimate of the bulk Lorentz factor $\Gamma_{bulk} \sim 2$ of the outflow. Finally, a 200-s quasi-periodic oscillation (QPO) was detected by both Suzaku and XMM, $\sim$ 10 and 19 days after the Swift/BAT trigger, respectively ([830]). QPOs are regularly detected in stellar mass BHs, but there is no firm physical interpretation of these phenomena. However, most models strongly link the origin of high-frequency QPO with orbits or resonances in the inner accretion disk close to the BH. This may cause variable energy injection into the jet, which consequently results in light variability in the X-ray band. This reasoning led [830] to estimate a BH mass between $5 \times 10^5 M_\odot$ and $5 \times 10^6 M_\odot$. As we will mention below, lower frequencies QPOs — linked to outer radius of the disc — may be instead related to the disc formation.

The LOFT Large Area Detector (LAD, [129]), with its breakthrough area (20 times larger than its predecessor RXTE/PCA), will be able to detect Swift J1644+57-like events out to redshift ~ 2. Moreover, as we will show in the following, the LAD will detect 200-s QPOs up to $z \sim 1$, with unprecedented precision.

In the following, we will focus on the synergy between SKA and LOFT in order to characterize the sub-sample of TDE candidates which present jet emission. SKA surveys will provide us with $\sim$ 150 triggers per year, which can be followed up by LOFT. Our goals are threefold. We aim at confirming and characterizing this class of TDEs. We will constrain the disc/jet formation processes using LOFT exquisite ability for variability studies. We will determine the efficiency of producing jets in sudden accretion events, comparing LAD detection rates with the complementary results from optical surveys like LSST.

7.6.1 Triggers by SKA

SKA, *in wide survey mode*, can cover an area of $A = 2 \times 10^4$ deg^2 every two days, reaching a limiting flux of $F_{\rm lim} = 90\mu$Jy at 1.4 GHz. In each of this observation, a J1644-like event (radio luminosity of

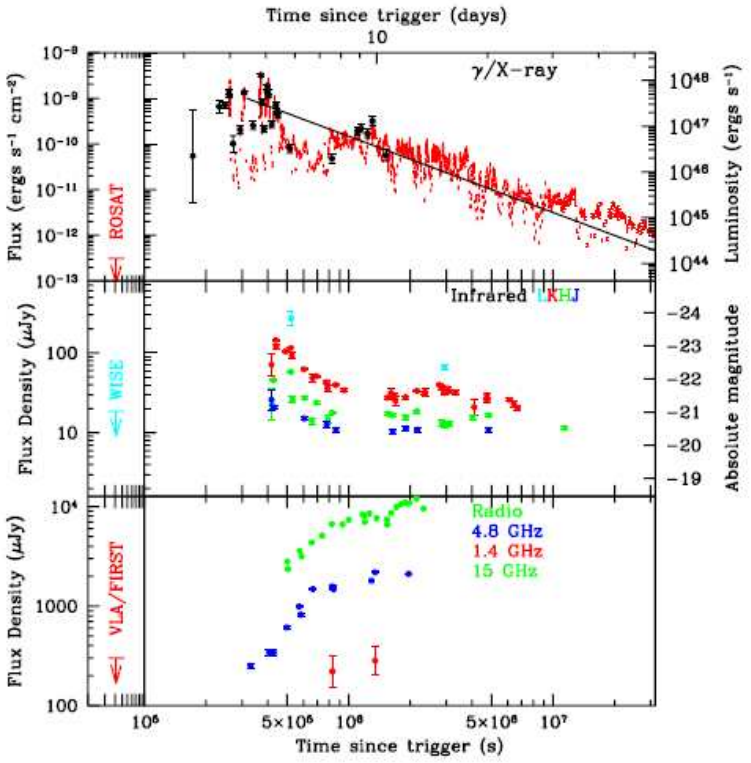

Figure 7.6. Multiwavelength γ/X-ray, optical/IR and radio light curves of Swift J1644+57 from [831], [832]. The panels show increasing wavelength, from γ/X-ray (top), optical/IR (middle) to radio (lower)

$\sim 10^{39}$ erg s^{-1} at 10 days after the trigger[3]) can be detected out to redshift $z \approx 0.5$. LOFT can observe the corresponding X-ray flux out to $z \sim 1-1.5$, therefore providing in principle follow-up to all SKA triggers. The rate of SKA TDEs can be estimated as ([833])

$$R \simeq 1.6 \times 10^{-2} \Gamma^{-2} A[\mathrm{deg}^2] \left(\frac{\mathrm{F_{sw}}}{\mathrm{F_{lim}}}\right)^{3/2} \frac{\mathrm{n_{BH}}}{10^{-2}\mathrm{Mpc}^{-3}}\ \mathrm{yr}^{-1} \tag{7.6.1}$$

which for the wide survey yields 265 events yr^{-1}. For this calculation we assumed $F_{\rm sw} \sim 200\mu$Jy, the flux at 1.4 GHz of the Swift J1644+57 (Figure 7.6). The number density of supermassive black holes ($n_{\rm BH}$) has been normalised with the local value (Merloni & Heinz 2008). The LOFT coverage of the sky, will allow us to follow up around 60% of these events, for a total of $\sim$ 160 events per year.

SKA in *deep wide survey mode* covers a smaller area of the sky, $A = 10$ deg^2, but the flux limit that can be reached observing this area twice, is almost 30 times lower, $F_{\rm lim} \simeq 3\mu$Jy at 1.4 GHz. We could thus reach TDE candidates out to $z \sim 1.8$, a similar redshift coverage than LOFT in the X-ray band. The rate of events however, is much lower $\sim$ 10 events per year when accounting for a factor

[3]Swift J1644+57 $F_{\rm sw} = 200\mu$Jy at 10 days after the trigger, at $z = 0.35$

of 2 lower BH number density (see e.g. eq. 7.6.1). The LOFT-SKA events will consequently be ∼ 6 events per year.

These calculations assume that all TDEs are accompanied by jet production. The Jet-disc connection is theoretically very uncertain and any observational constraint would be very valuable. With LOFT, we can constrain jet production efficiencies as low as 10% − 5%, which would yield 10-20 events per year.

In order to classify radio transients at 1.4 GHz as TDE candidate to activate a ToO with LOFT, some of SKA antennas should be repointed within a day from the alert towards the target, in order to detect the typical flux rise expected at higher — unabsorbed –frequencies (see Figure 7.6 lower panel). Moreover, in order to exclude any blazar activity, the quicklook analysis should first exclude that the host galaxy is an AGN. Finally, observations at higher radio frequencies should be crucial to pinpoint the position of the event within the host galaxy. A transient position *n*ot consistent with the host galactic centre would rule out a TDE, favoring a γ-ray burst explosion. For example SKA-phase II and/or ALMA should be able to locate the event within 100 pc from the galactic centre out to $z = 0.5$.

Variability: QPOs

Each of the SKA triggers from the wide survey are not only bright enough in X-ray to be detected by the LAD ($F_{\rm lim} \geq 5 \times 10^{-12}$ erg cm^{-2} s^{-1}), they can also maintain a flux above threshold for enough time to allow variability analysis. The main timescales in a TDE are linked to the jet or disc formation and feeding.

If the jet is powered by accretion, modulations of the accretion rate can results in variability imprinted in the X-ray light curve. Perhaps the longer timescale variability can be expected on the fallback timescale

$$t_{\rm fall} \simeq 40\, M_6^{1/2} m_*^{-1} \beta^{-3}\ {\rm d}, \tag{7.6.2}$$

which can be as short as $t_{\rm fall} \simeq 12$ d for a black hole with mass $M = 10^5 M_\odot$, while for $M = 10^8 M_\odot$ $t_{\rm fall} \simeq 400$ d. The star mass is in unit of solar masses $M_* = m_* M_\odot$ and the penetration factor $\beta = R_{\rm t}/R_{\rm p}$, where the tidal radius is $R_{\rm t} = R_* \left(\frac{M}{M_*}\right)^{1/3}$.

Variability on a shorter timescale can be caused from processes that accompanying the disc formation and circularization. The characteristic timescale is the dynamical time at the outer radius of the disc $R_{\rm d}$, which is expected to be twice the pericenter radius $R_{\rm d} = 2R_{\rm p}$,

$$t_{\rm dy}(R_{\rm d}) = 2\pi \sqrt{\frac{R_{\rm d}^3}{GM}} \simeq 8.3\ {\rm hr}\, \beta^{-3/2} r_*^{3/2} m_*^{1/2}, \tag{7.6.3}$$

where the star radius is in solar units $R_* = r_* R_\odot$.

Finally, the Keplerian frequency at the innermost stable circular orbit is the highest variability frequency that may be excited,

$$t_{\rm dy}(R_{\rm ISCO}) = \sqrt{\frac{R_{\rm ISCO}^3}{GM}} \simeq 2 \times 10^2\ {\rm s} \left(\frac{\alpha}{3}\right)^{3/2} \left(\frac{M}{4.5 \times 10^5}\right), \tag{7.6.4}$$

where $\alpha = 3$ for a non-rotating black hole and $\alpha = 0.5$ or maximally rotating black holes. For this latter case, a timescale of 200-s can be achieved with $M = 5 \times 10^6 M_\odot$. This QPO can be related to mechanisms of jet production, as well as powering.

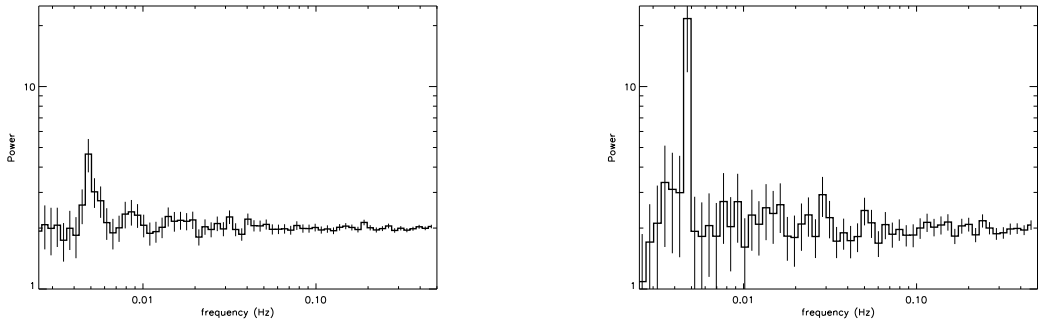

Figure 7.7. LOFT/LAD simulations of the QPO detected by both Suzaku and XMM in the Swift J1644 TDE (coherent frequency ~ 4.8 mHz, $\Delta\nu \sim 0.4$ mHz, fractional rms ~ 0.028). Left panel: ~ 100 ks on-source time for a flux of $\sim 5 \times 10^{-12}$ erg cm^{-2} s^{-1}. Right panel: ~ 10 ks on-source time for a flux of $\sim 10^{-11}$ erg cm^{-2} s^{-1}.

We have simulated the detection of this last high frequency QPO, which may be the hardest to detect. A $\geq 5-\sigma$ detection of a 200-s timescale QPO with rms $\sim 2.8\%$ (see Figure 7.7) requires ~ 10 ks (~ 100 ks) of integration time for a limiting flux of 10^{-11} erg cm^{-2} s^{-1} (5×10^{-12} erg cm^{-2} s^{-1}). Those integration times are both shorter than the time the event stays above threshold. For example an event at $z = 0.5$ is detected 10 days after the trigger, and it has a X-ray flux of 10^{-10} erg cm^{-2} s^{-1}, which will decay below threshold only after $\sim$ a month from the trigger. Events at lower redshift can be observed earlier, and the event stays above threshold even longer. Using candidates from the *deep* SKA survey, we can extend the QPOs analysis for objects out to redshift $z \sim 1$ (for an $\geq 5-\sigma$ detection). It is thus clear that SKA-LAT synergy can be a uniquely powerful to detect, identify and characterize TDEs.

8 Interstellar Medium, Solar System, Planetary Science, Bioastronomy

8.1 High-Mass Star Formation

M. Beltrán, S. Molinari, R. Cesaroni

Massive stars ($M > 8\ M_{\odot}$) of spectral types O and B play a crucial role in many areas of astrophysics. They dominate the appearance and evolution of galaxies, are responsible for the production of heavy elements and influence the interstellar medium through energetic stellar winds, ionizing radiation and supernova explosions. Understanding massive star formation is thus fundamental. However, in spite of the importance of high-mass stars, little is known about the physics that controls their formation. High-mass stars are rare objects that form very quickly ($< 10^4$-10^5 yr, [834]). What is more, high-mass star-forming regions are located farther away (typically a few kpc) than the nearest low-mass star-forming regions. This, together with the fact that massive stars form in crowded and very obscured ($A_V > 100$) regions, implies that the study of the massive star formation process encounters observational limitations that are difficult to circumvent. Furthermore, the fast collapse and contraction time scales and extreme conditions resulting from increasing turbulence and radiation pressure, make the theoretical treatment of their formation challenging. Nowadays, there are two contending models that propose a solution for the formation of massive stars based on non-spherical accretion and high accretion rates (e.g. [834–836]).

To make progress in our understanding of massive star formation and set constraints on the models, ones needs good observational knowledge of the star-formation environment and of the evolutionary steps through which OB star formation occurs. To circumvent the above mentioned observational problems, radio interferometric observations at subarcsecond angular resolution and sensitivity are required. At submillimeter wavelengths, ALMA is undoubtedly the instrument that can provide us with information on the dusty/molecular component, namely on structures such as, e.g., circumstellar disks around OB (proto)stars and the associated molecular outflows. However, ALMA cannot study a very important piece of the puzzle, needed to fully understand the formation mechanism of massive stars: the ionized material surrounding the newly borned early-type star. This important component must be studied at centimeter wavelengths and for this purpose the role of SKA is crucial.

8.1.1 Ionised Gas

The ionized material is important to study accretion and feedback in massive star-forming regions. Massive stars are very hot ($T>10^4$ K) and emit ultraviolet photons with enough energy to ionize the surrounding gas, giving rise to hypercompact (HC) and ultracompact (UCHII) HII regions [837], which are very bright at centimeter wavelengths. These regions are still deeply embedded in their parental molecular, dusty cores and possibly still accreting [838]. According to [839], the accretion process does not end as soon as an HII region is formed but it continues through the ionized region in the form of ionized accretion flows.

Feedback processes that act against gravitational collapse and accretion of gas onto protostars include radiation pressure, thermal pressure of photo-ionized gas, ram pressure from protostellar winds, and main sequence stellar winds. The first manifestations of fast ionized outflowing material comes in the form of thermal radio jets such as those of HH 80-81 [840], where proper motions reveal velocities of at least 600 km/s [841]. These jets are perpendicular to the rotating disk-like structures observed in molecular lines and dust continuum emission (e.g. [842] and references therein). Typical ionized mass-loss rates are about 1E-6 Msun/yr [843]. These radio jets, which are very weak if compared to HII regions, are similar to those that have been observed towards low-mass Young Stellar Objects (YSOs) (e.g. [844]), and hence, as suggested for the low-mass case [845], might play a role in driving the bipolar molecular outflows seen on a much larger scale.

Further strong feedback occurs when ionization of the surrounding material begins. The expanding ionization front of the nascent HII region moves faster in low density directions, creating bipolar compact HII regions. These regions tend to display broad recombination lines (> 40 km/s: [846]), which suggest that the expansion of the HII region cannot be led only by the thermal pressure of the ionized gas, but has to be driven by an additional mechanism, such as powerful stellar winds [847].

8.1.2 The Role of SKA

To study the different forms of feedback, jets, compact and hyper-compact HII regions, and ionized stellar winds, as well as the accretion flows taking place in the earliest stages of massive star formation, the current radio facilities have exhausted the targets that are bright enough to be imaged. These are basically just a few of the nearest and brightest objects, which do not represent a statistically significant sample. Here is where SKA, with its unprecedented angular resolution and sensitivity, plays a major role. For the typical distances of high-mass star-forming regions (5 kpc), angular resolutions of 0.01″ are needed to resolve the compact ionized regions, which in turn require sensitivities of 0.01 μJy to detect the optically thin emission from thermal jets and stellar winds.

Continuum emission

The 12-14 GHz window will be the highest frequency probe of the continuum available with SKA. Combined with observations at lower frequencies, this will allow us to determine the spectral index of the continuum emission and discriminate between thermal radio jets and HII regions. Thermal radio jets have a spectral index alpha ($S \propto \nu^{\alpha}$) in the range 0.25-1.1, depending on the collimation of the jet (for a prototypical biconical jet α= +0.6), while optically thick HII regions have a spectral index alpha=2. The angular size of radio jets varies with frequency ([848]; [844]) and its typical elongated morphology – sometimes made of a chain of well aligned radio peaks – is a distinctive feature. The angular resolution of SKA will allow allow us to resolve the jet and given that radio jets have flux densities of only a few mJy, its high-sensitivity will be needed to properly map their morphology. Therefore, the spectral index of the centimeter continuum emission together with the morphology will be used to identify radio jets. The jet properties (mass loss rate, momentum rate, collimation) will be derived from the radio flux [849] and compared with the corresponding parameters of the associated large-scale molecular outflows [844]. In addition, by sampling a large number of objects, one can study the variation of the jet parameters as a function of luminosity and evolution.

Continuum emission will also allow to study the expansion of the HC HII regions and will help to estimate the age of the central YSOs, as done by [850] for the massive protostar G24.78+0.08. In fact, if the HII region is expanding, for a given mechanical luminosity, the radius of the ionized region and its expansion velocity can be expressed as a function of time [851].

Recombination lines

Observations of recombination lines at centimeter wavelengths will allow us to trace the kinematics of the ionized gas in hypercompact and ultracompact HII regions, and will help to distinguish expansion motions from accretion. By tracing gas infall in the surroundings (< 0.001 pc) of the newly formed massive star [852], one can estimate the mass infall rate, which is an important parameter to constrain the theoretical models of high-mass star formation. To trace ionized accretion flows at scales of a few milliparsecs, angular resolutions «0.1″ are needed, together with high-sensitivities, taking into account that the recombination line strength is about 10% of the continuum level. These performances can only be attained by SKA at centimeter wavelengths. In particular, the 12-14 GHz frequency range of SKA, which will provide the highest angular resolution, includes four hydrogen recombination lines: H81α, H80α, H79α, and H78α.

8.2 Complex organic molecules in protostellar environments

C. Codella, F. Fontani, P. Caselli, C. Ceccarelli, M.T. Beltrań, J.R. Brucato, M.E. Palumbo

8.2.1 The formation of a Sun: from prestellar cores to planetary systems

The formation of Sun-like stars and the chemical complexity of the molecular gas involved in the process are sketched in Fig. 1, following [853]: (i) matter slowly accumulates toward the center of a molecular cloud. The central density increases while the temperature decrease. Atoms and molecules in the gas phase freeze-out onto the cold surfaces of the dust grains, forming the grain mantles. Hydrogenation of atoms and molecules takes place, forming molecules such as water (H_2O), formaldehyde (H_2CO) and methanol (CH_3OH). In these regions the formation of new molecules in icy mantles is also caused by the effects of UV photons and low-energy cosmic rays. (ii) the collapse starts, the gravitational energy is converted into radiation and the envelope around the central object warms up. The molecules frozen on the mantles acquire mobility and form new species. When the temperature reaches about 100 K mantle sublimates, and we have the so called hot corinos ($\leq$ 0.01 pc) phase. Molecules in the mantles are injected in the gas, where they react and form new, more complex, molecules. The abundance of COMs (such as methyl formate, $HCOOCH_3$, or dymethyl ether, CH_3OCH_3) dramatically increases. A classical example is provided by IRAS16293-2422 (e.g. [854; 855]), where recently also glycoaldehyde ($HCOCH_2OH$), crucial molecules for the formation of metabolic molecules, has been detected ([856]). (iii) Simultaneously to the collapse, a newborn protostar generates a fast and well collimated jet, possibly surrounded by a wider angle wind. In turn, the ejected material drives shocks travelling through the surrounding high-density medium. Shocks heat the gas up to thousands of K and trigger several processes such as endothermic chemical reactions and ice grain mantle sublimation or sputtering. Several molecular species undergo significant enhancements in their abundances. The prototypical chemical rich shock is L1157-B1. Toward this source, not only relatively simple complex molecules, like methanol, have been detected ([857]), but also molecules considered hot corinos tracers, like methyl formate ($HCOOCH_3$), ethanol (C_2H_5OH), formic acid (HCOOH) and methyl cyanide (CH_3CN) ([858]). The emission of these species is concentrated in a small (around 1000 AU) region associated with the violent shocks at the head of the outflowing material ([859]). The presence of COMs in molecular outflows strongly suggests that these species were part of the sputtered icy mantles as the time elapsed since the shock is too short for any gas-phase route to build up COMs. (iv) The envelope dissipates with time and eventually only a circumstellar disk remains, also called protoplanetary disk. In the hot regions, close to the central forming star, new complex molecules are synthesised by reactions between the species

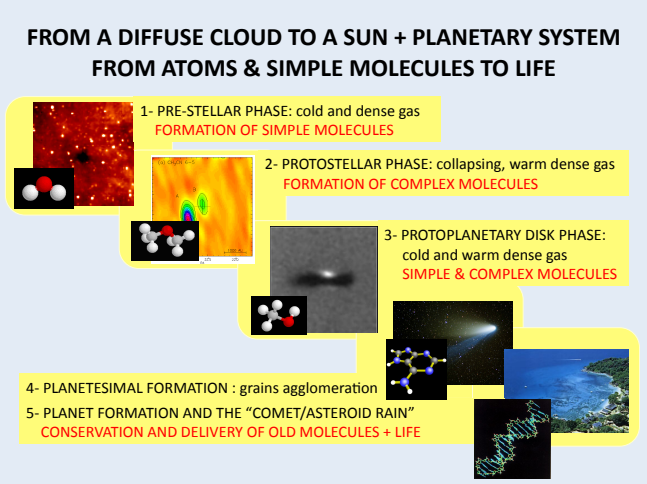

Figure 8.1. Star formation and chemical complexity ([853]). The formation of a star and a planetary system, like the Solar System, passes through different phases, marked in the sketch.

formed in the protostellar phase. In the cold regions of the disk, where the vast majority of matter resides, the molecules formed in the protostellar phase freeze-out onto the grain mantles again. Dust grains then coagulate into larger planetesimals, the bricks of future planets, comets, and asteroids.

8.2.2 Chemical complexity around massive stars

Our understanding of the formation of massive stars has largely improved in recent years. From a theoretical point of view, it has been demonstrated that radiation pressure is not a barrier to form stars with masses > 8 solar masses and spectral type O and B and that they could form through disk accretion. Two main theoretical scenarios proposed to explain the formation of massive stars are accretion-based mechanisms: (1) the core accretion model, where a massive star forms from a massive core fragmented from the natal molecular cloud, and (2) the competitive accretion model, where a molecular cloud initially fragments into low-mass cores, which form stars that compete to accrete mass from a common gas reservoir. Both models predict the existence of protostellar accretion disks around massive young stellar objects, and therefore it is reasonable to expect the presence of wind-driven molecular outflows. However, in the first scenario the disk-outflow system must be a well-collimated structure, while this is ruled out in the second scenario where the outflows-disk system is the result of the overlapping of many low-mass protostellar outflows oriented randomly.

The clustered mode of high-mass star formation and the typical large distances of high-mass star forming regions (usually larger than 1 kpc, definitely higher than those of typical low-mass star forming regions, such as Taurus, 140 pc, and Perseus, 250 pc) challenge direct observation of accretion disks. Nevertheless, over the last years, evidence of the existence of accretion disks have been provided by observations ([860]). Also collimated outflows and jets with properties similar to those originating from low-mass protostars have been detected, thus implying a similar formation mechanism for low- and high-mass stars. Indeed, jet-driven molecular outflows play an important role in the accretion scenario: an evolutionary sequence for the outflows driven by massive protostars has been proposed by [861], in which an initially well-collimated jet/outflow gradually evolves into a wide-angle wind as the ionising radiation powered by the central massive stellar object becomes more dominant.

The earliest stages of the massive star formation are characterised by the occurrence of the so called hot cores, i.e. hot (> 100 K), small (≤ 0.1 pc), and massive (up to thousands of solar masses) clumps warmed by the stellar radiation. Similarly to hot corinos around low-mass protostars, hot cores are powerful emitters of COMs (see e.g. [862]), evaporated from grain mantles, from methyl cyanide to glycoaldehyde and its isomers ([863]), whose line emission have been detected at millimetre wavelengths. Hot cores differ from hot corinos not only for the larger sizes, but also chemically. When normalised to methanol or formaldehyde, hot cores have typically one order of magnitude less abundant COMs (such as $HCOOCH_3$ or CH_3OCH_3) than hot corinos (e.g. [864]). Such difference is likely due to various factors, such as the composition of the sublimated ices, governed by the past prestellar history. Among these, deuterated species represent an important record of the early cold phase. In particular, recent surveys have shown that some of these species are evolutionary indicators and/or preferentially trace one specific evolutionary group (e.g. [865]).

8.2.3 The lessons provided by spectral surveys

Molecular complexity builds up at each step of the star formation process, starting from simple molecules and ending up in polyatomic species. Understanding in great detail the involved processes is likely the only way to predict the ultimate molecular complexity reached in the ISM, as the detection of large molecules is increasingly more difficult with the increase of the number of atoms constituting them. Thanks to the recent spectacular progress of astronomical observations, particularly due to the Herschel (sub-mm and IR), IRAM and SMA (mm and sub-mm), and NRAO (cm) telescopes, an enormous activity is being developed in the field of Astrochemistry, extending from astronomical observatories to chemical laboratories.

We are already involved in a strong international observational effort to detect complex and rare molecular species in the interstellar space through emission due to their ro-vibrational transitions. These efforts are carried out since many years using single-dishes with the IRAM ground based observatory (e.g. the ASAI 80-300 GHz spectral survey Large Programme), with the Herschel Space Observatory (e.g. the CHESS spectral survey Key Programme in the 500-2000 GHz window). Unbiased spectral surveys with unprecedented sensitivity of templates of dense cores, protostars, and young stars have been obtained, which covers the full formation process of low- and high-mass stars. Forest of lines, especially at 3mm, have been obtained. Major advances relevant to the objectives of this project are: (i) the discovery of a hugely enhanced molecular deuteration in low-mass protostars, with the detection of doubly and triply deuterated molecules (e.g. [866]); (ii) the discovery of large quantities of COMs in hot corinos and hot cores (e.g. [855; 862]) and shocked regions (e.g. [858; 859]). A huge effort is carried out also using interferometers to provide high-spatial resolution images. In particular, we are deeply involved in the CALYPSO PdB-IRAM Large Programme. CALYPSO is observing a large sample of low-mass protostellar objects in the 80-300 GHz window, obtaining high-angular resolution (less than 1–3 arcsec) maps of numerous COMs in the inner protostellar environment. Finally, we stress that we have been using the ALMA interferometer since the very beginning of Science Verification and Early Science, leading several projects accepted (and part of them recently observed) during the Cycle 0-1 calls. Also the first spectra provided by interferometers show spectacular forests of lines: in particular the 3mm band shows an amazing large number of COM lines at high excitation (see e.g. [867]).

8.2.4 Why SKA?

The numerous detections of high-excitation COM lines in the 3mm window call for observations at lower wavelengths, where heavy species are expected to emit (see e.g. the JCMT, http://spec.jpl.nasa.gov, and CDMS, http://www.astro.uni-koeln.de/cdms, spectral catalogues). In particular, if we consider

bright lines ($S\mu^2 > 1$ D^2) at low excitation ($E_u \leq 20$ K), then the 4-15 GHz band contains a considerable number of COMs transitions. Even more important, the millimeter frequency bands are often so full of lines that it is paradoxically difficult to identify species through a large number of emission lines simply due to confusion. On the other hand, this low frequency band is relatively clear, given that low energy transitions of light molecules fall at much higher frequencies. The completion of the results obtained at mm-wavelengths with spectral surveys in the cm-window will allow one to have the possibility of have, for different species, a large number of transitions, which is needed to reliably detect the largest COMs for which the population is distributed over many energy states, having large partition functions. An instructive view is given by the NRAO 100-m GBT PRIMOS Legacy Project, which recorded the spectrum from 300 MHz to 46 GHz towards the Sgr B2(N) molecular cloud. The PRIMOS data have resulted in numerous new detections in astrochemistry (e.g. [868], and references therein). SKA will observe at frequencies higher than 100 MHz, offering high-angular resolutions (1–10 mas, depending on frequency). If the SKA array will be optimised also for frequencies higher than 4–5 GHz, possibly reaching the 10-15 GHz spectral window, then the study of molecular line emission will be instructive. The typical sizes of the regions associated with COMs' emission is less than about 1 arcsec (hot corinos, hot cores, jets). Therefore, the spatial resolutions offered by SKA are fundamental to resolve the emitting region or at least to minimise beam dilution. In this way, (i) we will have bright line emission, and (ii) we will correctly evaluate COMs' abundances. To conclude, SKA could produce a complete inventory of known interstellar species accessible in the centimeter wavelength range that can be used to put severe constrains on the physical conditions of the emitting gas, as well as on COMs abundances.

8.2.5 The need of laboratory experiments

Laboratory experiments have shown that complex molecules are formed after ion bombardment (keV-MeV) and UV photolysis (6.9–13.6 eV) of simple solid phase molecules (such as methanol, methane, carbon monoxide) and their mixtures (e.g. [869; 870]). Complex molecules formed in the solid phase are released to the gas phase after desorption of icy grain mantles. Thus the comparison between observed gas phase chemical abundances and experimental results is essential to build up an accurate chemical network as well as determining the origin and history of the protostellar objects. At the *Laboratory for Experimental Astrophysics* in Catania there is a long-standing tradition of experimental studies of the chemical effects induced by ionising radiation (photons and energetic ions) bombarding astrophysically relevant ices. Furthermore the Catania Laboratory team plans to develop an innovative experimental set-up in order to detect minor complex species formed which cannot be detected with conventional techniques.

8.3 Galactic foregrounds versus Galactic astronomy

C. Burigana

The accurate study of Galactic emissions, other than intrinsically of extreme interest, is crucial for any cosmological exploitation of radio to infrared sky [871]. In this context, Galactic emissions are considered as sources of foreground. They can be divided in two wide categories: diffuse emissions and localized structures or discrete/point-like sources. By construction, the interferometric design of the SKA and of its precursors is more suitable for investigating on the latter kind of sources, object of previous discussions. On the other hand, as first probed by DASI [872], interferometers can be also fruitfully used to map the diffuse sky signal on relatively wide areas in both total intensity and polarization, Fourier transforming data from the U-V space to the real 2D space. The possibility of extending this opportunity to intermediate and large scales, or equivalently to low and intermediate

multipoles, largely relies on the capability of available mosaic techniques to assemble different FoVs into maps with appropriate large scale calibration and matching. This is of increasing complexity at SKA increasing frequency, since the smaller FoV sizes of higher frequencies. On the other hand, the high Galactic radio signal does not require the extreme accuracy demanded, for instance, by CMB fluctuation mapping at the SKA highest frequencies.

The SKA radio frequency coverage is of extreme interest to study the Galactic synchrotron emission, in both total intensity and polarization, and the unpolarized Galactic free-free emission, particularly remarkable at low and moderate Galactic latitudes. Extending the SKA frequency coverage to highest frequencies will allow to accurately derive the spectral behaviour of these emissions on a wide range. This is crucial for many applications in CMB studies, since the accuracy of many component separation methods (see e.g. [871; 873] and references therein) takes great benefit by the increasing of the frequency range of the templates adopted in the analysis and/or by a priori information about the spectral behaviour of the different components, related to the energy and properties of emitting particles, superimposed in the overall signal. This information contributes to the improvement of the physical knowledge of the so-called mixing-matrix adopted in the inversion process that derives the different physical components from multifrequency maps. Furthermore, SKA data can be used to map the Galactic HI 21-cm emission.

Regarding the synchrotron emission, produced by relativistic cosmic ray electrons spiraling in the Galactic magnetic field, a remarkable feature of the Galactic radio sky is the significant depolarization appearing in a wide region around the Galactic center. This effect is certainly much less relevant in the microwaves, as evident by the comparison [874] of available radio surveys with millimeter surveys like e.g. those provided by WMAP (see Fig. 8.2). Multifrequency, high sensitivity radio observations like those that will be available with the SKA will certainly put a firm light on this problem, allowing to disentangle between the various depolarization effects, i.e. *Faraday* depolarization associated to Galactic magnetic fields and *geometrical* depolarization coming from the averaging in the observed signal of contributions from cells with different polarization angles, both along the line of sight and within the angular directions of the observational effective beam.

If mosaic techniques will work successfully, a view of a very wide sky fraction will allow to map Galactic foregrounds at intermediate and large scales. This will have a tremendous impact for the development and verification of 3D physical models of the Galaxy and for the study of the large scale, almost regular component of the Galactic magnetic field [877–881]. Turbulence phenomena [882] predict a typical power law dependence of the power spectrum of diffuse emission with properties related to the physical conditions of the ISM in the considered area. Almost independently of the accuracy of mosaic techniques, SKA maps on many patches of sky of limited area will allow to reconstruct with unprecedented accuracy the correlation properties of the radio sky diffuse emission, thus providing crucial information for the comparison with theoretical models and and their implementation through numerical codes [883; 884].

Two other topics crucial for both Galactic science and foreground treatment for survey cosmological exploitation are the full understanding of the *anomalous microwave emission* (AME) and of the so-called *haze* component.

AME is the recently identified emission component which is well-correlated with far-infrared dust emission. It is produced by rapidly spinning small dust grains having an electric dipole moment [885] and its spectrum is expected to peak in the range 15–50 GHz. *Planck* has for the first time been able to define the shape of the spectrum on the high frequency side of the emission peak in a number of dust/molecular/HII regions [886]. In the frequency range 20–40 GHz AME is typically comparable in brightness to the free-free for the inner Galactic plane. Depending on the implementation of the high frequency channels, the SKA could provide precise mapping on the low frequency side of this

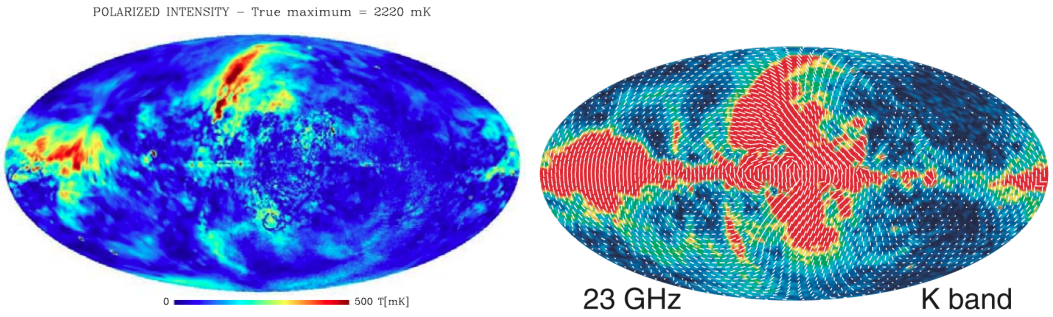

Figure 8.2. All-sky maps of Galactic polarized emission at radio (1.4 GHz, left image; adapted from [875]) and microwave (23 GHz, right image; adapted from [876]) frequencies.

emission.

Planck was also able to identify and characterize the emission from the Galactic haze at microwave wavelengths [887]. It is a distinct component of diffuse Galactic emission, roughly centered on the Galactic centre, and extends to $|b| \sim 35°$ in Galactic latitude and $|l| \sim 15°$ in longitude. By combining WMAP and *Planck* data, [887] were able to determine the spectrum of this emission to high accuracy, unhindered by the large systematic biases present in previous analyses. The derived spectrum is consistent with power-law emission with a spectral index of -2.55 ± 0.05, thus excluding free-free emission as the source and instead favoring hard-spectrum synchrotron radiation from an electron population with a spectrum (number density per energy) $dN/dE \sim E^{-2.1}$. At Galactic latitudes $|b| < 30°$, the microwave haze morphology is consistent with that of the Fermi gamma-ray haze or bubbles (see also [888]), indicating that we have a multi-wavelength view of a distinct component of our Galaxy. Given both the very hard spectrum and the extended nature of the emission, it is highly unlikely that the haze electrons result from supernova shocks in the Galactic disk. Instead, a new mechanism for cosmic-ray acceleration in the centre of our Galaxy is implied. With the SKA we will have the opportunity to firmly constrain these models, through a precise multifrequency mapping of this emission in both total intensity and polarization.

Summarizing, the SKA high resolution maps of the Galactic emission will contribute to a better comprehension of Galactic foreground providing key astrophysical information for the separation of CMB and the cosmological HI 21 cm emission. Also as a heritage of the studies carried out in the context of the *Planck* project, our team has a good expertise in both component separation techniques and in multifrequency analysis of Galactic foreground that will be fruitfully transferred to the analysis of SKA data, possibly in combination with other surveys.

8.4 SETI

C. Maccone

8.4.1 Summary

When the SKA will be working, for the first time it will be possible to detect TV programs broadcasted by Alien Civilizations in the Galaxy, up to a distance of about 10 light years. Though this is a modest distance, the possibility of detecting "Alien Leakage" is an absolute novelty for SETI. In fact, SETI radio astronomers could so far only hope to detect INTENTIONAL Alien messages, transmitted with huge omni-directional powers, which is rather unlikely even for more advanced civilizations than us. Maybe this is why we could not detect any Alien civilization in the first 52 years of traditional

SETI searches (1960–2012). In addition to that, the beam-forming capabilities of the SKA will enable us to conduct SETI searches in a much shorter time than possible today by aid of big dishes. Just as an example, using its beam-forming techniques, LOFAR is already capable today of conducting a full–sky SETI survey in 24 hours. But LOFAR can observe only in the MHz range, which is why the SKA will become crucial for SETI observations in the GHz range by virtue of beam-forming. Finally, it will be stressed the need to raise a new generation of radio astronomers capable of using the SKA for Astrobiology (also called "the Cradle of Life"). This means young radio astronomers expert in the detection of radio signatures testing for the chemistry of life on extrasolar planets, like the thousands of extrasolar planets already discovered by the NASA Kepler space mission. Such SETI searches on the Kepler exoplanets are already now ongoing at Green Bank by a team led by Andrew Seimion of Berkeley, and his example should be followed by young radio astronomers intending to work on the SKA.

8.4.2 Introduction to SETI

SETI, an acronym standing for "Search for Extra-Terrestrial Intelligence", is the search for electromagnetic waves carrying signals reaching the Earth from possible alien civilizations. It started back in 1960 (Project Ozma run by Frank Drake), and was later continued occasionally in several countries, with ever-increasing use of computer technology. No Alien Signal was ever found, tough there were some dubious cases in the past, all finally dismissed as RFI (Radio Frequency Interference). It should be noted, however, that our largest radio telescopes may be capable of detecting radio signals emitted "with typically human electric powers" only up to distances of a few hundred light years. This is a very, very small part of the Galaxy, and so the conclusion reached by many SETI scientists is that "we did not find any ETs because we did not explore far enough in the Galaxy". As of 2012, received electromagnetic waves of four types are considered to be of interest to SETI:

1. Radio waves in the "Terrestrial Microwave Window", roughly between 1 and 10 GHz. Basically these SETI searches are pursued by the Allen Telescope Array of the SETI Institute in California, by the Arecibo radio telescope (run by the Berkeley SETI Team), and at some other minor locations in the world, like the SETI Italia Program run at Medicina (near Bologna, Italy) by virtue of a "small" 32-meter dish.

2. Radio waves in the MHz range, currently explored by the LOFAR radio telescope in the Netherlands and other European countries.

3. Optical SETI, looking for optical laser pulses, basically done only in the United States and the United Kingdom, thought there are plans in Europe to do Optical SETI soon (in Italy at the FOAM13 Observatory in Tradate, Varese, then in Austria, etc.).

4. Infrared SETI: done no-where yet, but under consideration at Berkeley and Harward in the USA.

5. To the above four types of electromagnetic SETI, a fifth type should be added: neutrino SETI, so far never tried experimentally and only studied by paper research.

Currently five increasing levels of complexity exist in SETI:

1. Piggyback SETI, like the one SERENDIP IV spectrum analyzer installed at the Medicina 32–meter dish on the Hydrogen line receiver at 1.420 GHz. SERENDIP makes use of whatever observing plan (sequence of frequencies, sky coordinates, and polarizations) under way at its

host observatory. Moreover, the SERENDIP data acquisition system, once installed, operates autonomously. This approach makes it possible to obtain large amounts of high quality observing time in a manner that is economical and that does not adversely affect ongoing radio astronomy survey work. The criticism to this way of doing SETI, however, is that we will hardly find any ETs as long as we look at stars of "generic" astrophysical interest, i.e. possibly not interesting at all from the point of view of SETI and the origin of life on extrasolar planets. Thus, doing piggyback SETI is "the most superficial way of doing SETI", since we will hardly find ETs by looking at the least likely stars!

2. Wideband SETI by KLT. The KLT (Karhunen-Loève Transform) is an extremely powerful algorithm to extract very weak signals of any kind from noise of any kind (i.e. colored noise, not just white noise). Technically speaking, it is a principal component method, i.e. a principal axis transformation in the Hilbert space spanned by the eigenfunctions (i.e. eigenvectors) of the autocorrelation of the (noise+possible signal). Interested readers may wish to read [889]. The KLT, however, requires many more computations than the well-known FFT: for a an autocorrelation matrix $N \times N$, the KLT requires N^2 computations, while the FFT requires just $N \log N$. Since computer time is money, the vast majority of scientists and technologists refused to replace the cheaper FFT by the more expensive KLT, and thus they may have missed many SETI signals that the FFT "cannot see" because it applies to narrow-band signals only, and not to wide-band signals.

3. SETI targeted searches, that may be subdivided into searches from the ground and searches from space:

   a) Searches from the ground are exemplified by the creation of the HabCat and the relevant searches conducted by virtue of the Allen Telescope Array (ATA). The Catalog of Nearby Habitable Systems (HabCat) ([890; 891]) is a catalogue of 17,129 "HabStars" star systems which conceivably have habitable planets. The list was developed by scientists Jill Tarter and Margaret Turnbull under the auspices of Project Phoenix, by pruning the Hipparcos Catalogue (which has 118,218 stars) and filtering on a wide range of star system features. Later, in the decade 2003-2012, many of these stars were searched for SETI radio signals by virtue of the ATA Team led by Jill Tarter at the SETI Institute in Mountain View, California.

   b) Searches from space, exemplified by the Corot (2007-present) and Kepler (2009–present) space missions and the SETI searches conducted from the ground on the new exoplanets discovered by these space missions. A good reference on this very recent work is the paper presented by Andrew Siemion of the Berkeley SETI Team at the Fourth IAA Symposium on Searching for Life Signatures, organized by Claudio Maccone and held in the Republic of San Marino (September 25-28, 2012; [892]).

8.4.3 SKA for SETI

Figure 8.3 shows the typical behaviour of the signal flux vs. range for current SETI searches. The diagonal lines show transmitters of different effective powers. The x–axis is the sensitivity of the search. The y–axis on the right is the range in light years, and on the left is the number of sun-like stars within this range. The vertical line labeled SS is the typical sensitivity achieved by a full sky search, such as BETA above. The vertical line labeled TS is the typical signal flux achieved by a targeted search such as Phoenix. Clearly, a radio telescope sensitive to a flux of 10–30 W/m^2 would have a range of 100 light years, thus including about 1,000 stars of solar type in the search.

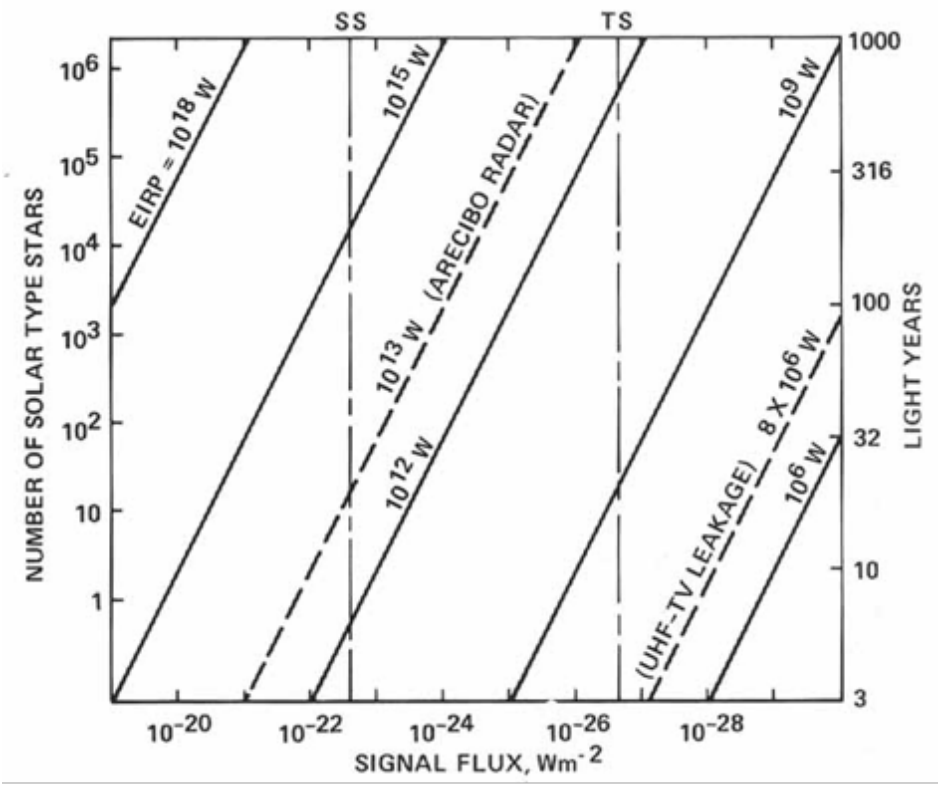

Figure 8.3. Signal flux vs. range for SETI radio searches. The diagonal lines show transmitters of different effective powers. The x–axis is the sensitivity of the search. The y–axis on the right is the range in light years, and on the left is the number of sun–like stars within this range. The vertical line labeled SS is the typical sensitivity achieved by a full sky search, such as BETA above. The vertical line labeled TS is the typical sensitivity achieved by a targeted search such as Phoenix. Figure taken from *http* : *//en.wikipedia.org/wiki/*).

Going now over to the SKA, the sensitivity, field-of-view and angular resolution of the SKA will make possible a program to create a multi-epoch data base of wide-angle relative astrometry to a few Îijas precision for about 10 million radio sources with $S > 10$ μJy (see [893]). Sub-AU imaging of thermal emission will trace the process of terrestrial planet formation. The raw sensitivity of the SKA will allow âĂIJleakageâĂİ radiation to be detected from potential civilizations in planetary systems around millions of solar-type stars, not to mention possible civilizations around M–stars, that might be many more and so much older than solar-type stars.

8.4.4 Conclusions

By the time the SKA becomes a reality a new generation of young radio astronomers capable of using the SKA for Astrobiology and SETI must be raised. It is thus a breakthrough in scientific culture what is now needed. Brand-new textbooks (like [894]) may only help to bring about this cultural change.

Part III

Appendices

A Telescope Specifications

The technical specifications for SKA and SKA precursors (Meerkat and ASKAP) are provided in Table A.1. Parameters for ASKAP and MeerKAT are from their telescope web sites. Parameters for SKA Phase 1 (SKA 1) and SKA Phase 2 (SKA 2) are from [895]. Such parameters should be considered as indicative. The different SKA 1 and SKA 2 arrays reported in Table A.1 are defined as following (see [895]):

- SKA 1 Low: Low-frequency Aperture Array (AA)
- SKA 1 Mid: Mid-frequency dish array with high sensitivity single pixel feeds
- SKA 1 AIP–Survey: Component of SKA 1 delivering high survey speed at mid frequencies, based on Phocal Array Feeds (PAF, part of AIP)
- SKA 2 Low: Low-frequency Aperture Array (AA)
- SKA 2 Mid–Dish: Mid-frequency dish array with high sensitivity single pixel feeds, and possibly equipped with PAFs
- SKA 2 AIP AA: Mid frequency dense Aperture Array (part of AIP)
- SKA 2 AIP–PAF: A component of SKA 2 delivering high survey speed at mid frequency, based on PAFs (part of AIP).

The AIP components are not guaranteed to be available but are subject to future engineering decisions based on cost/performance. Only PAFs are considered in the SKA engineering plan for inclusion in SKA 1.
The parameters listed in Table A.1 were used to derive the integration times and/or sensitivities, by using the *SKA Exposure Time Simulator*[1]. ASKAP typical sensitivities and survey speeds are reported also in Table A.2.

[1] www – astro.physics.ox.ac.uk/ hrk/SKA_EXPOSURE.html

Table A.1. Technical specifications for SKA Precursors, SKA Phase 1 and SKA Phase 2.

Telescope:	ASKAP (2016[a])	Meerkat 1 (2016)	Meerkat 2 (2018)	SKA 1 Low	SKA 1 Mid	SKA 1 AIP−Survey	SKA 2 Low	SKA 2 Mid–Dish	SKA 2 AIP−AA	SKA 2 AIP−PAF
Collector Type:	12m dish	13.5m dish	13.5m dish	Sparse AA	15m dish	15m dish + PAF	Sparse AA	15m dish	Dense AA	15m dish + PAF
No of Collectors:	36	64	64+7	280	250	96	280	2500	280	2000
Frequency Range (GHz):	0.7–1.8	0.9–1.7	0.58–1.7 8.0–14.5	0.07–0.45	0.45–3.0	0.7–1.8	0.07–0.45	0.45–10.0	0.4–1.4	0.45–3.0
Max Bandwidth (GHz):	0.3	0.75		0.38	1.5	0.3	0.38	Depends	1.0	0.3
< 1 GHz			0.435					on feeds		
1–1.7 GHz			0.75							
> 8 GHz			2 or 4							
Effective FoV (deg^2):	30	1.0				30	200			
0.5/0.6 GHz			5.6							144
1 GHz			1.9		1.0			1.0		36
1.7/2 GHz			0.62							9
8 GHz			0.03							
14 GHz			0.01							
Sensitivity[b] (m^2/K):	65	> 220				275		10000		
> 90 MHz							4000			
131 MHz				1515						
300 MHz				889						
< 1.2 GHz									10000	
0.45–1.4 GHz					773					
0.6–1.7 GHz			> 220							
1.4 GHz									5000	
1–2 GHz					1031					7000
8–14.5 GHz			> 200							
Telescope Configuration:						TBD				TBD
< 700 m	83%									
700 m – 6 km	17%									
< 1 km		70%	63%	50%	50%		30%	20%	30%	
1 – 5 km				20%	20%		36%	30%	36%	
1 – 8 km		30%	27%							
8 – 16 km			10%							
5 – 100/180 km				30%	30%		34%	30%	34%	
< 180 km								20%		

[a] First observations with ASKAP will be possible from 2014 with a limited number of antennas.

[b] Sensitivity defined as A/T, where A = total collecting area, $T = T_{sys}/\eta$, and η is the aperture efficiency.

Table A.2. ASKAP indicative sensitivities (for 1^h observation) and survey speeds for different angular resolutions (obtained assuming T_{sys} = 50 K and aperture efficiency η = 0.8).

Parameter	10"	18"	30"	90"	180"	Units
Continuum Sensitivity (300 MHz)	37	29	34	74	132	μJy/beam
Line Sensitivity (100 kHz)	2.1	1.6	1.9	4.1	7.3	mJy/beam
Surface Brightness Sensitivity (5 kHz)	–	–	5.2	1.3	0.56	K
Continuum Survey Speed (300 MHz, 100 μJy)	220	361	267	54	17	deg^2/hr
Line Survey Speed (100 kHz, 5 mJy)	184	301	223	45	14	deg^2/hr
Surface Brightness Survey Speed (5 kHz, 1 K)	–	–	1.1	18	94	deg^2/hr

B Bibliography

Bibliography

[1] Norris, R.P., et al., PASA, 30 (2013) e020

[2] Johnston, S., et al., PASA, 24 (2007) 174

[3] Johnston, S., et al., ExA, 22 (2008) 151

[4] Deboer, D. R., et al., IEEE Proc., 97 (2009) 1507

[5] Jonas, J. L., IEEE Proc., 97 (2009) 1522

[6] *Science with the Square Kilometre Array*, eds: C. Carilli, S. Rawlings, New Astronomy Reviews, Elsevier, Vol.48 (2004) Issue 11-12

[7] Giroletti, M., Paragi, Z., Bignall, H., et al., 2011, A&A, 528, L11

[8] Oosterloo, T., Verheijen, M. A. W., van Cappellen, W., et al., 2009, in *Wide Field Astronomy & Technology for the Square Kilometre Array (SKADS 2009)*, Eds. Torchinsky S.A. et al., POS, 132, id. 70

[9] Röttgering, H., Afonso, J., Barthel, P., et al. 2011, Journal of Astrophysics and Astronomy, 32, 557

[10] Röttgering, H. J. A., et al. 2010, in *ISKAF 2010*, POS, 112, 50

[11] Norris, R.P., Hopkins, A.M., Afonso, J., et al., 2011, PASA, 28, 215

[12] Field, G. B., Proceedings of the Institute of Radio Engineers, 46 (1958) 240

[13] Furlanetto, S. R., *Mon. Not. R. Astr. Soc.* , 371 (2006) 867

[14] Furlanetto, S. R., Oh, S. P., & Briggs, F. H., Physics Reports, 433 (2006) 181

[15] Harker, G. et al., *Mon. Not. R. Astr. Soc.* , 405 (2010) 2492

[16] Komatsu, E. et al., *Astrophys. J. Suppl. Ser.* , 192 (2011) 18

[17] Loeb, A., JCAP, 5 (2012) 28

[18] McQuinn, M., Lidz, A., Zahn, O., et al., *Mon. Not. R. Astr. Soc.* , 377 (2007) 1043

[19] McQuinn, M. & O'Leary, R. M., (2012) ArXiv e-prints:1204.1345

[20] Mellema, G. et al., (2012) ArXiv e-prints

[21] Mesinger, A., *Mon. Not. R. Astr. Soc.* , 407 (2010) 1328

[22] Mesinger, A., Ferrara, A., & Spiegel, D. S. , (2012) ArXiv e-prints:1210.7319

[23] Mesinger, A. & Furlanetto, S., *Astrophys. J.* , 669 (2007) 663

[24] Mesinger, A., Furlanetto, S., & Cen, R., *Mon. Not. R. Astr. Soc.* , 411 (2011) 955

[25] Mesinger, A., McQuinn, M., & Spergel, D. N. , *Mon. Not. R. Astr. Soc.* , 422 (2012) 1403

[26] Naoz, S., Noter, S., & Barkana, R., *Mon. Not. R. Astr. Soc.* , 373 (2006) L98

[27] Salvaterra, R., Ferrara, A., & Dayal, P., *Mon. Not. R. Astr. Soc.* , 414 (2011) 847

[28] Tingay, S. J. et al., (2012) ArXiv e-prints

[29] Tseliakhovich, D. & Hirata, C., PRD, 82 (2010) 083520

[30] Valdés, M., Evoli, C., Mesinger, A., Ferrara, A., & Yoshida, N., (2012) ArXiv e-prints:1209.2120

[31] Wise, J. H., Turk, M. J., Norman, M. L., & Abel, T., (2010) ArXiv e-prints:1011.2632

[32] Wouthuysen, S. A., AJ, 57 (1952) 31

[33] Zahn, . et al., *Astrophys. J.* , 756 (2012) 65

[34] Zahn, O., Mesinger, A., McQuinn, M., et al., *Mon. Not. R. Astr. Soc.* , 414 (2011) 727

[35] Perlmutter, S., Aldering, G., Goldhaber, G., et al., Astrophys.J. , 517 (1998) 565

[36] Riess, A. G., Filippenko, A. V., Challis, P., et al., Astron.J., 116 (1998) 1009

[37] de Bernardis, P., Ade, P. A. R., Bock, J. J., et al., Nature, 404 (2000) 955

[38] Stompor, R., Abroe, M., Ade, P., et al., Astrophys.J., 561 (2001) L7

[39] Spergel, D. N., Verde, L., Peiris, H. V., et al., Astrophys.J.Suppl., 148 (2003) 175

[40] Riess, A. G., Strolger, L.-G., Tonry, J., et al., Astrophys.J., 607 (2004) 665,

[41] Sahni, V. & Starobinsky, A. 2000, Int.J.Mod.Phys., D9 (2000) 373

[42] Padmanabhan, T., Phys.Rept., 380 (2003) 235

[43] Chen, G. & Ratra, B., Astrophys.J. ,582 (2002) 586

[44] Podariu, S., Daly, R. A., Mory, M. P., & Ratra, B., Astrophys.J., 584 (2002) 577

[45] Cardone, V. F., Troisi, A., & Capozziello, S., Phys.Rev. D, 69 (2004) 083517

[46] Capozziello, S., Cardone, V. F., Elizalde, E., Nojiri, S., & Odintsov, S. D. , Phys.Rev.D, 73 (2006) 043512

[47] Daly, R. A. & Djorgovski, S. G. 2004, Astrophys.J., 612, 652

[48] Wang, Y. & Mukherjee, P. 2004, Astrophys.J., 606, 654

[49] Wang, Y. & Tegmark, M. 2004, Phys.Rev.Lett., 92, 241302

[50] Hu, W. & Sugiyama, N. 1996, Astrophys.J., 471, 542

[51] Eisenstein, D. J., Zehavi, I., Hogg, D. W., et al. 2005, Astrophys.J., 633, 560

[52] Strauss, M. A., Weinberg, D. H., Lupton, R. H., & Narayanan, V. K. 2002, Astron.J., 124, 1810

[53] Dalal, N., Abazajian, K., Jenkins, E., & Manohar, A. V. 2001, Phys.Rev.Lett., 87, 141302

[54] Capozziello, S., Cardone, V. F., & Troisi, A. 2006, JCAP, 0608, 001

[55] Capozziello, S. 2002, Int.J.Mod.Phys.D, 11, 483

[56] Nojiri, S. & Odintsov, S. D. 2003, Phys.Rev.D, 68, 123512

[57] Carroll, S. M., Duvvuri, V., Trodden, M., & Turner, M. S. 2003, Phys.Rev.D, 70, 043528

[58] Sandvik, H., Tegmark, M., Zaldarriaga, M., & Waga, I. 2002, Phys.Rev.D, 69,123524

[59] Kamenshchik, A. Y., Moschella, U., & Pasquier, V. 2001, Phys.Lett. B, 511, 265

[60] Dewdney, P. E., Hall, P. J., Schilizzi, R. T., & Lazio, T. J. L. W. 2009, Proceedings of the IEEE, 97

[61] Torchinsky, S. et al. 2007, Proc. 19th Rencontres de Blois

[62] Smith R.E.S. et al. *Stable clustering, the halo model and non-linear cosmological power spectra*, *MNRAS* **341** (2003) pg. 1311

[63] Boyarsky, Alexey; Lesgourgues, Julien; Ruchayskiy, Oleg; Viel, Matteo *Lyman-α constraints on warm and on warm-plus-cold dark matter models*, *JCAP* **05** (2009) pg. 12

[64] Kang Xi, MacciŸ, Andrea V.; Dutton, Aaron A., *The Effect of Warm Dark Matter on Galaxy Properties: Constraints from the Stellar Mass Function and the Tully-Fisher Relation*, *ApJ* **767** (2013) pg. 22

[65] Planck Collaboration, *Planck 2013 results. XVI. Cosmological parameters*, arxiv:1303.5076

[66] Viel, Matteo; Haehnelt, Martin G.; Springel, Volker, *The effect of neutrinos on the matter distribution as probed by the intergalactic medium*, *JCAP* **06** (2010) pg. 15

[82] Xia, Jun-Qing; Granett, Benjamin R.; Viel, Matteo; Bird, Simeon; Guzzo, Luigi; Haehnelt, Martin G.; Coupon, Jean; McCracken, Henry Joy; Mellier, Yannick, *Constraints on massive neutrinos from the CFHTLS angular power spectrum*, *JCAP* **06** (2012) pg. 10

[68] Costanzi Alunno Cerbolini, M.; Sartoris, B.; Xia, Jun-Qing; Biviano, A.; Borgani, S.; Viel, M., *Constraining neutrino properties with a Euclid-like galaxy cluster survey*, arxiv:1303.4550

[69] Lovell, Mark R.; Eke, Vincent; Frenk, Carlos S.; Gao, Liang; Jenkins, Adrian; Theuns, Tom; Wang, Jie; White, Simon D. M.; Boyarsky, Alexey; Ruchayskiy, Oleg, *The haloes of bright satellite galaxies in a warm dark matter universe*, *MNRAS* **420** (2012) pg. 2318

[70] Viel, M.; Markovic, K.; Baldi, M.; Weller, J., *The non-linear matter power spectrum in warm dark matter cosmologies*, *MNRAS* **421** (2012) pg. 50

[71] Viel, Matteo; Becker, George D.; Bolton, James S.; Haehnelt, Martin G.; Rauch, Michael; Sargent, Wallace L. W., *How Cold Is Cold Dark Matter? Small-Scales Constraints from the Flux Power Spectrum of the High-Redshift Lyman-α Forest*, *Physical Review Letters* **100** (2008) pg. 1304

[72] Valdes, M.; Ferrara, A.; Mapelli, M.; Ripamonti, E., *Constraining dark matter through 21-cm observations*, *MNRAS* **377** (2007) pg. 245

[73] Scaramella, R., Zamorani, G., Vetolani, G., *ApJ* **376L** (1991) 1

[74] Branchini, E., Plionis M., Sciama D., *ApJ* **461L** (1996) 17

[75] Bilicki, M., Chodorowski, M, Jarrett T., Mamon G.A., *ApJ* **741** (2011) 31

[76] Condon, J.J., Cotton, W.D., Greisen, E.W., Yin, Q.F., Perley, R.A., Taylor, G.B., Broderick, J.J., *AJ* **115** (1998) 1693.

[77] Blake, C., Wall, J., *MNRAS* **337** (2002) 993.

[78] Overzier, R.A., Röttgering, H.J.A., Rengelink, R.B., Wilman, R.J., *A&A* **405** (2003) 53.

[79] Hernandez-Monteagudo, C., *A&A* **520** (2010) A101.

[80] Negrello, M., Magliocchetti, M., De Zotti, G., *MNRAS* **368** (2006) 935.

[81] Massardi, M., Bonaldi, A., Negrello, M., Ricciardi, S., Raccanelli, A., de Zotti, G., *MNRAS* **404** (2010) 532.

[82] Xia, J.-Q., Viel, M., Baccigalupi, C., De Zotti, G., Matarrese, S., Verde, L., *ApJ* **717** (2010) L17.

[83] Raccanelli, A., *et al. MNRAS* **424** (2012) 801

[84] Blake, C., Bacon, D., Fluke C., Kitching, T., Miller, L., Power, C., Wilman, R., *SKADS Virtual Telescope Proposal* (2007) available at http://www.skadseu.org/p/svt/svt blake.pdf

[85] Simpson, F., *et al. MNRAS* **429** (2013) 2249

[86] Colless, M., and the 2dF Team *MNRAS* **328** (2001) 1039

[87] Abazajan, K., and the SDSS Team, *ApJS* **182** (2009) 543.

[88] Drinkwater, M. J., and the WiggleZ Team, *MNRAS*, **401**, (2010) 1429

[89] Ahn, C. P., and the BOSS Team. *ApJS* **2013** (2012) 21

[90] Guzzo, L., and the VIPERS Team, arXiv:1303.2623 (2013)

[91] Giovanelli, R., Haynes, M. P., *Apj* **360L** (1986) 55

[92] Meyer, M.J. *et al.*, *MNRAS* **350** (2004) 1195

[93] Haynes, M. P., Giovanelli, R., *et al.*, *AJ* **142** (2011) 170

[94] Abdalla, F.B., Blake, C., Rawlings, S., *MNRAS* **401** (2010) 743
[95] Laurejis, R., *et al.,* arXiv:1110.3193 (2011)
[96] Abdalla, F.B., Rawlings S., *MNRAS* **360** (2005) 27
[97] Guzzo, L., *et. al.*, *Nature* **451** (2008) 541
[98] Basilakos S., Plionis M., Kovac K., Voglis N., *MNRAS* **378** (2007) 301
[99] Martin, A.M. et al., *ApJ* **750** (2012) 38
[100] Bianchi, D. *et al.*, *MNRAS*, **427** (2012) 2420.
[101] Magliocchetti, M., et al. 2013, submitted to *MNRAS*
[102] Piran, T. 2004, Rev. Mod. Phys., 76, 1143
[103] Mészaros, P. 2006, Rep. Prog. Phys., 69, 2259
[104] Gehrels, N., Ramirez–Ruiz, E., Fox, D. B. 2009, ARA&A, 47, 567
[105] Zhang, B. 2011, Comptes Rendus Physique, 12, 206 (arXiv:1104.0932)
[106] Salvaterra, R., Della Valle, M., Campana, S., et al. 2009, Nature, 461, 1258
[107] Cucchiara, A., Cenko, S.B., Bloom, J.S., et al. 2011, ApJ, 743, 154
[108] Suzuki, N., Rubin, D., Lidman, C., et al. 2012, ApJ, 746, 85
[109] Amati, L., Guidorzi, C., Frontera, F., et al. 2008, MNRAS, 391, 577
[110] Della Valle, M. & Amati, L. 2009, AIP Conference Proceedings, Volume 1053, pp. 299-308
[111] Amati, L., Frontera, F., Tavani, M., et al. 2002, A&A, 390, 81
[112] Amati, L. 2006, MNRAS, 372, 233
[113] Band, D. L. et al. 1993, ApJ, 413, 281
[114] Amati, L. 2012, IJMPS, 12, 19
[115] Guetta, D. & Della Valle, M. 2007, ApJ, 657, L73
[116] Amati, L., Della Valle, M., Frontera, F., et al. 2007, A&A, 463, 913
[117] Ghirlanda, G.. Ghisellini, G.. Salvaterra, R., et al. 2013, MNRAS, 428, 1410
[118] Amati, L., Frontera, F. & Guidorzi, C. 2009, A&A, 508, 173
[119] Amati, L., Della Valle, M., Frontera, F., et al. 2013, in prep.
[120] Ghirlanda, G., Ghisellini, G., Lazzati, D. 2004, ApJ, 616, 331
[121] Dai, Z.G., Liang, E.W. & Xu, D. 2004, ApJ, 612, L101
[122] Sari, R., Piran, T. & Halpern, J.P. 1999, ApJ, 519, L17
[123] Ghirlanda, G., Ghisellini, G., Firmani, 2006, New J. Phys., 8, 123
[124] Panaitescu, A., Mészáros, P., Burrows, D.N., et al. 2006, MNRAS, 369, 2059
[125] Curran, P.A., van der Horst, A.J., Wijers, R.A.M.J. 2008, MNRAS, 386, 859
[126] Liang, E.-W., Racusin, J.L., Zhang, B., et al. 2008, ApJ, 675, 528
[127] Reichart, D.,E. 2001, ApJ, 553, 235
[128] Chandra, P. & Frail, D.A. 2012, ApJ, 746, 156
[129] M. Feroci, L. Stella, M. van der Klis, et al., Experimental Astronomy 34 (2012) 415.
[130] M. Feroci, J.W. den Herder, E. Bozzo, et al., Proceedings of the SPIE 8443 (2012) id.2.
[131] Amati, L., del Monte, V. D'Elia, et al., Nucl. Phys. B Proc. Suppl. (2013) in press, (arXiv:1302.5276).

[132] Sunyaev R.A., Zeldovich Ya.B., 1972, Comm. Astrophys. Space Phys., 4, 173

[133] Rephaeli Y., 1995, ARA&A, 33, 541

[134] Zeldovich Ya.B., Sunyaev R.A., 1969, Ap&SS, 4, 301

[135] *Planck* Collaboration, 2013, A&A, submitted, arXiv:1303.5089

[136] Subrahmanyan R., Ekers R.D., 2002, in the XXVIIth General Assembly of the URSI, August 17-24, Maastricht, The Netherlands, astro-ph/0209569

[137] Ostriker J.P., Vishniac E.T., 1986, ApJ, 306, L51

[138] Vishniac E.T., 1987, ApJ, 322, 597

[139] Gnedin N.Y., Jaffe A.H., 2001, ApJ, 551, 3

[140] Springel V., White M., Hernquist L., 2001, ApJ, 549, 681

[141] da Silva A.C., et al., 2001, ApJ, 561, L15

[142] Ma C.-P., Fry J.N., 2002, PRL, 88, 211301

[143] Silk J., 1968, ApJ, 151, 459

[144] Burigana C., de Zotti G., Feretti L., 2004, New Astronomy Reviews, 48, 1107

[145] Rees M.J., Ostriker J.P., 1977, MNRAS, 179, 541

[146] White S.D.M., Rees M.J., 1978, MNRAS, 183, 341

[147] Ikeuchi S., 1981, PASJ, 33, 211

[148] Natarajan P., Sigurdsson S., Silk J., 1998, MNRAS, 298, 577

[149] Natarajan P., Sigurdsson S., 1999, MNRAS, 302, 288

[150] Aghanim N., Balland C., Silk, J., 2000, A&A, 357, 1

[151] Platania P., Burigana C., De Zotti G., Lazzaro E., Bersanelli M., 2002, MNRAS, 337, 242

[152] Lapi A., Cavaliere A., De Zotti G., 2003, ApJ, 597, L93

[153] de Zotti G., C. Burigana, A. Cavaliere, et al., 2004, in Proc. Int. Symp. *Plasmas in the Laboratory and in the Universe: new insights and new challenges*, Como, September 2003, eds. Bertin G., Farina D., Pozzoli R., pg. 375, astro-ph/0401191

[154] Navarro J.F., Frenk C.S., White S.D.M., 1997, ApJ, 490, 393

[155] Bullock J.S., et al., 2001, MNRAS, 321, 559

[156] Tremaine S., et al., 2002, ApJ, 574, 740

[157] Granato G.L., et al., 2001, MNRAS, 324, 757

[158] Ferrarese L., 2002, in *Current high-energy emission around black holes*, eds. C.-H. Lee & H.-Y. Chang, Singapore: World Scientific Pub.

[159] Mason B.S., et al., 2003, ApJ, 591, 540

[160] Dawson K.S., et al., 2002, ApJ, 581, 86

[161] Pei Y.,1995, ApJ, 438, 623

[162] Oh S.P., Cooray A., Kamionkowski M., 2003, MNRAS, 342, L20

[163] Salvaterra R., Burigana C., 2002, MNRAS, 336, 592

[164] Mather J.C., et al., 1990, ApJ, 354, L37

[165] Fixsen D.J., et al., 1996, ApJ, 473, 576

[166] Kogut A., 1996, in XVI Moriond Astrophysics meeting *Microwave Background Anisotropies*, March 16-23, Les Arcs, France, astro-ph/9607100

[167] Kogut A., 2003, in the Proc. of *The Cosmic Microwave Background and its Polarization*, New Astronomy Reviews, eds. Hanany S., Olive K.A., Vol. 47, Issues 11-12, p. 945

[168] Fixsen D.J., Mather J.C., 2002, ApJ, 581, 817

[169] Sunyaev R.A., Zeldovich Ya.B., 1970, Ap&SS, 7, 20

[170] Danese L., de Zotti G., 1980, A&A, 84, 364

[171] Burigana C., Danese L., De Zotti G., 1991, A&A, 246, 59

[172] Barlett J.G., Stebbins A., 1991, ApJ, 371, 8

[173] Stebbins A., Silk J., 1986, ApJ, 169, 1

[174] Burigana C., Salvaterra R., 2003, MNRAS, 342, 543

[175] Kogut A., Fixsen D.J., Chuss D.T., et al., 2011, JCAP, 07, article id. 025

[176] COrE Collaboration, COrE – Cosmic Origins Explorer – A White Paper, 2011, arXiv:1102.2181

[177] PRISM Collaboration, 2013, arXiv:1306.2259

[178] Burigana C., Finelli F., Salvaterra R., Popa L.A., Mandolesi N., 2004, in *Recent Research Developments in Astronomy & Astrophysics* – Vol. 2, 59

[179] Procopio P., Burigana C., 2009, A&A, 507, 1243

[180] Khatri R., Sunyaev R.A., 2012, JCAP, 09, 016

[181] Prandoni I., et al., 2001, A&A, 365, 392

[182] Gervasi M., Tartari A., Zannoni M., Boella G., Sironi G., 2008, ApJ, 682, 223

[183] Toffolatti L., et al., MNRAS, 1998, 297, 117

[184] Singal J., Fixsen D., Kogut A., et al., 2011, ApJ, 730, article id. 138

[185] Seiffert M.D., Fixsen D.J., Kogut A., et al., 2011, ApJ, 734, article id. 6

[186] Singal J., Stawarz L.,Lawrence A., Petrosian V., 2010, MNRAS, 409, 1172

[187] Condon J.J., Cotton W.D., Fomalont E.B., et al., 2012, ApJ, 758, article id. 23

[188] Sachs, R. K. Wolfe, A. M., 1967, ApJ, 147, 73

[189] Crittenden R. G., Turok N., 1996, Physical Review Letters, 76, 575

[190] Peiris H. V., Spergel D. N., 2000, ApJ , 540, 605

[191] Fosalba P., GaztaÃĂÃžnaga E., Castander F. J., 2003, ApJL, 597, L89

[192] Padmanabhan N., Hirata C. M., Seljak U., et al. 2005, Physical Review D, 72, 043525

[193] Granett B. R., Neyrinck M. C., Szapudi I., 2008, ApJL, 683, L99

[194] Granett B. R., Neyrinck M. C., Szapudi I., 2009, ApJ, 701, 414

[195] Papai P., Szapudi I., Granett B. R., 2011, ApJL, 732, 27

[196] Fosalba P., Gaztanaga E., 2004, MNRAS, 350, L37

[197] Afshordi, N., Loh, Y. S., & Strauss, M. A., 2004, Phys. Rev. D, 69, 083524

[198] Nolta M. R.,Wright E. L., et al. 2004, ApJL, 608, 10

[199] Raccanelli A., Bonaldi A., Negrello M., et al. 2008,MNRAS, 386, 2161

[200] Boughn S., Crittenden R., 2004a, Nature, 427, 45

[201] Boughn S. P., Crittenden R. G., 2004b, ApJL, 612, 64

[202] Rassat A., Land K., et al. 2007, MNRAS, 377, 1085

[203] Francis C. L., Peacock J. A., 2010, MNRAS, 406, 2

[204] Xia, J.Q-; Viel, M.; Baccigalupi, C.; Matarrese, S., JCAP 09, 003 (2009)

[205] Xia, J.Q-; Viel, M.; Baccigalupi, C.; De Zotti, G.; Matarrese, S., Verde L., ApJL 717, L17 (2010a)

[206] Xia, J.Q-; Bonaldi, A.; Baccigalupi, C.; De Zotti, G.; Matarrese, S., Verde L., JCAP 08, 013 (2010b)

[207] Xia J.Q., Baccigalupi C., Matarrese S., Verde L., Viel M. (2011) Journal of Cosmology and Astroparticle Physics, Vol. 08:033 (JCAP08(2011)033).

[208] Schiavon F., Finelli F., Gruppuso A., Marcos-Caballero A., Vielva P., Crittenden R.G., Barreiro R.B., Martínez-González E., 2012, MNRAS, 427, 3044

[209] Tegmark M., 1997, Phys. Rev. D, 55, 5895

[210] *Planck* Collaboration, 2013, A&A, submitted, arXiv:1303.5079

[211] Komatsu E., et al., 2010, Astro2010: The Astronomy and Astrophysics Decadal Survey, Science White Papers, Vol. 158

[212] Bartolo N., Komatsu E., Matarrese S., Riotto A., 2010, Physics Report, 402, 103

[213] Verde L., Wang L.M., Heavens A., Kamionkowski M., 2000, MNRAS, 313, L141

[214] Komatsu E., Spergel D.N., 2001, Physical Rev. D, 63, 063002

[215] Babich D., Creminelli P., Zaldarriaga M., 2004, JCAP, 08, 009

[216] *Planck* Collaboration, 2013, A&A, submitted, arXiv:1303.5084

[217] Kurz R., Shaver P., 1999, Messenger, 96, 7

[218] Schneider R., Salvaterra R., Choudhury T.R., Ferrara A., Burigana C., Popa L.A., 2008, MNRAS, 384, 1525

[219] Burigana C., De Zotti G., Danese L., 1995, A&A, 303, 323

[220] Burigana C., Popa L.A., Salvaterra R., Schneider R., Choudhury T.R., Ferrara A., 2008, MNRAS, 385, 404

[221] Trombetti T., Burigana C., 2013, in prep.

[222] Naselsky P., Chiang L.Y., 2004, MNRAS, 347, 921

[223] Trombetti T., Burigana C., 2012, JMP, 3, 1918

[224] Oh S.P., 1999, ApJ, 527, 16

[225] Press W.H., Schechter P., 1974, ApJ, 187, 452

[226] Bond J.R., Cole S., Efstathiou G., Kaiser N., 1991, ApJ, 379, 440

[227] Sasaki S., 1994, PASJ, 46, 427

[228] Hummer D.G., Storey P.J., 1987, MNRAS, 224, 801

[229] Rybicki G.B., Lightman A.P., 1979, *Radiative Processes in Astrophysics*, Wiley, New York

[230] Haiman Z., Loeb A., 1998, ApJ, 503, 505

[231] Partridge R.B., Richards E.A., Fomalont E.B., Kllerman K.I., Windhorst R., 1997 ApJ, 483, 38

[232] Ponente P.P., Diego J.M., Sheth R.K., Burigana C., Knollmann S.R., Ascasibar Y., 2011, MNRAS, 410, 2353

[233] Miniati F., Ferrara A., White S.D.M., Bianchi S., 2004, MNRAS, 348, 964

[234] Springel V., 2005, MNRAS, 364, 1105

[235] Hernquist L., Katz N., 1989, ApJS, 70, 419

[236] Crocce M., Pueblas S., Scoccimarro R., 2006, MNRAS, 373, 369

[237] Bersanelli M., Bensadoun M., de Amici G., Levin S., Limon M., Smoot G.F., Vinje W., 1994, ApJ, 424, 517

[238] White S.D.M., Rees M.J. 1978, MNRAS, 183, 341

[239] Birnboim Y., Dekel A. 2003, MNRAS, 345, 349

[240] Rees M.J., Ostriker J.P. 1977, MNRAS, 179, 541

[241] Heckman T.M. 2002, in ASP Conf. Ser. Vol. 254, Astron. Soc. Pac., San Francisco, p. 292

[242] Oppenheimer B.D., Davé R. 2006, MNRAS, 373, 1265

[243] Tornatore L., Borgani S., Dolag K., Matteucci F. 2007, MNRAS, 382, 1050

[244] McNamara B.R., Nulsen P.E.J. 2012, New Journal of Physics, 14, 5023

[245] Raccanelli, A., Zhao, G.-B., Bacon, D. J., et al. 2012, MNRAS, 424, 801

[246] Papastergis, E., Martin, A. M., Giovanelli, R., & Haynes, M. P. 2011, ApJ, 739, 38

[247] Haynes, M. P., Giovanelli, R., Martin, A. M., et al. 2011, AJ, 142, 170

[248] Baugh C.M. 2006, Reports on Progress in Physics, 69, 3101

[249] Springel V., Hernquist L. 2003, MNRAS, 339, 289

[250] De Lucia G., Blaizot J. 2007, MNRAS, 375, 2

[251] Monaco P., Fontanot F., Taffoni G. 2007, MNRAS, 375, 1189

[252] Fontanot F., De Lucia G., Monaco P., Somerville R.S., Santini P. 2009, MNRAS, 397, 1776

[253] De Lucia G., Boylan-Kolchin M., Benson A.J., Fontanot F., Monaco P. 2010, MNRAS, 406, 1533

[254] Fontanot F., Pasquali A., De Lucia G., van den Bosch F.C., Somerville R.S., Kang X. 2011, MNRAS, 413, 957

[255] De Lucia G., Fontanot F., Wilman D., Monaco P. 2011, MNRAS, 414, 1439

[256] Obreschkow D., Croton D., De Lucia G., Khochfar S., Rawlings S. 2009, ApJ, 698, 1467

[257] Duffy A.R., Meyer M.J., Staveley-Smith L., Bernyk M., Croton D.J., Koribalski B.S., Gerstmann D., Westerlund S. 2012, MNRAS, 426, 3385

[258] Fu J., Guo Q., Kauffmann G., Krumholz M. 2010, MNRAS, 409, 515

[259] Lagos C., Lacey C.G., Baugh C.M., Bower R.G., Benson A.J. 2011, MNRAS, 416, 1566

[260] Blitz L., Rosolowsky E. 2006, ApJ, 650, 933

[261] Krumholz M.R., McKee C.F., Tumlinson J. 2009, ApJ, 699, 850

[262] Murante G., Monaco P., Giovalli M., Borgani S., Diaferio A. 2010, MNRAS, 405, 1491

[263] Murante G., Calabrese M., De Lucia G., Monaco P., Borgani S., Dolag K. 2012, ApJL, 749, 34

[264] De Lucia G., Kauffmann G., White S.D.M. 2004, MNRAS, 349, 1101

[265] Viel, M., Lesgourgues, J., Haehnelt, M. G., Matarrese, S., & Riotto, A. 2005, Phys. Rev. D, 71, 063534

[266] Merson, A. I., Baugh, C. M., Helly, J. C., et al. 2013, MNRAS, 429, 556

[267] Manera, M., Scoccimarro, R., Percival, W. J., et al. 2013, MNRAS, 428, 1036

[268] Monaco P., Safusatti E., Borgani S., Crocce M., Fosalba P., Sheth R., Theuns T. 2013, MNRAS, to be submitted

[269] Berlind, A. A., & Weinberg, D. H. 2002, APJ, 575, 587

[270] Lilly, S. J., Le Fevre, O., Hammer, F., & Crampton, D. *ApJL*, **460** (1996) L1.

[271] Madau, P., Ferguson, H. C., Dickinson, M. E., et al., *MNRAS*, **283** (1996) 1388.

[272] Buat, V., Giovannoli, E., Burgarella, D., et al., *MNRAS* **409** (2010) L1.

[444] Erb, D. K., et al., *ApJ* **647** (2006) 128.

[274] Bouwens, R. J., et al., *ApJ*, **705** (2009) 705.

[275] Bell, E. F., & Kennicutt, R. C., Jr., *ApJ* **548** (2001) 681.

[276] Castellano, M., Fontana, A., Grazian, A., et al., *A&A* (2012) **540** 39.

[277] Hopkins, A. M., Connolly, A. J., Haarsma, D. B., & Cram, L. E., *AJ* **122** (2001) 288.

[278] Garn, T., & Best, P. N., *MNRAS* **409** (2010) 421.

[279] Casey, C. M., Berta, S., Béthermin, M., et al., *ApJ* **761** (2012) 139.

[280] Oliver, S. J., Bock, J., Altieri, B., et al., *MNRAS* **424** 1614

[281] Condon, J. J., *ARA&A* **30** (1992) 575.

[282] Ivison, R. J., Chapman, S. C., Faber, S. M., et al., *ApJL* **660** (2007) L77.

[283] Pannella, M., Carilli, C. L., Daddi, E., et al., *ApJL* **698** (2009) L116.

[284] Lilly, S., Schade, D., Ellis, R., et al., *ApJ* **500** (1998) 75.

[285] Bruce, V. A., Dunlop, J. S., Cirasuolo, M., et al., *MNRAS* **427** (2012) 1666.

[286] McLure, R. J., Pearce, H. J., Dunlop, J. S., et al., *MNRAS* **428** (2013) 1088.

[287] Szomoru, D., Franx, M., Bouwens, R. J., et al., *ApJ* **735** (2011) 22.

[288] Hirschmann, M., Naab, T., Somerville, R. S., Burkert, A., & Oser, L., *MNRAS* **419** (2012) 3200.

[289] Guo, Q., White, S., Boylan-Kolchin, M., et al., {emphMNRAS **413** (2011) 101.

[290] Lapi, A., et al., *ApJ* **742** (2011) 24.

[464] Hopkins, A. M., & Beacom, J. F., *ApJ* **651** (2006) 142.

[292] Bouwens, R. J., et al., *ApJ*, **737** (2011) 90.

[293] Granato, G. L., De Zotti, G., Silva, L., et al., {emphApJ **600** (2004) 580.

[294] Cirasuolo, M., Shankar, F., Granato, G. L. et al., *ApJ* **629** (2005) 816.

[295] Bower, R. G., Benson, A. J., Malbon, R., et al., *MNRAS* **370** (2006) 645.

[296] Ferrarese, L., & Ford, H., *Space Science Reviews* **116** (2005) 523.

[297] Magorrian, J., Tremaine, S., Richstone, D., et al., *AJ* **115** (1998) 2285.

[298] Gebhardt, K., Bender, R., Bower, G., et al., *ApJL* **539** (2000) L13.

[299] Marconi, A., & Hunt, L. K., *ApJL* **589** (2003) L21.

[300] Hasinger, G., Miyaji, T., & Schmidt, M., *A&A* **441** (2005) 417.

[301] Hopkins, P. F., Richards, G. T., & Hernquist, L., *ApJ* **654** (2007) 731.

[302] Kauffmann, G., & Haehnelt, M., *MNRAS* **311** (2000) 576.

[303] Volonteri, M., Haardt, F., & Madau, P., *ApJ* **582** (2003) 559.

[304] Marconi, A., Risaliti, G., Gilli, R., et al., *MNRAS* **351** (2004) 169.

[305] Di Matteo, T., Springel, V., & Hernquist, L. , *Nature* **433** (2005) 604.

[306] Gilli, R., Comastri, A., & Hasinger, G., *A&A* **463** (2007) 79.

[307] Daddi, E., Alexander, D. M., Dickinson, M., et al., *ApJ* **670** (2007) 173.

[308] Fiore, F., Puccetti, S., Brusa, M., et al., *ApJ* **693** (2009) 447.

[309] Del Moro, A., Alexander, D. M., Mullaney, J. R., et al., *A&A*, **549** (2013) 59.

[310] Fiore, F., Puccetti, S., Grazian, A., et al., *A&A* **537** (2012) A16.

[311] Bothwell, M. S., Kenicutt, R. C., Johnson, B. D., et al., *MNRAS* **415** (2011) 1815.

[312] Rodighiero, G., Daddi, E., Baronchelli, I., et al., *ApJL* **739** (2011) L40.

[313] Michałowski, M., Hjorth, J., & Watson, D., *A&A* **514** (2010) A67.

[314] Ivison, R. J., et al., *A&A* **518** (2010) L31.

[315] Helou, G., Soifer, B. T., Rowan-Robinson, M., *ApJ* **298** (1985) L7.

[316] Gavazzi, G., Cocito, A., Vettolani, G., *ApJ* **305** (1986) L15.

[317] Bell, E. F., *ApJ* **586** (2003) 794.

[318] Garn, T., Green, D. A., Riley, J. M., Alexander, P., *MNRAS* **397** (2009) 1101.

[319] Jarvis, M. J., et al., *MNRAS* **409** (2010) 92.

[320] Haarsma, D. B., Partridge, R. B., Windhorst, R. A., Richards, E. A., *ApJ* **544** (2000) 641.

[321] Beswick, R. J., Muxlow, T. W. B., Thrall, H., Richards, A. M. S., & Garrington, S. T., *MNRAS* **385** (2008) 1143.

[322] Murphy, E. J., Condon, J. J., Schinnerer, E., et al., *ApJ* **737** (2011) 67.

[323] Hirashita, H., & Hunt, L. K., *A&A* **460** (2006) 67.

[324] Elmegreen, B. G., & Elmegreen, D. M., *ApJ* **627** (2005) 632.

[325] Genzel, R., Newman, S., Jones, T., et al., *ApJ* **733** (2011) 101.

[326] Chapman, S. C., Smail, I., Windhorst, R., Muxlow, T., & Ivison, R. J., *ApJ* **611** (2004) 732.

[327] Daddi, E., Elbaz, D., Walter, F., et al., *ApJL* **714** (2010) L118.

[328] Tacconi, L. J., Neri, R., Chapman, S. C., et al., *ApJ* **640** (2006) 228.

[329] Prandoni, I., Morganti R., Mignano A., in *Panoramic Radio Astronomy*, PoS **36** (2009)

[330] Padovani, P., Miller, N., Kellermann, K. I., Mainieri, V., Rosati, P., Tozzi, P., *ApJ* **740** (2011) 20.

[331] Jarvis, M. J., & Rawlings, S., *NewAR* **48** (2004) 1173.

[332] Wilman, R. J., et al., *MNRAS* **388** (2008) 1335.

[333] Kukula M.J., Dunlop J.S., Hughes D.H., Rawlings S. *MNRAS* **297** (1998) 366.

[334] Cirasuolo, M., et al., *MNRAS* **346** (2003) 447.

[335] Cattaneo, A., Faber, S. M., Binney, J., et al. *Nature* **460** (2009) 213.

[336] Silk, J., & Rees, M.,*A&A* **331** (1998) L1.

[337] Croton, D. J., et al. *MNRAS* **365** (2006) 11.

[338] Fabian, A. C., et al., *MNRAS* **344** L43.

[339] Merloni, A., & Heinz, S., *MNRAS* **381** (2007) 589.

[340] Hardcastle, M. J., et al., *MNRAS* **376** (2007) 1849.

[341] Best, P.N., & Heckman T.M., *MNRAS* (2012) **421** (2012) 1569.

[342] Best, P.N., et al., *MNRAS* **362** (2005) 25.

[343] Metcalf, R. B., & Magliocchetti, M., *MNRAS* **365** (2006) 101.

[344] Prandoni, I., Parma, P., Wieringa, M.H., et al., *A&A* **457** (2006) 517.

[345] Prandoni, I., de Ruiter, H.R., Ricci, R., et al., *A&A* **510** (2010) A42.

[346] Ibar E., Ivison R.J., Biggs A.D., Lal D.V., Best P.N., Green D.A., *MNRAS* **397** (2009) 281.

[347] Ibar, E., Ivison, R. J., Best, P. N., Coppin, K., Pope, A., Smail, I., Dunlop, J. S., *MNRAS* **401** (2010) L53.

[348] Baldwin, J. A., Phillips, M. M., Terlevich, R., *PASP* **93** (1981) 5.

[349] Norris, R. P., Tingay, S., Phillips, C., Middelberg, E., Deller, A., Appleton, P. N., *MNRAS* **378** (2007) 1434.

[350] Lacy, M., Storrie-Lombardi, M.J., Sajina, A., et al., *ApJS* **154** (2004) 166.

[351] Vattakunnel, S., Tozzi, P., Matteucci, F., et al., *MNRAS* **420** (2012) 2190.

[352] Roy, A. L., Norris, R. P., Kesteven, M. J., Troup, E. R., Reynolds, J. E., *MNRAS* **301** (1998) 1019.

[353] Gruppioni, C., Pozzi, F., Zamorani, G., Vignali, C., *MNRAS* **416** (2011) 70.

[354] Afonso, J., Mobasher, B., Chan, B., Cram, L., *ApJ* **559** (2001) L101.

[355] Kewley L. J., *ApJ* **530** (2000) 704.

[356] Garrett M. A., *A&A* **384** (2002) L19.

[357] Parra R., Conway J. E., Aalto S., Appleton P. N., Norris R. P., PihlstrÂĺom Y. M., Kewley L. J., *ApJ* **720** (2010) 555.

[358] Chi, S., Barthel P. D, Garrett M. A., *A&A* **550** (2013) 68.

[359] Waddington I., Windhorst R.A., Cohen S.H., Partridge R.B., Spinrad H., Stern D., *ApJ* **526** (1999) L77.

[360] Muxlow T.W.B., et al., *MNRAS* **358** (2005) 1159.

[361] Guidetti, D., Bondi, M., Prandoni, I., et al., *MNRAS* (2013) in press.

[362] Silk, J., *MNRAS* **364** (2005) 1337.

[363] Biggs, A. D., Younger, J. D., Ivison, R. J., *MNRAS* **408** (2010) 342.

[364] Owen, F.N, Morrison, G.E., *AJ* **136** 1889.

[365] Bunker, A. J., Stanway, E. R., Ellis, R. S., & McMahon, R. G., *MNRAS* **355** (2004) 374.

[366] Cai, Z.-Y., et al., (2013) in prep.

[367] Béthermin, M., et al., *HerMES: deep number counts at 250 μm, 350 μm and 500 μm in the COSMOS and GOODS-N fields and the build-up of the cosmic infrared background*, *A&A* **542** (2012) A58.

[368] Bothwell, M. S., Smail, I., Chapman, S. C., et al., *MNRAS* **429** (2013) 3047.

[369] Tacconi, L. J., Genzel, R., Neri, R., et al., *Nature* **463** (2010) 781.

[370] Krumholz, M. R., *ApJ* **759** (2012) 9.

[371] Gnedin, N. Y., Tassis, K., & Kravtsov, A. V., *ApJ* **697** (2009) 55.

[372] Krumholz, M. R., McKee, C. F., & Tumlinson, J., *ApJ* **699** (2009) 850.

[373] Zwaan, M. A., Staveley-Smith, L., Koribalski, B. S., et al., *AJ* **125** (2003) 2842.

[374] Ferrarese, L. & Merritt, D. 2000, ApJ, 539, L9

[375] Gebhardt, K., Bender, R., Bower, G., et al. 2000, ApJ, 539, L13

[376] Marconi, A. & Hunt, L. K. 2003, ApJ, 589, L21

[377] Marconi, A., Risaliti, G., Gilli, R., et al. 2004, *Mon. Not. R. Astr. Soc.* , 351, 169

[378] Granato, G. L., De Zotti, G., Silva, L., Bressan, A., & Danese, L. 2004, *Astrophys. J.* , 600, 580

[379] Di Matteo, T., Springel, V., & Hernquist, L. 2005, Nature, 433, 604

[380] Hopkins, P. F., Hernquist, L., Cox, T. J., et al. 2005, *Astrophys. J.* , 630, 705

[381] Hopkins, P. F., Hernquist, L., Cox, T. J., et al. 2006, *Astrophys. J. Suppl. Ser.* , 163, 1

[382] Menci, N., Fiore, F., Puccetti, S., & Cavaliere, A. 2008, *Astrophys. J.* , 686, 219

[383] Gruppioni, C., Pozzi, F., Zamorani, G., & Vignali, C. 2011, *Mon. Not. R. Astr. Soc.* , 416, 70

[384] Santini, P., Rosario, D. J., Shao, L., et al. 2012, A&A, 540, A109

[385] King, A. R. 2010, *Mon. Not. R. Astr. Soc.* , 402, 1516

[386] Fabian, A. C. 2012, ArXiv e-prints

[387] Heckman, T. M., Smith, E. P., Baum, S. A., et al. 1986, *Astrophys. J.* , 311, 526

[388] Sakamoto, K., Okumura, S. K., Ishizuki, S., & Scoville, N. Z. 1999, *Astrophys. J. Suppl. Ser.* , 124, 403

[389] Combes, F. 2001, Advanced Lectures on the Starburst-AGN, 223

[390] Friedli, D., & Martinet, L. 1993, A&A, 277, 27

[391] Schinnerer, E., Eckart, A., & Tacconi, L. J. 2000, *Astrophys. J.* , 533, 826

[392] Schinnerer, E., Eckart, A., Tacconi, L. J., Genzel, R., & Downes, D. 2000, *Astrophys. J.* , 533, 850

[393] Heckman, T. M. 2008, ArXiv e-prints, 809

[394] Macchetto, F., Marconi, A., Axon, D. J., et al. 1997, *Astrophys. J.* , 489, 579

[395] Marconi, A., Capetti, A., Axon, D. J., et al. 2001, *Astrophys. J.* , 549, 915

[396] Capetti, A., Marconi, A., Macchetto, D., & Axon, D. 2005, A&A, 431, 465

[397] Pastorini, G., Marconi, A., Capetti, A., et al. 2007, A&A, 469, 405

[398] de Francesco, G., Capetti, A., & Marconi, A. 2008, A&A, 479, 355

[399] Dalla Bontá, E., Ferrarese, L., Corsini, E. M., et al. 2008, ArXiv e-prints, 809

[400] Ferrarese, L. 2002, *Astrophys. J.* , 578, 90

[401] Ferrarese, L., Cote, P., Blakeslee, J. P., et al. 2006, ArXiv Astrophysics e-prints

[402] Sani, E., Marconi, A., Hunt, L. K., & Risaliti, G. 2010, ArXiv e-prints

[403] Beifiori, A., Courteau, S., Corsini, E. M., & Zhu, Y. 2012, *Mon. Not. R. Astr. Soc.* , 419, 2497

[404] Labita, M., Treves, A., Falomo, R., & Uslenghi, M. 2006, *Mon. Not. R. Astr. Soc.* , 373, 551

[405] Decarli, R., Falomo, R., Treves, A., et al. 2010, *Mon. Not. R. Astr. Soc.* , 402, 2441

[406] Decarli, R., Falomo, R., Treves, A., et al. 2010, *Mon. Not. R. Astr. Soc.* , 402, 2453

[407] Merloni, A., Bongiorno, A., Bolzonella, M., et al. 2010, *Astrophys. J.* , 708, 137

[408] Sarria, J. E., Maiolino, R., La Franca, F., et al. 2010, A&A, 522, L3

[409] Portinari, L., Kotilainen, J., Falomo, R., & Decarli, R. 2012, *Mon. Not. R. Astr. Soc.* , 420, 732

[410] Fiore, F., Puccetti, S., Brusa, M., et al. 2009, *Astrophys. J.* , 693, 447

[411] Fiore, F., Puccetti, S., Grazian, A., et al. 2011, ArXiv e-prints

[412] Fiore, F., Puccetti, S., Grazian, A., et al. 2012, A&A, 537, A16

[413] Brusa, M., Comastri, A., Gilli, R., et al. 2008, ArXiv e-prints, 809

[414] Brusa, M., Fiore, F., Santini, P., et al. 2009, ArXiv e-prints

[415] Brusa, M., Civano, F., Comastri, A., et al. 2010, ArXiv e-prints

[416] Comastri, A., Ranalli, P., Iwasawa, K., et al. 2011, A&A, 526, L9+

[417] Shankar, F., Salucci, P., Granato, G. L., De Zotti, G., & Danese, L. 2004, *Mon. Not. R. Astr. Soc.* , 354, 1020

[418] Gruppioni, C., Pozzi, F., Polletta, M., et al. 2008, ArXiv e-prints, 805

[419] Feruglio, C., Maiolino, R., Piconcelli, E., et al. 2010, A&A, 518, L155+

[420] Cano-Diaz, M., Maiolino, R., Marconi, A., et al. 2011, ArXiv e-prints

[421] Cicone, C., Feruglio, C., Maiolino, R., et al. 2012, ArXiv e-prints

[422] Maiolino, R. & et al. 2012, Science

[423] Maiolino, R., Gallerani, S., Neri, R., et al. 2012, ArXiv e-prints

[424] Fontanot, F., De Lucia, G., Monaco, P., Somerville, R. S., & Santini, P. 2009, ArXiv e-prints

[425] Fontanot, F., Monaco, P., Cristiani, S., & Tozzi, P. 2006, *Mon. Not. R. Astr. Soc.* , 373, 1173

[426] Menci, N., Cavaliere, A., Fontana, A., et al. 2004, *Astrophys. J.* , 604, 12

[427] Lamastra, A., Menci, N., Maiolino, R., Fiore, F., & Merloni, A. 2010, ArXiv e-prints

[428] Vestergaard, M. & Peterson, B. M. 2006, *Astrophys. J.* , 641, 689

[429] Inskip, K. J., Jahnke, K., Rix, H., & van de Ven, G. 2011, ArXiv e-prints

[430] Vattakunnel, S., Tozzi, P., Matteucci, F., et al. 2012, *Mon. Not. R. Astr. Soc.* , 420, 2190

[431] McClure, R. D., & van den Bergh, S. 1968, AJ, 73, 1008

[432] Lequeux, J., Peimbert, M., Rayo, J. F., Serrano, A., & Torres-Peimbert, S. 1979, A&A, 80, 155

[433] Garnett, D. R. 2002, arXiv:astro-ph/0211148

[434] Tremonti, C. A., Heckman, T. M., Kauffmann, G., et al. 2004, *Astrophys. J.* , 613, 898

[435] Lee, H., Skillman, E. D., Cannon, J. M., et al. 2006, *Astrophys. J.* , 647, 970

[436] Edmunds, M. G. 1990, *Mon. Not. R. Astr. Soc.* , 246, 678

[437] Lehnert, M. D., & Heckman, T. M. 1996, *Astrophys. J.* , 472, 546

[438] Brooks, A. M., Governato, F., Booth, C. M., et al. 2007, ApJ, 655, L17

[439] Mouchine, M., Gibson, B. K., Renda, A., & Kawata, D. 2008, arXiv:0801.2476

[440] Calura, F., & Menci, N. 2009, *Mon. Not. R. Astr. Soc.* , 400, 1347

[441] Köppen, J., Weidner, C., & Kroupa, P. 2007, *Mon. Not. R. Astr. Soc.* , 375, 673

[442] Finlator, K., & Davé, R. 2008, *Mon. Not. R. Astr. Soc.* , 385, 2181

[443] Davé, R., Finlator, K., & Oppenheimer, B. D. 2011, *Mon. Not. R. Astr. Soc.* , 416, 1354

[444] Erb, D. K., Shapley, A. E., Pettini, M., et al. 2006, *Astrophys. J.* , 644, 813

[445] Maiolino, R., Nagao, T., Grazian, A., et al. 2008, A&A, 488, 463

[446] Mannucci, F., Cresci, G., Maiolino, R., et al. 2009, *Mon. Not. R. Astr. Soc.* , 398, 1915

[447] Mannucci, F., Cresci, G., Maiolino, R., Marconi, A., & Gnerucci, A. 2010, *Mon. Not. R. Astr. Soc.* , 408, 2115

[448] Cresci, G., Mannucci, F., Sommariva, V., et al. 2012, *Mon. Not. R. Astr. Soc.* , 421, 262

[449] Hughes, T. M., Cortese, L., Boselli, A., Gavazzi, G., & Davies, J. I. 2013, A&A, 550, A115

[450] Barnes, J. E. and Hibbard, J. E., *AJ* **137** (2009) 3071

[451] Binney, J., Nipoti, C., and Fraternali, F., *MNRAS* **397** (2009) 1804

[452] Bregman, J. N., *ARA&A* **45** (2007) 221

[453] Carilli, C. L., Daddi, E., Riechers, D., Walter, F., Weiss, A., Dannerbauer, H., Morrison, G. E., Wagg, J., Davé, R., Elbaz, D., Stern, D., Dickinson, M., Krips, M., and Aravena, M., *ApJ* **714** (2010) 1407

[454] Chiappini, C., Matteucci, F., and Gratton, R., *ApJ* **477** (1997) 765

[455] Chomiuk, L. and Povich, M. S., *AJ* **142** (2011) 197

[456] Crain, R. A., McCarthy, I. G., Frenk, C. S., Theuns, T., and Schaye, J., *MNRAS* **407** (2010) 1403

[457] Fernandez, X., Joung, M. R., and Putman, M. E., *ApJ* **749** (2012) 181

[458] Forster Schreiber, N. M., Genzel, R., Bouché;, N., Cresci, G., Davies, R., Buschkamp, P., Shapiro, K., Tacconi, L. J., Hicks, E. K. S., Genel, S., Shapley, A. E., Erb, D. K., Steidel, C. C., Lutz, D., Eisenhauer, F., Gillessen, S., Sternberg, A., Renzini, A., Cimatti, A., Daddi, E., Kurk, J., Lilly, S., Kong, X., Lehnert, M. D., Nesvadba, N., Verma, A., McCracken, H., Arimoto, N., Mignoli, M., and Onodera, M., *ApJ* **706** (2009) 1364

[459] Fraternali, F., van Moorsel, G., Sancisi, R., and Oosterloo, T., *AJ* **123** (2002) 3124

[460] Fraternali, F. and Binney, J. J., *MNRAS* **386** (2008) 935

[461] Fraternali, F. and Tomassetti, M. *MNRAS* **426** (2012) 2166

[462] Gastaldello, F., ApJ, **693** (2009) 43

[463] Governato, F., Willman, B., Mayer, L., Brooks, A., Stinson, G., Valenzuela, O., Wadsley, J., and Quinn, T., *MNRAS* **374** (2007) 1479

[464] Hopkins, P. F., Hernquist, L., Cox, T. J., Di Matteo, T., Robertson, B., and Springel, V., *ApJS* **163** (2006) 1

[465] Hopkins, A. M., McClure-Griffiths, N. M., and Gaensler, B. M., *ApJ* **682** (2008) L13

[466] Jogee, S., Miller, S. H., Penner, K., Skelton, R. E., Conselice, C. J., Somerville, R. S., Bell, E. F., Zheng, X. Z., Rix, H.-W., Robaina, A. R., Barazza, F. D., Barden, M., Borch, A., Beckwith, S. V. W., Caldwell, J. A. R., Peng, C. Y., Heymans, C., McIntosh, D. H., Huler, B., Jahnke, K., Meisenheimer, K., Sanchez, S. F., Wisotzki, L., Wolf, C., and Papovich, C., *ApJ* **697** (2009) 1971

[467] Kaufmann, T., Bullock, J. S., Maller, A. H., Fang, T., and Wadsley, J., *MNRAS* **396** (2009) 191

[468] Kennicutt, R. C., Jr., *ApJ* **272** (1983) 54

[469] Keres, D., Katz, N., Fardal, M., Davé, R., and Weinberg, D. H., *MNRAS* **395** (2009) 160

[470] Lelli, F., Fraternali, F., and Sancisi, R., *A&A* **516** (2010) A11

[471] Lopez-Sanjuan, C., Balcells, M., Pérez-González, P. G., Barro, G., García-Dabó, C. E., Gallego, J., and Zamorano, J., *A&A* **501** (2009) 505

[472] Lotz, J. M., Jonsson, P., Cox, T. J., Croton, D., Primack, J. R., Somerville, R. S., and Stewart, K., *ApJ* **742** (2011) 103

[473] Marinacci, F., Binney, J., Fraternali, F., Nipoti, C., Ciotti, L., and Londrillo, P., *MNRAS* **404** (2010) 1464

[474] Martinez-Delgado, D., Gabany, R. J., Crawford, K., Zibetti, S., Majewski, S. R., Rix, H.-W., Fliri, J., Carballo-Bello, J. A., Bardalez-Gagliuffi, D. C., Penarrubia, J., Chonis, T. S., Madore, B., Trujillo, I., Schirmer, M., and McDavid, D. A., *AJ* **140** (2010) 962

[475] Oosterloo, T.A., Morganti, R., Sadler, E.M., Vergani, D., Caldwell, N., *Aj***123** (2002) 729

[476] Oosterloo, T., Fraternali, F., and Sancisi, R., *AJ* **134** (2007) 1019

[477] Panter, B., Jimenez, R., Heavens, A. F., and Charlot, S., *MNRAS* **378** (2007) 1550

[478] Pisano, D. J., Barnes, D. G., Gibson, B. K., Staveley-Smith, L., Freeman, K. C., and Kilborn, V. A., *ApJ* **662** (2007) 959

[479] Putman, M. E., Peek, J. E. G., and Joung, M. R., *ARA&A* **50** (2012) 491

[480] Queyrel, J., Contini, T., Kissler-Patig, M., Epinat, B., Amram, P., Garilli, B., Le FÃÍvre, O., Moultaka, J., Paioro, L., Tasca, L., Tresse, L., Vergani, D., LÃşpez-Sanjuan, C., Perez-Montero, E. *A&A***539** (2012) 93

[481] Sancisi, R. and Allen, R. J., *A&A* **74** (1979) 73

[482] Sancisi, R., Fraternali, F., Oosterloo, T., and van der Hulst, T., *A&ARv* **15** (2008) 189

[483] Schönrich, R. and Binney, J., *MNRAS* **396** (2009) 203

[484] Springel, V., Frenk, C. S., and White, S. D. M., *Natur* **440** (2006) 1137

[485] Swaters, R. A., Sancisi, R., and van der Hulst, J. M., *ApJ* **491** (1997) 140

[486] Vergani D., Pizzella, A., Corsini, E. M., van Driel, W., Buson, L. M., Dettmar, R.-J., Bertola, F. *A&A***463** (2007) 883

[487] Vergani, D., Epinat, B., Contini, T., Tasca, L., Tresse, L., Amram, P., Garilli, B., Kissler-Patig, M., Le Fevre, O., Moultaka, J., Paioro, L., Queyrel, J., Lopez-Sanjuan, C., *A&A***546** (2012) 118

[488] Wolfe, A. M., Gawiser, E., and Prochaska, J. X., *ARA&A* **43** (2005) 861

[489] Athanassoula, E., Makino, J., Bosma, A., *MNRAS* **286** (1997) 825

[490] Barnes, J. E., *Nature* **338** (1989) 123

[491] Brassington, N., Ponman, T.J., Read, A.M., *MNRAS* **377** (2007) 1439

[492] Boroson B., Kim, D-W., Fabbiano, G., *ApJ* **729** (2011) 12

[493] Cooper, M. C., Newman, J. A., Croton, D. J., Weiner, B. J., Willmer, C. N. A., Gerke, B. F., Madgwick, D. S., Faber, S. M., Davis, M., Coil, A. L., Finkbeiner, D. P., Guhathakurta, P., Koo, D. C., *MNRAS* **370** (2006) 198

[494] De Lucia, G., Springel, V., White, S.D.M., Croton, D., Kauffmann, G., *MNRAS* **366** (2006) 499

[495] Diehl S., & Statler, T.S., *ApJ* (2007) **668** 150

[496] Dressler, A., *ApJ* **236** (1980) 351

[497] Ellis, S.C., & O'Sullivan E., *MNRAS* **367** (2006) 627

[498] Fabbiano, G., & Schweizer, F., *ApJ* **447** 572

[499] Freeland, E., Sengupta, C., Croston, J. H., *MNRAS* **409** (2010) 1518

[500] Giovanelli, R. and Haynes, M. P., *ApJ* **292** (1985) 404

[501] Hibbard, J.E., *PhD, Columbia University* (1995)

[502] Kauffmann, G., *MNRAS* **281** (1996) 487

[503] Kawata, D. and Mulchaey, J. S., *ApJL* **672** (2008) L103

[504] Kern, K. M., Kilborn, V. A., Forbes, D. A., Koribalski, B., *MNRAS* **384** (2008) 305

[505] Machacek, M. E., Jerius, D., Kraft, R., Forman, W. R., Jones, C., Randall, S., Giacintucci, S., Sun, M., *ApJ* **743** (2011) 15

[506] Memola, E., Trinchieri, G., Wolter, A., Focardi, P., Kelm, B., *A&A* **497** (2009) 359

[507] Mulchaey J.S., & Jeltema T., *ApJ* **715** (2010) L1

[508] Nolan L A., Ponman, T.J., Read, A.M., Schweizer, F., *MNRAS* **353** (2004) 221

[509] Rasmussen, J., Ponman, T. J., Mulchaey, J. S., *MNRAS* **370** (2006) 453

[510] Sandage, A., *JRAS*, **84** (1990) 70

[511] Sansom A.E., O'Sullivan, E., Forbes, D.A., Proctor, R.N., Davis, D.S., *AJ* **120** 1946

[512] Sansom A.E., Hibbard, J.E., Schweizer, F., *MNRAS* **370** 1541

[513] Scodeggio, M., Silva, D.R., *A&A* **359** (2000) 953

[514] Verdes-Montenegro, L., Yun, M. S., Williams, B. A., Huchtmeier, W. K., Del Olm, A., Perea, J., *A&A* **377** (2001) 812

[515] Villalobos Á., De Lucia, G., Borgani, S., Murante, G., *MNRAS* **424** (2012) 2401

[516] Vollmer, B., *A&A* **398** (2003) 525

[517] Wolter, A., Vergani, D., Trinchieri, G., *ASPC* **421** (2010) 297

[518] Bicknell, G. V., Jones, D. L., & Lister, M. 2004, NewAR, 48, 1151

[519] Giroletti, M., Giovannini, G., Feretti, L., et al. 2004, ApJ, 600, 127

[520] Ghisellini, G., Tavecchio, F., Chiaberge, M., 2005, A&A, 432, 401

[521] Murphy, E., Cawthorne, T. V., & Gabuzda, D. C. 2013, MNRAS, 682

[522] Pudritz, R. E., Hardcastle, M. J., & Gabuzda, D. C. 2012, SSRv, 169, 27

[523] Giroletti, M., Hada, K., Giovannini, G., et al. 2012, A&A, 538, L10

[524] Aharonian et al., *ApJL* **696** (2009) pg. L150-L155

[525] Albert et al., *ApJ* **669** (2007) pg. 862-883

[526] Tramacere et al., *ApJ* **739** (2011) article id. 66.

[527] Ho, L. C., & Ulvestad, J. S. 2001, ApJS, 133, 77

[528] Nagar, N. M., Falcke, H., Wilson, A. S., & Ulvestad, J. S. 2002, A&A, 392, 53

[529] Narayan, R., & Yi, I. 1994, ApJ, 428, L13

[530] Gallimore, J. F., Baum, S. A., & O'Dea, C. P. 2004, ApJ, 613, 794

[531] Ulvestad, J. S., & Ho, L. C. 2001, ApJ, 562, L133

[532] Falcke, H., Nagar, N. M., Wilson, A. S., & Ulvestad, J. S. 2000, ApJ, 542, 197

[533] Ghisellini, G., Haardt, F., & Matt, G. 2004, A&A, 413, 535

[534] Giroletti, M., & Panessa, F. 2009, ApJ, 706, L260

[535] Bontempi, P., Giroletti, M., Panessa, F., Orienti, M., & Doi, A. 2012, MNRAS, 426, 588

[536] Panessa, F., & Giroletti, M., , 2013, MNRAS, in press, arXiv1304.0794

[537] Allen, S. W., Dunn, R. J. H., Fabian, A. C., Taylor, G. B., & Reynolds, C. S. 2006, MNRAS, 372, 21

[538] Balmaverde, B., Baldi, R. D., & Capetti, A. 2008, A&A, 486, 119

[539] Binette, L., Magris, C. G., Stasińska, G., & Bruzual, A. G. 1994, A&A, 292, 13

[540] Bondi, H. 1952, MNRAS, 112, 195

[541] Capetti, A., Kharb, P., Axon, D. J., Merritt, D., & Baldi, R. D. 2009, AJ, 138, 1990

[542] Ferrarese, L. & Merritt, D. 2000, ApJL, 539, L9

[543] Gebhardt, K., Bender, R., Bower, G., et al. 2000, ApJL, 539, L13

[544] Revnivtsev, M., Churazov, E., Sazonov, S., Forman, W., & Jones, C. 2008, A&A, 490, 37

[545] Trinchieri, G. & di Serego Alighieri, S. 1991, AJ, 101, 1647

[546] Vattakunnel, S., Trussoni, E., Capetti, A., & Baldi, R. D. 2010, A&A, 522, A89

[547] Yusef-Zadeh, F., Wardle, M., Miller-Jones, J. C. A., et al. 2011, ApJ, 729, 44

[548] Cordey, R. A. 1987, MNRAS, 227, 695

[549] Parma, P., Murgia, M., de Ruiter, et al. 2007, A&A, 470, 875

[550] Murgia, M., Parma, P., Mack, K.-H., et al. 2011, A&A, 526, A148

[551] Murgia, M., Markevitch, M., Govoni, F., et al. 2012, A%A, 548, A75

[552] Xu, H., Li, H., Collins, D.C., Li, S., Norman, M.L., 2011, ApJ, 739, 77

[553] Antonucci, R. 1993, *ARAA*, 31, 473

[554] Bennert, N., Barvainis, R., Henkel, C., & Antonucci, R. 2009, *ApJ*, 695, 276

[555] Braatz, J. A., Reid, M. J., Humphreys, E. M. L., et al. 2010, *ApJ*, 718, 657

[556] Braatz, J. A., Condon, J. J., Henkel, C., Lo, K. -Y., Reid, M. J. 2010a, in *Astro2010: The Astronomy and Astrophysics Decadal Survey, Science White Papers*, no. 23

[557] Castangia, P., Impellizzeri, C. M. V.., McKean, J. P., Henkel, C., Brunthaler, A., Roy, A. L., Wucknitz, O., Ott, J., & Momjian, E. 2011 *A&A*, 529, 150

[558] Greene, J. E., Peng, C. Y., Kim, M., Kuo, C. -Y., et al. 2010, *ApJ*, 721, 26

[559] Greenhill, L. J., Booth, R. S., Ellingsen, S. P., et al. 2003, *ApJ*, 590, 162

[560] Henkel, C., Peck, A. B., Tarchi, A., et al. 2005 *A&A*, 436, 75

[561] Herrnstein, J. R., Moran, J. M., Greenhill, L. J., Diamond, P. J., Inoue, M., Nakai, N., Miyoshi, M., Henkel, C., & Riess, A. 1999, *Nature*, 400, 539

[562] Impellizzeri, C. M. V., McKean, J. P., Castangia, P., Roy, A. L., Henkel, C., Brunthaler, A., & Wucknitz, O. 2008, *Nature*, 456, 927

[563] Kuo, C. Y., Braatz, J. A., Condon, J. J., et al. 2011, *ApJ*, 727, 20

[564] McKean, J. P., Impellizzeri, C. M. V., Roy, A. L., Castangia, P., Samuel, F., Brunthaler, A., Henkel, C., & Wucknitz, O. 2011, *MNRAS*, 410, 2506, M11

[565] Miyoshi, M., Moran, J., Herrnstein, J., Greenhill, L., Nakai, N., Diamond, P., & Inoue, M. 1995, *Nature*, 373, 127

[566] Omont, A., Yang, P., Cox, P., et al. 2013, *arXiv:1301.6618*

[567] Peck, A. B., Henkel, C., Ulvestad, J. S., Brunthaler, A., Falcke, H., Elitzur, M., Menten, K. M., & Gallimore, J. F. 2003, *ApJ*, 590, 149

[568] Tarchi, A., Brunthaler, A., Henkel, C., Menten, K. M., Braatz, J., & Weiß, A. 2007b, *A&A*, 475, 497

[569] Urry, C. M. & Padovani, P. 1995, *PASP*, 107, 803

[570] Borgani, S., Fabjan, D., Tornatore, L., et al., 2008, Space Science Reviews, 134, 379

[571] Feretti, L., Giovannini, G., Govoni, F., Murgia, M., 2012, A&A Rev., 20, 54

[572] Peterson, J. R.; Fabian, A. C., 2006, PhR 427, 1

[573] Blasi, P., Gabici, S., Brunetti, G., 2007, International Journal of Modern Physics A, 22, 681

[574] Buote, D.A., 2001, ApJ, 553, L15

[575] Cassano, R., Ettori, S., Giacintucci, S., et al., 2010, ApJ, 721, L82

[576] Brunetti, G., Cassano, R., Dolag, K., Setti, G., 2009, A&A, 507, 661

[577] Keshet, U., & Loeb, A., 2010, ApJ, 722, 737

[578] Brunetti, G., 2011, Mem. SAIt, 82, 515

[579] Venturi, T., 2011, Mem. SAIt, 82, 499

[580] Venturi T., Giacintucci S., Dallacasa D., et al., 2013, A&A, 551, A24

[581] Murgia M., Govoni F., Feretti L., et al., 2004, A&A, 424, 429

[582] Govoni, F., Murgia, M., Feretti, L., et al., 2006, A&A, 460, 425

[583] Vacca, V., Murgia, M., Govoni, F., et al., 2010, A&A, 514, A71

[584] Govoni, F., Enßlin, T. A., Feretti, L., & Giovannini, G., 2001, A&A, 369, 441

[585] Planck Collaboration, Ade, P. A. R., Aghanim, N., et al., 2012, arXiv:1208.3611

[586] Brown, S., & Rudnick, L., 2011, MNRAS, 412, 2

[587] Bonafede A., Brüggen M., van Weeren R., et al., 2012, MNRAS, 426, 40

[588] Hanisch, R. J., 1982, A&A, 116, 137

[589] Giovannini, G., Tordi, M., Feretti, L., 1999, New Astronomy, 4, 141

[590] Kempner, J. C., Sarazin, C. L., 2001, ApJ, 548, 639

[591] Venturi, T., Giacintucci, S., Brunetti, G., et al., 2007, A&A, 463, 937

[592] Venturi, T., Giacintucci, S., Dallacasa, D., et al., 2008, A&A, 484, 327

[593] Cassano, R., Brunetti, G., Venturi, T., Setti, G., Dallacasa, D., Giacintucci, S., Bardelli, S., 2008 A&A, 480, 687

[594] Giovannini, G., Feretti, L., Girardi, M., et al., 2011, A&A, 530, L5

[595] Brown, S., Duesterhoeft, J., & Rudnick, L., 2011, ApJ, 727, L25

[596] Cassano, R., Brunetti, G., & Setti, G., 2006, MNRAS, 369, 1577

[597] Brunetti, G., Giacintucci, S., Cassano, R., et al., 2008, Nature, 455, 944

[598] Lazarian, A., & Brunetti, G., 2011, Mem. SAIt, 82, 636

[599] Cassano, R., Brunetti, G., Norris, R. P., et al., 2012, A&A, 548, A100

[600] Sutter, P. M., & Ricker, P. M., 2012, ApJ, 759, 92

[601] Kushnir, D., Katz, B., & Waxman, E, 2009, Journal of Cosmology and Astroparticle Physics, 9, 24

[602] Brunetti, G., & Lazarian, A., 2011, MNRAS, 410, 127

[603] Ensslin, T., Pfrommer, C., Miniati, F., Subramanian, K., 2011, A&A, 527, A99

[604] Donnert, J., Dolag, K., Brunetti, G., Cassano, R., 2013, MNRAS, 429, 3564

[605] Wiener, J. Zweibel, E. G., Oh, S. Peng, 2013, arXiv 1303.4746

[606] Brown, S., Emerick, A., Rudnick, L., Brunetti, G., 2011, ApJ, 740, L28

[607] Condon, J. J., 1987, In: *Scientific Benefits of an Upgraded Arecibo Telescope* (NAIC, ed. Taylor & Davis), p. 89

[608] Ackermann, M., Ajello, M., Allafort, A., Baldini, L., Ballet, J., et al., 2010, ApJ, 717, L71

[609] Reimer, A., Reimer, O., Schlickeiser, R., Iyudin, A., 2004 A&A, 424, 773

[610] Brunetti, G., Venturi, T., Dallacasa, D., Cassano, R., Dolag, K., Giacintucci, S., Setti, G., 2007, ApJ, 670, L5

[611] Ackermann M., Ajello M., Allafort P., et al., 2010, JCAP, 05, 025

[612] Ando S., Nagai D., 2012, JCAP, 07, 017

[613] Aleksic J., Antonelli L.A., Antoranz P., et al., ApJ, 710, 634

[614] Abramowski A., Acero F., Aharonian F., et al., 2012, ApJ, 750, 123

[615] Storm E., Jeltema T.E., Profumo S., Rudnick L., 2013, ApJ, 768, 106

[616] Gao L., Frenk C.S., Jenkins A., Pringel V., White S.D.M., 2012, MNRAS, 419, 1721

[617] Fabian, A. 1994, ARA&A, 32, 277

[618] Peterson, J. R., et al. 2001, A&A, 365, 104

[619] Gitti, M., et al. 2010, ApJ, 714, 758
[620] Gitti, M., et al. 2006, A&A, 448, 853
[621] McNamara, B. R., & Nulsen, P. E. J. 2007, ARA&A, 45, 117
[622] Gitti, M., et al. 2012, Advances in Astronomy, 2012, 1
[623] Birzan, L., et al. 2004, ApJ, 607, 800
[624] Birzan, L., et al. 2008, ApJ, 686, 859
[625] Croton, D.J., et al. 2006, MNRS, 365 11
[626] McNamara, B.R., et al. 2006, ApJ, 648, 164
[627] Rafferty, D.A., et al. 2008, ApJ, 687, 899
[628] Hlavacek-Larrondo J., et al. 2012, MNRAS, 421, 1360
[629] Santos, J.S., et al. 2010, A&A, 521, 64
[630] Santos, J.S., et al. 2012, A&A, 539, 105
[631] Sun, M., 2009, ApJ, 704, 1586
[632] Miley, G., et al. 2006, ApJ, 650, 29-L32
[633] Zhuravleva I. et al., 2012, MNRAS, 422, 2712
[634] Markevitch M. & Vikhlinin A., 2007, Phys. Rep., 443, 1
[635] Bagchi, J., Enßlin, T. A., Miniati, F., et al., 2002, New Astronomy, 7, 249
[636] Ryu, D., Schleicher, D. R. G., Treumann, R. A., Tsagas, C. G., & Widrow, L. M.,
[637] Widrow, L. M., Ryu, D. Schleicher, D. R. G., et al., *Space Sci.Rev* **166** (2012) 37
[638] Kawasaki, M., & Kusakabe, M., *Phys.Rev.D* **86** (2012) 063003
[639] Paoletti, D., & Finelli, F., arXiv:1208.2625 2012
[640] Paoletti, D., & Finelli, F., *Phys.Rev.D*, **83** (2011) 123533
[641] Shaw, J. R., & Lewis A., *Phys.Rev.D* **86** (2012) 043510
[642] Caprini, C., Finelli, F., Paoletti, D., & Riotto, A., *JCAP* **6** (2009) 21
[643] Seshadri, T. R., & Subramanian, K., *Phys. Rev. Lett.* **103** (2009) 081303
[644] Shiraishi, M., Nitta, D., Yokojama, S., & Ichiki, K., *JCAP* **1203** (2012) 041
[645] Trivedi, P., Subramanian, K., & Seshadri, T. R., *Phys.Rev.D***82**(2010) 123006
[646] Trivedi, P., & Subramanian, K., *Phys.Rev.Lett.* **108** (2012) 231301
[647] Dolag, K., e-print astro-ph/0601484 (2006)
[648] A. Neronov and I. Vovk, *Science Vol.* **328** (2010) 5974 73
[649] A. M. Taylor, I. Vovk and A. Neronov, *Astronomy & Astrophysics*, **529** (2011) A144
[650] I. Vovk, A. M. Taylor, D. Semikoz and A. Neronov, *Astrophys. J.* **747** (2012) L14
[651] Kosowsky, A., & Loeb, A., *Astrophys.J.* **469** (1996) 1
[652] Clarke, T.E., Kronberg, P.P., Böhringer, H., 2001, ApJ, 547, L111
[653] Bonafede, A., Govoni, F., Feretti, L., et al., 2011, A&A, 530, A24
[654] Carilli, C.L., & Taylor, G.B., 2002, ARA&A 40, 319
[655] Govoni, F., Feretti, L., 2004, Int. J. Mod. Phys. D, Vol. 13, N.8, p. 1549
[656] Ferrari, C., Govoni, F., Schindler, S., Bykov, A.M., Rephaeli, Y., 2008, Space Science Reviews, 134, 93

[657] Dolag, K., Bykov, A. M., Diaferio, A., 2008, Space Science Reviews, 134, 311
[658] Guidetti, D., Murgia, M., Govoni, F., et al., 2008, A&A, 483, 699
[659] Guidetti, D., Laing, R.A., Murgia, M., et al., 2010, A&A, 514, A50
[660] Govoni, F., Dolag, K., Murgia, M., et al., 2010, A&A, 522, A105
[661] Vacca, V., Murgia, M., Govoni, F., et al., 2012, A&A, 540, A38
[662] Bonafede, A., Feretti, L., Murgia, M., et al., 2010, A&A, 513, A30
[663] Guidetti, D., Laing, R.A., Bridle, A.H., Parma, P., Gregorini, L., 2011, MNRAS, 413, 2525
[664] Rudnick, L., & Blundell, K.M., 2003, ApJ, 588, 143
[665] O'Sullivan, S.P., Feain, I.J., McClure-Griffiths, N.M., et al., 2013, ApJ, 764, 162
[666] Enßlin T.A., & Vogt C., 2003, A&A, 401, 835
[667] Laing, R.A., Bridle, A.H., Parma, P., Murgia, M., 2008, MNRAS, 391, 521
[668] Kuchar, P., & Enßlin, T.A., 2011, A&A 529, A13
[669] Krause, M., Alexander, P., Bolton, R., et al., 2009, MNRAS, 400, 646
[670] Bogdanović, T., Reynolds, C. S., Massey, R., 2011, ApJ, 731, 7
[671] Bonafede, A., Giovannini, G., Feretti, L., Govoni, F., Murgia, M., 2009a, A&A, 494, 429
[672] van Weeren, R. J., Röttgering, H. J. A., Brüggen, M., & Hoeft, M. 2010, Science, 330, 347
[673] Govoni, F., Murgia, M., Feretti, L., et al., 2005, A&A, 430, L5
[674] Pizzo, R.F., de Bruyn, A.G., Bernardi, G., Brentjens, M.A., 2011, A&A, 525, A104
[675] Bonafede, A., Feretti, L, Giovannini, G., et al., 2009b, A&A, 503, 707
[676] Govoni, F., Murgia, M., Xu, H., et al., 2013, A&A, 554, A102
[677] Xu, H., Govoni, F., Murgia, M., et al., 2012, ApJ, 759, 40
[678] Antonucci E., Gabriel A.H., Dennis B.R., 1984, ApJ, 287, 917
[679] Phillips K.J.H., Neupert W.M., 2008, SoPh, 32, 209
[680] Guedel M., 2009, LNP, 778, 269
[681] Hallinan G., Antonova A., Doyle J.G., Bourke S., Lane C., Golden A., 2008, ApJ, 684, 644
[682] Ravi V., Hallinan G., Hobbs G., Champion D.J., 2011, ApJ, 735, L2
[683] Trigilio C., Leto P., Leone F., Umana G., Buemi C., 2000, A&A, 362, 281
[684] Trigilio C., Leto P., Umana G., Buemi C.S., Leone F., 2011, MNRAS, 739, L10
[685] Slee O.B., Wilson W., Ramsay G., 2008, PASA, 25, 94
[686] Trigilio C., Leto P., Umana G., Buemi C.S., Leone F., 2008, MNRAS, 384, 1437
[687] Ravi V., Hobbs G., Wickramasinghe D. et al., 2010, MNRAS, , 408, 99
[688] Seaquist E.R., 1993, RPPh, 56, 1145
[689] Umana G., Trigilio C., Tumino M., Catalano S., Rodonó M., 1993, A&A, 267, 126
[690] Guedel M., 2002, ARA&A, 40, 2017
[691] Benz A.O., Guedel M., 2010, ARA&A, 48, 241
[692] Berger E., Rutledge R.E., Reid I.N. et al., 2005, ApJ, 627,960
[693] Lorimer, D. & Kramer, M. 2005, *Handbook of pulsar astronomy*, Cambridge
[694] Smits, R. et al. 2009, A&A, 493, 1161

[695] Possenti, A., 2013, *Neutron Stars and Pulsars*, ed. J. van Leeuwen, IAU 291
[696] Kramer, M. *et al.*, 2004, New Astr. Rev., 48, 993
[697] Burgay, M., et al. 2003, Nature, 426, 531
[698] Kramer M., et al., 2006, Science, 314, 97
[699] Freire, P.P.C., et al. 2012, MNRAS, 423, 3328
[700] Damour T., Esposito-Farèse, D., 1996, Phys. Rev. D. 54, 1474
[701] Kramer M., & Wex N., 2009, Class. Quantum Grav. 26, 073001
[702] Damour T. & Schafer G. 1988, Nuovo Cimento, 101, 127
[703] Pfahl, E., Podsiadlowski, P., Rappaport, S. 2005, ApJ, 628, 343
[704] Devecchi, B,, Colpi, M., Mapelli, M., Possenti, A. 2007, MNRAS, 380, 691
[705] Deneva, I.S. 2010, Ph.D. dissert., Cornell Univ.
[706] Liu, K., et al. 2012, ApJ, 747, L1
[707] Hawking, S.W. & Penrose, R., 1970, in *Royal Soc. Proceed. Ser. A*, 314, 529
[708] Hellings, R.W. & Downs, G.S. 1993, ApJ, 265, 39
[709] Lee, K., et al., 2010, ApJ, 722, 1589
[710] Sesana, A. & Vecchio, A. 2010, Phys. Rev. D., 81, 104008
[711] Phinney, S. & Kulkarni, S. 1994, ARA&A, 32, 591
[712] Freire, P.P.C. 2013, at *http://www.naic.edu/ pfreire/GCpsr.html*
[713] Lattimer, J.M. & Schutz, B.F. 2005, ApJ, 629, 979
[714] Smits, R. et al. 2011, A&A, 528, 108
[715] Alpar, A., et al. 1982, Nature, 300, 728
[716] Davies, M.B. & Hansen, B.M.S. 1998, MNRAS, 301, 15
[717] Sesana, A., Sartore, N., De Vecchi, B., Possenti, A., 2012, MNRAS, 427, 502
[718] Boffi, F. & Branch, D. 1995, PASP, 107, 347
[719] Bower C.G et al. D. 2007, ApJ, 666, 346
[720] Branch, D. et al. 1995, PASP, 107, 1019
[721] Cappellaro, E., Evans, R., Turatto, M. 1999, A&A, 351, 459
[722] Della Valle, M. 2011, IJMPD, 20, 1745
[723] Maund, J. et al. 2004, Natur, 427, 129
[724] Guetta, D. & Della Valle, M. 2007, ApJ, 657, L73
[725] Immler, S. et al. 2001, ApJ, 561, L107
[726] Livio, M. 2001, STScI symposium series, Vol. 13, Cambridge University Press, p. 334
[727] Mannucci, F., Della Valle, M., Panagia, N. 2006, MNRAS, 370, 773
[728] Nakar, E. & Piran, T. 2011, Natur, 478, 82
[729] Ofek, E. et al. 2013, Natur, 494, 65
[730] Montes, M. et al. 1998, ApJ, 506, 874
[731] Panagia, N. et al. 2006, ApJ, 646, 369
[732] Pastorello, A. et al. 2007, Natur, 447, 829

[733] Prialnik, D. & Kovetz, A. 1995, ApJ, 445, 789
[734] Raskin, C. et al. 2008, ApJ, 689, 358
[735] Soderberg, A. et al. 2010, Natur, 463, 513
[736] Weiler, K. et al. 2004, NewAR, 48, 1377
[737] Zhiping et al. 2013, ApJ, submitted
[738] Salvaterra R., Della Valle M., Campana S., et al., Nat, 461, 1258, (2009)
[739] Frail D. A., Kulkarni S. R., Sari R., et al., ApJ, 526, L55, (2001)
[740] Berger E., ApJ, 690, 231 (2009)
[741] Woosley S. E., ApJ, 405, 273, (1993)
[742] Lazzati D., Morsony B. J., Blackwell C. H., et al., ApJ, 759, 68, (2012)
[743] Rosswog S., Ramirez-Ruiz E. MNRAS, 343, L36, (2003)
[744] Rees M. J., Meszaros P., ApJ, 430, L93, (1994)
[745] Meszaros P., Rees M. J. ApJ, 405, 278 (1993)
[746] Meszaros P., RPPh, 69, 2259, (2006)
[747] Chandra P., Frail D. A., ApJ, 746, 156 (2012)
[748] Frail D. A., Kulkarni S. R., Nicastro L., Nat., 389, 261, (1997)
[749] Frail D. A., Metzger B. D., Berger E., et al., ApJ, 600, 828, (2004)
[750] Frail D. A., Soderberg A. M., Kulkarni S. R., ApJ, 619, 994, (2005)
[751] Berger E., Kulkarni S. R., Frail D. A. ApJ, 612, 966, (2004)
[752] Berger E., Kulkarni S. R., Frail D. A., et al., ApJ, 599, 408, (2003)
[753] Soderberg A. M., Nakar E., Berger E., Kulkarni S. R. ApJ, 638, 930, (2006)
[754] Stanway, Elizabeth R.; Davies, Luke J. M.; Levan, Andrew J. MNRAS, 409, L74, (2010)
[755] Hatsukade B., Hashimoto T., Ohta K., et al., ApJ, 748, 108, (2012)
[756] Zauderer, B. A.; Berger, E.; Margutti, R., et al. arXiv1209.4654, (2012)
[757] Ghirlanda G., et al., (2013) in preparation
[758] Toma K., Ioka K., Nakamura T., ApJ, 673, L123, (2008)
[759] Giannios D., Spitkovsky A., MNRAS, 400, 330, (2009)
[760] Covino S., Ghisellini G., Lazzati D., et al., MSAIS, 5, 160, (2004)
[761] Lazzati D., NJPh, 8, 131, (2006)
[762] Kobayashi S., ApJ, 545, 807, (2000)
[763] Ioka K., Meszaros P., ApJ, 631, 429 (2005)
[764] Livio M., Waxman E., ApJ, 538, 187, (2000)
[765] Bloom J. S., Frail D. A., Kulkarni S. R., ApJ, 594, 674, (2003)
[766] Ghirlanda G., Ghisellini G., Lazzati D. ApJ, 594, 674, (2003)
[767] Ghirlanda G., Ghisellini G., Lazzati D., et al. ApJ, 613, L13, (2004)
[768] Kodama Y., Yonetoku D., Murakami T., et al., MNRAS, 391, L1, (2008)
[769] Berger E., Cowie L. L., Kulkarni S. R., et al., ApJ, 588, 99, (2003)
[770] Michalowski M. J., Kamble A., Hjorth J., ApJ, 755, 85, (2012)

[771] Meszaros P. & Rees M. ApJ, 715, 967 (2012)

[772] Ciardi B., Loeb A. ApJ, 540, 687, (2000)

[773] Whalen D., Abel T., Norman M. L. ApJ, 610, 14, (2004)

[774] Ciardi B., Labropoulos P., Maselli A., et al., MNRAS, 428, 1755, (2013)

[775] Meszaros P & Rees M., ApJ, 715, 967, (2010)

[776] Suwa Y. & Ioka K. ApJ, 726, 107, (2011)

[777] Toma K., Sakamoto T., Meszaros P. ApJ, 731, 127, (2011)

[778] Xu Y., Ferrara A., Chen X. MNRAS, 410, 2025, (2011)

[779] Furlanetto S. R., Loeb A. ApJ, 579, 1

[780] Fabbiano, G., *ARA&A* **44** (2006) 323

[781] Begelman, M.C., *ApJ* **568** (2002) 97

[782] King, A.R., Davies, M.B., Ward, M. J., Fabbiano, G., Elvis, M., *ApJ*, **552** (2001) L109

[783] King, A., *MNRAS* **292** (2009) L41

[784] Colbert, E.J.M., Mushotzky, R.F., *ApJ* **519** (1999) 89

[785] Portegies-Zwart, S.F., Dewi, J., Maccarone, T., *MNRAS* **355** (2004) 413

[786] Portegies Zwart, S.F., Baumgardt, H., Hut, P., Makino, J., McMillan, S.L.W., *Nature* **428** (2004) 724

[787] Freitag, M., Gürkan, M.A., Rasio, F.A., *MNRAS* **368** (2006) 141

[788] Pakull, M.W., Mirioni, L., *RMxAA* **15** (2003) 197

[789] Pakull, M.W., *KITP Conference: Supernova and Gamma-Ray Burst Remnants* (2006) 48

[790] Liu, J.-F., Bregman, J.N., and Seitzer, P., *ApJ* **580** (2002) L31

[791] Terashima, Y., Inoue, H., and Wilson, A.S., *ApJ* **645** (2006) 264

[792] Roberts, T.P., Levan, A.J., Goad, M.R., *MNRAS* **387** (2008) 73

[793] Grisé, F., Pakull, M.W., Soria, R., Motch, C., Smith, I.A., Ryder, S.D., Böttcher, M., *A&A* **486** (2008) 151

[794] Tao, L., Feng, H., Grisé, F., Kaaret, P., *ApJ* **737** (2011) 81

[795] Swartz, D.A., Ghosh, K.K., Tennant, A.F., Wu, K., *ApJS* **154** 519

[796] Swartz, D.A., Soria, R., Tennant, A.F., Yukita, M., *ApJ* **741** (2011) 49

[797] Liu, J.F., Bregman, J.N., Irwin, J., *ApJ* **642** (2006) 171

[798] Ranalli, P., Comastri, A., Setti, G., *A&A* **399** (2003) 39

[799] Persic, M., Rephaeli, Y., *A&A* **463** (2007) 481

[800] Grimm, H.-J., Gilfanov, M., Sunyaev, R., *MNRAS* **339** (2003) 793

[801] Mineo, S., Gilfanov, M., Sunyaev, R., *MNRAS* **419** (2012) 2095

[802] Kaaret, P., Prestwich, A.H., Zezas, A., Murray, S.S., Kim, D.-W., Kilgard, R.E., Schlegel, E.M., Ward, M.J., *MNRAS* **321** L29

[803] Matsumoto, H., *ApJ* **547** (2001) L25

[804] Wolter, A., Trinchieri, G., and Colpi, M., *MNRAS* **373** (2006) 1627

[805] Farrell, S.A.,; Webb, N.A., Barret, D., Godet, O., Rodrigues, J.M., *Nature* **460** (2009) 73

[806] Sutton, A.D., Roberts, T.P., Walton, D.J., *AN* **332** (2011) 362

[807] Servillat, M., Farrell, S.A., Lin, D., Godet, O., Barret, D., Webb, N.A., *ApJ* **743** (2011) 6

[808] Zampieri, L., Roberts, T.P., *MNRAS* **400** (2009) 677

[809] Corbel, S., Nowak, M.A., Fender, R.P., Tzioumis, A.K., Markoff, S., *A&A* **400** (2003) 1007

[810] Gallo, E., Fender, R.P., Pooley, G.G., *MNRAS* **344** (2003) 60

[811] Merloni, A., Heinz, S., di Matteo, T., *MNRAS* **345** (2003) 1057

[812] Falcke, H., Körding, E., Markoff, S., *A&A* **414** (2004) 895

[813] Weiler, W.K., Panagia, N., Montes, M.J., Sramek, R.A., *ARA&A* **40** (2002) 387

[814] Chevalier, R.A., *ESO ASTROPHYSICS SYMPOSIA* (2003) 299

[815] Webb, N.A., et al., *SF2A-2012* (2012) 631

[816] Cseh, D., Corbel, S., Kaaret, P,. Lang, C., Grisé, F., Paragi, Z., Tzioumis, A., Tudose, V., Feng, H., *ApJ* **749** (2012) 17

[817] Belloni, T. M. 2010, *Lecture Notes in Physics*, Berlin Springer Verlag, **794** (2010) 53

[818] Muñoz-Darias, T., Motta, S., Belloni, T., *MNRAS* **410** (2011) 679

[819] M. J. Rees. *Nature*, 333:523–528, June 1988.

[820] E. S. Phinney. *Nature*, 340:595–596, August 1989.

[821] S. Komossa. In R. E. Schielicke, editor, *Reviews in Modern Astronomy*, volume 15 of *Reviews in Modern Astronomy*, page 27, 2002.

[822] J. L. Donley, W. N. Brandt, M. Eracleous, and T. Boller. *A&A*, 124:1308–1321, September 2002.

[823] S. Gezari, T. Heckman, S. B. Cenko, M. Eracleous, K. Forster, T. S. Goncalves, D. C. Martin, P. Morrissey, S. G. Neff, M. Seibert, D. Schiminovich, and T. K. Wyder. *ApJ*, 698:1367–1379, June 2009.

[824] S. Gezari, R. Chornock, A. Rest et al. *Nature*, 485:217–220, May 2012.

[825] S. Campana, G. Lodato, P. D'Avanzo et al. *Nature*, 480:69–71, December 2011.

[826] L. E. Strubbe and E. Quataert. *MNRAS*, 400:2070–2084, December 2009.

[827] D. N. Burrows, J. A. Kennea, G. Ghisellini et al. *Nature*, 476:421–424, August 2011.

[828] S. B. Cenko, H. A. Krimm, A. Horesh et al. *ApJ*, 753:77, July 2012.

[829] B. A. Zauderer, E. Berger, A. M. Soderberg et al. *Nature*, 476:425–428, August 2011.

[830] R. C. Reis, J. M. Miller, M. T. Reynolds et al. *Science*, 337:949–, August 2012.

[831] A. J. Levan, N. R. Tanvir, S. B. Cenko et al. *Science*, 333:199–, July 2011.

[832] A. Levan. In *European Physical Journal Web of Conferences*, volume 39 of *European Physical Journal Web of Conferences*, page 2005, December 2012.

[833] van Velzen, S. and Frail, D. A. and Körding, E. and Falcke, H. *A&A*, 552, A5, Apr 2013.

[834] McKee C. F., Tan J. C., *ApJ*, **585** (2003), 850

[835] Bonnell I. A., Vine S. G., Bate M. R., *MNRAS*, **349** (2004), 735

[836] Krumholz M. R., Klein R. I., McKee C. F., Offner S. S. R., Cunningham, A., *Science*, **323** (2009), 754

[837] Wood D. O. S., Churchwell E., *ApJS*, **69** (1989), 831

[838] Keto E., *ApJ*, **666** (2007), 976

[839] Keto E., *ApJ*, **580** (2002), 980

[840] Martí J., Rodríguez L. F., Reipurth B., *ApJ*, **416** (1993), 208

[841] Martí J., Rodríguez L. F., Reipurth B., *ApJ*, **449** (1995), 184

[842] Cesaroni R., Galli D., Lodato G., Walmsley C. M., Zhang Q. 2007, in *Protostars and Planets V*, p. 197

[843] Martí J., Rodríguez L. F., Torrelles J. M., *A&A*, **345** (1999), L5

[844] Anglada G. 1996, in *Radio emission from the stars and the sun*, Astronomical Society of the Pacific Conference Series (1996), Volume 93, p. 3

[845] Anglada G., Villuendas E., Estalella R., Beltrán M. T., et al., *AJ*, **116** (1998), 2953

[846] Sewilo M., Churchwell E., Kurtz S., Goss W. M., Hofner P., *ApJ*, **605** (2004), 285

[847] Moscadelli L., Goddi C., Cesaroni R., Beltrán M. T., Furuya R. S., *A&A*, **472** (2007), 867

[848] Reynolds S. P., *ApJ*, **304** (1986), 713

[849] Curiel S., Rodríguez L. F., Cantó J., Torrelles J. M., *RMxAA*, **17** (1989), 137

[850] Beltrán M. T., Cesaroni R., Moscadelli L., Codella C., *A&A*, **471** (2007), L13

[851] Shull J. M., *ApJ*, **238** (1980), 860

[852] Keto E., Wood K., *ApJ*, **637** (2006), 850

[853] Caselli P., Ceccarelli C., 2012 The Astronomy and Astrophysics Review, 20, 56

[854] Ceccarelli, C., Caselli, P., Herbst, E., Tielens, A.G.G.M., Caux, E. 2007 Protostars and Planets V, University of Arizona Press, Tucson, p.47

[855] Bottinelli, S., Ceccarelli, C., Williams, J.P., Lefloch, B. 2007, A&A 463, 601

[856] Jorgensen, J.K., Favre, C. Bisschop, S.E., Bourke, T.L., van Dishoeck, E.F., Schmalzl, M. 2012, ApJ 757, L4

[857] Bachiller, R., Pérez Gutiérrez, M., Kumar, M.S.N., Tafalla, M. 2001, A&A 372, 899

[858] Arce, H.G., Santiago-García, J., Jorgensen, JK., Tafalla, M., Bachiller, R. 2008, A&A 681, L21

[859] Codella, C., Benedettini, M., Beltrán, M.T., Gueth, F., Viti, S., Bachiller, R., Tafalla, M., Cabrit, S., Fuente, A., Lefloch, B. 2007, A&A 507, L25

[860] Cesaroni, R., Galli, D., Lodato, G., Walmsley, C.M., Zhang, Q. 2007 Protostars and Planets V, University of Arizona Press, Tucson, p.197

[861] Beuther, H., Shepherd, D. 2005, in *Cores to Clusters: Star Formation with Next Generation Telescopes*, Astrophysics and Space Science Library, 324, 105

[862] Kurtz, S., Cesaroni, R., Churchwell, E., Hofner, P., Walmsley, C.M. 2000 in *Protostars and Planets IV*, University of Arizona Press, Tucson, p. 299

[863] Beltrán, M.T., Codella, C., Viti, S., Neri, R., Cesaroni, R. 2009, ApJ, L93

[864] Herbst, E., van Dishoeck, E.F. 2009, ARA&A 47, 427

[865] Fontani, F., Palau, A., Caselli, P., Sánchez-Monge, Á., Butler, M.J., Tan, J.C., Jiménez-Serra, I., Busquet, G., Leurini, S., Audard, M. 2011, A&A 529, L11

[866] Parise, B., Castets, A., Herbst, E., Caux, E., Ceccarelli, C., Mukhopadhyay, I., Tielens, A.G.G.M. 2004, A&A 416, 159

[867] Maury, A.J., André, Ph., Maret, S., Codella, C., Gueth, F., Belloche, A., Cabrit, S., Bacman, A. 2013, in *The Labyrinth of Star Formation*, Springer, in press

[868] Loomis, R.A., Zaleski, D.P.; Steber, A.L., et al. 2013, ApJ 765, L9

[869] Oberg, K.I., Garrod, R.T., van Dishoeck, E.F., Linnartz, H., 2009, A&A 504, 891

[870] Modica, P., Palumbo, M. E., 2012, A&A 519, 22

[871] Burigana C., Davies R.D., de Bernardis P., et al., 2013, IJMPD, in press, arXiv:1302.3474

[872] Kovac J.M., Leitch E.M., Pryke C., Carlstrom J.E., Halverson N.W., Holzapfel W.L., 2002, Nature, 420, 772

[873] Leach S.M., Cardoso J.-F., Baccigalupi C., et al., 2008, A&A, 491, 597

[874] Burigana C., La Porta L., Reich W., Reich P., Gónzalez-Nuevo J., Massardi M., De Zotti G., in *CMB and Physics of the Early Universe* (CMB2006), G. De Zotti et al., eds., PoS(CMB2006)016 (http://pos.sissa.it//archive/conferences/027/016/CMB2006_016.pdf).

[875] Burigana C., La Porta L., Reich P., Reich W., 2006, AN, 327, 491

[876] Bennett C.L., Larson D., Weiland J.L., et al., 2013, ApJS, submitted, arXiv:1212.5225

[877] Sun X.H., Reich W., Waelkens A., Ensslin T.A., 2008, A&A, 477, 573

[878] Sun X.H., Reich W., 2009, A&A, 507, 1087

[879] Sun X.H., Reich W., 2010, Research in Astron. Astrophys., 10, 1287

[880] Fauvet L., Macias-Perez J.F., Aumont J., et al., 2011, A&A, 526, id. A145

[881] Fauvet L., Macias-Perez J.F., Désert F.X., 2012, Astroparticle Physics, 36, 57

[882] Cho J., Lazarian A., ApJ, 575, L63

[883] Strong A.W., Moskalenko I.V., 1998, ApJ, 509, 212

[884] Waelkens A., Jaffe T., Reinecke M., Kitaura F.S., Ensslin, T.A., et al., 2009, A&A, 495, 697

[885] Draine B.T., Lazarian A., 1998, ApJ, 494,, L19

[886] *Planck* Collaboration. XX, 2011, A&A, 536, A20

[887] *Planck* Collaboration. IX, 2013, A&A, in press, arXiv://1208.5483v1

[888] Carretti, E., Crocker R.M., Staveley-Smith L., et al., 2012, Nature, 493, 66

[889] Maccone, C., *Acta Astronautica* **67** (2010) 1427.

[890] Turnbull, M.C., & Tarter, J.C., *ApJ Suppl. Series* **145** (2003) 181.

[891] Turnbull, M.C., & Tarter, J.C., *ApJ Suppl. Series* **149** (2003) 423.

[892] Siemion, A., et al., *Acta Astronautica* (2013) in press.

[893] Taylor, A. R., *www.skatelescope.org/* .

[894] Maccone, C., *Mathematical SETI*, Praxis-Springer, ISBN–10: 3642274366 | ISBN–13: 978-3642274367 (2012).

[895] *Report of the SKA Siting Options Working Group* (2012) www.skatelescope.org
agreement n. 202781.